GULF LISTEN
LONG-TERM INVESTIGATIONS INTO
SOUNDSCAPES, TRENDS, ECOSYSTEMS AND NOISE

# LISTEN GoMex: 2020-2023

## *Long-term Investigations into Soundscapes, Trends, Ecosystems, and Noise in the Gulf of Mexico*

**Report Authors:**

Kaitlin E. Frasier[1], Melissa S. Soldevilla[2], Macey A. Kadifa[1], Lynne Hodge[2 3], Héloïse Frouin-Mouy[2], Ludovic Tenorio-Hallé[2], Amanda Debich[2],Itzel Pérez Carballo[4], Katrina Johnson[1], Isabel Catalina Barrera Diaz[5], Adolfo Gracia [5], Arturo Serrano[4], Lance P. Garrison[1], John A. Hildebrand[1], Matthieu Le Henaff[6], Joel Ortega Ortiz[6], Carrie Wall-Bell[7]

[1]Scripps Institution of Oceanography, University of California, San Diego

[2]NOAA NMFS Southeast Fisheries Science Center

[3]University Corporation for Atmospheric Research's (UCAR) Cooperative Programs for the Advancement of Earth System Science (CPAESS)

[4]Universidad Veracruzana

[5]Instituto de Ciencias del Mar y Limnología, UNAM

[6]Cooperative Institute for Marine and Atmospheric Studies, University of Miami

[7]University of Colorado Boulder and NOAA National Centers for Environmental Information

March 19, 2024

DOI: // 10.25923/3ma1-b145

## Suggested Citation

Frasier K.E., Soldevilla, M.S., Kadifa, M.A., Hodge, L., Frouin-Mouy, H., Tenorio-Hallé, L., Debich, A., Pérez Carballo, I., Johnson, K., Barrera Diaz, I.C., Gracia, A., Serrano, A., Garrison, L.P., Hildebrand, J.A., Le Henaff, M., Ortega Ortiz, J., Wall-Bell, C. (2023) LISTEN GoMex: 2020-2023 - Long-term Investigations into Soundscapes, Trends, Ecosystems, and Noise in the Gulf of Mexico. Marine Physical Laboratory, Scripps Institution of Oceanography, University of California San Diego, La Jolla, CA. MPL Technical Memorandum #667. Version 1.3.

DOI: // 10.25923/3ma1-b145

# Table of Contents

# 1 Executive Summary

In 2010, the *Deepwater Horizon* (DWH) oil spill had unprecedented impacts on the Gulf of Mexico ecosystem, including the twenty cetacean species inhabiting the oceanic waters of this semi-enclosed large marine ecosystem. Due to the impacts from DWH oil, restoration projects focused on oceanic cetaceans are being enacted in the Gulf. These projects require basic information on species' spatiotemporal density patterns, Gulf-wide movement patterns, Gulf-wide population sizes, long-term abundance trends, and species' responses to oceanographic and anthropogenic processes, along with information on Gulf-wide ambient noise levels and the contributions from anthropogenic noise sources. To address these needs, NOAA's Southeast Fisheries Science Center (SEFSC), UCSD's Scripps Institution of Oceanography (SIO), and partners initiated a comprehensive, long-term, multi-scale passive acoustic monitoring program throughout US and Mexican Gulf waters over the 2020 – 2025 period. This program collects data needed to develop predictive habitat models to assess the processes driving seasonal, interannual, and decadal trends in spatial distribution, density, and abundance of oceanic cetaceans and to assess contributions of ambient noise sources to the Gulf soundscape. This collaborative study annually deploys moored HARP instruments, continuously recording over the 10 Hz to 100 kHz band, over the five-year period at a total of:

- 8 five-year long-term sites to identify temporal trends and variability at reference sites over the study period,
- 20 one-year short-term sites over a broad area of the Gulf to capture spatial trends and variability in cetacean density and environmental processes,
- 3 six-month sites with targeted sampling using tracking arrays to obtain acoustic behavior data for density estimation, and
- 2 three-to-five-year sites focused on areas of importance to the DWH Restoration noise reduction project.

Additionally, the study leverages 10 years of historic HARP recordings at 5 long-term sites, collected by SIO as part of the DWH damage assessment to enhance the assessment of trends in cetacean density and noise.

This report compiles the preliminary results from three years of HARP recordings over the 2020-2023 period. Sites are distributed across the Gulf of Mexico, primarily in deep waters, with regional coverage including the north and northeastern Gulf (long-term sites MC & DC respectively), Loop-Current-adjacent regions (long-term sites LC & DT, and short-term sites Y1D/B, Y2A/B/D & Y3B), northwestern Gulf upper slope and Sigsbee Escarpment (long-term sites AC & GC, and short-term site Y3D), Sigsbee Deep (short-term site Y3A), southern Gulf Bay of Campeche (long-term site MR and short-term sites Y1C, Y2C & Y3C) and Campeche Escarpment (CE), and northern Gulf shelf-break shipping lanes (long-term sites GA & SL). The two long-term noise-focused sites Galveston (site GA) at site 215 m depth and Southern Louisiana (site SL) are shallow (220 m seafloor depth), as is the De Soto Canyon site (260 m seafloor depth). Short-term sites Y1D and Y2B had intermediate seafloor depths (550 m

and 700m respectively) while all other sites had seafloor depths of 1000 m or more with hydrophones positioned near 1000 m depth. Tracking arrays were deployed at long-term sites MC, GC, and MR during the 2020-2023 period.

Data analysis primarily consisted of automated detection and classification of marine mammal echolocation signals followed by density estimation, and characterization of anthropogenic noise sources. Data analyses for specific sound sources were conducted in two versions of the dataset: a "low frequency" decimated version of the dataset with an effective bandwidth of 10 - 1,000 Hz, and a broadband version with an effective bandwidth of 10 Hz - 100 kHz. Ambient soundscape, seismic airgun, vessel source level, and baleen whale analyses were conducted using the low-frequency dataset. Odontocete and local ship noise analyses were conducted using the broadband dataset.

This report, which combines three years of monitoring data from long-term and short-term sites, yields new preliminary insights into Gulf-wide distributions of marine mammals. Patterns in Cuvier's beaked whale distributions suggest two hot spots in the vicinity of the Campeche Escarpment and the Loop Current-adjacent regions near the southern end of the Florida Escarpment. Gervais' beaked whales appeared to primarily occupy the Loop Current-adjacent sites in the east, and were secondarily found in deep southwestern Mexican waters (Mexican Ridges region). Blainville's beaked whale, a rarity in the northern GoMex was primarily present from the Bay of Campeche up to the Sigsbee Escarpment, at sites with bottom depths over 2000 m. Beaked whale tracking allowed estimation of swim speeds and echolocation click source levels for three species of beaked whales from a total of 53 acoustically-tracked dives. This Gulf-specific dive and acoustic behavior data will be used to improve conversion of beaked whale click detections at long-term and short-term sites into animal counts for more robust density trends.

Sperm whale densities were highest in the region near Mississippi Canyon, with a secondary hot spot in the vicinity of Mexican Ridges. During this three-year period, densities at MC were similar to historic 2010 estimates, while while those at GC were lower, and densities at the southern end of the Florida Escarpment were higher than previous 2010 estimates, matching findings from decadal trends. Unidentified high-frequency dolphin (UD, presumed primarily *Stenella* spp. and offshore *Tursiops truncatus*) hourly presence was highest at the eastern Gulf sites, including relatively high densities and occurrence at abyssal plain sites with bottom depths greater than 2,500 m. Differences in seasonal peaks in density across sites for dolphins (Risso's dolphin & UD) and sperm whales suggest possible seasonal movement patterns within the Gulf. Analyses of the 2020-2022 deployments found Rice's whale call detections at seven of the 17 sites including the core habitat and adjacent waters (DC, Y1D, LC), at shallow shipping lane sites (SL and GA), and in Mexican waters of the southwestern Gulf (MR, Y2C).

At most of the 21 locations over the August 2020 to July 2023 recording period, the ambient soundscape below 100 Hz is dominated by seismic survey signals (airguns) nearly year-round. Moreover, throughout the three years, the same surveys appear simultaneously across

most acoustic recorders, illustrating the long-range propagation of these intense low-frequency signals. At the sites with the highest detection rates, airguns are typically detected in 50% of minutes per day, and can approach 100% of minutes. Airgun received levels were highest at the Green Canyon site due to many months of close range surveys in the fall of 2020 and winter of 2022.

Vessel traffic noise from commercial shipping is apparent in the quieter periods between seismic surveys, and noise from weather events is visible at higher frequencies, especially at the sites with the overall lowest sound levels, such as De Soto Canyon. Shipping activity in the GoMex is high, with cargo ships and tankers making up the majority of identifiable vessels. From 2020 to 2023, tens of thousands of ships passed within 15 km of the Gulf HARPs, with thousands passing multiple times, and some vessels making 100 - 1500 different close approaches. Source levels were estimated for over 5,000 vessels using two recording stations positioned within the shipping lanes adjacent to the ports of Houston/Galveston and Southern Louisiana. Median monopole source levels were highest for cargo ships and tankers, with energy peaks around 50 Hz.

# 2 Introduction

## 2.1 Project Background

In 2010, the *Deepwater Horizon* (DWH) oil spill had unprecedented impacts on the Gulf of Mexico ecosystem, including the twenty cetacean species inhabiting the oceanic waters of this semi-enclosed large marine ecosystem. Due to the impacts from DWH oil, science and restoration projects focused on oceanic cetaceans are being enacted in the Gulf to enhance their conservation and recovery, including one focused on reducing impacts of noise on marine mammals. These science and restoration projects require basic information on species' spatio-temporal density patterns, Gulf-wide movement patterns, Gulf-wide population sizes, long-term abundance trends, and species' responses to oceanographic and anthropogenic processes, along with information on Gulf-wide ambient noise levels and the contributions from anthropogenic noise sources.

To address these needs, NOAA's Southeast Fisheries Science Center (SEFSC), UCSD's Scripps Institution of Oceanography (SIO), and partners initiated the LISTEN GoMex program, a comprehensive, long-term, multi-scale passive acoustic monitoring program throughout US and Mexican Gulf waters. The LISTEN GoMex project combines several collaborative projects including:

- *"Assessing Long-term Trends and Processes Driving Variability in Cetacean Density throughout the Gulf of Mexico using Passive Acoustic Monitoring and Habitat Modeling"*, funded by the RESTORE Science Program to improve our understanding of where and when cetaceans occur throughout the Gulf and how and why that is changing over time.
- *"Reduce Impacts of Anthropogenic Noise on Cetaceans"*, a restoration project funded by the *Deepwater Horizon* Open Ocean Trustee Implementation Group to improve understanding of how noise-producing human activities affect the Gulf soundscape and cetaceans, and to work with industry partners to reduce human-produced noise impacts on cetaceans.
- *"Environmental Characterization using Ambient Seismic Sources"*, funded by the US Navy Task Force Ocean to improve understanding of how we can use opportunistic sound sources to characterize the inner structure of the ocean, for example, deep Loop Current features.

To meet these objectives, the Gulf-wide passive acoustic monitoring program is being implemented over the 2020 – 2025 period to collect data needed to develop predictive habitat models to assess the processes driving seasonal, interannual, and decadal trends in spatial distribution, density, and abundance of oceanic cetaceans and to assess contributions of ambient noise sources to the Gulf soundscape. The collaborative, multi-scale study annually deploys moored High-frequency Acoustic Recording Package (HARP) instruments over the five-year period at a total of A) 8 five-year long-term sites to identify temporal trends and variabil-

ity at reference sites over the study period, B) 20 one-year short-term sites over a broad area of the Gulf to capture spatial trends and variability in cetacean density and environmental processes, C) 3 six-month sites with targeted sampling using tracking arrays to obtain acoustic behavior data for density estimation, and D) 2 or more one-year sites focused on areas of importance to the DWH Restoration noise reduction project. Additionally, the study leverages 10 years of historic HARP recordings at 5 long-term sites, collected by SIO as part of the DWH damage assessment to enhance the assessment of trends in cetacean density and noise.

This report compiles the preliminary results from three years of HARP recordings over the 2020-2023 period. The 8 offshore, long-term sites named for nearby oceanographic features include:

- De Soto Canyon (site DC) located within the Rice's whale core habitat at 260 m depth,
- Dry Tortugas (site DT) at 1,200 m depth
- Green Canyon (site GC) at 1,100 m depth
- Mississippi Canyon (site MC) at 1,200 m depth
- Alaminos Canyon (site AC) at 1,100 m depth
- Campeche Escarpment (site CE) at 2,100 m depth
- Loop Current (site LC) at 3,200 m depth
- Mexican Ridges (site MR) at 1,100 m depth

The 11 one-year sites include:

- Y1B at 3,330 m depth
- Y1C at 2,900 m depth
- Y1D at 550 m depth
- Y2A at 2,500 m depth
- Y2B at 700 m depth
- Y2C at 2,100 m depth
- Y2D at 2,100 m depth
- Y3A at 3,700 m depth
- Y3B at 3,200 m depth
- Y3C at 2,200 m depth
- Y3D at 3,100 m depth

The 2 short-term noise-focused sites include:

- Galveston (site GA) at 215 m depth
- Southern Louisiana (site SL) at 220 m depth

Tracking arrays were deployed at long-term sites MC, GC, and MR during the 2020-2023 period. These sites are all located in oceanic Gulf waters beyond the continental shelf in the US and Mexico (Figure 1).

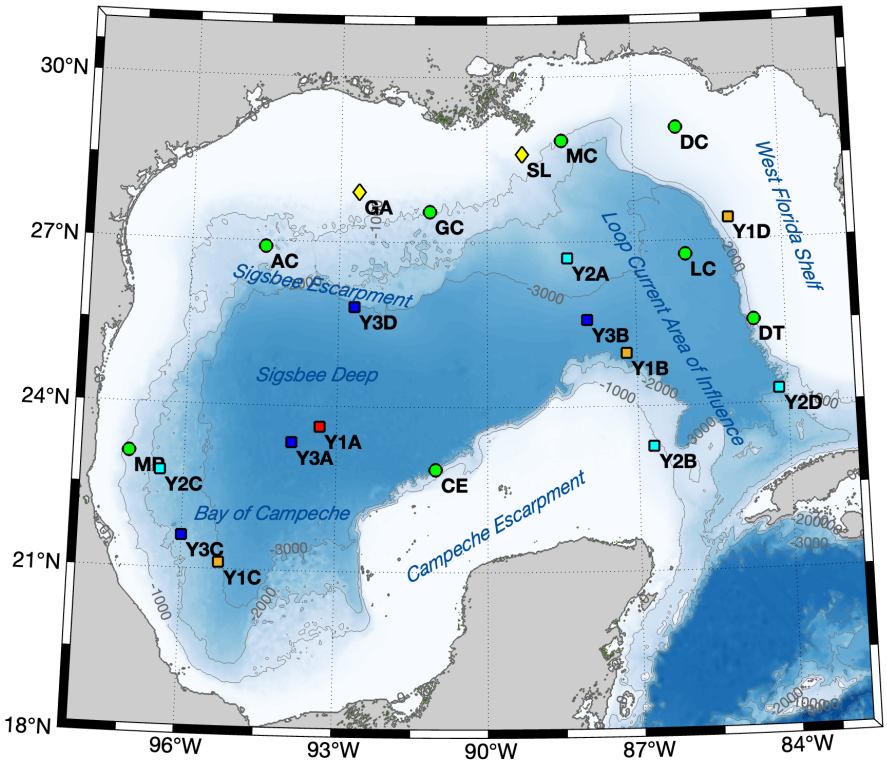


**Figure 1:** Location of the High-frequency Acoustic Recording Packages (HARPs) and Mid-Frequency Acoustic Recording Packages (MARPs). Green circles represent multi-year HARP sites; orange, cyan, and dark blue squares represent single-year HARP sites from years one, two, and three, respectively; yellow diamonds represent MARP sites; and a red square represents a site where there was no effort due to a data quality issue.

## 2.2 High Level Data Description

High-frequency Acoustic Recording Packages (HARPs) are autonomous underwater acoustic recording devices that, dependent on configuration, can record sounds over a bandwidth from 10 Hz up to 160 kHz and are capable of approximately one year of continuous recording. During all historic recordings and at 12 of the new sites, the HARPs were set to record continuously at a sampling rate of 200 kHz, sufficient to record sounds from all sources of interest. At the two soundscape sites (GA and SL), the HARPs were set to record continuously at a sample rate of 20 kHz, sufficient to record anthropogenic noise sources of interest, and are referred to as Mid-frequency Acoustic Recording Packages (MARPs). At three of the sites (GC, MC, and MR), two additional 4-ch HARPs deployed as part of a 3-unit tracking array (a total of 6 HARPs), were set to record continuously at 100 kHz (MR recorded at 200 kHz), sufficient to record most sounds from odontocetes and all lower frequency sounds. In summary, of the 48 HARPs deployed over this period, 36 were deployed to record signals from all marine mammal species, anthropogenic sound sources, and ambient soundscapes, 6 were deployed to focus on ambient soundscapes and anthropogenic sound sources, and 6 were deployed as part of an array for marine mammal tracking.

The HARPs at sites with seafloor depths less than 1200 m were deployed in small mooring configurations with the hydrophones suspended approximately 20 m above the seafloor. At sites with seafloor depths greater than 1200 m, deep mooring configurations were used, with the hydrophones buoyed to approximately 1000 m depth. Each HARP hydrophone was calibrated in the laboratory to allow for quantitative analysis of the received sound field. Representative data loggers and hydrophones have also been calibrated at the Navy's TRANSDEC facility to verify the laboratory calibrations (Wiggins and Hildebrand 2007).

Of the 48 HARPs deployed over the August 2020 - September 2023 period, 41 HARPs were successfully recovered with high-quality data recordings (Figure 2, Table 2).

Three HARPs did not record data successfully: The HARP at Y1A exhibited internal corrosion issues that prevented recovery of recordings. One of the HARPS, the 2020 deployment of the 200 kHz HARP at MC, is presumed to have become entangled upon release and is awaiting recovery. The second 4-channel HARP deployed at site MC in 2020 did not wake up to start recording due to an unexpected software reset, an issue which has since been corrected in the 4-channel HARP firmware.

Five HARPs recorded successfully but had data quality issues: The GC15 HARP had hydrophone problems due to a manufacturing defect. Data was recorded successfully from 7/8/2022 to 10/11/2022. Recording resumed from 11/2/2022 to 11/18/2022 and the instrument did not record usable data thereafter, resulting in only 111 of 360 projected total days of data (Figure 2, Table 2). The MC17 HARP recorded continuously but intermittent high amplitude noise was recorded from 3/4/2023 through the end of the recording. This may have been due to an hydrophone malfunction or caused by equipment rubbing on the hydrophone, possibly due to loss of top float buoyancy. Noisy periods were excluded from the analyses us-

ing amplitude-based filters, resulting in recovery and analysis of approximately 80% of the dataset. The LC03 HARP deployment ended prematurely after 18 of 384 projected days due to excessive power consumption, the precise cause of which is still under investigation. One of the 4-channel HARPs deployed at MR03 had a microSD controller chip failure resulting in a loss of 6 days of data (207 of 213 projected total days of data recorded) (Figure 2, Table 2). The second 4-channel HARP at MR03 stopped recording during the last week of the deployment on 2/3/2023 due to a shark bite into the hydrophone cable, resulting in two weeks of lost data (2/3/2023 - 2/17/2023),ultimately recording 197 of 211 of total projected days of data (Figure 2, Table 2). Three recordings, DC14, GC14, and MC16 were 2-3 months shorter than expected due to a battery wiring issue.

| Site | Deployment | Start Date | End Date | Recording Duration (Days) |
|---|---|---|---|---|
| AC | 01 | 8/29/2020 | 9/5/2021 | 372 |
| AC | 02 | 9/6/2021 | 7/21/2022 | 318 |
| AC | 03 | 7/21/2022 | 7/6/2023 | 359 |
| CE | 01 | 9/1/2020 | 9/1/2021 | 365 |
| CE | 02 | 9/1/2021 | 7/16/2022 | 317 |
| CE | 03 | 7/27/2022 | 7/9/2023 | 367 |
| DC | 13 | 8/15/2020 | 8/23/2021 | 372 |
| DC | 14 | 8/23/2021 | 6/3/2022 | 284 |
| DC | 15 | 9/21/2022 | 7/4/2023 | 286 |
| DT | 13 | 8/17/2020 | 8/27/2021 | 374 |
| DT | 14 | 8/27/2021 | 7/12/2022 | 319 |
| DT | 15 | 7/13/2022 | 6/26/2023 | 348 |
| GA | 01 | 8/30/2020 | 9/6/2021 | 371 |
| GA | 02 | 9/6/2021 | 7/23/2022 | 319 |
| GA | 03 | 7/23/2022 | 7/18/2023 | 359 |
| GC | 13 | 8/12/2020 | 8/20/2021 | 373 |
| GC | 14 | 8/20/2021 | 5/5/2022 | 257 |
| GC | 14_01_C4 | 9/7/2021 | 3/26/2022 | 199 |
| GC | 14_02_C4 | 9/7/2021 | 3/25/2022 | 198 |
| GC | 15* | 7/8/2022 | 11/8/2022 | 111 |
| LC | 01 | 8/16/2020 | 8/24/2021 | 372 |
| LC | 02 | 8/24/2021 | 7/10/2022 | 319 |
| LC | 03* | 7/10/2022 | 7/29/2023 | 18 |
| MC | 15* | 8/13/2020 | – | – |
| MC | 15_01_C4 | 8/13/2020 | 2/28/2021 | 199 |
| MC | 15_02_C4* | 8/13/2020 | – | – |
| MC | 16 | 8/22/2021 | 4/28/2022 | 249 |
| MC | 17* | 7/9/2022 | 7/4/2023 | 359 |
| MR | 01 | 9/7/2020 | 9/4/2021 | 362 |
| MR | 02 | 9/4/2021 | 7/19/2022 | 318 |
| MR | 03 | 7/19/2022 | 7/12/2023 | 357 |

| | | | | |
|---|---|---|---|---|
| MR | 03_01_C4* | 7/19/2022 | 2/17/2023 | 207 |
| MR | 03_02_C4* | 7/19/2022 | 2/15/2023 | 197 |
| SL | 01 | 8/13/2020 | 8/21/2021 | 372 |
| SL | 02 | 8/21/2021 | 7/9/2022 | 321 |
| SL | 03 | 7/9/2022 | 7/3/2023 | 359 |
| Y1 | Y1A_01* | – | – | – |
| Y1 | Y1B_01 | 8/21/2020 | 8/26/2021 | 370 |
| Y1 | Y1C_01 | 9/5/2020 | 9/3/2021 | 363 |
| Y1 | Y1D_01 | 8/15/2020 | 8/23/2021 | 373 |
| Y2 | Y2A_01 | 8/25/2021 | 7/11/2022 | 319 |
| Y2 | Y2B_01 | 8/31/2021 | 7/15/2022 | 318 |
| Y2 | Y2C_01 | 9/4/2021 | 7/19/2022 | 318 |
| Y2 | Y2D_01 | 8/29/2021 | 7/14/2022 | 318 |
| Y3 | Y3A_01 | 7/17/2022 | 7/13/2023 | 361 |
| Y3 | Y3B_01 | 7/12/2022 | 7/7/2023 | 360 |
| Y3 | Y3C_01 | 7/18/2022 | 7/11/2023 | 358 |
| Y3 | Y3D_01 | 7/22/2022 | 7/17/2023 | 359 |
| | | | Total Days | 14,220 |
| | | | Total Years | 38.95 |

**Table 2:** Dates and durations of high-quality HARP recordings spanning from 2020-2023. Deployments with a (*) denote deployments with hardware or processing issues or are that still deployed, resulting in incomplete data (see text for more information).

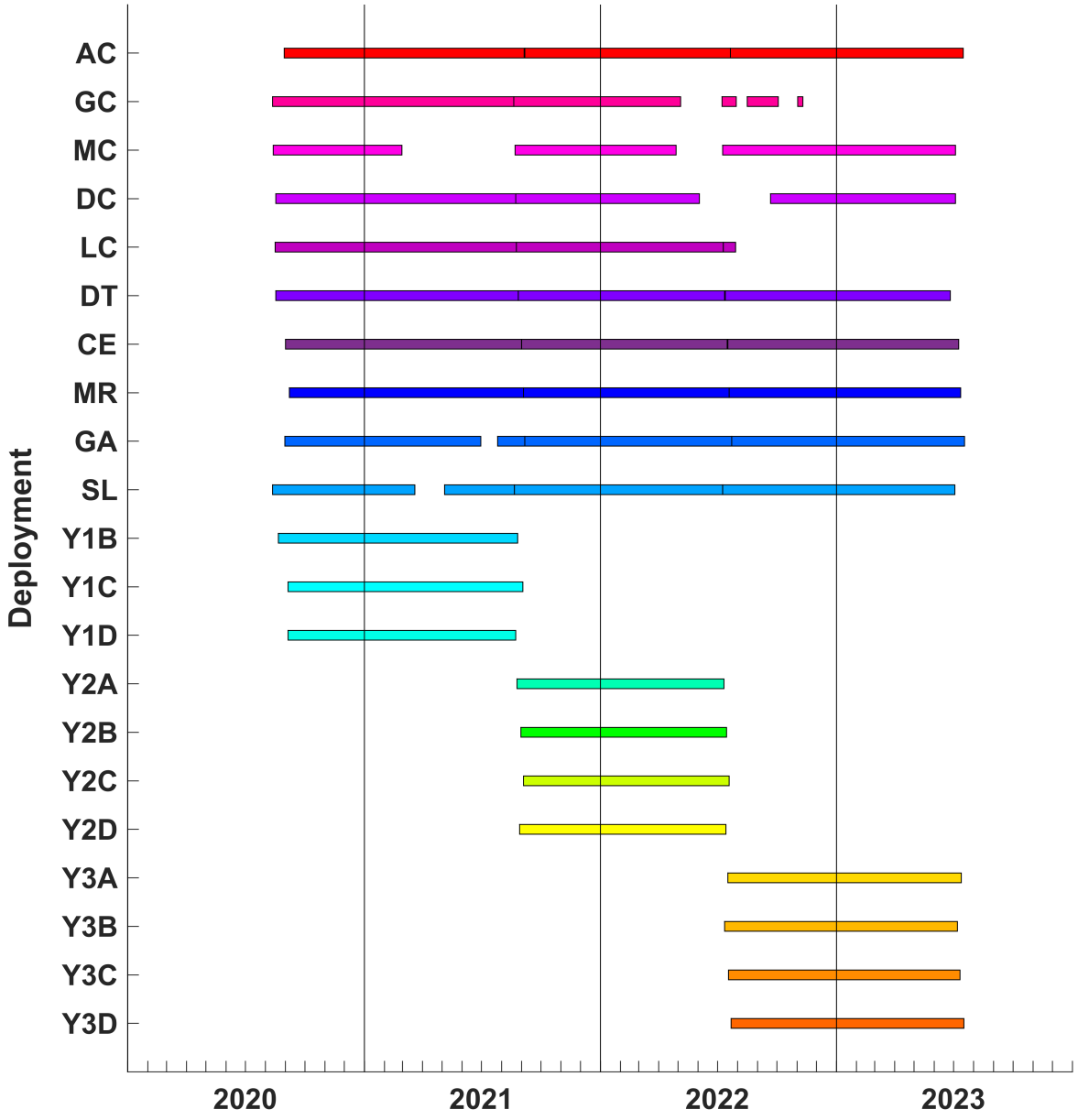


**Figure 2:** Recording effort for Gulf of Mexico HARP sites from 2020-2023. Data collection is ongoing.

# 3 Data Analysis

The data analysis process is described below in terms of the major classes of odontocete vocalizations, anthropogenic sounds, and low-frequency ambient soundscape in the Gulf of Mexico region, and the procedures used to detect and characterize them.

We summarize and characterize sounds detected at all the sites across the Gulf of Mexico. Weekly estimated density was calculated for each species or species group where appropriate. Weekly occurrence is reported for non-biological signals. Diel, seasonal and interannual patterns of the occurrence of various signals are reported for each monitoring site and compared across sites. Vessel noise analyses detail vessel categories and sound levels. Low frequency ambient noise dominated by anthropogenic sound sources is compared across sites.

## 3.1 Odontocete Analyses

### 3.1.1 Click Classification

Odontocete sounds can be categorized as echolocation clicks, burst pulses, or whistles. Echolocation clicks are broadband impulses with peak energy between 1 and 150 kHz, dependent upon the species. Buzzes or burst pulses are rapidly repeated clicks that have a creak, squeal, screech, or buzz-like sound quality; they are often lower in frequency than echolocation clicks. Dolphin whistles are tonal calls predominantly between 1 and 20 kHz that vary in frequency content, their degree of frequency modulation, as well as duration. These signals are easily detectable in a long-term spectral average (LTSA) as well as the spectrogram. Analyses in this report focus only on echolocation clicks as a proxy for odontocete presence because they are currently the most promising call type for species classification in the region. Future analysis might identify distinguishing whistle or burst pulse characteristics.

Odontocete echolocation clicks were detected automatically using an energy detector with a minimum received level threshold of 120 dBpp re: 1 $\mu$Pa (Roch et al. 2011; Frasier et al. 2016). To classify detected clicks to putative taxonomic groups, dominant click types and false positive categories at these sites were identified using automated unsupervised clustering methods (Frasier, 2021). Detections were clustered within successive five-minute windows and dominant click types were identified in each window using spectral features, inter-click intervals, and waveform envelopes. Regular clicks were the focus of this analysis; therefore, clicks with an ICI less than 0.001 sec were excluded from this analysis to limit the inclusion of buzz clicks. An automated clustering algorithm was then used to identify recurrent types based on spectral features, inter-click interval (ICI), and waveform distributions at each site (Frasier et al. 2017). Common click types were manually aggregated across all of the sites in the Gulf of Mexico to form classifier training and testing sets for 13 signal types including 9 odontocete signals and 4 sources of false positives. Click types were attributed to a specific species if acoustically identifiable (e.g., beaked whales and Risso's dolphin) or

assigned an unidentified category if the species was unknown. A deep neural network was trained to classify these signal types with 98% classification accuracy on a balanced test set. This trained network was used to classify all five-minute windows across all sites. Classifications were retained if classification probability exceeded 90% and the classified bin contained at least 5 clicks. Classifier confusion was evaluated manually using a subset of the recordings from the historic data set (sites MC, GC, DT & DC) from 2010-2020 (Table 3). An analyst manually annotated 3% of all hours for estimation of species-specific error rates (ER), based on the occurrence of false positive (FP), false negative (FN), true positive (TP) and true negative (TN) detections of each species, computed as:

$$ER = (FP + FN)/(FN + FP + TP + TN) \quad (1)$$

Standard odontocete detectors were not run on the 2020-2023 GC_14 4-channel HARPs, MC_15 4-channel HARP, or GA & SL MARP datasets since the recording bandwidth was not sufficient. Odontocete detectors were not run on MR_03 4-channel HARP data because the single channel deployment was longer, and overlapped in time with the MR 4-channel deployments. Tracking-specific odontocete detection algorithms were run on the GC_14 4-channel and MC_15 4-channel data, and will be run in the future on the MR_03 4-channel data. SL_03 was a HARP deployment, but as a noise-focused station, it was not analyzed for odontocetes for this report.

### 3.1.2 Density Estimation

Point-transect-based density estimation methods were used to convert presence in 5-minute windows into weekly estimates of marine mammal densities at each site for each putative marine mammal taxonomic class. For each class and site combination, the probability of detecting a group of animals in a five-minute time window was estimated using a Monte Carlo simulation, taking into account minimum detection thresholds, echolocation click frequency content and signal attenuation, taxon-specific dive depths and vocalization rates, and local oceanographic conditions (Table. 4). Weekly animal densities were computed following Marques et al. (2009) for group counting, using previously-published parameter estimates for beaked whales (Hildebrand et al. 2015), sperm whales (Solsona Berga 2019), delphinids (Frasier 2015), and *Kogia* spp. (Hildebrand et al. 2019). This study used a different minimum received level threshold than that used in previously published studies. All models were therefore re-evaluated for this project with a consistent minimum received level (125 dB peak-to-peak) for all species (Table 4). Climatological mean sound speed profiles for the month of January were extracted from the Generalized Digital Environment Model (GDEM v 3.0) and used for frequency-dependent propagation loss estimation at each site. Summer sound speed profiles may result in slightly different detection probability estimates for some species (Frasier et al. In Review) and may be incorporated in subsequent analyses. The goal of our analysis is estimation of animal densities from the passive acoustic monitoring data. Our basic assumption is that the acoustic detections for each species at each site give a mea-

sure of the relative density over time. The analysis was conducted for each HARP site, and to provide sufficient data for each density estimate, the data were averaged over weekly time intervals.

| Species | Mean Error Rate |
|---|---|
| Sperm whale | 2.23% |
| Cuvier's beaked whale | 0.47% |
| Gervais' beaked whale | 0.27% |
| Blainville's beaked whale | 0.03% |
| Risso's dolphins | 2.50% |
| Other delphinids (All) | 7.17% |
| *Kogia* spp. | 0.27% |

**Table 3:** Mean error rates for each species for each site based on manual review of 3% of hours of data sampled across the historic dataset (2010-2020, Rafter et al. 2022). Error rates for other delphinids represent all three groups of unidentified delphinids. Individual confusion statistics and error rates for the various delphinid categories will be computed once final categories have been defined in future reports.

| Site | Sperm whale | Cuvier's BW | Gervais' BW | Blainville's BW | Risso's dolphin | Unid. delphinid | *Kogia* spp. |
|---|---|---|---|---|---|---|---|
| **AC** | 59.2 (3.8) | 29.8 (2.5) | 22.7 (1.9) | 23.8 (2.2) | 19.6 (4.4) | 8.1 (2.4) | 20.8 (2.1) |
| **CE** | 52.2 (3.7) | 28.4 (2.5) | 21.3 (2.1) | 21.7 (2.2) | 20.0 (4.2) | 8.7 (2.8) | 22.2 (2.1) |
| **DC** | – | – | – | – | 19.6 (2.4) | 12.5 (2.4) | – |
| **DT** | 38.7 (3.3) | 29.3 (2.3) | 22.4 (2.0) | 23.5 (2.3) | 20.8 (4.5) | 8.4 (2.5) | 19.4 (2.3) |
| **GC** | 43.6 (2.7) | 29.4 (2.4) | 22.5 (2.0) | 23.5 (2.2) | 20.9 (4.4) | 8.4 (2.5) | 19.5 (2.0) |
| **LC** | 58.4 (5.2) | 29.4 (2.3) | 22.4 (2.1) | 23.4 (2.2) | 19.0 (4.1) | 7.7 (2.4) | 19.5 (2.2) |
| **MC** | 37.7 (2.1) | 29.7 (2.3) | 22.6 (2.0) | 23.7 (2.2) | 20.9 (4.4) | 9.2 (2.6) | 23.3 (1.9) |
| **MR** | 47.1 (2.7) | 30.2 (2.4) | 23.1 (2.0) | 24.3 (2.2) | 20.3 (4.4) | 8.0 (2.4) | 20.6 (2.1) |
| **Y1B, Y3D, Y3B, Y2A, Y2D** | 56.7 (4.9) | 29.4 (2.5) | 22.1 (2.0) | 22.4 (2.2) | 19.2 (4.1) | 7.1 (2.2) | 19.5 (2.1) |
| **Y1C, Y3C, Y3A, Y2C** | 56.9 (5.3) | 29.4 (2.3) | 22.3 (2.0) | 23.1 (2.2) | 19.0 (4.5) | 7.7 (2.3) | 19.5 (2.4) |
| **Y1D, Y2B** | 56.7 (4.9) | 29.4 (2.5) | 22.5 (2.0) | 23.4 (2.2) | 20.7 (3.7) | 10.7 (2.5) | 23.3 (1.9) |

**Table 4:** Detection probability by species computed based on species-specific Monte Carlo simulations within a defined maximum detection radius (Sperm whales: 35 km, Beaked whales: 4 km, Dolphins: 5 km, *Kogia*: 1.5 km). Y# sites with presumed similar mean detection probabilities were grouped based on site depth and mooring design for preliminary analysis. More detailed modeling of site-specific detection probabilities is planned.

### 3.1.3 Beaked Whale Tracking for Density Estimation Parameterization

In 2021, two 4-channel High-frequency Acoustic Recording Packages (tracking HARPs) were deployed 772 m apart at site GC (depth $\sim$1100 m). Each tracking HARP was equipped with four calibrated hydrophones positioned in a tetrahedral array (Wiggins et al. 2012). The spacing between hydrophones was $\sim$1 m, with the top hydrophone located $\sim$6 m above the seafloor. All HARPs were deployed on a seafloor slope in an area of known beaked whale habitat in the Gulf of Mexico (Hildebrand et al. 2015). Acoustic analysis was conducted using custom MATLAB-based software programs in a two-step approach. First, automated detection and classification of echolocation clicks was implemented using the SPICE detector remora, an add-on of the acoustic analysis tool *Triton* (Frasier et al. 2017). A minimum received level threshold of 115 dBpp re: 1 $\mu$ Pa (Frasier et al. 2017) was used to trigger detection of the candidate clicks. Then, custom software for analyst-assisted species classification (*DetEdit*, Solsona-Berga et al. 2020) was used for manual validation and annotation of each detected beaked whale click bout. Echolocation pulses from Cuvier's, Gervais' and Blainville's beaked whales detected on both recorders at GC were used to reconstruct individual tracks (three-dimensional localizations) using a toolkit called *Where's Whaledo* (Snyder et al., *Submitted*). Dives were rejected from analysis when 1) they represented groups of animals whose individual detection angles could not be unambiguously discriminated, 2) the track had too few detections to be reliably localized, or 3) the track was of too short duration (less than 7 min). To investigate the directionality of beaked whale clicks, each peak-to-peak source level ($SL_{pp}$) was associated with an angle measured between the acoustic axis of the whale's click sound beam, and the vector connecting the whale with the HARP from which the $SL_{pp}$ was estimated. This angle ranges from 0° (looking forward along the acoustic axis) to 180° (looking backward along the acoustic axis), with 90° as perpendicular to the acoustic axis, and is referred to as the off-axis angle, $\gamma$ (Gassmann et al. 2015).

## 3.2 Odontocete Species Call Descriptions

Nineteen odontocetes are resident to the Gulf of Mexico, and numerous human-made noise sources are also common in these waters. A description of the identifying features of each species' call types and identified noise sources follows. For all odontocete species and noise source descriptions, the following figures are presented, from top to bottom, and left to right, representing 1) a long-term average spectrogram of an acoustic encounter over 1 hour, 2) a standard spectrogram of acoustic signals over 5 minutes, 3) the average spectrum of an acoustic signal type with associated variance, 4) a histogram of average ICIs for an acoustic signal type, and 5) the envelope of the signal waveform.

**List of odontocete species found in the Gulf of Mexico:**

- Sperm whale (*Physeter macrocephalus*) (ESA-Listed)
- Dwarf sperm whale (*Kogia sima*)
- Pygmy sperm whale (*Kogia breviceps*)
- Cuvier's beaked whale (*Ziphius cavirostris*)
- Blainville's beaked whale (*Mesoplodon densirostris*)
- Gervais' beaked whale (*Mesoplodon europaeus*)
- Short-finned pilot whale (*Globicephala macrorhynchus*)
- Killer whale (*Orcinus orca*)
- False killer whale (*Pseudorca crassidens*)
- Pygmy killer whale (*Feresa attenuata*)
- Melon-headed whale (*Peponocephala electra*)
- Common bottlenose dolphin (*Tursiops truncatus*)
- Risso's dolphin (*Grampus griseus*)
- Rough-toothed dolphin (*Steno bredanensis*)
- Fraser's dolphin (*Lagenodelphis hosei*)
- Pantropical spotted dolphin (*Stenella attenuata*)
- Striped dolphin (*Stenella coeruleoalba*)
- Clymene dolphin (*Stenella clymene*)
- Spinner dolphin (*Stenella longirostris*)

### 3.2.1 Cuvier's Beaked Whale

Beaked whales can be identified acoustically by their echolocation signals (Baumann-Pickering et al. 2014). These signals are frequency-modulated (FM) upsweep pulses, which appear to be species specific and distinguishable by their spectral and temporal features. Identifiable signals are described for all beaked whales known to occur in the region, namely Blainville's, Cuvier's, and Gervais' beaked whales.

Cuvier's echolocation signals are polycyclic, with a characteristic FM pulse upsweep, peak frequency around 40 kHz (Figures 3 & 4), and uniform inter-click interval (ICI) of about 0.5 s (Johnson et al. 2004; Zimmer et al. 2005). An additional feature that helps with the identification of Cuvier's FM pulses is that they have two characteristic spectral peaks around 17 and 23 kHz.

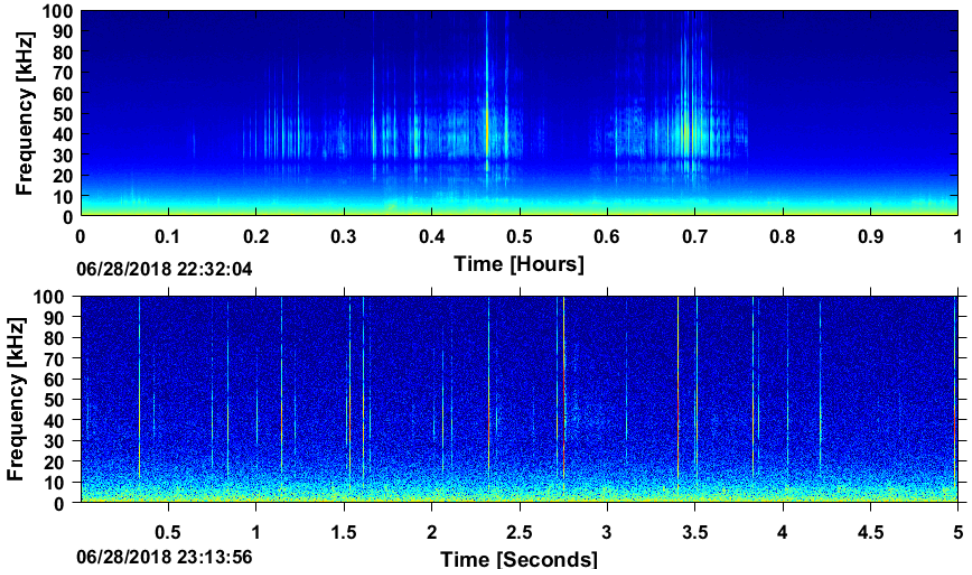


**Figure 3:** Cuvier's beaked whale signal in LTSA (top) and spectrogram (bottom).

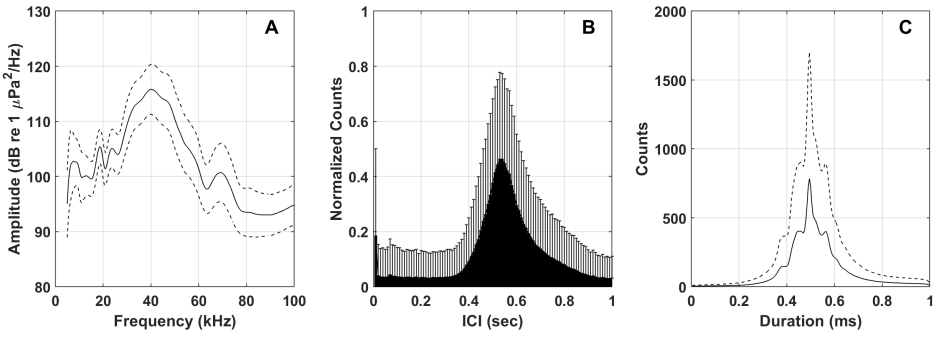


**Figure 4:** Left: Mean frequency spectrum of Cuvier's beaked whale echolocation clicks (solid line) and 25th and 75th percentiles (dashed lines); Center: Inter-click interval distribution with peak near 0.5 s; Right: Mean waveform envelope (solid line) and standard deviation (dashed line) of representative clicks.

### 3.2.2 Gervais' Beaked Whale

Gervais' beaked whale echolocation signals have energy concentrated in the 30-50 kHz band (Gillespie et al. 2009), with a peak at 44 kHz (Baumann-Pickering et al. 2013) (Figures 5 & 6). While Gervais' beaked whale signals are similar to those of Cuvier's and Blainville's beaked whales, the Gervais' beaked whale FM pulses are at a slightly higher frequency than those of the other two species. Similar to all beaked whales, Gervais' beaked whale FM pulses sweep up in frequency. The ICI for Gervais' beaked whale signals is typically around 0.28 s (Baumann-Pickering et al. 2013).

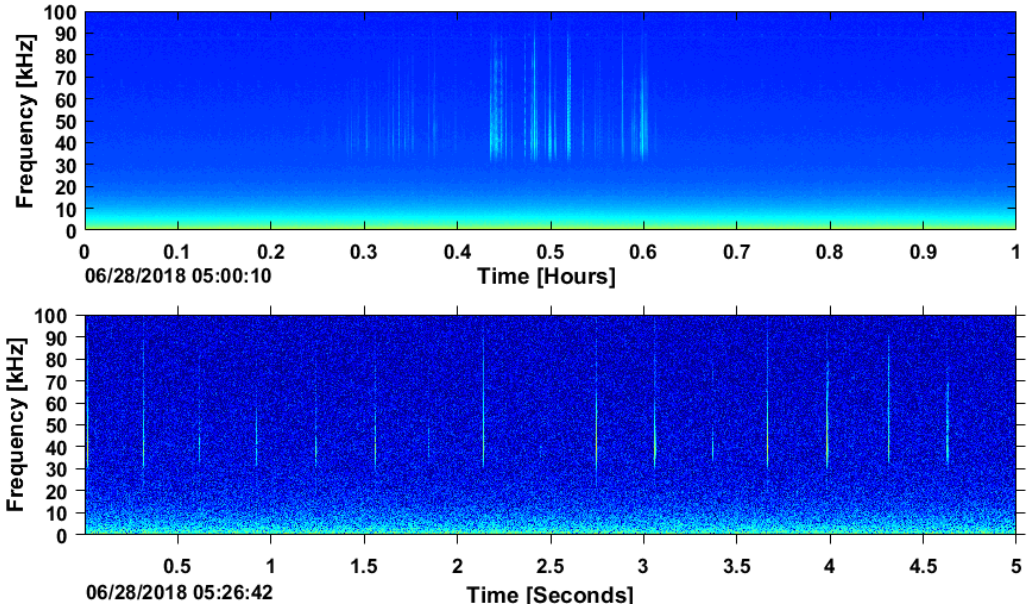


**Figure 5:** Gervais' beaked whale signal in LTSA (top) and spectrogram (bottom).

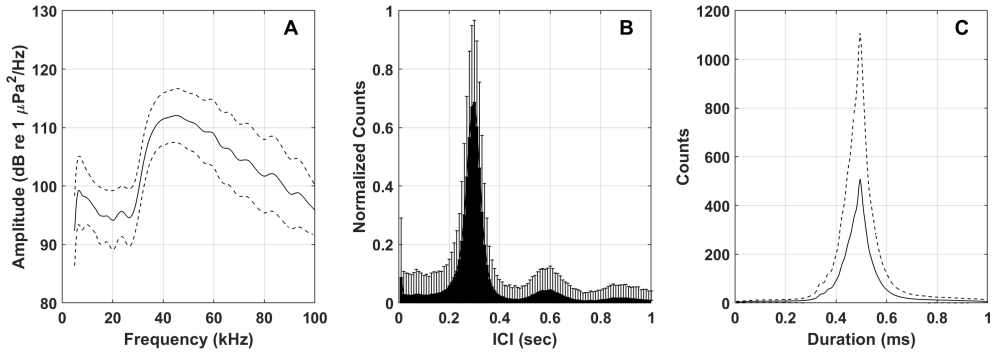


**Figure 6:** Left: Mean frequency spectrum of Gervais' beaked whale echolocation clicks (solid line) and 25th and 75th percentiles (dashed lines); Center: Inter-click interval distribution with peak near 0.3 s. Smaller peaks can occur at multiples of the main peak, and represent cases where a subset of clicks in a click train have been missed by the detector or classifier; Right: Mean waveform envelope of representative clicks.

### 3.2.3 Blainville's Beaked Whale

Blainville's beaked whale echolocation signals are, like most beaked whales' signals, poly-cyclic with a characteristic frequency-modulated upsweep, and are identifiable by a peak frequency around 34 kHz and uniform ICI of about 0.28 s (Johnson et al. 2004, Baumann-Pickering et al. 2013). Blainville's FM pulses are also distinguishable in the spectral domain by their sharp energy onset around 25 kHz with only a small energy peak at around 22 kHz (Figures 7 & 8).

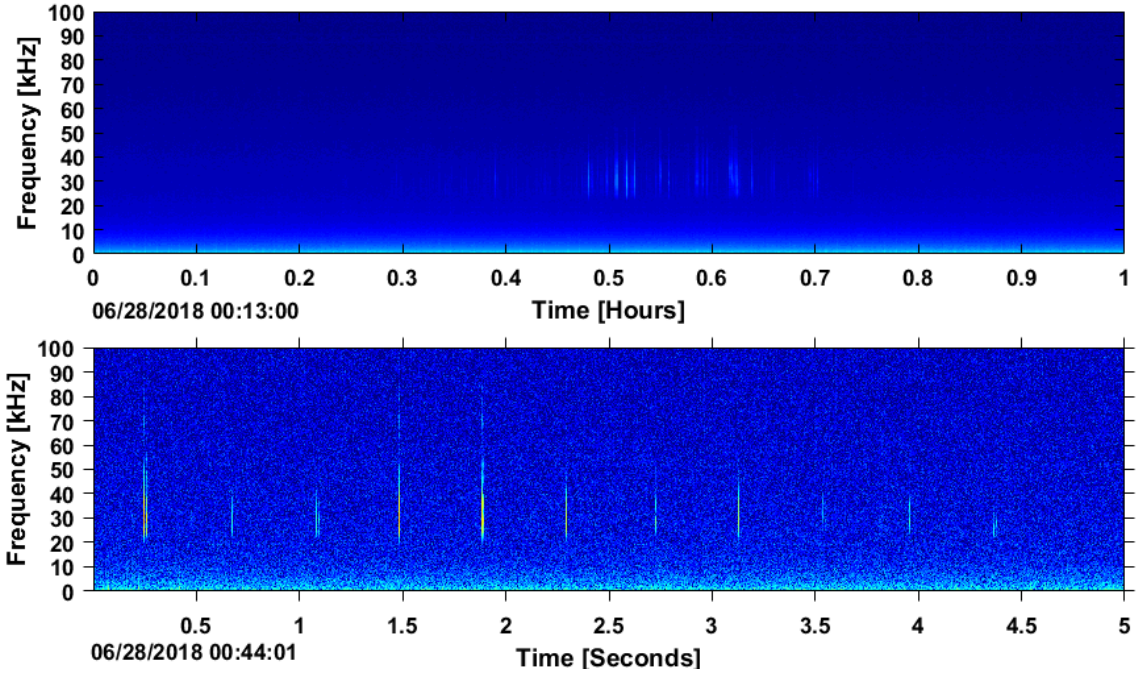


**Figure 7:** Blainville's beaked whale signal in LTSA (top) and spectrogram (bottom).

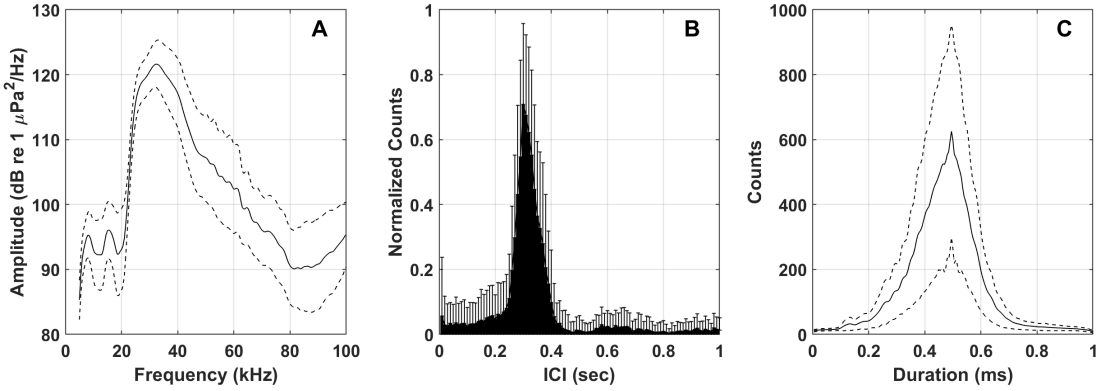


**Figure 8:** Left: Mean frequency spectrum of Blainville's beaked whale echolocation clicks (solid line) and 25th and 75th percentiles (dashed lines); Center: Inter-click interval distribution with peak near 0.3 s; Right: Mean waveform envelope of representative clicks.

### 3.2.4 Sperm Whales

Sperm whale clicks contain energy from 1-20 kHz, with the majority of energy between 10-15 kHz (Møhl et al. 2003) (Figures 9 & 10). With predominantly lower frequency energy, their echolocation clicks are highly distinguishable from those of other odontocetes. Regular clicks, observed during foraging dives, demonstrate an ICI from 0.25-2 s (Goold and Jones 1995, Madsen et al. 2002). Short bursts of closely spaced clicks called creaks are observed during foraging dives and are believed to indicate a predation attempt (Watwood et al. 2006). Effort was not expended to denote whether sperm whale detections were codas, creaks, regular or slow clicks, or to associate clicks with demographic groups (e.g. males vs. females, Solsona-Berga et al. 2022). Most sperm whale clicks in this dataset are likely produced by females and juveniles, as indicated by the relatively short modal ICI near 0.5 s.

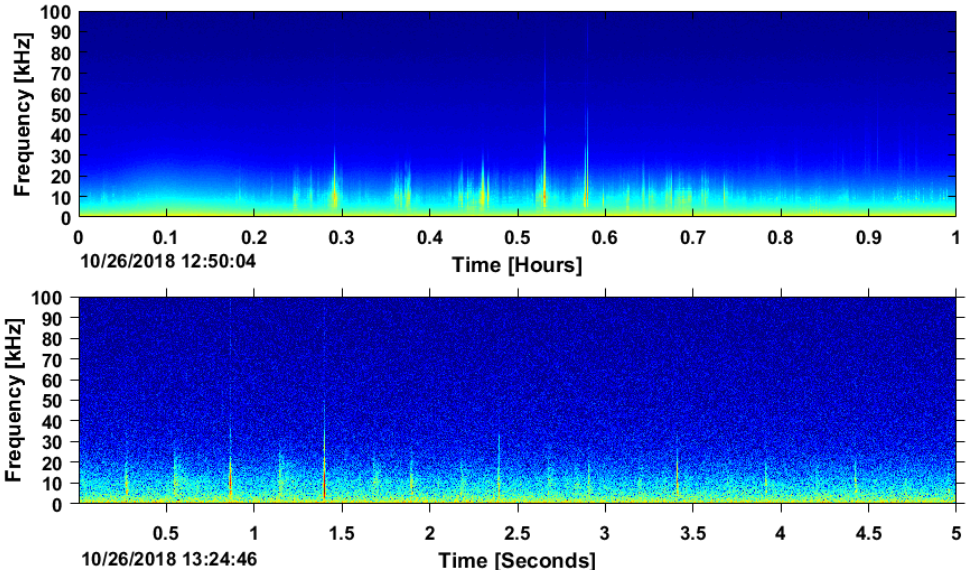


**Figure 9:** Sperm whale signals in LTSA (top) and spectrogram (bottom).

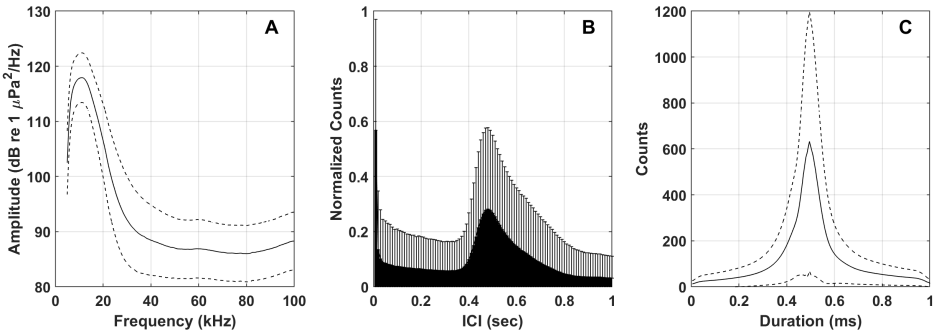


**Figure 10:** Left: Mean frequency spectrum of sperm whale echolocation clicks (solid line) and 25th and 75th percentiles (dashed lines); Center: Inter-click interval distribution with peak near 0.5 s; Right: Mean waveform envelope of representative clicks.

### 3.2.5 *Kogia* spp.

Dwarf and pygmy sperm whales emit echolocation signals which have peak energy at frequencies near 130 kHz (Au 1993). Their clicks can readily be distinguished from other species in the Gulf, but not from each other. While the peak frequency of these clicks is above the upper frequency band recorded by the HARP during these deployments, energy from *Kogia* clicks can be recorded within the 100 kHz HARP bandwidth (Figure 11). The observed signal may result both from the low-frequency tail of the *Kogia* echolocation click spectra, and from aliasing of energy from above the Nyquist frequency of 100 kHz (Figures 11 & 12). Typical modal ICIs for *Kogia* spp. are near 0.1 s.

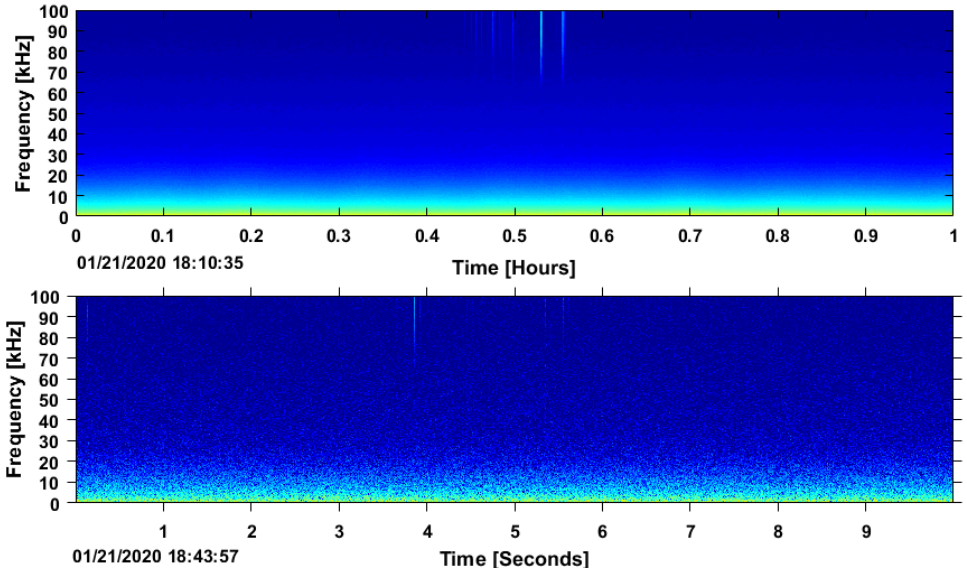


**Figure 11:** *Kogia* spp. signals in LTSA (top) and spectrogram (bottom).

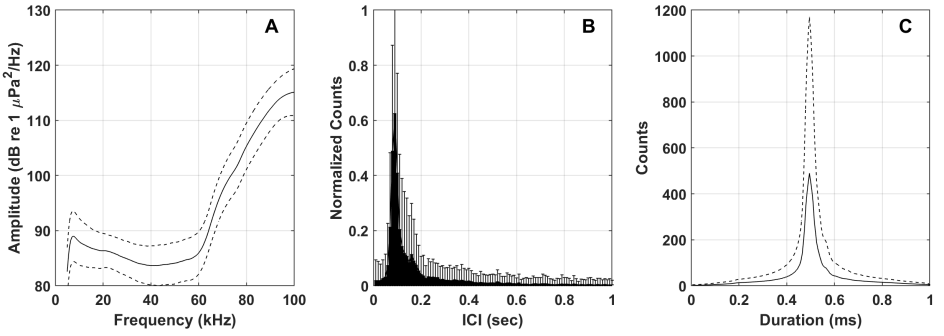


**Figure 12:** Left: Mean frequency spectrum of *Kogia* spp. echolocation clicks (solid line) and 25th and 75th percentiles (dashed lines); Center: Inter-click interval distribution with peak near 0.1 s; Right: Mean waveform envelope of representative clicks.

### 3.2.6 Risso's Dolphins

Risso's dolphin clicks (Figures 13 & 14) have frequency peaks at approximately 22, 26, and 33 kHz. These clicks have a modal ICI of approximately 0.15 seconds. Past studies have shown that spectral properties of Risso's dolphin clicks have slight variations with geographic region (Soldevilla et al. 2017), although the multiple sharp frequency peaks and average ICI found in the Gulf of Mexico are similar to what has been found elsewhere.

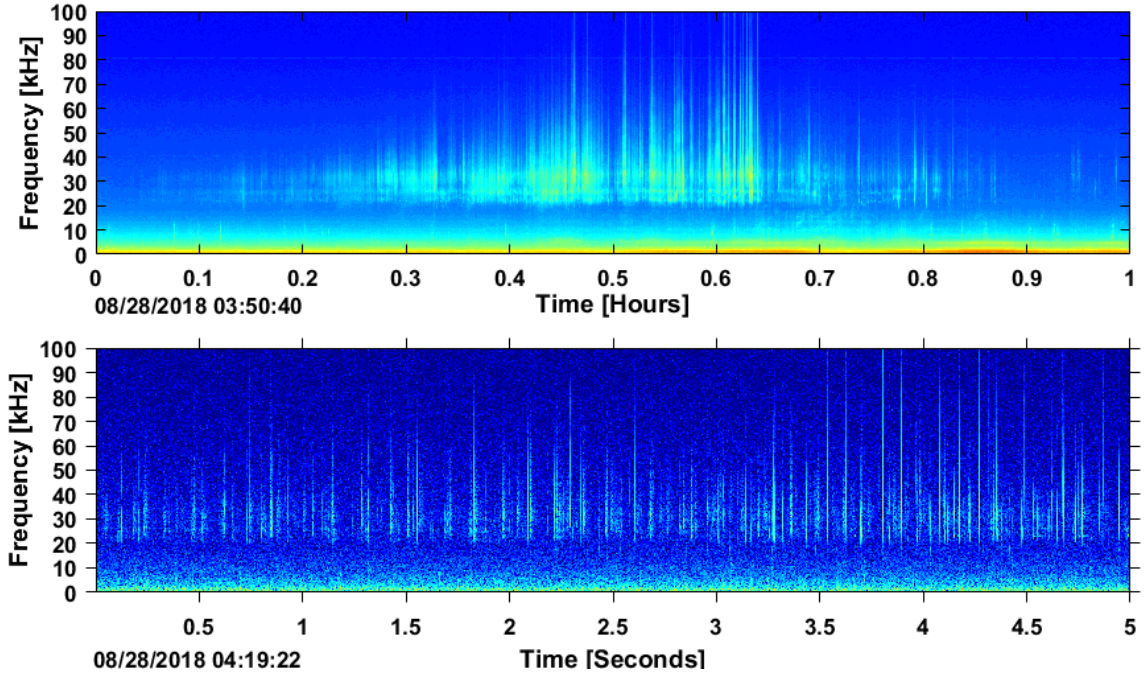


**Figure 13:** Risso's dolphins signals in LTSA (top) and spectrogram (bottom).

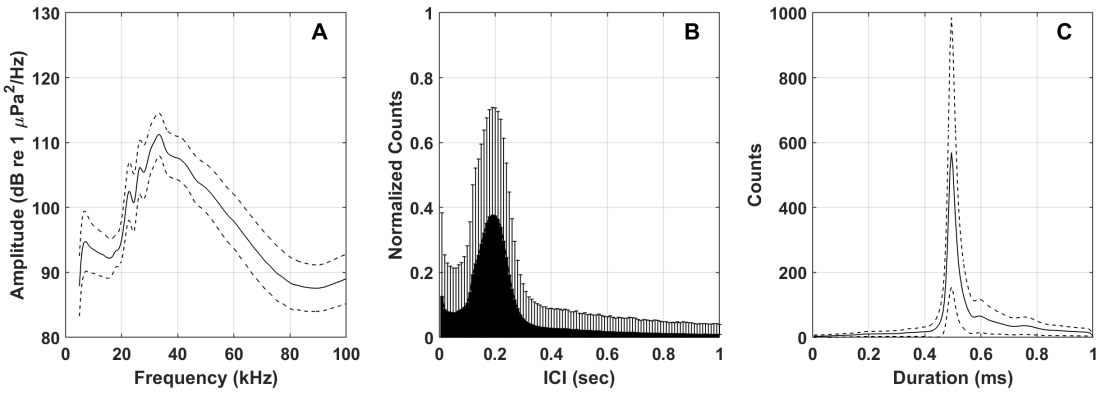


**Figure 14:** Left: Mean frequency spectrum of Risso's dolphins echolocation clicks (solid line) and 25th and 75th percentiles (dashed lines); Center: Inter-click interval distribution with peak near 0.2 s; Right: Mean waveform envelope of representative clicks.

### 3.2.7 Unidentified Dolphins: High-Frequency

High-frequency unidentified dolphins clicks (UD HF) were one of the dominant click types identified by the unsupervised cluster classification algorithm. They are distinctive, but have not previously been associated with a specific species. The majority of events in this grouping likely represents delphinids in the genus *Stenella*, primarily pantropical spotted dolphins (*Stenella attenuata*). Spinner dolphins (*Stenella longirostris*), Clymene dolphins (*Stenella clymene*), and striped dolphins (*Stenella coeruleoalba*) are also likely included, and their clicks may or may not be acoustically distinguishable from the dominant pantropical spotted dolphin (Frasier et al. 2017). Oceanic common bottlenose and Atlantic spotted dolphins (*Tursiops trucatus* and *Stenella frontalis*, respectively) may be included in this category. These two may be acoustically distinguishable from the other Stenella species based on observed differences between click spectral features and ICI at shallow sites (e.g., DC), where closely-related shelf populations of Atlantic spotted dolphins are presumed to be the dominant species, and deep sites, where oceanic Stenella species dominate. This distinction effort is in progress. It remains to be determined whether further distinctions are possible within this group. The majority of the UD HF clicks have peak frequencies between 30 and 45 kHz (Figures 15 & 16). Two peaks are visible in the ICI distribution. The dominant peak at 65 ms is likely associated with the Stenella category (primarily *S. attenuata*). The secondary peak at approximately 0.1 s is likely associated with offshore bottlenose dolphins. In the future, further analyses will be undertaken to refine this type into two or more click types and to reduce classification confusion between similar types.

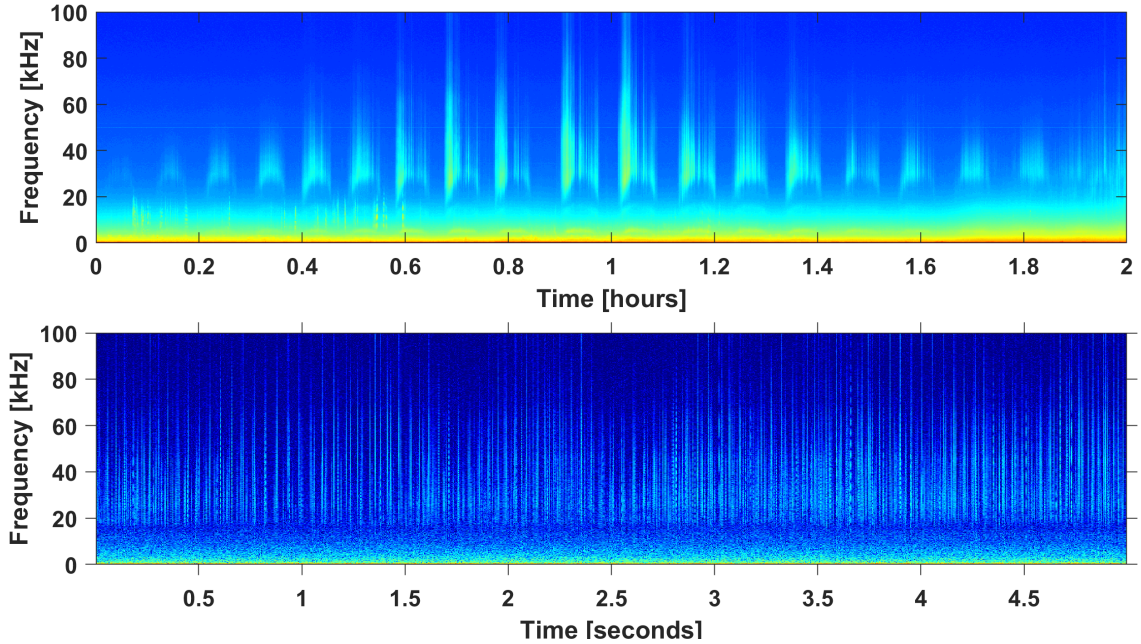


**Figure 15:** Unidentified dolphin high-frequency (UD HF) echolocation signals in LTSA (top) and spectrogram (bottom).

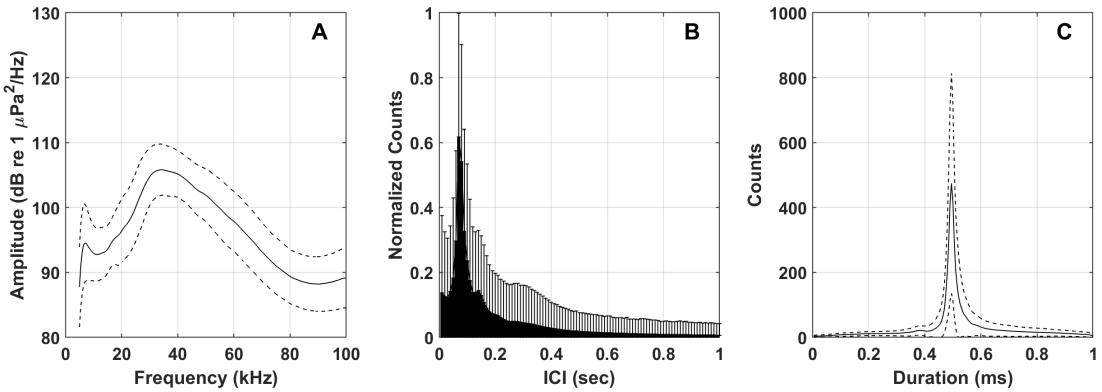


**Figure 16:** Left: Mean frequency spectrum of unidentified dolphin high-frequency (UD HF) echolocation clicks (solid line) and 25th and 75th percentiles (dashed lines); Center: Inter-click interval distribution with peak near 0.06 s; Right: Mean waveform envelope of representative clicks.

### 3.2.8 Unidentified Dolphins: Three-Peak

An unidentified dolphin click type with three distinct spectral peaks (UD 3P) was one of the dominant click types identified by the unsupervised cluster classification algorithm. The type is distinctive, but has not previously been associated with a specific species. UD 3P type clicks (Figures 17 & 18) have small spectral peaks at 13 and 19 kHz, with a large, broad energy peak between 30 and 50 kHz. These clicks have a modal ICI of approximately 0.1 s. In the future, further analysis will be required to refine unidentified click types and reduce classification confusion between similar types.

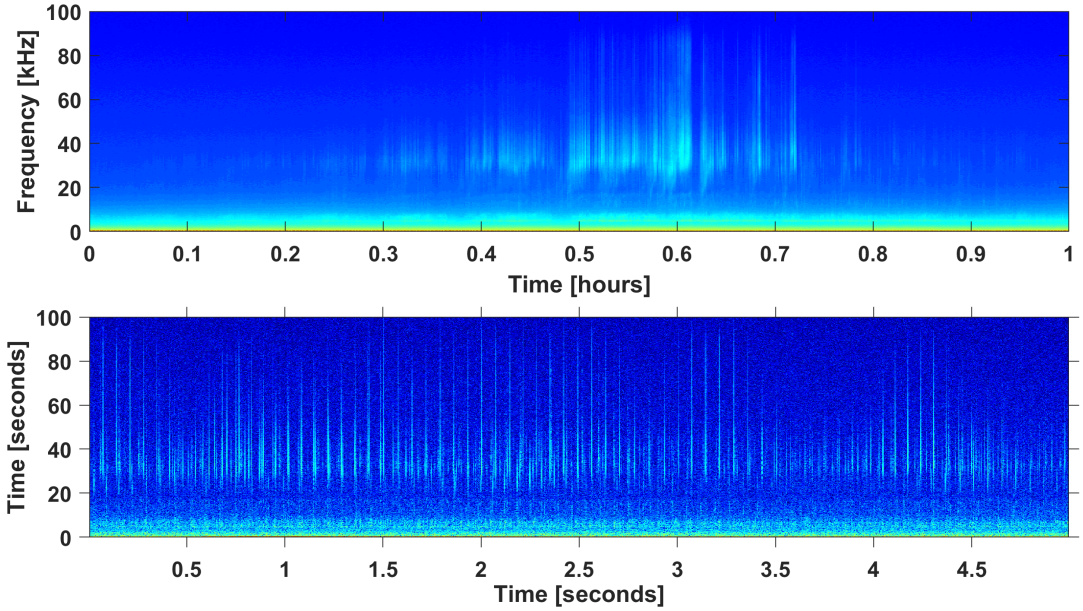


**Figure 17:** Unidentified dolphin three-peak (UD 3P) echolocation signals in LTSA (top) and spectrogram (bottom).

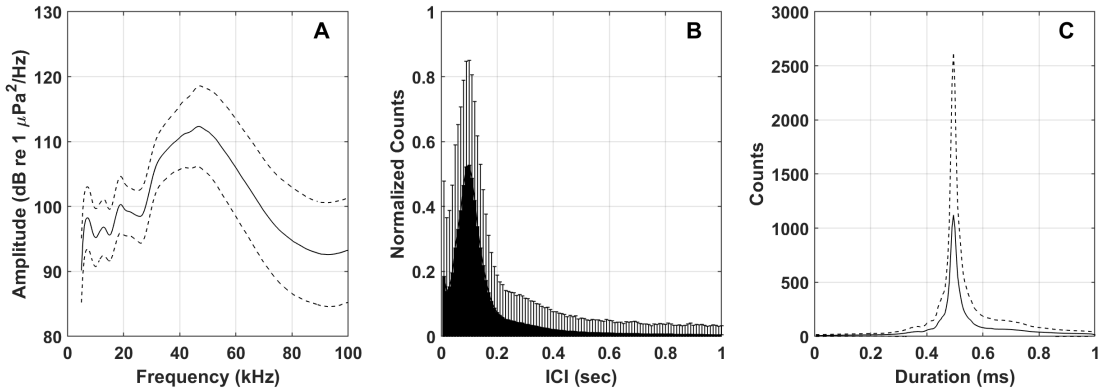


**Figure 18:** Left: Mean frequency spectrum of unidentified dolphin three-peak (UD 3P) echolocation clicks (solid line) and 25th and 75th percentiles (dashed lines); Center: Inter-click interval distribution with peak near 0.1 s; Right: Mean waveform envelope of representative clicks.

### 3.2.9 Unidentified Dolphins: Low-Frequency

A low frequency delphinid echolocation click category (UD LF) was another dominant click category identified by the unsupervised clustering algorithm. This category likely represents some of the large delphinid species including short finned pilot whale (*Globicephala macrorhynchus*; Cohen et al. 2022), melon-headed whale (*Peponocephala electra*), false killer whale (*Pseudorca crassidens*), and killer whale (*Orcinus orca*; Leu et al. 2022 ). UD LF type clicks (Figures 19 & 20) are characterized by a peak frequency below 30 kHz and a variable modal ICI near 0.2 s. This is a diverse category, and further analyses currently in progress are likely to result in the identification of multiple subtypes which may be attributable to individual species.

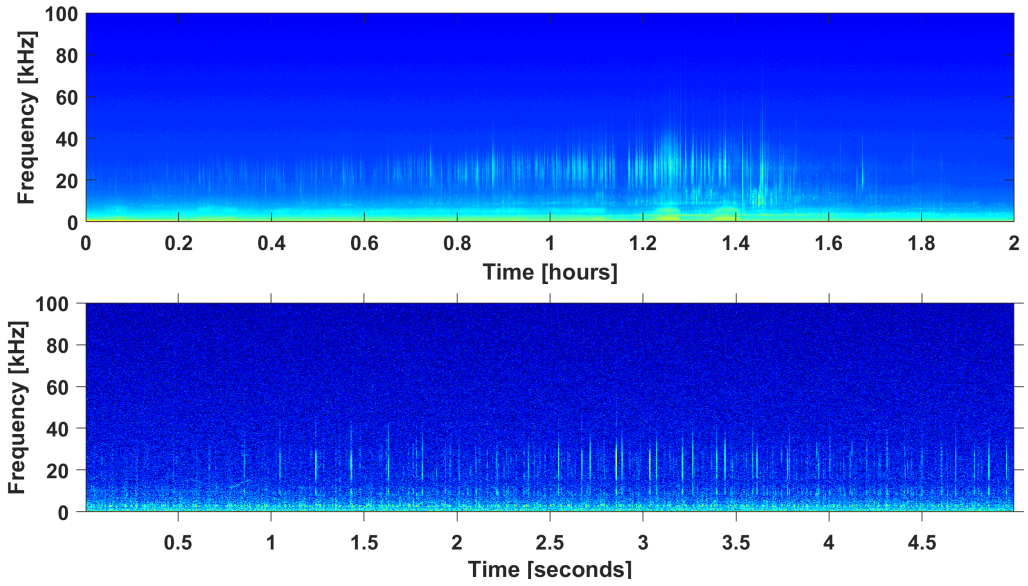


**Figure 19:** Unidentified dolphin low-frequency (UD LF) echolocation signals in LTSA (top) and spectrogram (bottom).

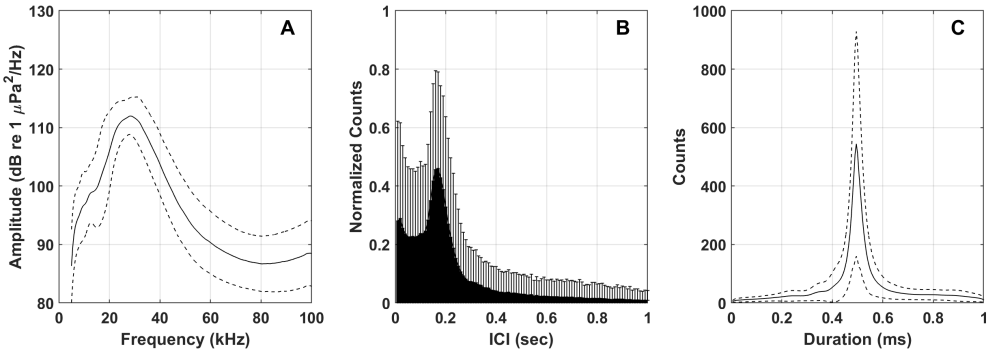


**Figure 20:** Left: Mean frequency spectrum unidentified dolphin low-frequency (UD LF) echolocation clicks (solid line) and 25th and 75th percentiles (dashed lines); Center: Inter-click interval distribution with peak near 0.18 s; Right: Mean waveform envelope of representative clicks.

## 3.3 Mysticete Whale Analyses

Analyses focused on calls of the Rice's whale, the only resident baleen whale found in the GOM, required only the low-frequency data for these analyses. The HARP recordings were decimated by factors of 100 and 10 for 200 kHz and 20 kHz data, respectively, to yield 2000 Hz data with an effective bandwidth of 10 to 1000 Hz. While low-frequency call detection effort was focused on Rice's whale calls, rare opportunistic detections of other baleen whale species were noted when they occurred, as were sounds of unknown origin that could potentially be produced by baleen whales.

## 3.4 Mysticete Whale Species Call Descriptions

In the Gulf of Mexico, three call types have been identified and attributed to free-ranging Rice's whales (Rice et al. 2014, Širović et al. 2014, Soldevilla et al. 2022a), and one additional call type has been proposed as a likely candidate (Širović et al. 2014; Figure 21).

### 3.4.1 Pulsed Calls

Rice's whales produce downsweep pulse sequence calls made up of a series of two or more short-duration downsweeps (mean: 8 downsweeps, range: 2-25) ranging from 110 ± 4 to 78 ± 7 Hz, with a mean duration of 0.4 ± 0.1 s, an inter-pulse interval of 1.3 ± 0.1 s, and source levels of 155 ± 14 dB re: 1 µPa at 1 m (Rice et al. 2014, Širović et al. 2014, Soldevilla et al. 2022a). A second downsweep call type, higher in frequency (170 to 110 Hz), segmented, and typically occurring in repeated sequences of doublets, also has been detected in autonomous recordings and is proposed to be a possible Rice's whale call (Širović et al. 2014).

### 3.4.2 Tonal Calls

Rice's whales produce two tonal call types: long-moan calls and tonal-sequence calls (Rice et al. 2014, Soldevilla et al. 2022a). The long-moan call type is a long-duration, amplitude-modulated downsweep ranging from 150 to 75 Hz with a mean center frequency of 107 Hz, mean 22.2 s duration, and 3.4 pulse/s amplitude pulse rate (Rice et al. 2014, Soldevilla et al. 2022a). Stereotyped variants of the long moan are common in the western Gulf and are occasionally detected in the core habitat as well (Soldevilla et al. 2022b). The second tonal call type, the tonal-sequence, consists of 1-6 narrow-band constant-frequency tones in sequence following some long-moans, with individual tonals having a mean center frequency of 103 Hz and mean 3.6 s duration (Rice et al. 2014).

### 3.4.3 Rice's Whale Automated Call Detectors

Spectrogram cross-correlation detectors for Rice's whale long-moan calls and downsweep pulse sequences were developed in Ishmael (Version 1.0; Mellinger and Clark 2000) using a two-day training dataset and a separate testing dataset to characterize miss rates and false detection rates (Soldevilla et al. 2022b). For all analyses, spectrograms were calculated using an FFT frame size of 512 samples, no zero-padding, 50% overlap, and spectrogram equalization with 3 s spectral averaging.

### 3.4.4 Long-Moan Detector Settings

Eastern long-moan call contours contain five sections which include the preliminary upsweep, the approximately 150 Hz tone, the first part of the downsweep (slope 1), the second part of the downsweep (slope 2), and the long nearly-constant-frequency tail (Figure 3). The cross-correlation contour kernel for the long-moan call focused on the 150 Hz tone and slope 1, the most consistent parts of the frequency-modulated tonal call. The kernel contour is defined by a 1.1 s tone from 146 Hz to 145 Hz followed by a 3.7 s downsweep from 145 Hz to 112 Hz, each with a 14 Hz contour bandwidth. Detection function smoothing was enabled. The detection threshold was set to 4.5, and minimum and maximum detection durations were 0.5 s and 3.0 s, respectively. The minimum time allowed between subsequent detection events was 0.5 s. The threshold of 4.5, yielding a 6.4% missed call rate and a 26.4% false detection rate on a test dataset, was selected to minimize miss rates without excessive false detection rates. Missed detections were typically associated with calls with low signal to noise ratios. The majority of false alarms were associated with disk write noise from the recording instrument and tonal sounds from passing ships. While this detector was developed on eastern long-moan calls, it is also effective at detecting western long-moan variants since the 150 Hz tone component is consistent across all long-moan types. A subsequent manual review step further reduces the false detection rate (see Validation of Automated Call Detections) .

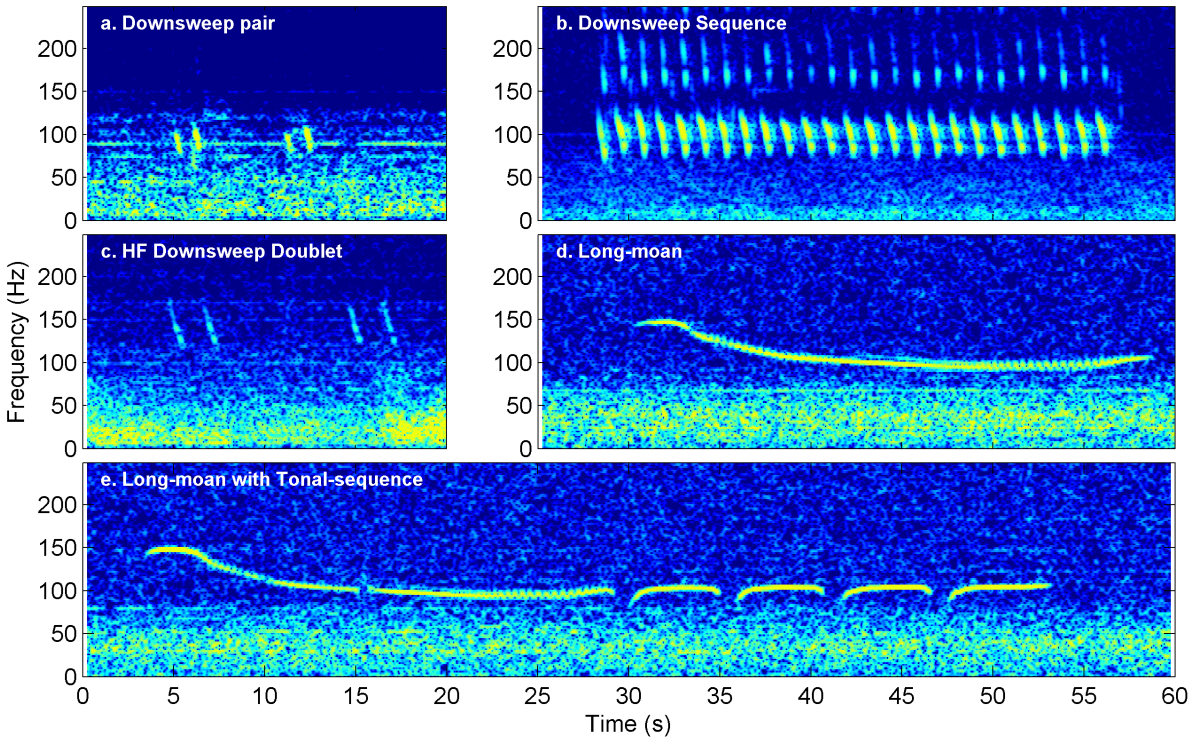


**Figure 21:** Spectrograms of stereotyped Rice's whale calls from northeastern Gulf of Mexico.

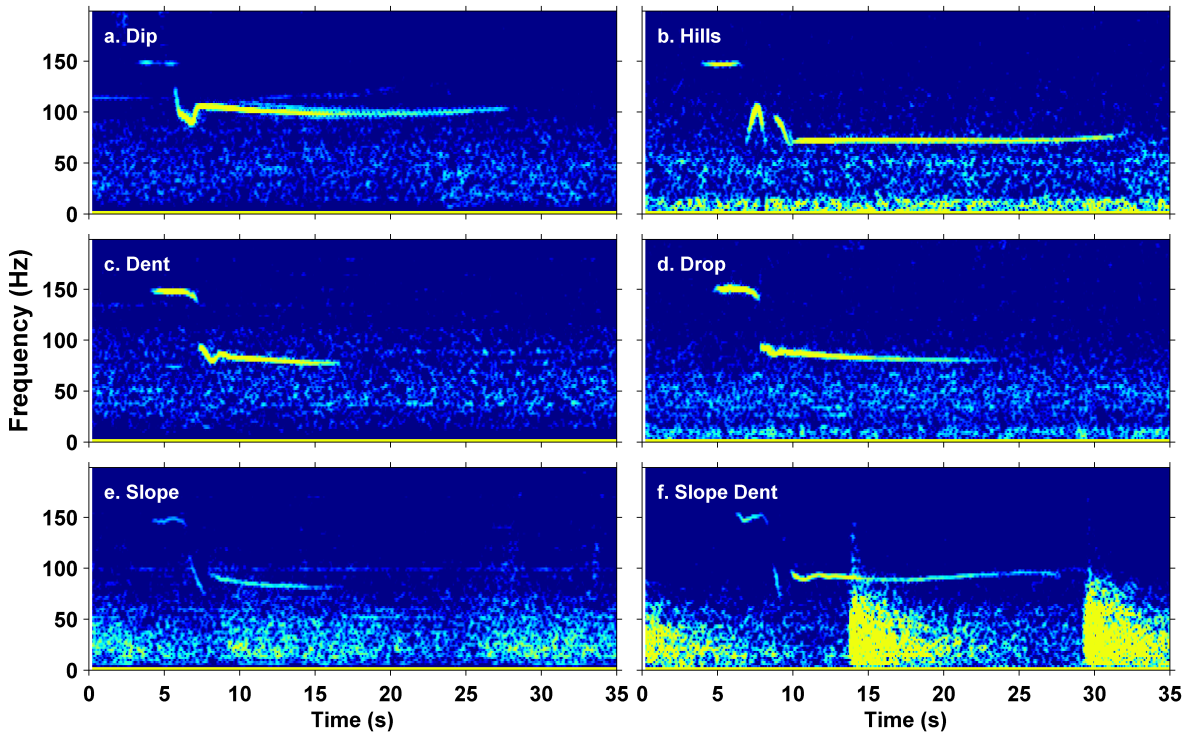


**Figure 22:** Spectrograms of stereotyped Rice's whale calls from northwestern Gulf of Mexico.

### 3.4.5 Downsweep Pulse Sequence Detector Settings

The *Ishmael* downsweep pulse sequence detector used the regular sequence feature to detect sequences of individual downsweep pulses as a single call. The cross-correlation contour kernel was defined as a single 0.4 s downsweep from 120 Hz to 80 Hz, with a 20 Hz contour bandwidth. For regular sequences, the minimum and maximum repetition period between individual pulse detections were set to 0.9 s and 1.1 s, respectively, and an 11 s window with 75% overlap was used. The detection threshold was set to 11, and minimum and maximum detection durations were set to 0.1 s and 40 s, respectively. The minimum time allowed between detection events was 0.4 s. The threshold of 11, yielding a 12.6% missed sequences rate and a 69.1% false detection rate on a test dataset, was selected to minimize miss rates without excessive false detection rates. Missed detections were typically associated with calls with low signal to noise ratios. The majority of false alarms were associated with long-moan calls with strongly pulsed tails and seismic survey airgun pulses with unusually short inter-pulse intervals or strong multipath effects.

### 3.4.6 Validation of Automated Call Detections

Given the critically endangered status of Rice's whales, automated detector thresholds were intentionally set to minimize missed detections at the cost of increased false positive detections, rather than selecting a threshold with equal miss and false alarm rates. The threshold selections aimed to reduce missed detections as much as possible while balancing the need to keep false detections within a reasonable number. Therefore, these preliminary detections require a follow-up step to manually validate and remove all false detections for a final dataset. This semi-automated process is both more efficient and consistent than a complete manual detection process and more accurate than a fully automated process. In the validation step, each automated detection is manually reviewed and scored as a true or false detection, and false positive rates are calculated as the percentage of false positives to total detections.

## 3.5 Other Noise Source Descriptions

In addition to odontocete echolocation clicks, other noise sources are commonly detected by the automated click detection algorithm. A description of the signal features of these common noise sources follows. The automated neural network classifiers of odontocete clicks were trained on these categories to avoid misclassification as marine mammal signals.

### 3.5.1 Ship Noise

Broadband ship sound occurs when a ship passes within a few kilometers of the hydrophone. Ship sound can occur for many hours at a time, but broadband ship sound typically lasts from 10 minutes up to 3 hours. Noise can extend above 10 kHz, although sound levels typically decrease rapidly above a few kHz (Figure 23). Impulsive signals generated during vessel propulsion can be confused with sperm whale echolocation clicks, therefore a ship noise category representing the noise energy above 5 kHz is included in the click classifier (24).

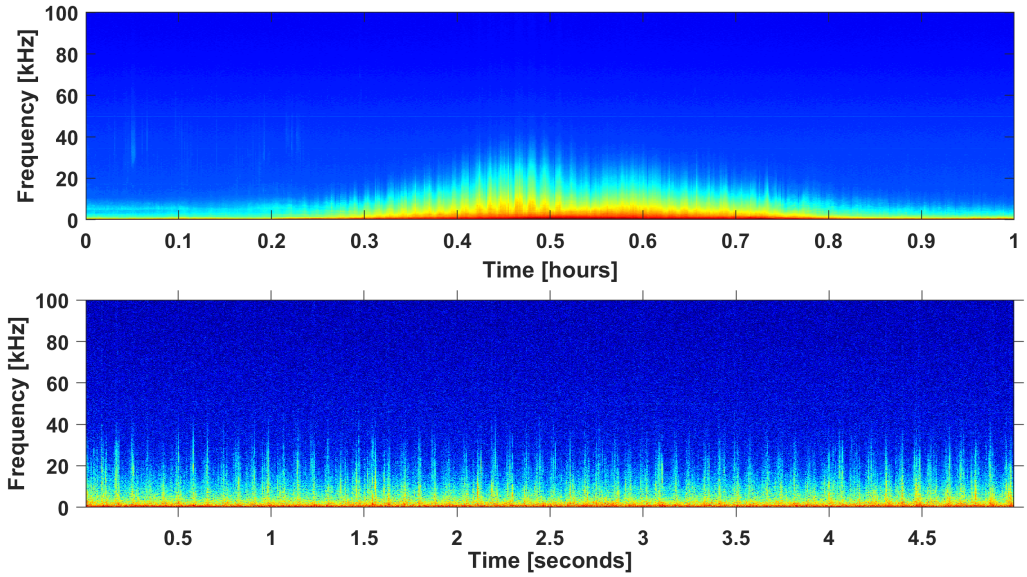


**Figure 23:** Broadband ship signals in LTSA (top) and spectrogram (bottom).

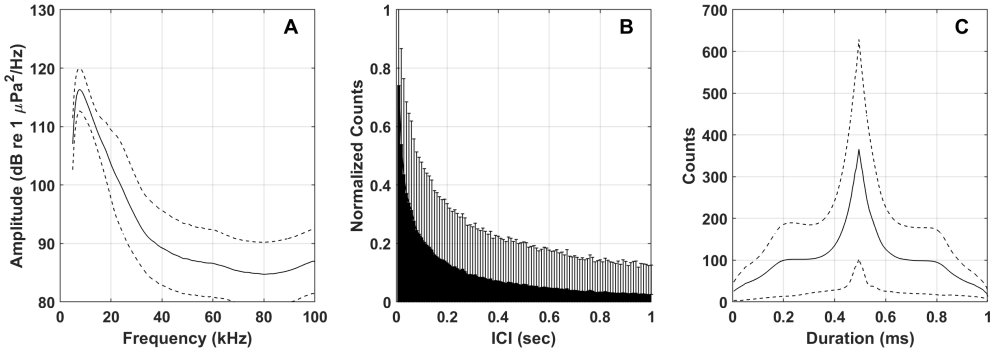


**Figure 24:** Left: Mean frequency spectrum of broadband ship noise (solid line) and 25th and 75th percentiles (dashed lines) as represented for the click classification step; Center: Inter-detection interval distribution; Right: Mean waveform envelope of representative signals. Note that this representation of ship noise is used in the context of the echolocation click classification process. Therefore, it is band passed to exclude frequencies below 5 kHz.

### 3.5.2 Noise - High and Low Frequency

Noise is a general category used to recognize and classify occasional and unusual signals, often within a particular dataset. Sources may include mooring noise generated during high current events, recording system noise, and other short, broadband signals that might be mistaken for echolocation. These signals are therefore included as a class within the click classifier (25).

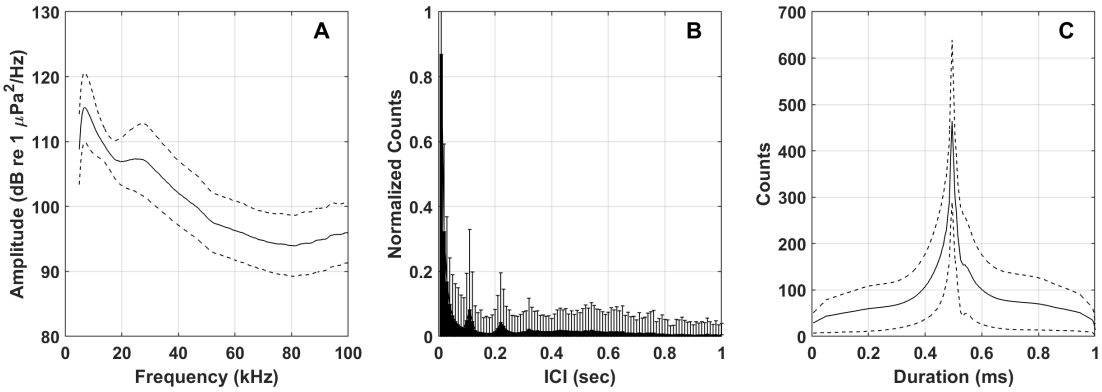


**Figure 25:** Left: Mean frequency spectrum of noise (solid line) and 25th and 75th percentiles (dashed lines); Center: Inter-detection interval distribution; Right: Mean waveform envelope of representative signals. Note that this representation of noise is used in the context of the echolocation click classification process. Therefore, it is band passed to exclude frequencies below 5 kHz.

### 3.5.3 Sonar

The sonar category consists of three types of sonar: mid-frequency, high-frequency, and echosounders. Sounds from mid-frequency active (MFA) sonar vary in frequency (1–10 kHz) and are composed of pulses of both frequency modulated (FM) sweeps and continuous wave (CW) tones (Henderson et al. 2022). High-frequency active (HFA) sonar is used for specialty military and commercial applications including high-resolution seafloor mapping, short-range communications, such as with Autonomous Underwater Vehicles (AUVs), multi-beam fath-ometers, and submarine navigation (Cox 2004). Echosounders are used by many varieties of commercial and private vessels and vary in frequency from 5-75 kHz (e.g., 26). This category was included when classifying impulsive signals at all sites (27).

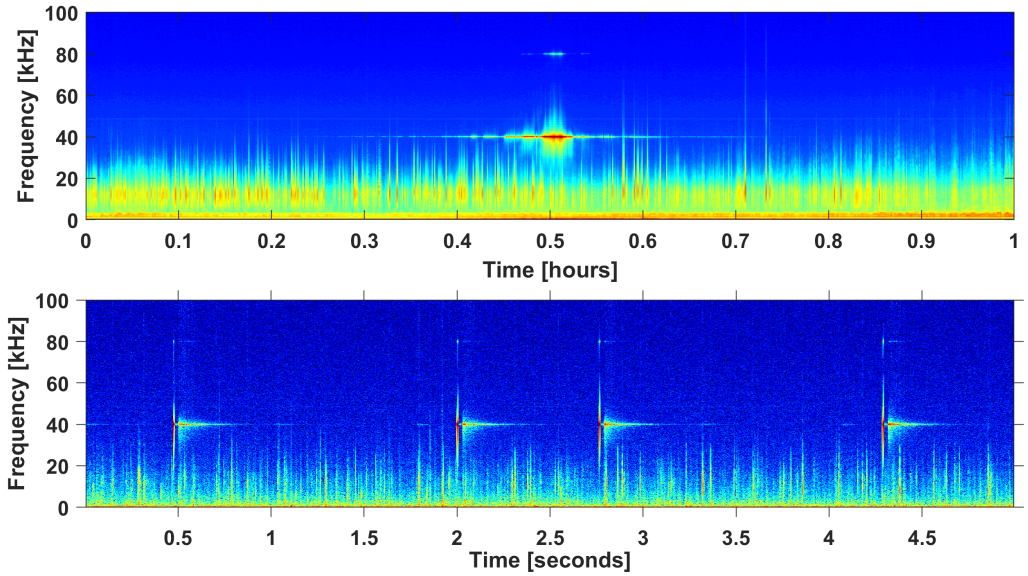


**Figure 26:** Echosounder signals (40 kHz) in LTSA (top) and spectrogram (bottom). This example image also includes sperm whale echolocation clicks.

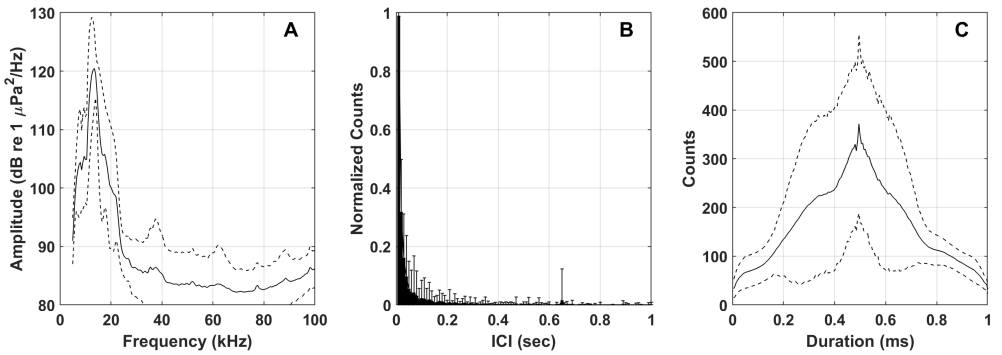


**Figure 27:** Left: Mean frequency spectrum of sonar (solid line) and 25th and 75th percentiles (dashed lines); Center: Inter-detection interval distribution; Right: Mean waveform envelope of representative signals.

## 3.6 Ambient and Anthropogenic Noise Analyses

Analyses of ambient noise levels provide information on the natural and anthropogenic contributions of noise sources and how they vary over time and space. Hourly long-term spectrograms were produced at each site to document ambient noise levels over time. The statistical distributions of ambient noise curves and third-octave and octave band sound levels were computed for the low-frequency band.

Several anthropogenic sound sources that are prolific in the Gulf of Mexico may be of interest for the noise reduction restoration project. The previously described noise classes were included in the odontocete signal analyses only to reduce misclassification errors for marine mammal detections. Additional automated detectors, described below, were developed specifically to document the occurrence of anthropogenic noise sources of interest, including: broadband ship noise, explosions, airguns, and echosounders. The start and end of each individual sound or the overall acoustic event was logged and their durations were summed to estimate cumulative hours present per week.

At the two noise-restoration-project shipping noise monitoring sites (GA and SL), additional analyses were conducted to estimate the source levels of commercial vessels transiting directly over the HARPs (those with a Closest Point of Approach (CPA) <= 200 m). Radiated noise levels and monopole source levels for identified cargo ships, tug-tows, tankers, cruise ships and a number of other vessels were developed during these analyses.

### 3.6.1 Ambient Noise Levels

Long-term spectrograms and ambient noise curves were estimated from the following methods from Wiggins et al. 2016 at three different resolutions:

- Low frequency, factor of 100 decimated data, 10 Hz-1 kHz in 1 Hz bins.
- Mid frequency, factor of 20 decimated data, 10 Hz-5 kHz in 10 Hz bins.
- Full frequency, 10 Hz-100 kHz in 100 Hz bins.

In each case, consecutive, five-s waveforms were transformed into sequential sound pressure spectral density estimates with 1 Hz bin resolution using the Welch method (Welch 1967). During recording, HARPs write sequential 75 s acoustic records to standard laptop-style computer hard disk drives such that there were 15 five-s spectra for each 75 s acoustic record. However, system self-noise can be present when the HARP is writing to disk (12 s out of each 75 s record), so the first three five-s spectra were not used for the following soundscape analyses. Statistical distributions of the noise spectra were computed per hour and per day after discarding partial days and days with deployment/recovery ships sounds or with known instrument self-noise problems. These distributions were calculated with custom MATLAB-based software to provide hourly and daily average and percentile sound pressure spectrum levels for all sites over the deployment periods in addition to long-term spectrograms. For conciseness, this report focuses on the low frequency output, which is most indicative of an-

thropogenic noise sources.

### 3.6.2 Broadband Ships

Broadband ship noise, from sources including the engine, propeller, and cavitation, occurs in the 30 Hz to 10 kHz or higher frequency range when a ship passes within a few kilometers of the hydrophone. At lower frequencies, particularly in the 30-150 Hz band, noise from more distant global shipping can occur near-continuously. While elevated low-frequency noise levels from distant ships can occur for many hours at a time, broadband ship noise during closer approaches typically lasts from 10 minutes up to 3 hours. Ship noise has a characteristic frequency-range-dependent pattern of constructive and destructive interference (bright and dark bands) in the LTSA due to the combination of direct and surface reflected sound paths (Figure 28; McKenna et al. 2012). Noise can extend above 10 kHz when vessels are very close to the recorders, while sound levels typically decrease rapidly above a few kHz. To determine the contribution of shipping noise to the soundscape at the Gulf of Mexico HARP sites between 2020-2023, and to determine the ship types that transit near each recording location, a combination of (1) automated ship detections in the HARP acoustic recordings and (2) Automatic Identification System (AIS) data were used. The AIS data, obtained from Marine Cadastre, included ship information such as MMSI, vessel name, vessel type, vessel size, time and position at the time of each detection, and other vessel specifics. These data were used to examine ship types commonly found within 15 km of the deployed HARPs and the distances at which the ships passed each site (up to 15 km).

To analyze the HARP acoustic data for ship noise, a modified version of the custom ship detector in Matlab-based software Triton (github.com/MarineBioAcousticsRC/Triton/wiki /ShipDetector) was used. The detector identifies shipping events within LTSAs by examining power spectral density estimates in three user-defined frequency bands. Events meeting three conditions based on amplitude above a threshold and duration are logged as a ship passage. The original ship detector was designed to run on full bandwidth LTSAs to prevent misclassification of ship noise at sperm whale frequencies (1-10 kHz) as sperm whale clicks during odontocete detection and classification analyses. This detector was modified to meet the current objective of detecting all close approaches of ships (within 15 km) over the full bandwidth of shipping noise (30 Hz to 10 kHz). To meet these objectives, the original ship detector was modified to: 1) use the higher-resolution mid-frequency band LTSAs, 2) extend the three user-defined frequency bands to frequencies below 5 kHz, and 3) expand the 1-step detector to a 2-step detector to enhance detection of both ships with only low-frequency energy content and those with broader band energy. The frequencies for the three user-defined frequency bands were chosen to maximize the detection of shipping noise while minimizing the detection of airgun surveys. In general, for the first-step parameters, the low-frequency band ranged from 100-250 Hz or 300-850 Hz, the mid-frequency band from 250-500 Hz or 850-3000 Hz, and the high-frequency band from 500-1000 Hz or 3000-5000 Hz. For the second-step parameters, the low-frequency band ranged from either 300-850 Hz (site DC only) or 100-500 Hz, the mid-frequency band from 850-3000 Hz (site DC only) or 500-1000 Hz, and

the high-frequency band from 3000-5000 Hz. At each site, optimal settings were selected by comparing detector results with manual ship detections in a subset of data.

After running the ship detector with the optimal settings, the Evaluation Interface in the ship sound detector Triton Remora was used to review the detector output and correct false detections as needed. The detector's performance was assessed by calculating precision and recall rates using the results of a manual review of 5% of each HARP dataset that was randomly selected. A quality score was given to the manual detections based on signal quality, with "1" representing a ship that would likely be detected (higher SNR), "2" a ship that possibly would be detected, and "3" a ship that would unlikely be detected (low SNR, representing more distant ships). When calculating precision and recall rates, true positives were ships detected both automatically and manually, missed calls were ships detected manually (quality scores 1 and 2 only) but not automatically, and false positives were detections made automatically that were not ships. These precision and recall values were high across sites, indicating the ship detector performed well at most sites (Figure 29).

Broadband received levels (RLs), between 10-5000 Hz, were calculated for both ships detected automatically and those identified by AIS. To calculate broadband RL, data for the duration of each ship detection were divided into one-second bins and a Fast Fourier Transform (FFT) was applied to provide a frequency bin resolution of 1 Hz. Airgun pulses were removed from the data by using a 50% sliding window over 20 seconds of data at a time and removing mean noise levels (one second at a time) between 20-60 Hz that were above a specified threshold (presumed to be airgun pulses). Broadband RLs were then calculated using the remaining data for each one-minute time bin, as the summed band level over the 10-5000 Hz band. For ships detected automatically, the maximum broadband RL during the duration of the detection is reported as the RL at CPA. For ships identified by AIS, the broadband RL in the minute bin from 30 seconds before to 30 seconds after the CPA is reported.

To better understand received ship levels with respect to ship type, distance, speed, and other characteristics, and to understand the frequency of occurrence of shipping noise from vessels not equipped with AIS, automated ship detections were linked to associated ship tracks in the AIS data. Shipping data results are presented at each site as the number of acoustic detections of passing ships, the daily duration of vessel noise presence, the broadband RLs of the ships detected automatically as well as those identified by AIS, the daily number of AIS-equipped ships passing nearby, and the annual percentage of ships per ship type passing nearby. Multiple ship passings close in time are typically detected as a single detection; therefore, ship detection results represent a minimum number.

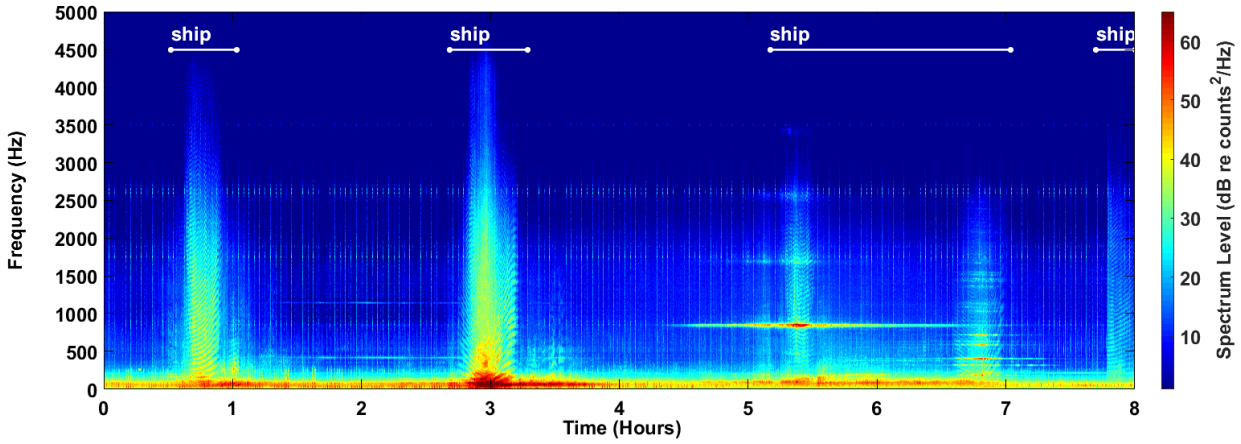


**Figure 28:** Example of ship detections made over an 8-hr period with the customized ship sound detector. Note the presence of tonal sound associated with the 3rd ship, as well as the merging of the 3rd and 4th ship transits into one detection.

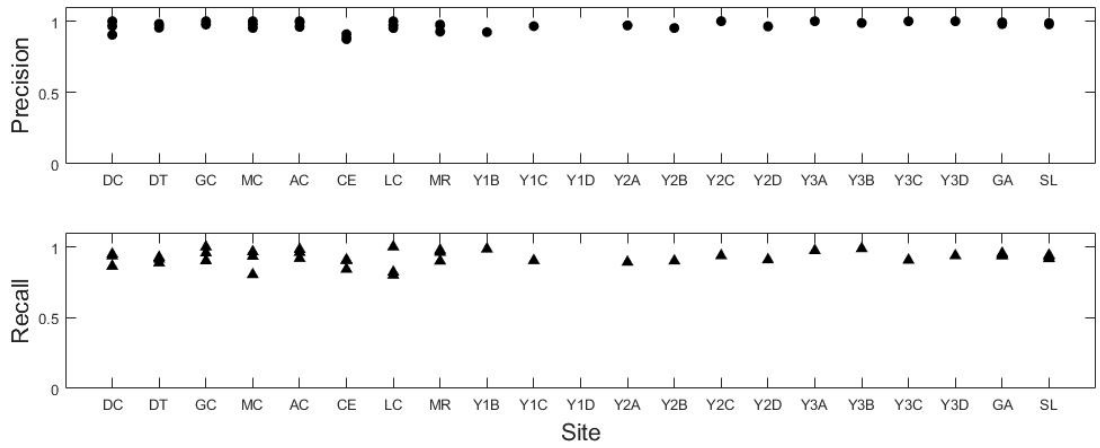


**Figure 29:** Automated ship noise detector performance (precision and recall) based on manual review of 5% of the data recorded at HARP locations between 2020-2023.

### 3.6.3 Ship Radiated Noise Levels and Monopole Source Levels

Radiated Noise Levels (RNL) were calculated based on ASA/ANSI (2009) and ISO (2019) specifications. Monopole Source Levels (MSL), correcting for the effect of Lloyd's mirror, were estimated using the approach of Gassmann et al 2017. Both sound levels, RNL and MSL, were estimated for one-third-octave bands from 10 Hz to 4 kHz. Each vessel transit recording was divided into non-overlapping segments with a duration of 1 s. A 10,000-point (NFFT) Fast Fourier Transform (FFT) was applied to each 1-second segment to provide a frequency bin resolution of 1 Hz. The magnitude of the FFT squared was multiplied by $2/\text{NFFT}^2$ to correct for the processing gain of the FFT. Over the duration of the transit, the mean sound pressure level (SPL) was computed over each 5-s segment every 3 s to smooth the time-frequency distribution. The resulting SPLs were reported in decibels (dB) summed from 5 to 1000 Hz with a reference pressure of 1 $\mu$Pa$^2$, and at 1 Hz and third-octave band resolution with a reference pressure of 1 $\mu$Pa$^2$/Hz. To estimate RNL, a spherical spreading propagation loss model ($N_{SS}$) was calculated with the following equation:

$$N_{SS} = 20log_{10}(R/r_0) \tag{2}$$

where R is the distance from the dipole source to the receiver and $r_0$ is the reference distance (1 m). The $N_{SS}$ used to compute RNL does not require a source depth ($d_S$), therefore the $d_S$ is assumed to be the dipole source for all transits. The $N_{SS}$ was applied to the SPL to achieve RNL (3).

$$RNL = SPL + N_{SS} \tag{3}$$

A propagation loss model that corrects for the Lloyd's mirror effect ($N_{PL}$) was applied to estimate MSL to account for reflected image interference at the sea surface and for compliance with ISO (2019, Equation 4). The $N_{PL}$ model ignores sound refraction in the water column and reflections with the seafloor and solely accounts for reflections from the sea surface (Gassmann et al. 2017; Audoly and Meyer 2017). The propagation loss of a sound source near the surface in deep water considering the Lloyd's mirror effect is given by:

$$N_{PL} = -20log_{10}\left(r_0\left|\frac{e^{ijkr_1}}{r_1} - \frac{e^{ijkr_2}}{r_2}\right|\right) \tag{4}$$

$$MSL = SPL + N_{PL} \tag{5}$$

where $r_1$ is the distance from the source to the receiver, $r_2$ is the distance from the reflected image source to the receiver, and k is the wave number ($k = 2\pi f/c$) in rad/m. Source depth was taken to be equal to 50% of the actual vessel draft. Harmonic mean sound speeds were calculated from depth, temperature, and salinity data obtained from the Global Ocean Forecasting System (GOFS) 3.1: 41-layer HYCOM + NCODA Global 1/12$^o$ analysis.

A modification of the Lloyd's mirror model was established in Gassmann et al. (2017) to remove mismatched interference lobes identified with ship noise measurements in compliance with ANSI/ASA (2009) and ISO (2016). The modification includes using the Lloyd's mirror model from 5 Hz up to the lowest frequency at which the Lloyd's mirror model and the spherical spreading model intersect. At the higher frequencies, the spherical spreading model was used (Gassmann et al. 2017). The intersection frequency was unique for each passage.

### 3.6.4 Airguns

Airguns are regularly used in seismic surveys for oil and gas exploration to investigate the ocean floor and what lies beneath it. An airgun is a container of high-pressure air that periodically vents into the surrounding water, producing an air-filled cavity which expands and contracts several times (Barger and Hamblen, 1980) producing an intense low-frequency broadband explosive impulse. Airgun pulses have energy as low as 5 Hz and can extend up to 250 Hz or higher (Blackman et al. 2004), lasting up to a few seconds including the reverberations depending on propagation conditions and the distance between the source and receiver. While most of the energy produced by an airgun array falls below 250 Hz, airguns can produce significant energy at frequencies up to at least 1 kHz (Blackman et al. 2004). Source levels generally are over 200 dB p-p re 1 $\mu$Pa · m (Amundsen and Landro, 2010), and have been measured up to 260 dB rms re 1 $\mu$Pa · m (Hildebrand 2009). These pulses typically have an inter-pulse interval of approximately 10 s and bouts can last from several hours to months at a time (Figure 30).

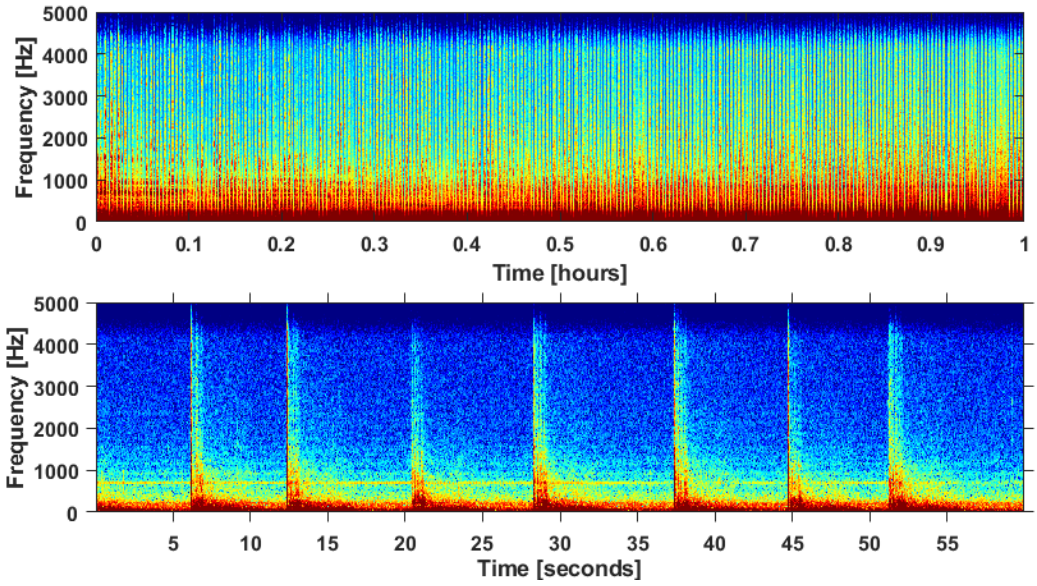


**Figure 30:** Airgun signals in LTSA (top) and spectrogram (bottom).

Airguns were detected automatically using a matched filter detector on the low-frequency band data. The acoustic recording timeseries were filtered with a 10th order Butterworth bandpass filter between 25 and 200 Hz. Cross correlation was computed between 75 s of

the envelope of the filtered timeseries and the envelope of a filtered example airgun explosion (0.7 s, Hann windowed) as the matched filter signal. The cross correlation was squared to 'sharpen' peaks of airgun pulse detections. A floating threshold was calculated by taking the median cross-correlation value over the current 75 s of data to account for detecting airguns within varying noise conditions, such as ship passings. A cross-correlation threshold of $2*10^{-6}$ above the median was set. When the correlation coefficient exceeded this threshold, the detection was sent to a phase 2 detection and classification step. Thresholds were determined based on a manual review of a subset of data.

Consecutive airgun pulse detections were required to have a minimum start time difference of 2 s. A 0.03 s running average energy across the detection was computed. The start and end times of the detection were marked when the energy rose by more than 0.5 dB above the median energy across the detection. The peak-to-peak (pp) and root-mean-square (rms) received levels (RLs) were computed over the potential pulse as well as before and after the explosion. The potential airgun pulse was classified as a false detection and removed if 1) the signal dB difference of pp and rms RLs between the during and AFTER detection periods was < 0.5 dB; 2) the dB difference of pp and rms RLs between the signal and the time BEFORE the signal was < 0.5 dB; and 3) the detection duration was shorter than 0.5 s. Further, detections with a peak-to-peak amplitude of < 120 dB were removed for this analysis.

# 4 Results

## 4.1 Odontocetes

A comparison of the number of hours that echolocation clicks were present for each odontocete species group shows that sperm whales were the most commonly detected species across all sites except the two shallowest locations DC and Y1D (Figure 31). Sperm whale clicks are lower frequency and higher amplitude than those of other species, resulting in longer detection ranges, which at least in part explains their more common occurrence. Unidentified delphinids were commonly detected along the continental slope in the north, and at Loop Current-affected sites in the eastern GoMx (Figure 31). Risso's dolphin click detections were common at eastern slope sites and at site Y2B (Figure 31). At site DC, UD 3p was the dominant odontocete signal, both in hours present and days present, but this type was rarely identified elsewhere (Figures 31 and 32). Species composition appears more varied at all sites when represented as presence and absence at the daily time scale, which is less biased toward the more detectable species (e.g., ten minutes of Kogia presence is given the same weight as many hours of sperm whale presence for a given day). Beaked whales and *Kogia* species were common at daily timescales, with higher occurrence in the southern and western regions (Figure 32) and high occurrence of Cuvier's beaked whales was also notable at the hourly scale at site CE (Figure 31).

Preliminary densities were computed for each odontocete species group category at each site (Table 5). The density estimation methods require estimates of subsurface behavior and odontocete group sizes. Where behavior is not well quantified (e.g., deep divers in shallow waters at site DC) or group sizes are not appropriate, density is not estimated, and other more suitable metrics such as duration of occurrence are reported. Density estimates are reviewed in detail in each species' section below.

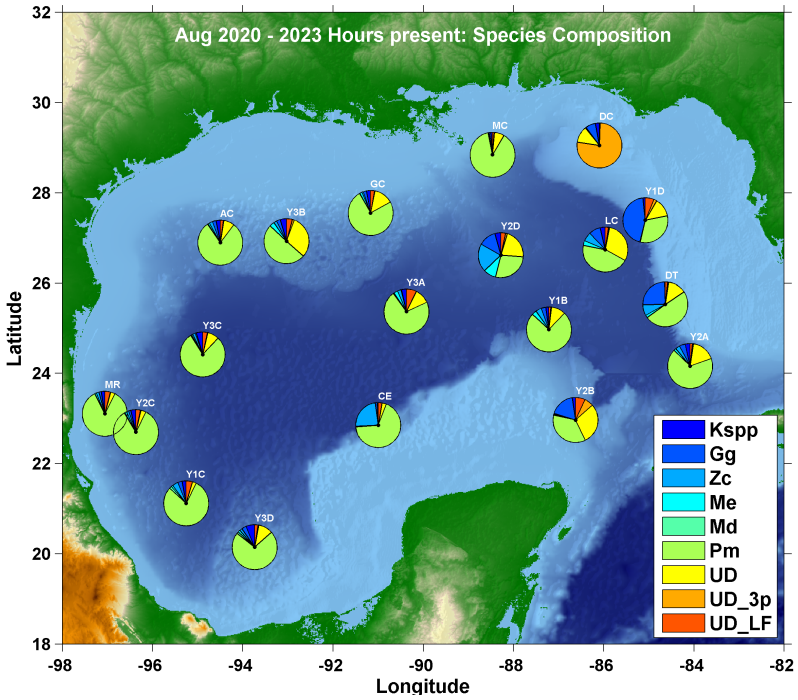


**Figure 31:** Overview of odontocete species composition from 2020-2023, based on the total number of hours during which each species was detected at each site.

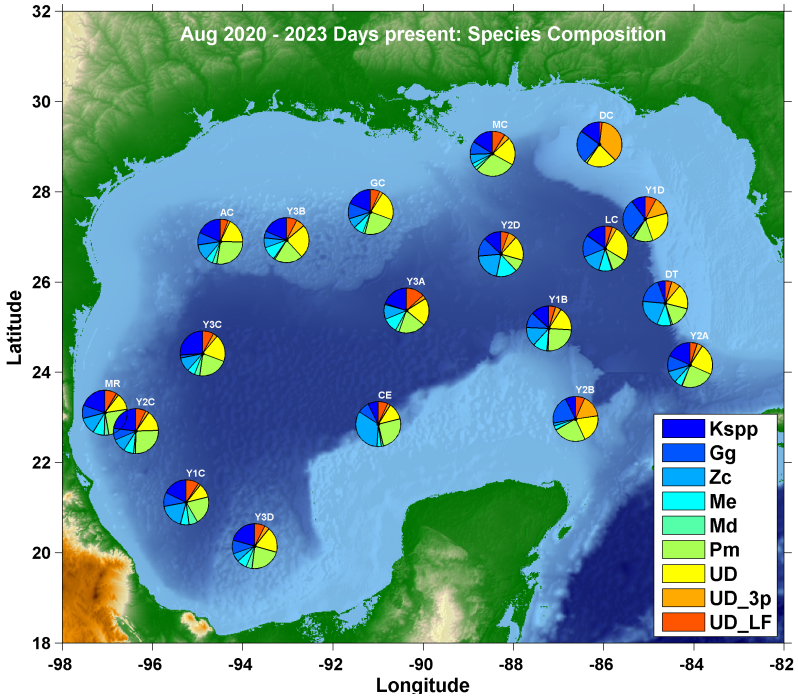


**Figure 32:** Overview of odontocete species composition from 2020-2023, based on the total number of days during which each species was detected at each site.

| | Pm | Zc | Me | Md | Kspp | Gg | UD | UD 3P | UD LF |
|---|---|---|---|---|---|---|---|---|---|
| **AC** | 1.1 | 2.0 | 0.7 | 0.7 | 18.5 | 6.0 | 236.8 | 3.2 | 15.1 |
| **GC** | 0.9 | 1.0 | 1.0 | 0.4 | 17.9 | 4.7 | 392.7 | 5.2 | 11.3 |
| **MC** | 4.0 | 1.1 | 0.8 | 0.3 | 11.2 | 11.4 | 703.2 | 5.5 | 19.4 |
| **DC** | - | - | - | Not estimated | Not estimated | 9.0 | 98.8 | 565.6 | 1.3 |
| **DT** | 0.9 | 10.9 | 2.1 | 0.1 | 4.8 | 99.8 | 603.0 | 29.7 | 11.7 |
| **LC** | 0.3 | 3.1 | 1.2 | 0.0 | 13.2 | 9.4 | 508.3 | 11.2 | 8.2 |
| **CE** | 0.9 | 24.2 | 0.3 | 0.3 | 4.4 | 4.0 | 91.5 | 3.8 | 20.3 |
| **MR** | 1.5 | 2.2 | 1.1 | 0.4 | 24.5 | 5.5 | 125.2 | 3.5 | 37.1 |
| **Y1B** | 0.9 | 3.1 | 2.3 | 0.1 | 15.3 | 6.1 | 308.0 | 14.0 | 7.2 |
| **Y1C** | 1.2 | 4.0 | 1.3 | 5.6 | 23.3 | 7.8 | 95.4 | 4.7 | 34.1 |
| **Y1D** | 0.2 | 0.1 | 0.0 | 0.0 | 4.8 | 45.5 | 124.2 | 22.8 | 15.2 |
| **Y2A** | 0.7 | 2.1 | 0.8 | 0.2 | 17.8 | 7.9 | 432.8 | 12.8 | 9.6 |
| **Y2B** | 0.2 | 0.2 | 0.2 | 0.0 | 7.7 | 22.0 | 341.8 | 79.4 | 20.4 |
| **Y2C** | 1.1 | 1.8 | 1.1 | 1.4 | 27.0 | 4.3 | 117.9 | 4.6 | 23.5 |
| **Y2D** | 0.2 | 12.1 | 4.3 | 0.0 | 15.9 | 19.2 | 444.8 | 27.7 | 7.5 |
| **Y3A** | 0.9 | 2.5 | 2.3 | 1.5 | 22.0 | 0.9 | 250.1 | 6.7 | 40.6 |
| **Y3B** | 0.4 | 1.2 | 1.7 | 0.1 | 22.3 | 4.4 | 583.5 | 24.2 | 18.7 |
| **Y3C** | 1.1 | 1.9 | 1.0 | 2.3 | 34.9 | 2.3 | 262.2 | 8.1 | 25.0 |
| **Y3D** | 0.9 | 1.6 | 1.0 | 2.4 | 44.1 | 8.5 | 321.1 | 9.6 | 14.7 |

**Table 5:** Mean density by species group as number of animals per 1000 $km^2$ over the entire recording period from 2020-2023.

### 4.1.1 Cuvier's Beaked Whale

Among the three beaked whale species, Cuvier's beaked whales generally had the highest mean densities across all sites throughout the study period (Table 5). Among long-term sites over this three year time period, Cuvier's beaked whale densities were highest at the Campeche Escarpment site (CE) with 24.2 animals estimated per 1,000 $km^2$ followed by Dry Tortugas (DT) with 10.9 animals per 1,000 $km^2$ (Figure 33, Table 5). Preliminary densities estimated during this period at site DT were approximately 60% lower than 2010 estimates (Frasier et al. In Review). Among the single year sites, Cuvier's beaked whale densities were high at Y2D, located in a deep canyon south of DT, with 12.1 animals per 1,000 $km^2$ (Figure 34, Table 5). Mean densities at all other sites were considerably lower, between 0.1 and 4.0 animals per 1,000 $km^2$ (Table 5). Beaked whales are not typically found at the shallow De Soto Canyon site (DC), therefore they were not classified at this location (Table 5).

Cuvier's beaked whale clicks were consistently detected throughout the year at nearly every site (Figures 33 and 34). Some seasonality is observed, with higher occurrence in winter months at sites DT, MR, Y2D, and Y3C (near MR). At Y1C (southeast of Y3C) the pattern appeared to be reversed with higher densities in summer, while densities were consistent throughout the year at site CE. No diel pattern in acoustic detections is observed at any site, suggesting no dependence of presence or foraging behavior on time of day (Figures 35 & 36). Spatial distributions based on monitoring to date suggests two hot spots in the vicinity of the Campeche Escarpment and the Loop Current-affected regions of the southern end of the West Florida Shelf (Figures 31, 37 and 38).

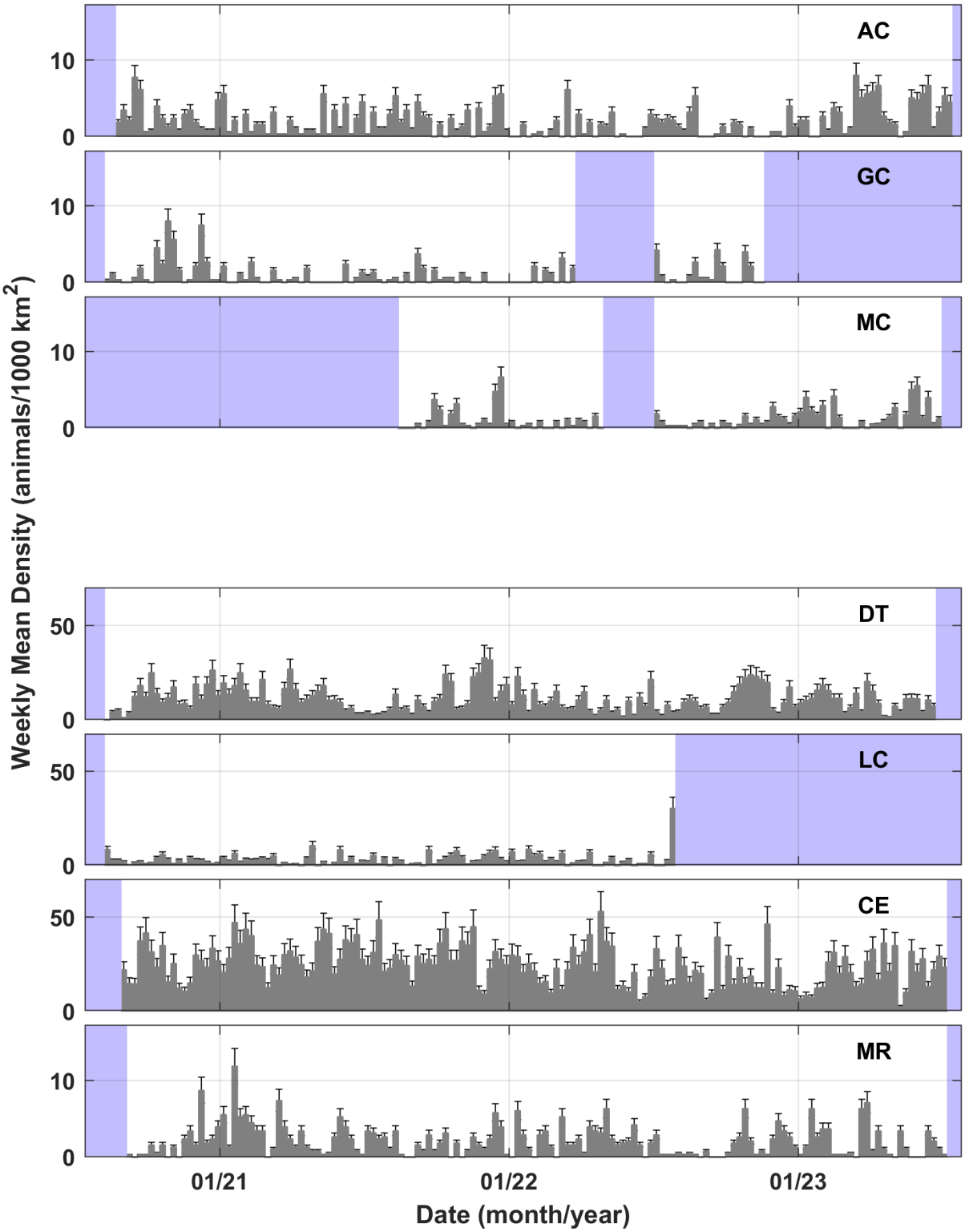


**Figure 33:** Weekly mean density (gray bars) of Cuvier's beaked whales at long-term sites from 2020 to 2023. No detection effort was expended for beaked whales at the shallow site DC. Error bars represent ± 1 standard deviation. Shaded blue sections represent periods with no recording effort. Note: y-axis values vary in some cases based on maximum densities.

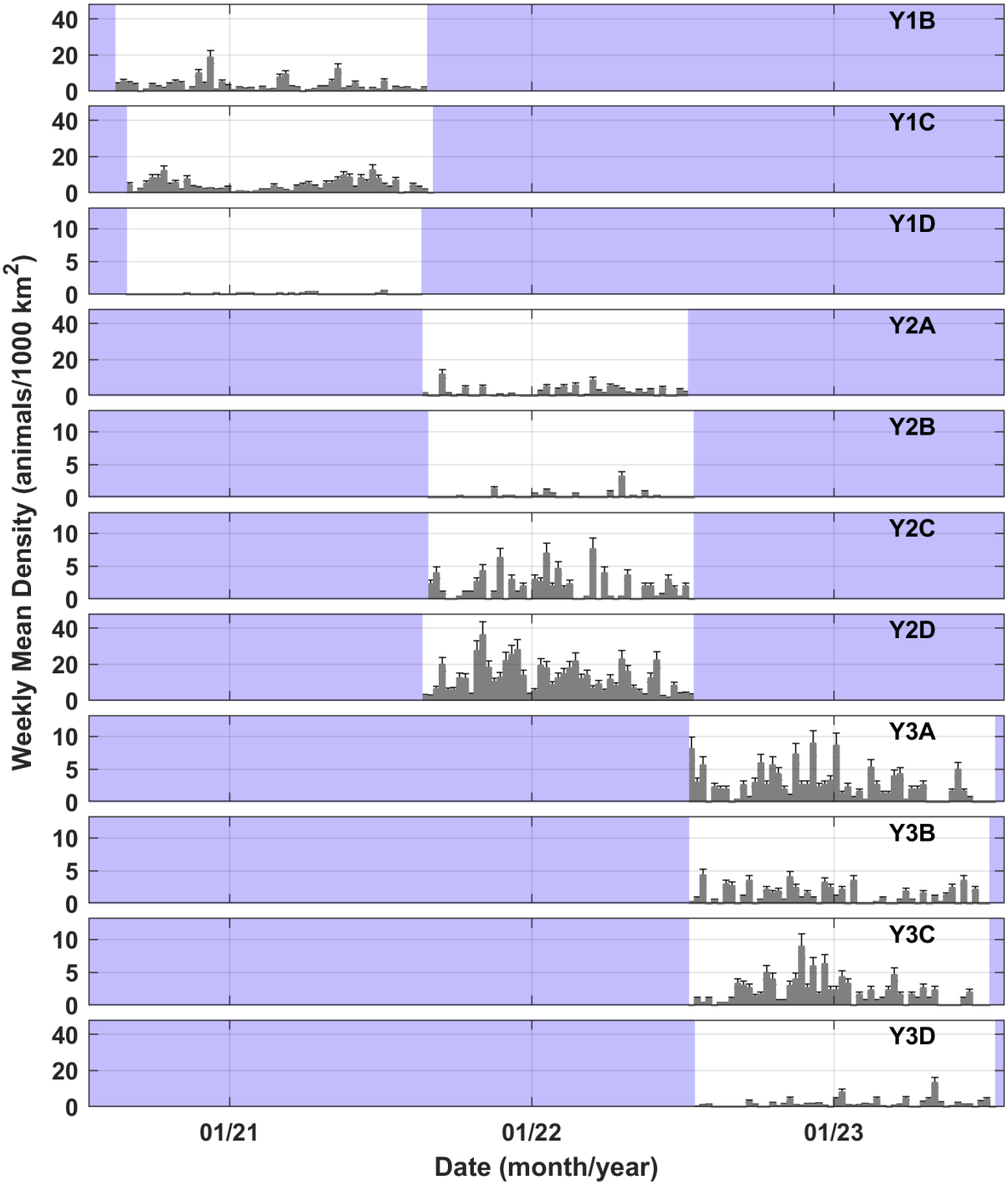


**Figure 34:** Weekly mean density (gray bars) of Cuvier's beaked whales at short-term sites from 2020 to 2023. Error bars represent ± 1 standard deviation. Shaded blue sections represent periods with no recording effort. Note: y-axis values vary in some cases based on maximum densities.

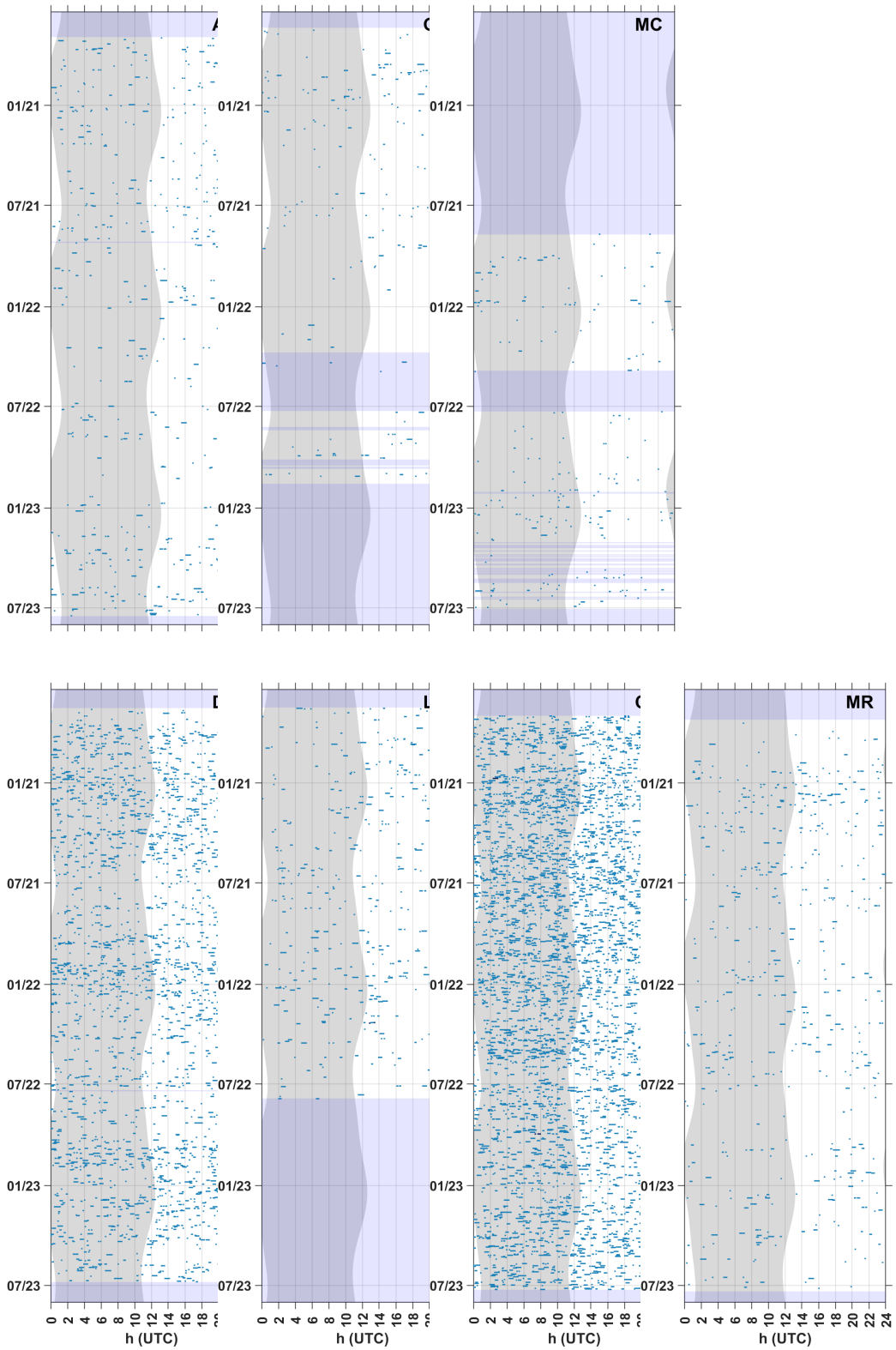


**Figure 35:** Cuvier's beaked whale echolocation clicks in five-minute bins at long-term sites from 2020-2023. Gray vertical shading denotes nighttime and light blue horizontal shading denotes absence of acoustic data. Color denotes number of detections per 5 minutes (light blue: <100; mid blue: 100-1000; dark blue: >1000). No detection effort was expended for beaked whales at the shallow site DC.

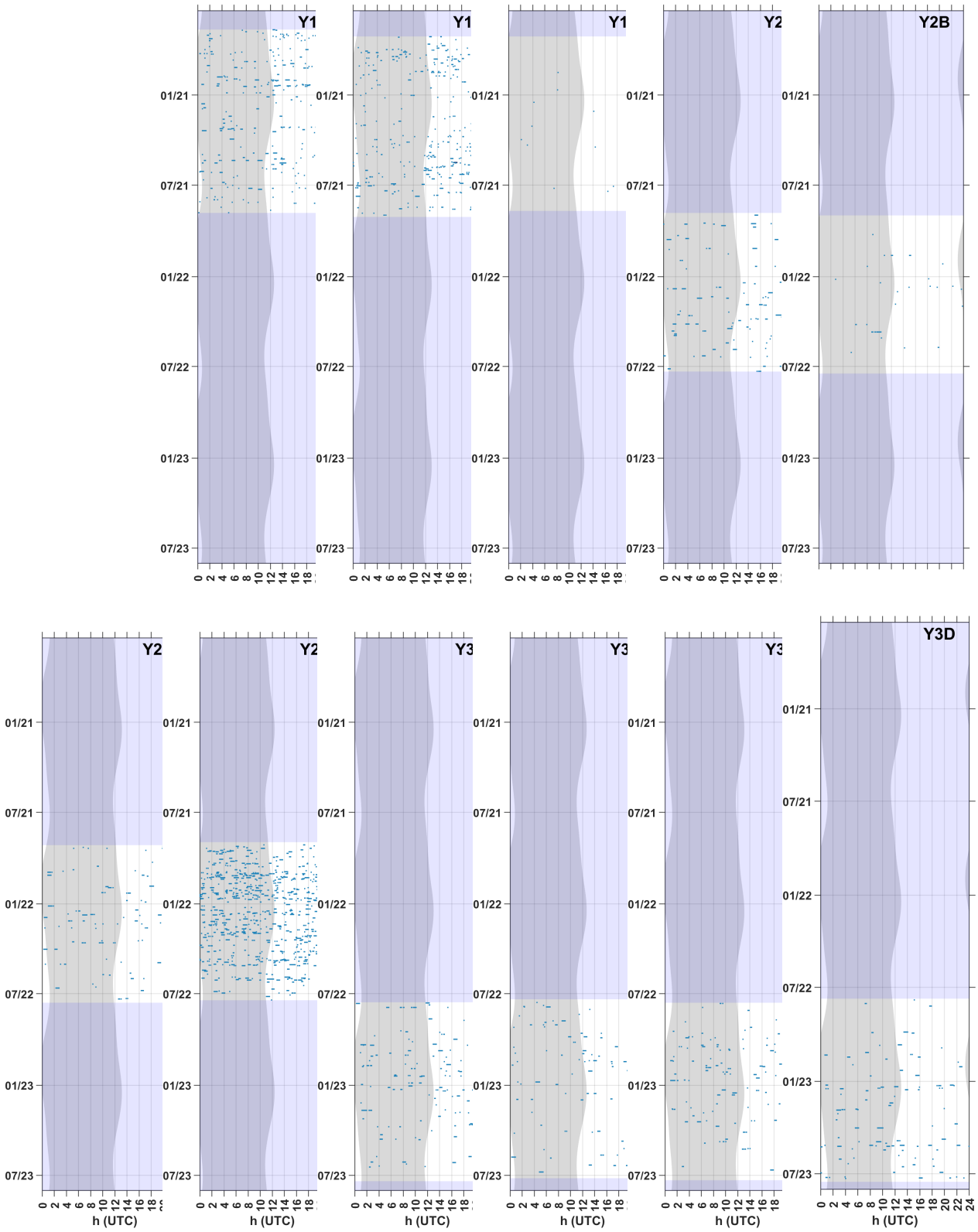


**Figure 36:** Cuvier's beaked whale echolocation clicks in five-minute bins at short-term sites from 2020 to 2023. Gray vertical shading denotes nighttime and light blue horizontal shading denotes absence of acoustic data. Color denotes number of detections per 5 minutes (light blue: <100; mid blue: 100-1000; dark blue: >1000).

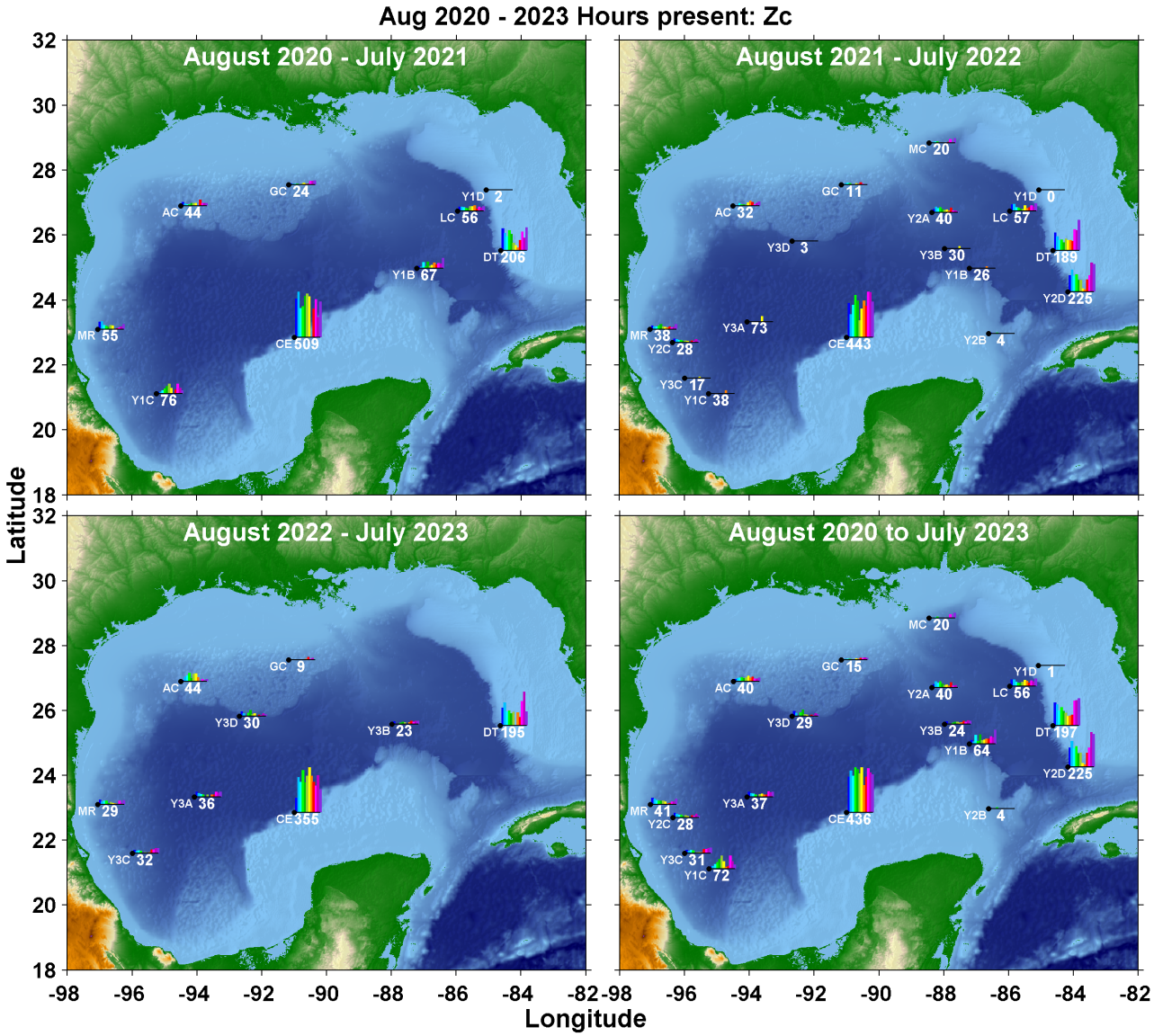


**Figure 37:** Average hourly presence of Cuvier's beaked whale echolocation clicks per month, represented as bar plots, from 2020 to 2023. Values below bar plots represent mean hours of presence per year. Panels represent presence in each of the three years of recordings with the bottom right panel representing all years combined.

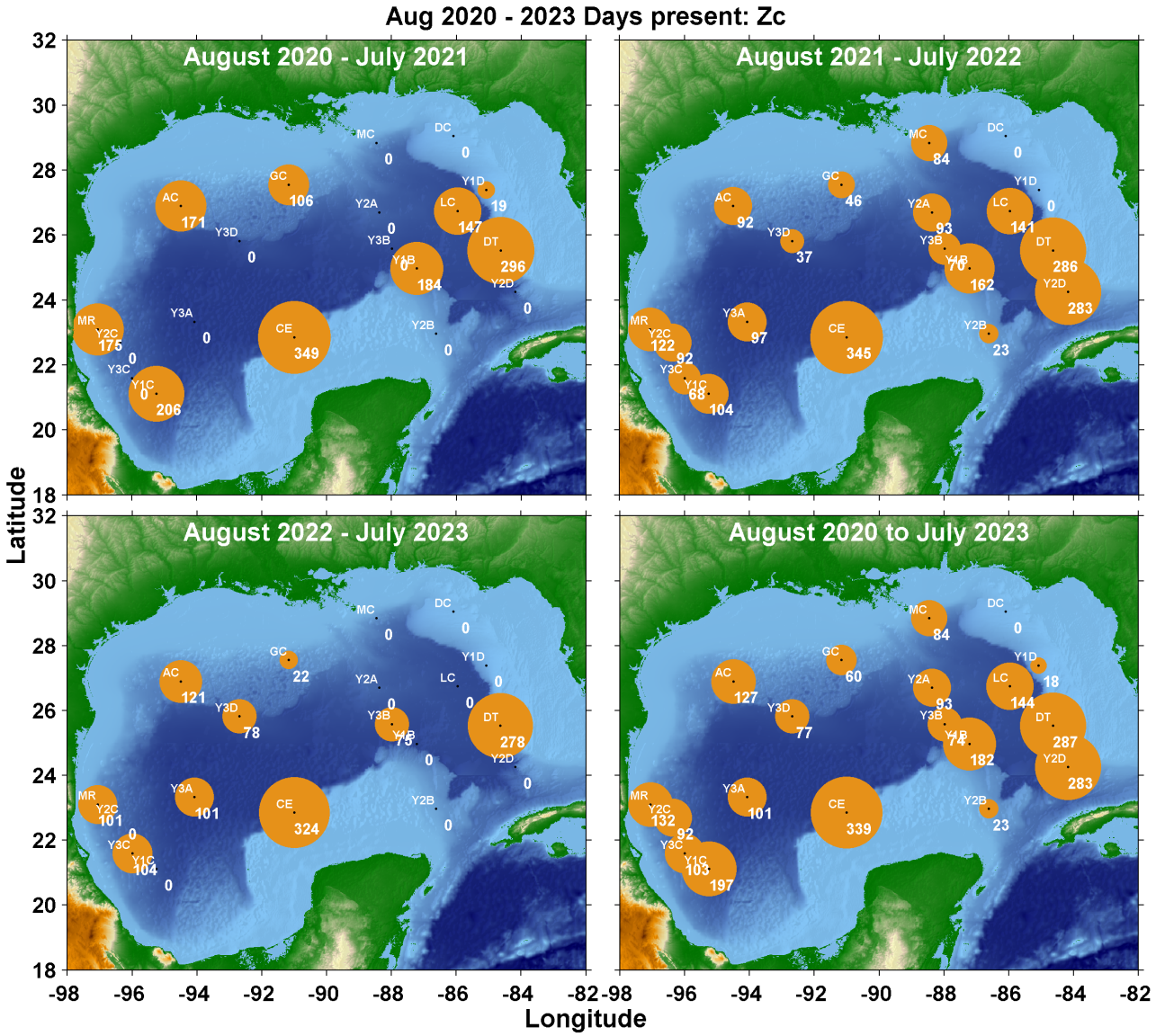


**Figure 38:** Average annual days with Cuvier's beaked whale echolocation click presence from 2020-2023. Panels represent presence in each of the three monitoring years, with the bottom right panel representing yearly means computed across the three years, adjusted for recording effort.

### 4.1.2 Gervais' Beaked Whale

Gervais' beaked whale was the second-most commonly detected beaked whale across all sites. Densities were highest at Y2D with 4.3 animals estimated per 1,000 $km^2$, south of the historically beaked whale-rich DT site (2.1 per 1,000 $km^2$; Table 5). Densities were also relatively high at sites Y1B and Y3A, along the western margin of the Loop Current and in the Sigsbee Deep region respectively, with 2.3 animals per 1,000 $km^2$. Mean densities at all other sites were considerably lower, between 0.2 and 1.7 animals per 1,000 $km^2$ (Table 5). Preliminary densities estimated during this period across all sites were lower than historical estimates at site DT from 2010-2015 ($\sim$10 per 1,000 $km^2$; Frasier et al. In Review). Beaked whales are not typically found at the shallow De Soto Canyon site (DC), therefore they were not classified at this location.

Gervais' beaked whale clicks were consistently detected throughout the year at nearly every site (Figures 39 & 40). No diel pattern in acoustic detections is observed at any site, suggesting no dependence of foraging behavior on time of day (Figures 41 & 42). Densities appear to be somewhat higher in spring, summer and early fall at site DT, while at Y1B and Y3B, density peaks were observed in winter. Gervais' beaked whales had high days present per year along most of the continental slope and deep sites, with notably low occurrence at site CE, where Cuvier's beaked whale densities were highest (Figure 43). Rather, Gervais' beaked whales appeared to primarily occupy the Loop Current-affected sites in the east, and were secondarily found in deep southwestern Mexican waters near sites MR and Y3A (Sigsbee Deep). Very few detections occurred at shallow sites Y1D and Y2B, consistent with prior observations from shallow water. There was high variability in numbers of days with Gervais' beaked whales present throughout the year among sites, ranging between 4 to 211 days (Figure 44).

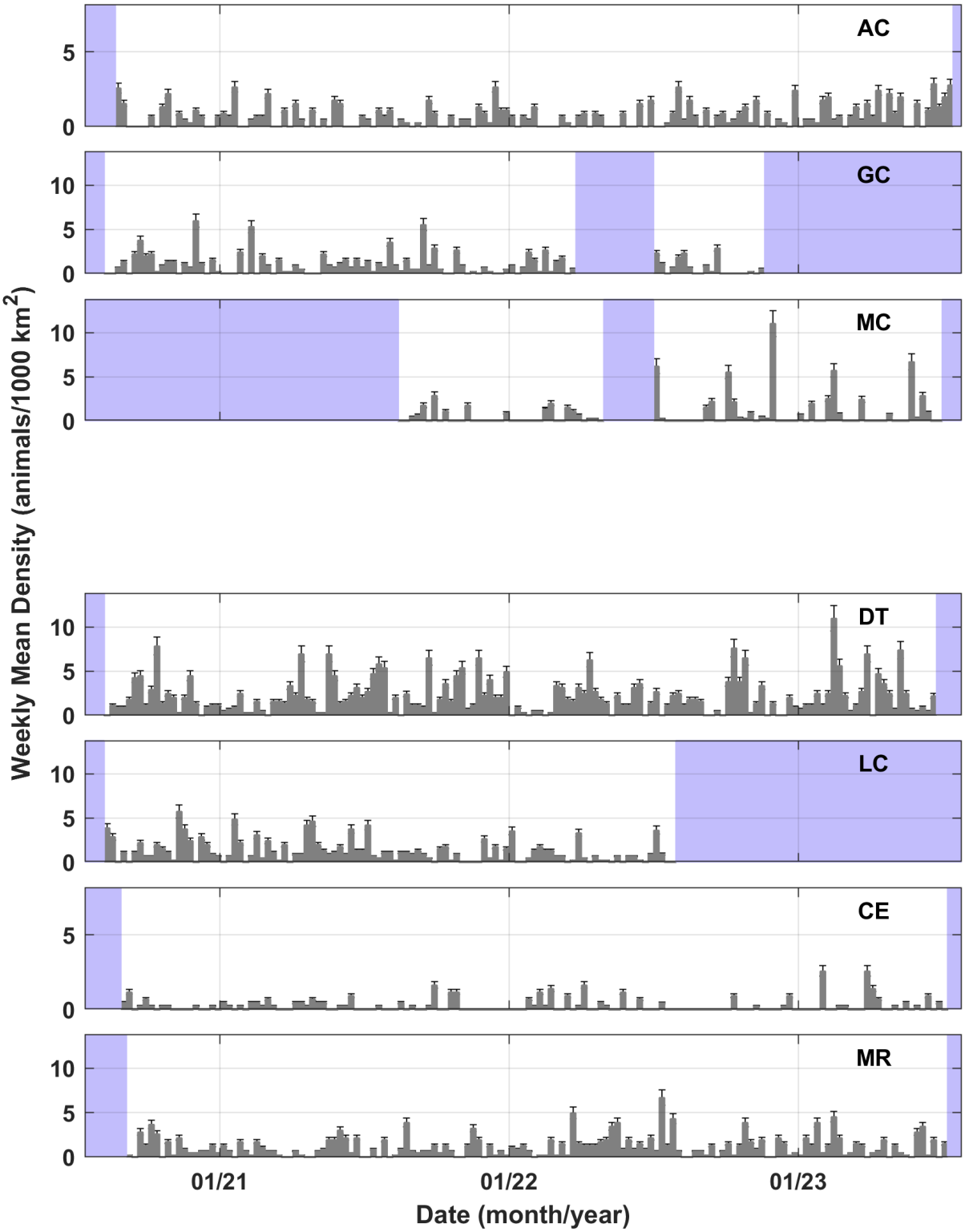


**Figure 39:** Weekly mean density (gray bars) of Gervais' beaked whales at long-term sites from 2020 to 2023. No detection effort was expended for beaked whales at the shallow site DC. Error bars represent ± 1 standard deviation. Shaded blue sections represent periods with no recording effort. Note: y-axis values vary in some cases based on detection levels.

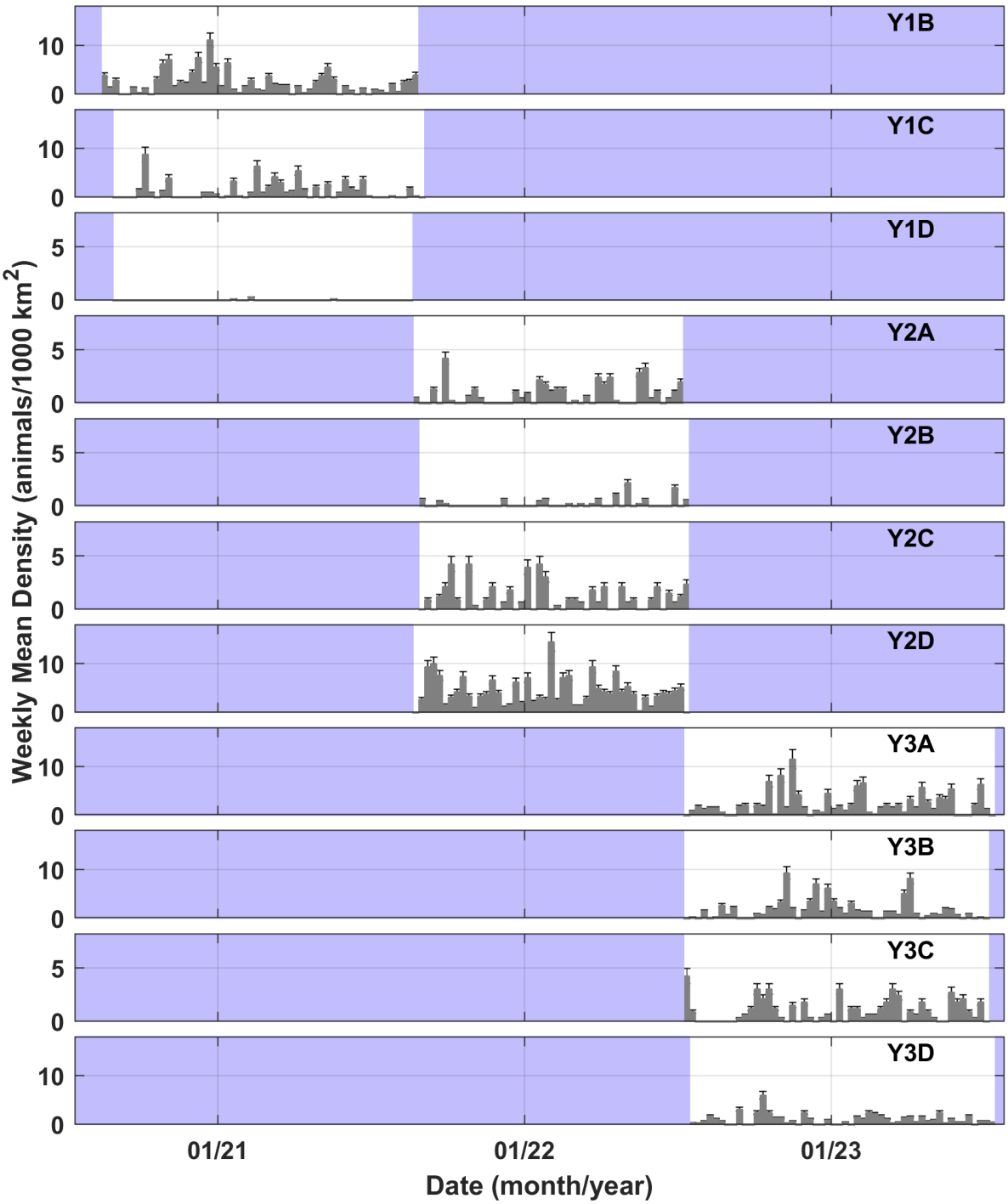


**Figure 40:** Weekly mean daily density (gray bars) of Gervais' beaked whales at short-term sites from 2020 to 2023. Error bars represent ± 1 standard deviation. Shaded blue sections represent periods with no recording effort. Note: y-axis values vary in some cases based on detection levels.

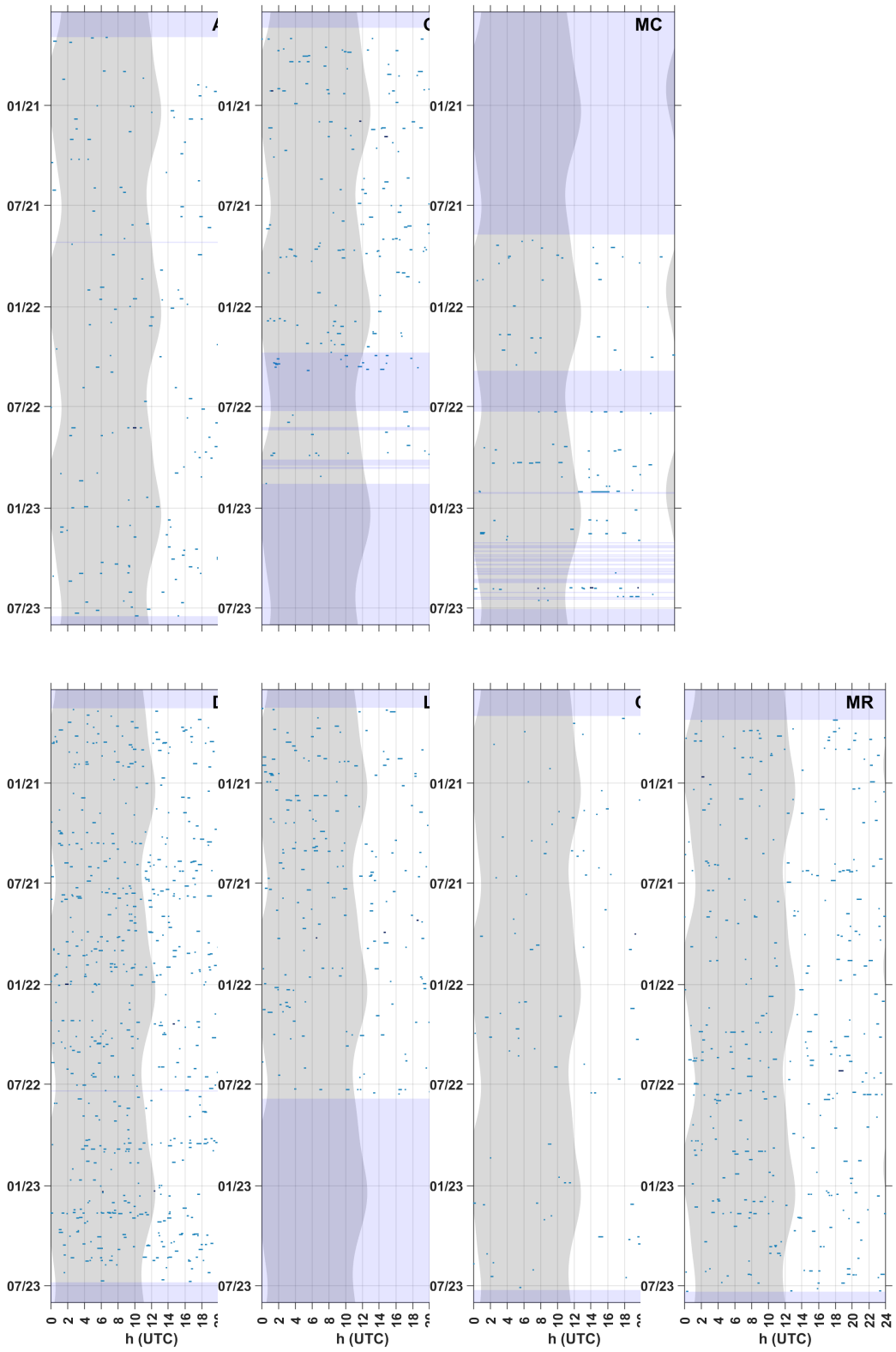


**Figure 41:** Gervais' beaked whale echolocation clicks in five-minute bins at long-term sites from 2020-2023. Gray vertical shading denotes nighttime and light blue horizontal shading denotes absence of acoustic data. Color denotes number of detections per 5 minutes (light blue: <100; mid blue: 100-1000; dark blue: >1000). No detection effort was expended for beaked whales at the shallow site DC.

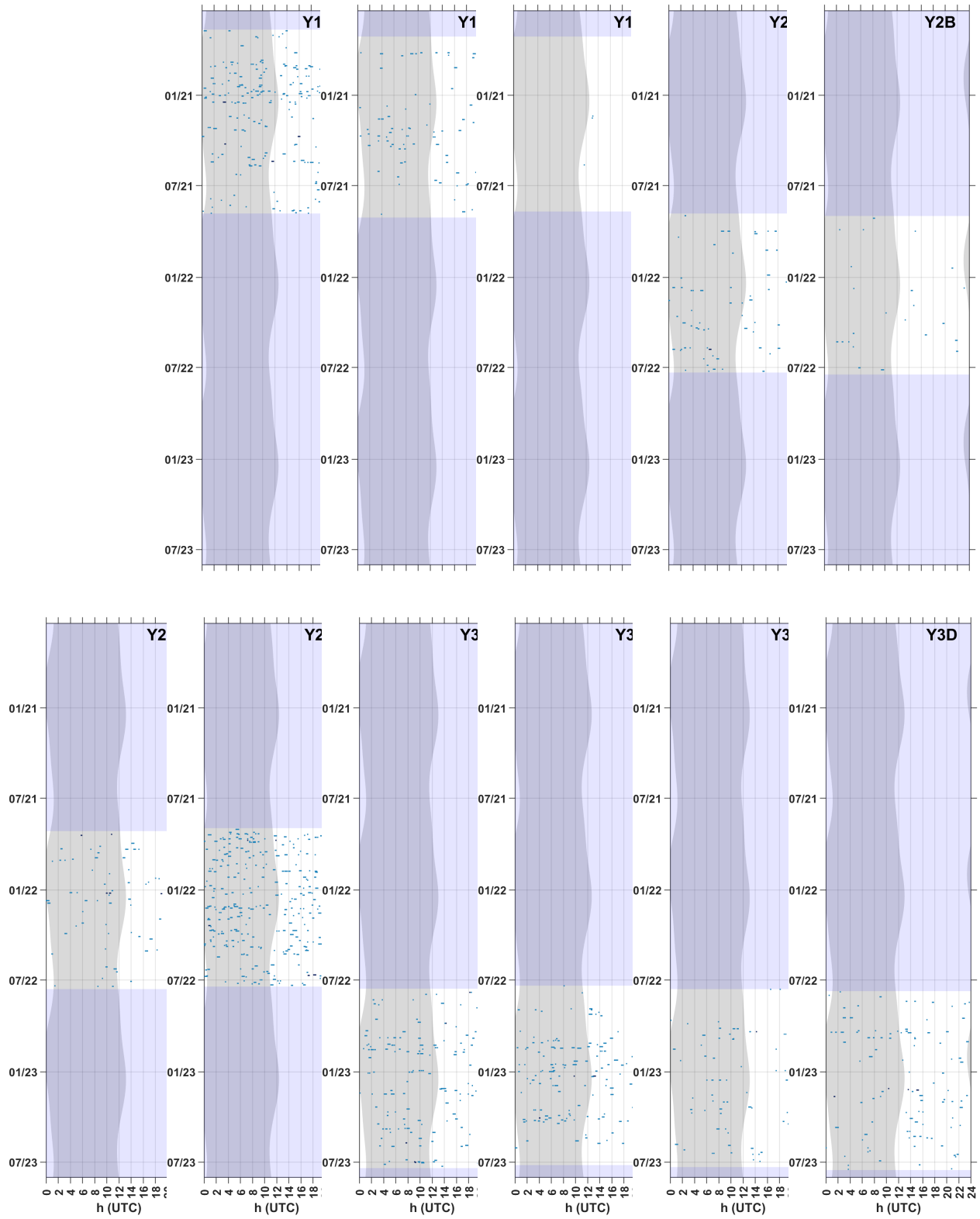


**Figure 42:** Gervais' beaked whale echolocation clicks in five-minute bins at short-term sites from 2020-2023. Gray vertical shading denotes nighttime and light blue horizontal shading denotes absence of acoustic data. Color denotes number of detections per 5 minutes (light blue: <100; mid blue: 100-1000; dark blue: >1000).

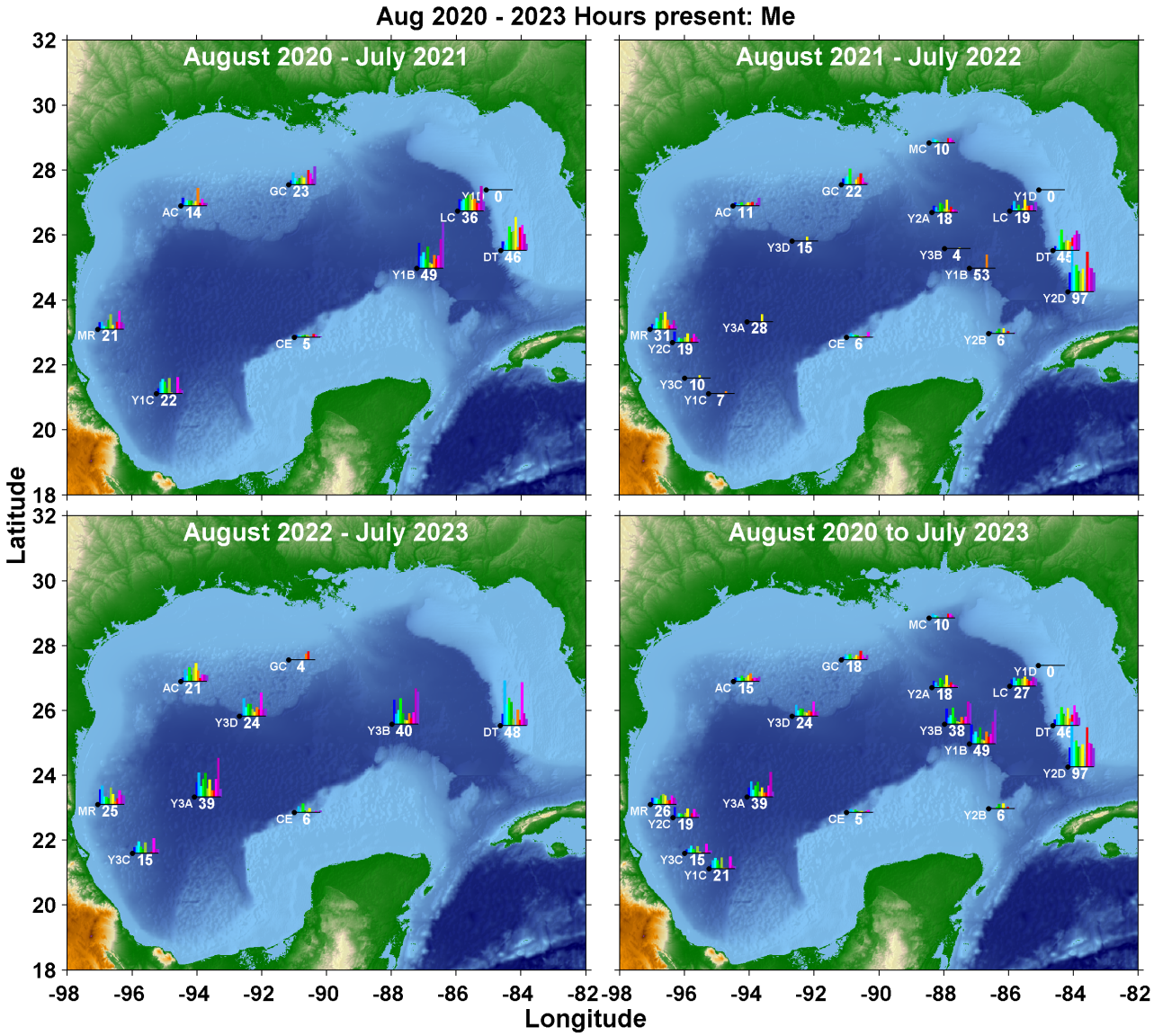


**Figure 43:** Average hourly presence of Gervais' beaked whale echolocation clicks per month, represented as bar plots, from 2020-2023. Values below bar plots represent mean hours of presence per year. Panels represent presence in each of the three years of recordings with the bottom right panel representing all years combined.

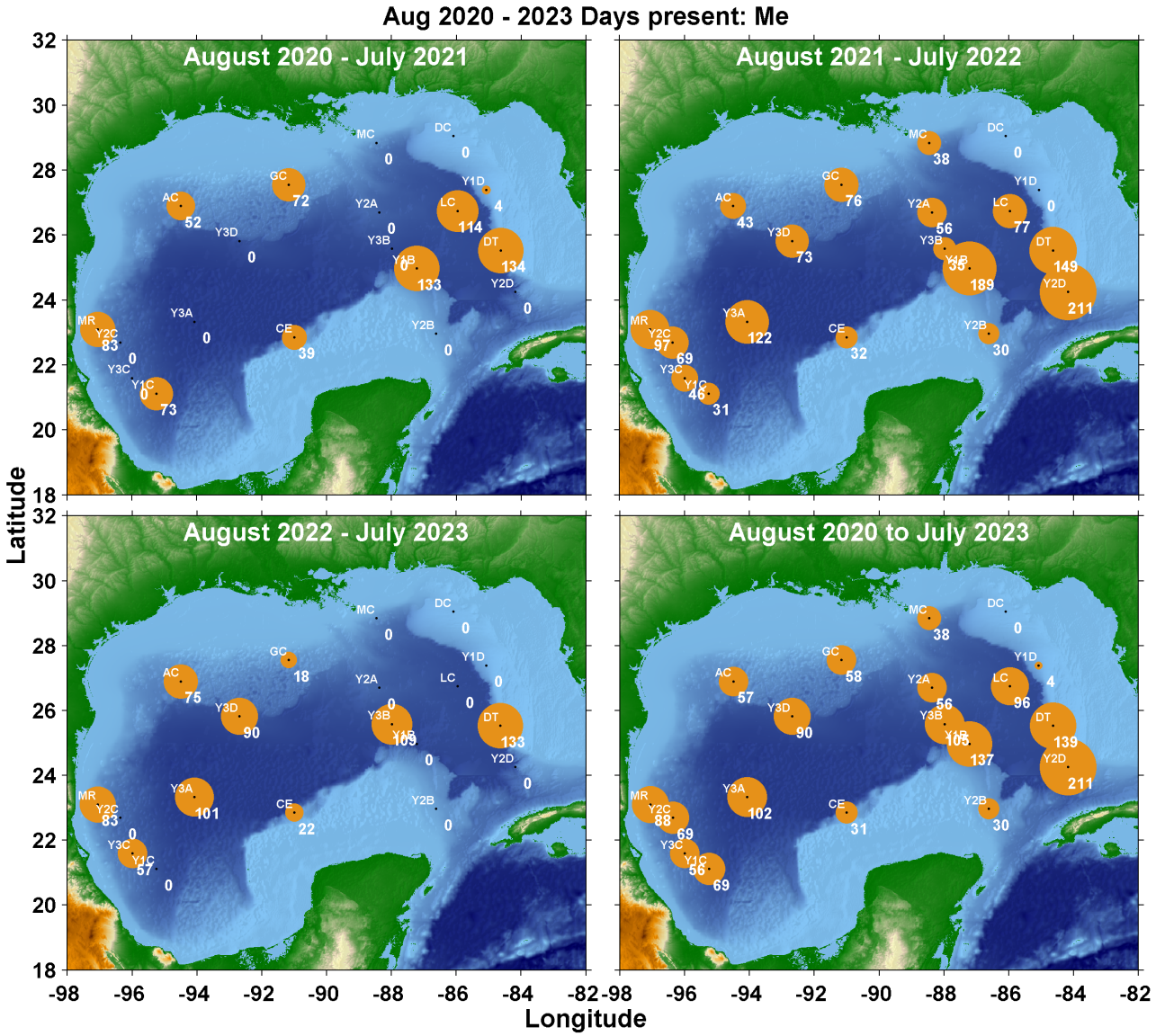


**Figure 44:** Average annual days with Gervais' beaked whale echolocation click presence from 2020-2023. Panels represent presence in each of the three monitoring years, with the bottom right panel representing yearly means computed across the three years, adjusted for recording effort.

### 4.1.3 Blainville's Beaked Whale

Blainville's beaked whales were the least-commonly detected beaked whale species on average with the lowest estimated densities during the 2020-2023 monitoring period (Table 5) though densities exceeded those of Gervais' beaked whales at a few sites. This species was predominantly detected in the southwestern Gulf and at a central Gulf site, Y3D. Site Y1C, a deep site in the Bay of Campeche, had the highest densities of Blainville's beaked whales with 5.6 animals per 1,000 $km^2$. Another Bay of Campeche site, Y3C also had relatively high densities (2.3 animals per 1,000 $km^2$), as did Y3D at the edge of the Sigsbee Escarpment (2.4 animals per 1,000 $km^2$) (Table 5). These are deep water sites well beyond the continental slope, with bottom depths over 2000 m. Density trends for Blainville's beaked whale at the historic sites are uncertain due to very low occurrence of this species. Beaked whales are not typically found at the shallow De Soto Canyon site (DC), therefore they were not classified at this location.

No seasonal patterns in Blainville's beaked whale occurrence were observed (Figures 39 &40). No diel pattern in acoustic detections were observed at any site, suggesting no dependence of foraging behavior on time of day (Figures 47 &48). The sparsity of the time series due to low overall numbers of Blainville's beaked whale detections may limit the ability to resolve such patterns. This species was primarily present from the Bay of Campeche up to the southern edge of the Sigsbee Escarpment (Figure 49). Blainville's beaked whales had the lowest daily presence of all species across sites throughout the Gulf, with detections present an average of 55 days per year at site Y3D, 66 days per year at site Y1C, and lower detection-positive days elsewhere (Figure 50).

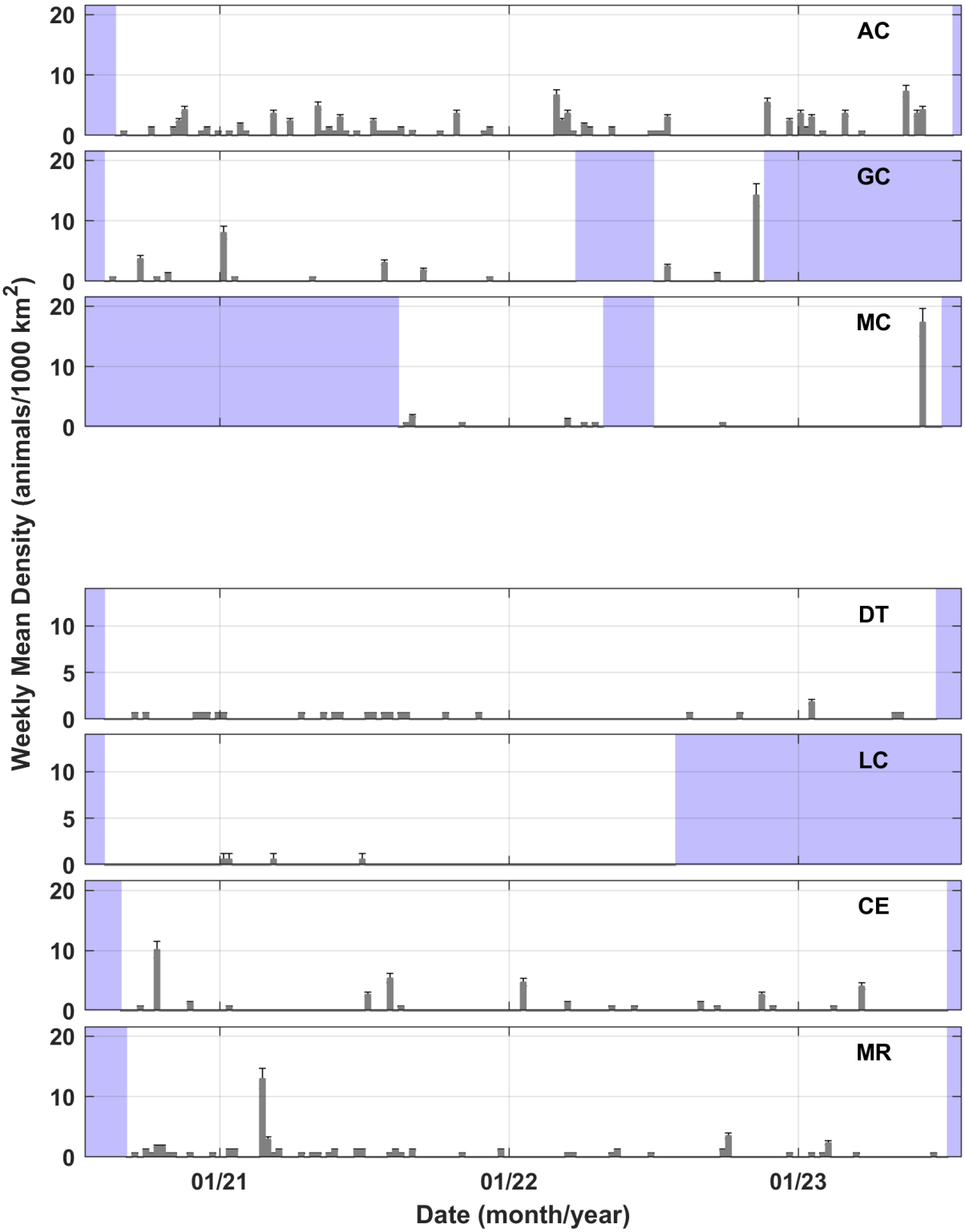


**Figure 45:** Weekly mean density (gray bars) of Blainville's beaked whales at long-term sites from 2020 to 2023. Error bars represent ± 1 standard deviation. Shaded blue sections represent periods with no recording effort. Note: y-axis values vary for each site based on maximum densities. No detection effort was expended for beaked whales at the shallow site DC.

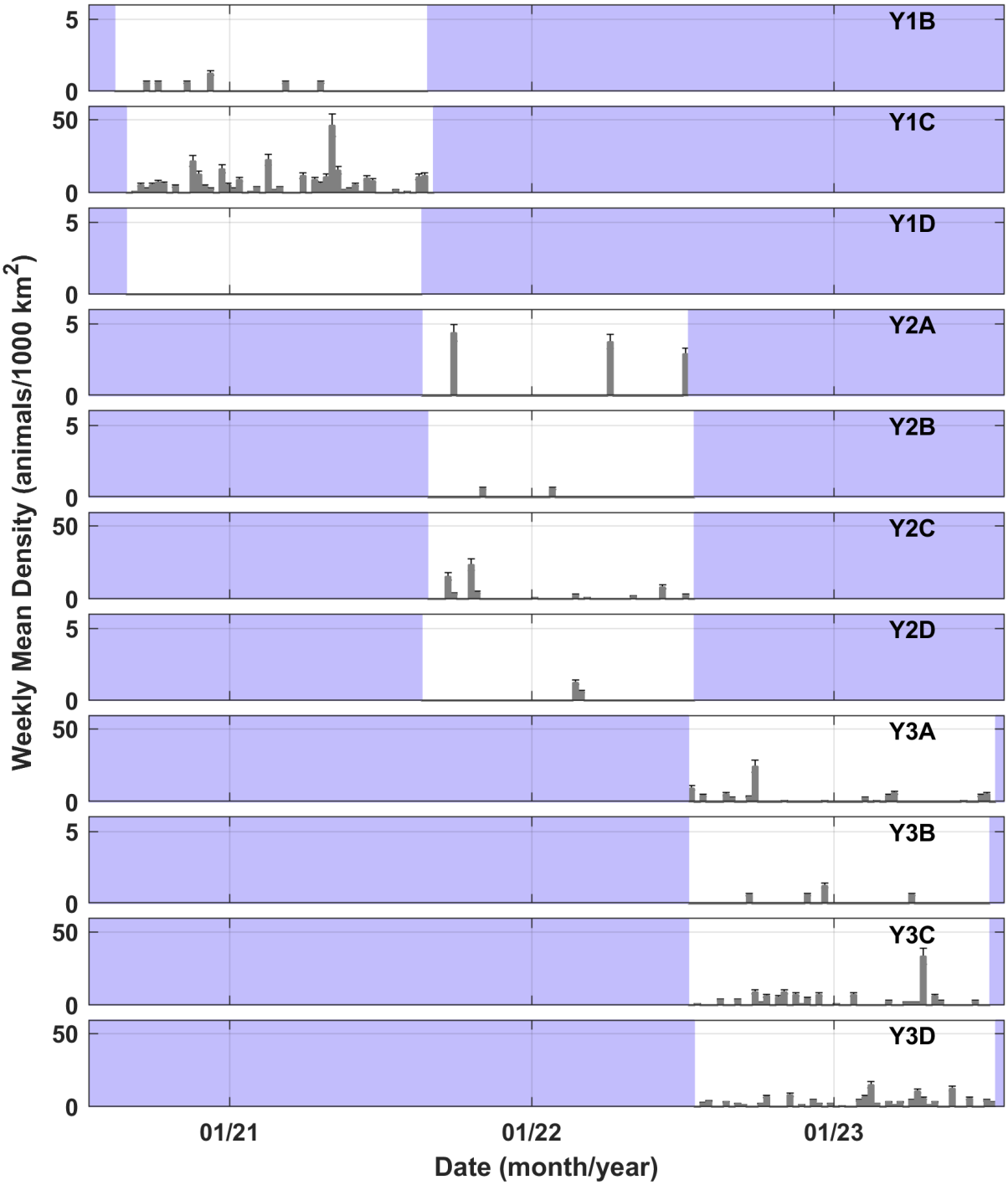


**Figure 46:** Weekly mean density (gray bars) of Blainville's beaked whales at short-term sites from 2020 to 2023. Shaded blue sections represent periods with no recording effort. Note: y-axis values vary for each site based on maximum densities.

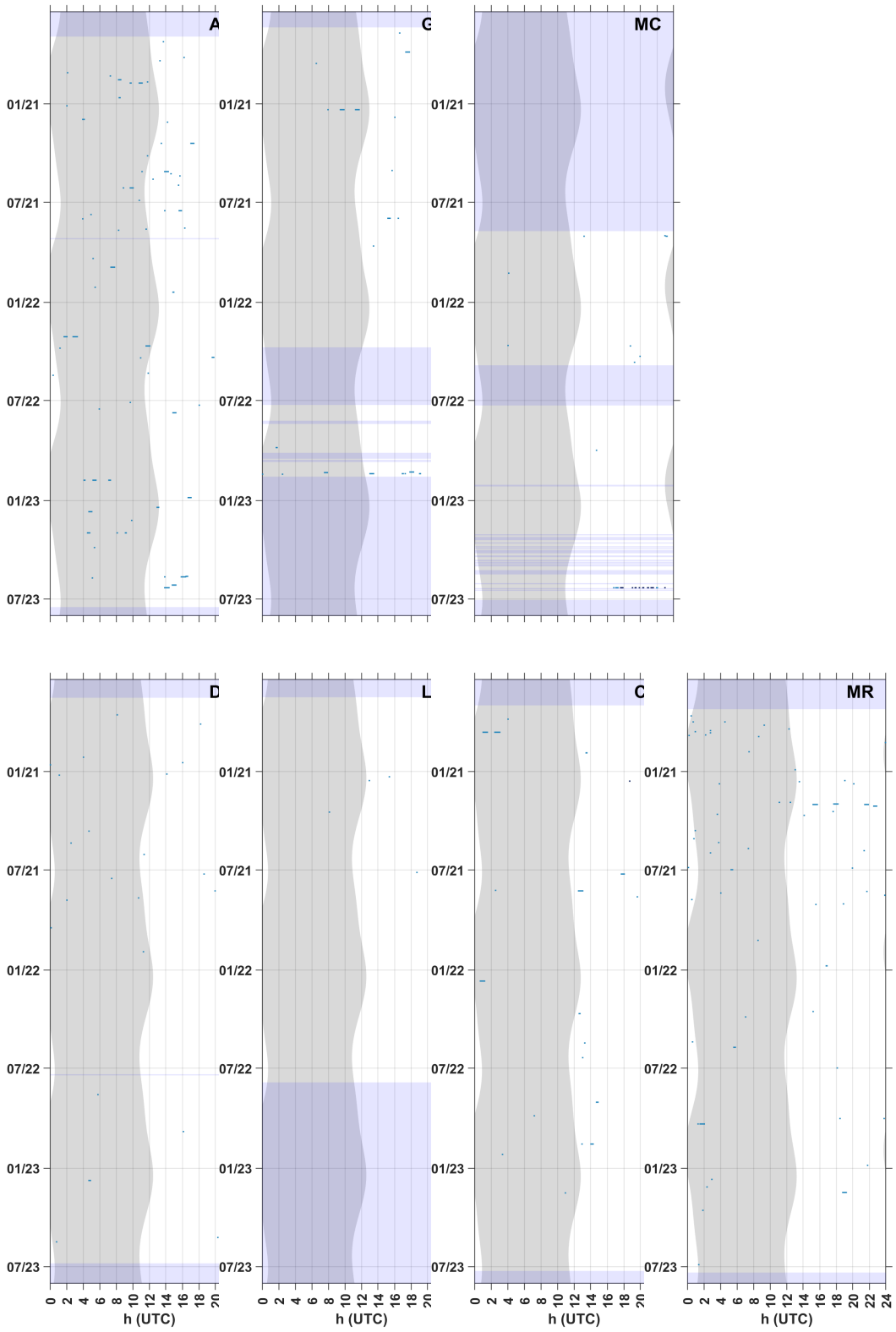


**Figure 47:** Blainville's beaked whale echolocation clicks in five-minute bins at long-term sites from 2020 to 2023. Gray vertical shading denotes nighttime and light blue horizontal shading denotes absence of acoustic data. Color denotes number of detections per 5 minutes (light blue: <100; mid blue: 100-1000; dark blue: >1000). No detection effort was expended for beaked whales at the shallow site DC.

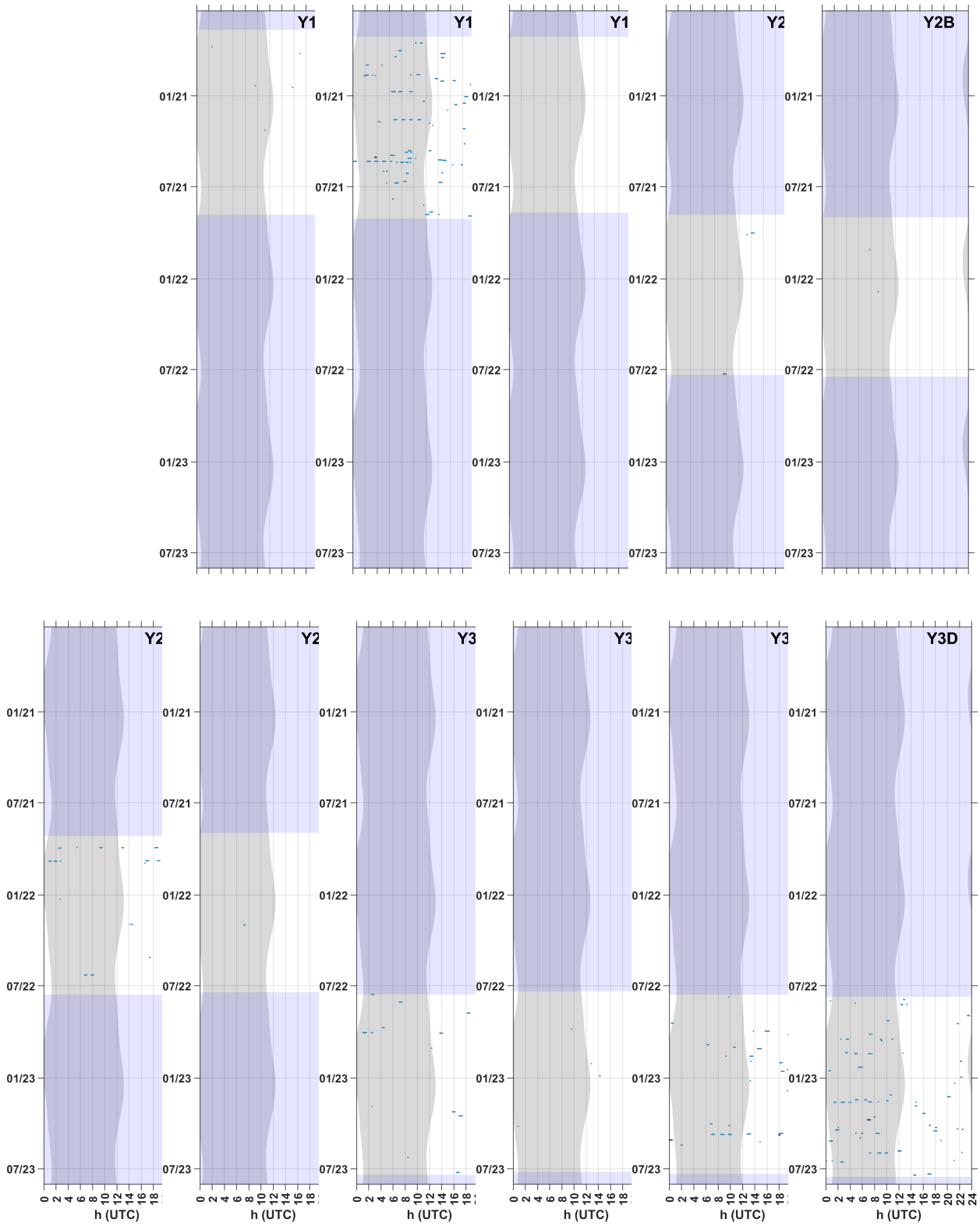


**Figure 48:** Blainville's beaked whale echolocation clicks in five-minute bins at short-term sites from 2020 to 2023. Gray vertical shading denotes nighttime and light blue horizontal shading denotes absence of acoustic data. Color denotes number of detections per 5 minutes (light blue: <100; mid blue: 100-1000; dark blue: >1000).

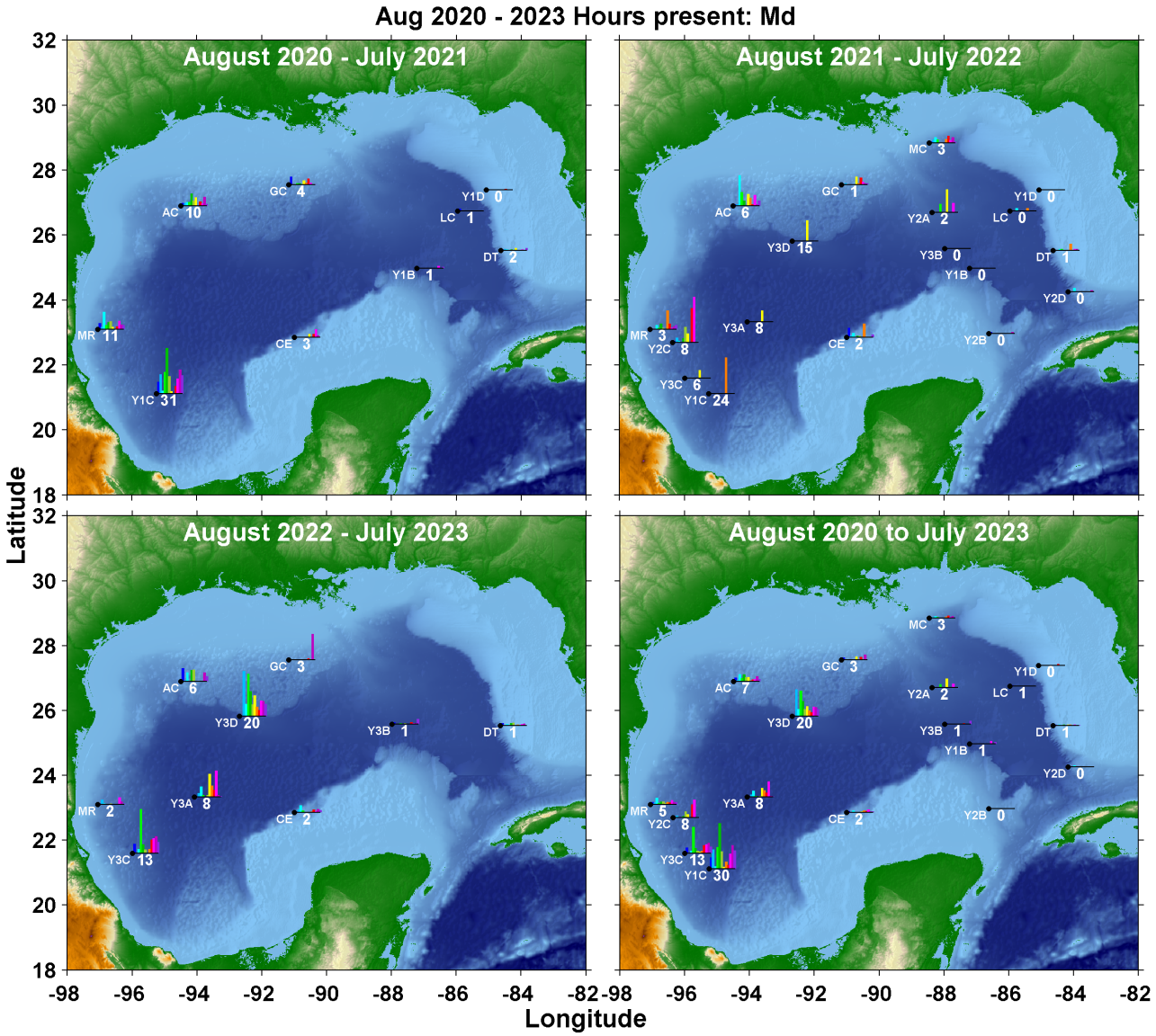


**Figure 49:** Average hourly presence of Blainville's beaked whale echolocation clicks per month, represented as bar plots, from 2020 to 2023. Values below bar plots represent mean hours of presence per year. Panels represent presence in each of the three years of recordings with the bottom right panel representing all years combined.

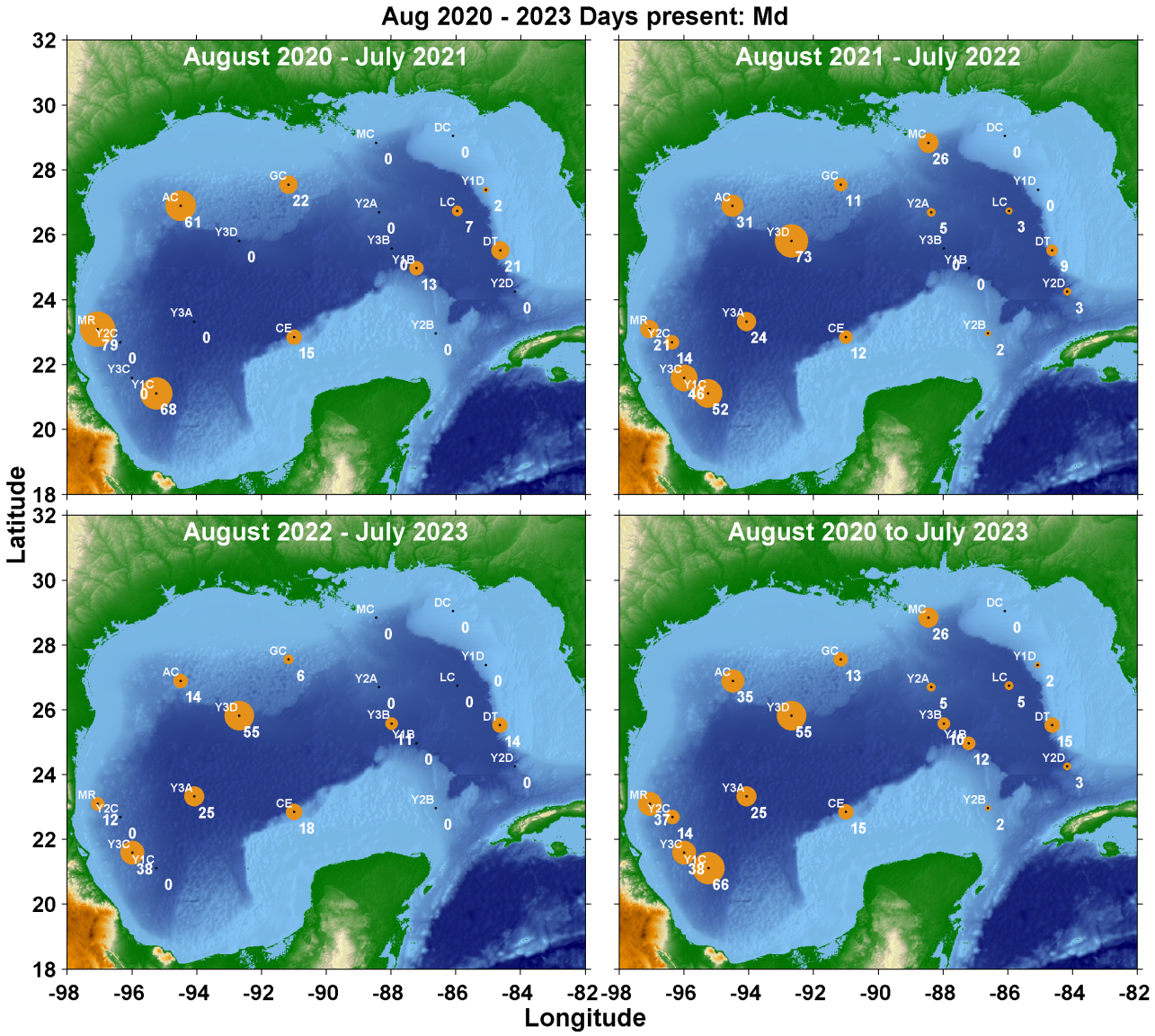


**Figure 50:** Average annual days with Blainville's beaked whale echolocation click presence per year from 2020-2023. Panels represent presence in each of the three monitoring years, with the bottom right panel representing yearly means computed across the three years, adjusted for recording effort.

### 4.1.4 Sperm Whale

During the 2020-2023 monitoring period, sperm whale densities were highest at Mississippi Canyon (MC) with 3.6 animals per 1,000 $km^2$ (Table 5) followed by site MR, in western the Mexican Ridges region (1.5 animals per 1,000 $km^2$). Densities at all other sites ranged from 0.2 to 1.2 animals per 1,000 $km^2$. Preliminary site MC densities (mean of 4.0 animals per 1,000 $km^2$) during this period were comparable with estimated 2010 densities at this site (4.1 animals per 1,000 $km^2$ based on historic data 2010-2020 mean; Frasier et al. In Review). Densities at site GC were lower than historic values (0.9 animals per 1,000 $km^2$ during 2020-2023 compared to 1.3 animals per 1,000 $km^2$ during 2010) but were higher at site DT where densities of sperm whales have been steadily increasing over the past decade (0.9 animals per 1,000 $km^2$ during 2020-2023 compared to 0.3 animals per 1,000 $km^2$ historically). Sperm whales were infrequently detected at site DC, and densities were not estimated for this location due to insufficient understanding of sperm whale behavior in shallow waters. Sperm whale occurrence is episodic with periods of high and low densities lasting weeks to months across sites (Figure 51 & 52).

Seasonality is observed at Loop-Current-adjacent sites including LC, Y1D, Y2B, and Y2D, with peaks in winter months, which may be associated with migration of males in and out of the region (Solsona-Berga et al. Submitted). Summer season peaks were observed at sites DT and Y2A, on the West Florida Shelf, and at one Bay of Campeche site, Y1C. Diel patterns in sperm whale echolocation activity may occur at some sites, including periods of primarily daytime foraging, and frequent gaps in acoustic activity at sunrise, however these patterns are not stable over long periods (Figures 53 & 54). Sperm whale daily presence is high across most sites, in part due to the long detection distances associated with their high source level, low to mid-frequency echolocation clicks (Figures 55 & 56). Sperm whale clicks are present most days of the year at all sites, ranging from 110 to 337 days per year on average at sites with moderate densities (Figure 56, Table 5).

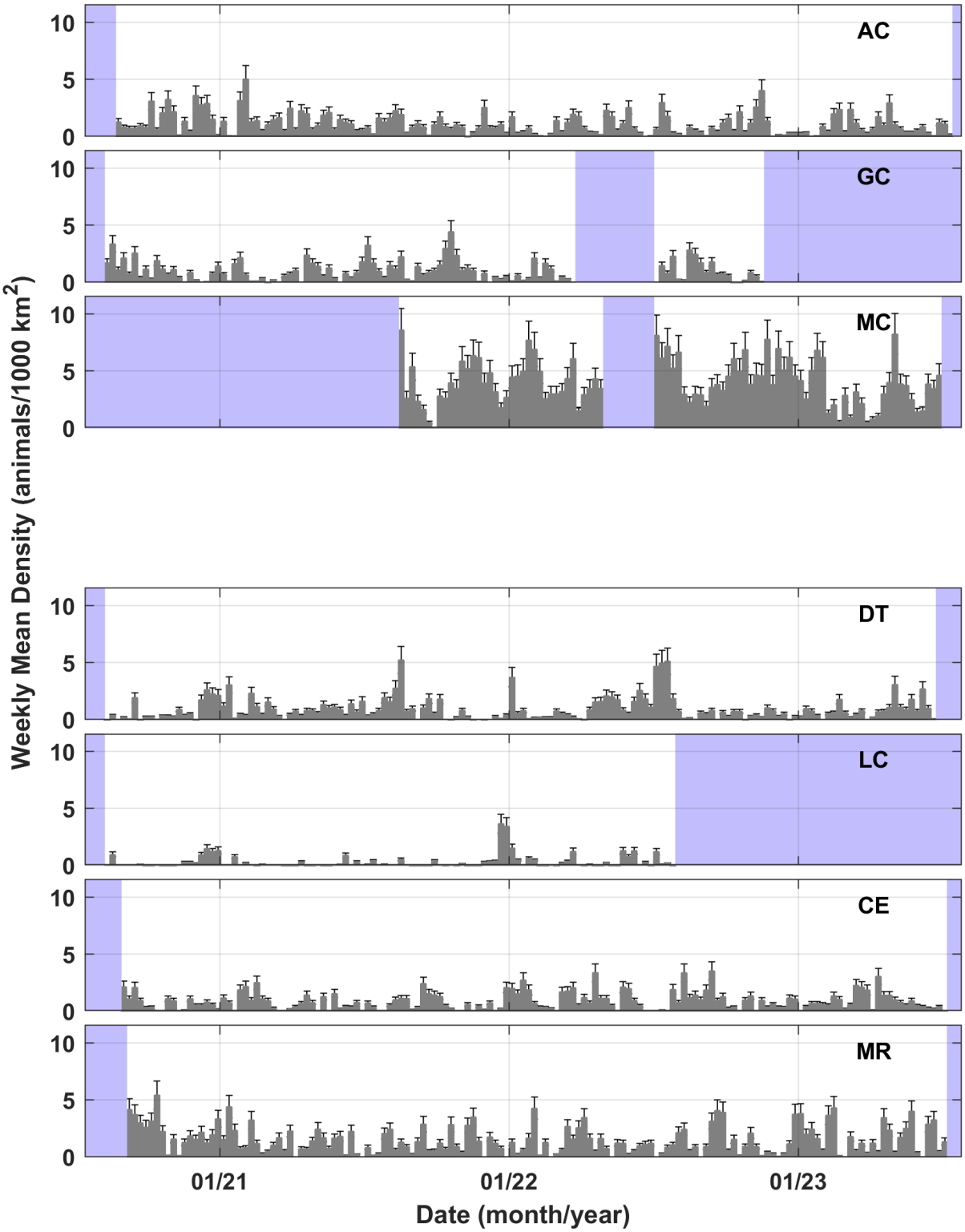


**Figure 51:** Weekly mean density (gray bars) of sperm whales at long-term sites from 2020 to 2023. Error bars represent ± 1 standard deviation. Shaded blue sections represent periods with no recording effort. Note: y-axis values vary in some cases based on maximum densities. Sperm whale densities were not estimated for the shallow site DC.

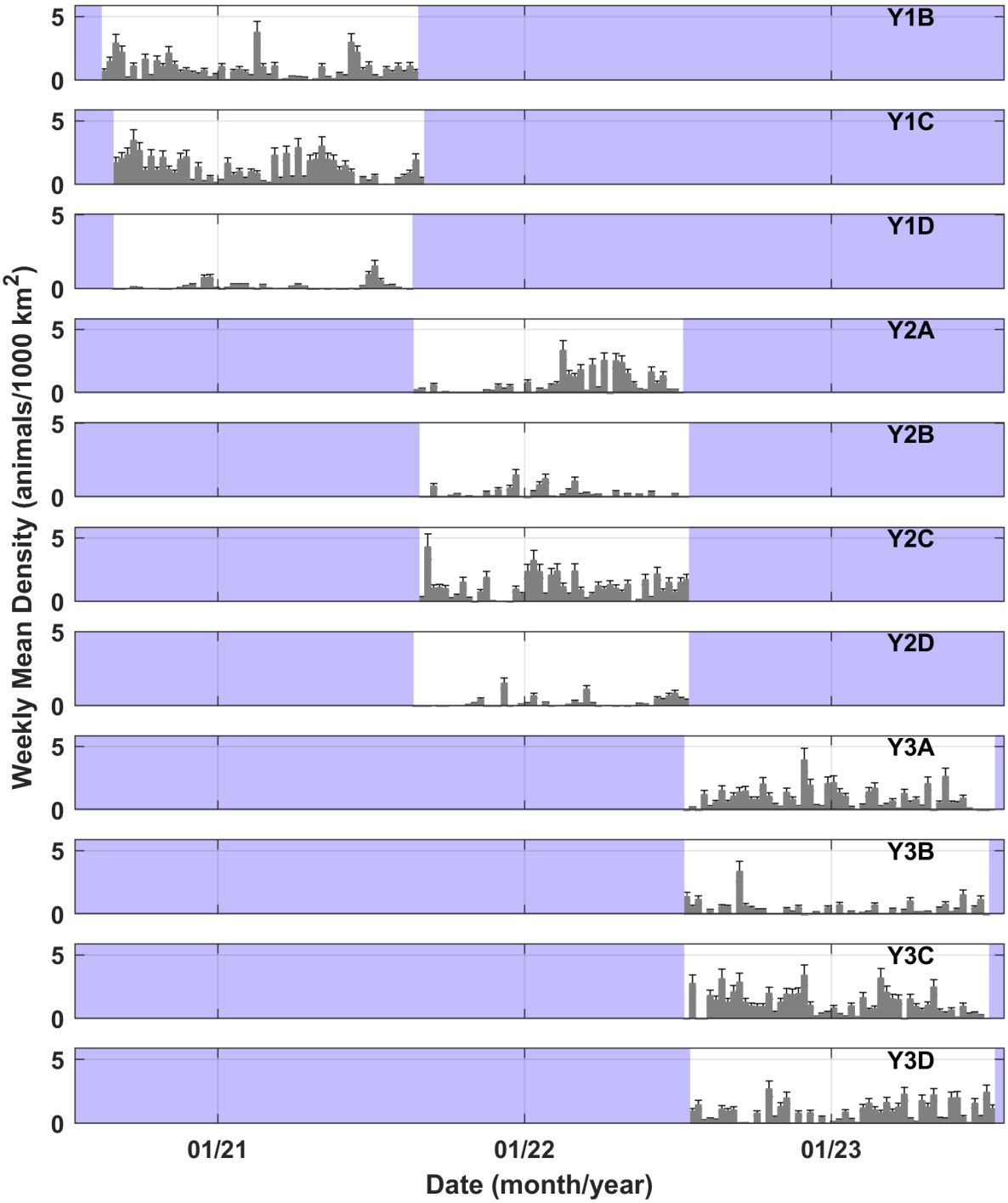


**Figure 52:** Weekly mean density (gray bars) of sperm whales at short-term sites from 2020 to 2023. Error bars represent ± 1 standard deviation. Shaded blue sections represent periods with no recording effort. Note: y-axis values vary in some cases based on maximum densities.

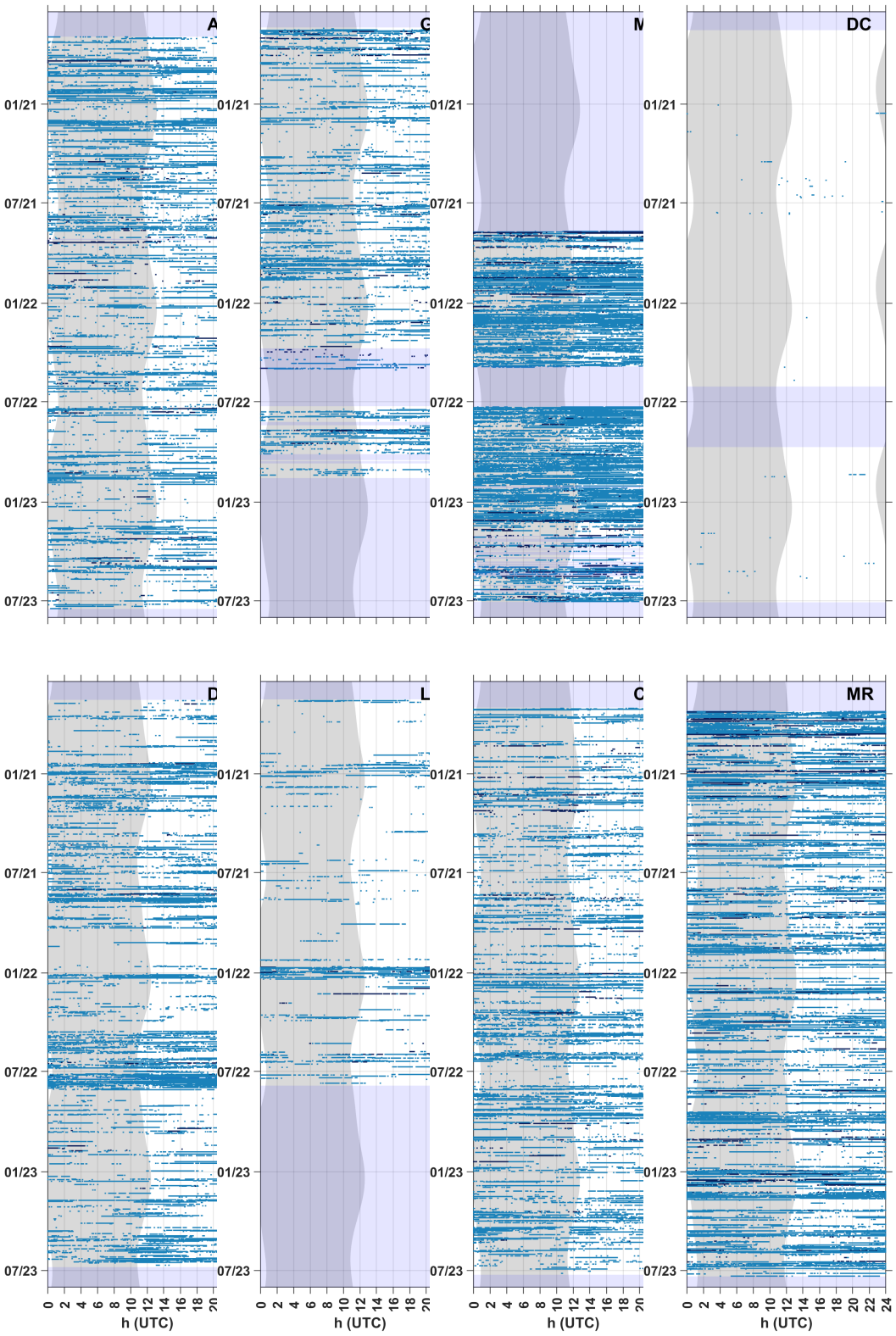


**Figure 53:** Sperm whale echolocation clicks in five-minute bins at long-term sites 2020-2023. Gray vertical shading denotes nighttime and light blue horizontal shading denotes absence of acoustic data. Color denotes number of detections per 5 minutes (light blue: <100; mid blue: 100-1000; dark blue: >1000).

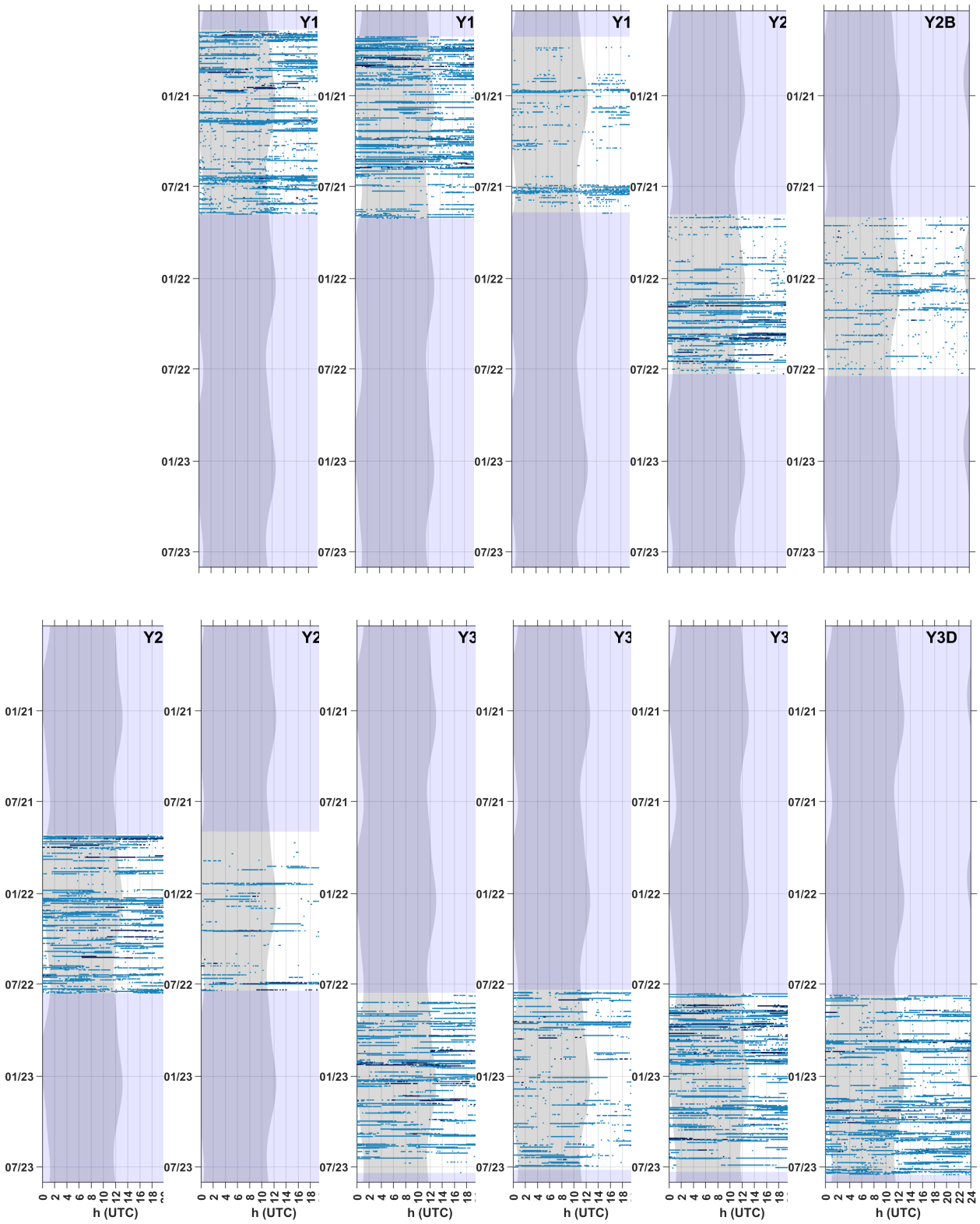


**Figure 54:** Sperm whale echolocation clicks in five-minute bins at short-term sites from 2020-2023. Gray vertical shading denotes nighttime and light blue horizontal shading denotes absence of acoustic data. Color denotes number of detections per 5 minutes (light blue: <100; mid blue: 100-1000; dark blue: >1000).

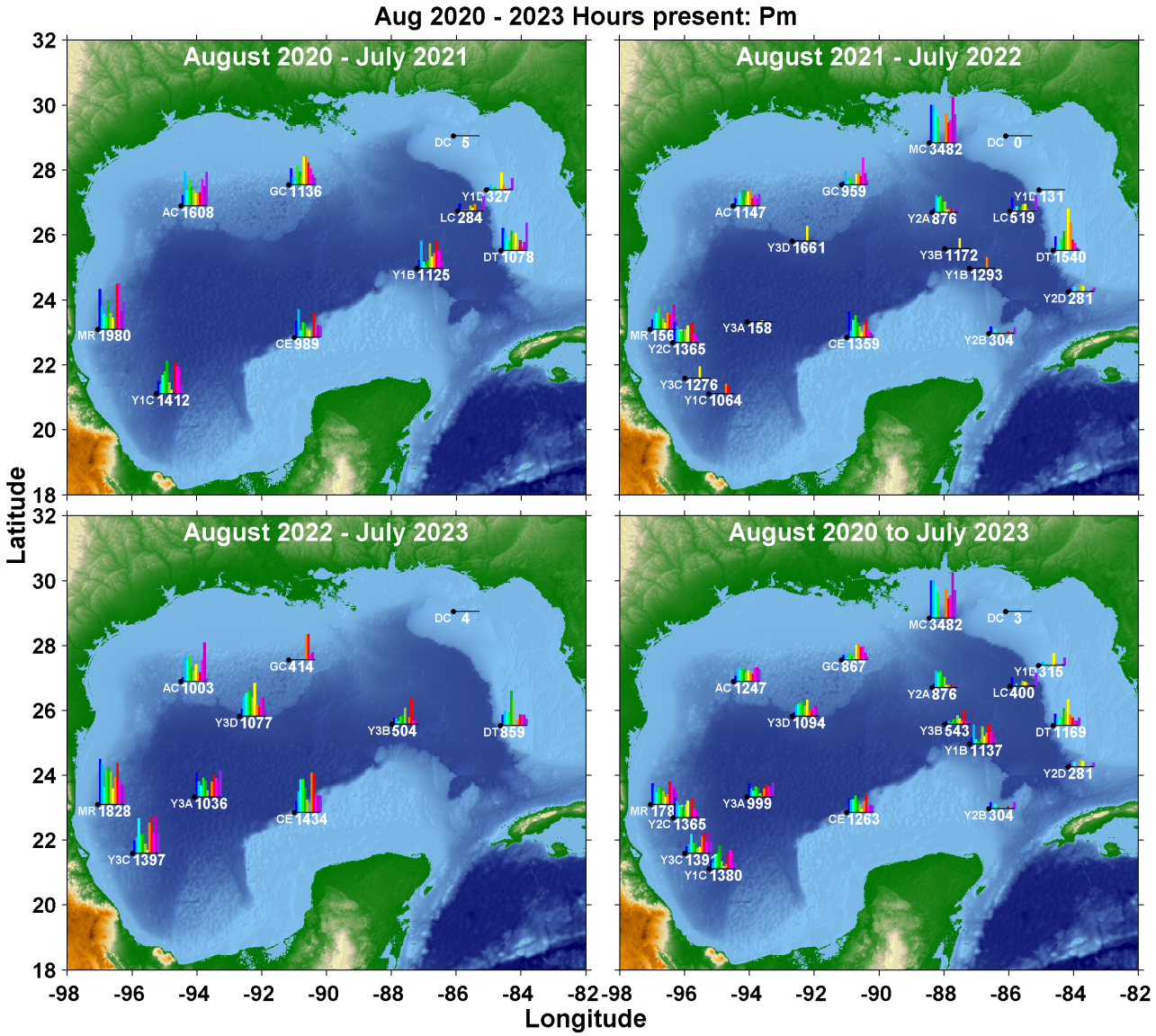


**Figure 55:** Average hourly presence of sperm whale echolocation clicks per month, represented as bar plots, from 2020-2023. Values below bar plots represent mean hours of presence per year. Panels represent presence in each of the three years of recordings with the bottom right panel representing all years combined.

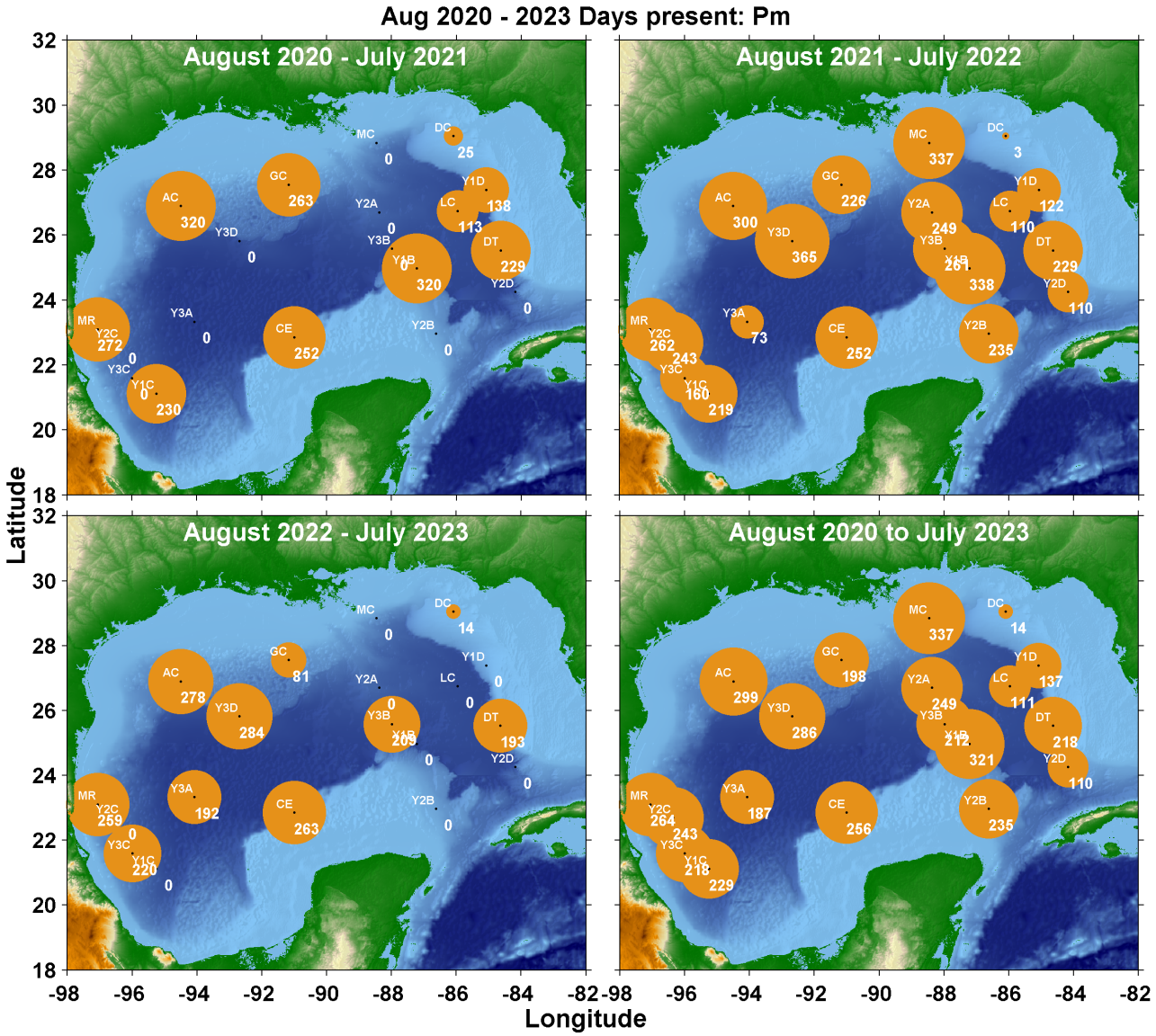


**Figure 56:** Average annual days with sperm whale echolocation click presence from 2020-2023. Panels represent presence in each of the three monitoring years, with the bottom right panel representing yearly means computed across the three years, adjusted for recording effort.

### 4.1.5 *Kogia* spp.

Over this three-year time period, *Kogia* spp. densities were relatively high at most sites, ranging from 4.8 to 44.1 animals estimated per 1,000 $km^2$ (Table 5). Estimated densities of *Kogia* spp. were highest at single year sites Y3D (south of the Sigsbee Escarpment) and Y3C and Y2C (southwestern Gulf) with 44.1, 34.9, and 27.0 animals per 1,000 $km^2$ respectively. Among the long-term sites, the highest densities of *Kogia* spp. was found at Mexican Ridges (MR) with 24.5 animals per 1,000 $km^2$, near the high-density Y2C and Y3C sites. Mean densities at all other long-term sites were lower, between 4.3 and 18.5 animals per 1,000 $km^2$ (Table 5). No clear evidence of seasonal variation in densities (Figures 57 & 58) or diel patterns in acoustic detections were observed at any site (Figures 59 & 60). Encounter durations are short due to limited detection ranges of this species' high frequency clicks. Density estimates from this report are preliminary and require further review to be made directly comparable with historical estimates due to sensor sensitivity differences above 90 kHz.

Hourly presence of *Kogia* spp. was higher at western Gulf sites in the vicinity of Mexican Ridges and in the deep basin (Figure 61). Presence was widespread and common across sites, ranging from an average of presence on 21% of days per year at site CE to 72% of days per year at site Y3D (Figure 62). At shallow site DC, *Kogia* spp. detections were present an average of 133 days per year from 2020-2023, but densities were not estimated due to a lack of information on dive behaviors of this species in shallow water.

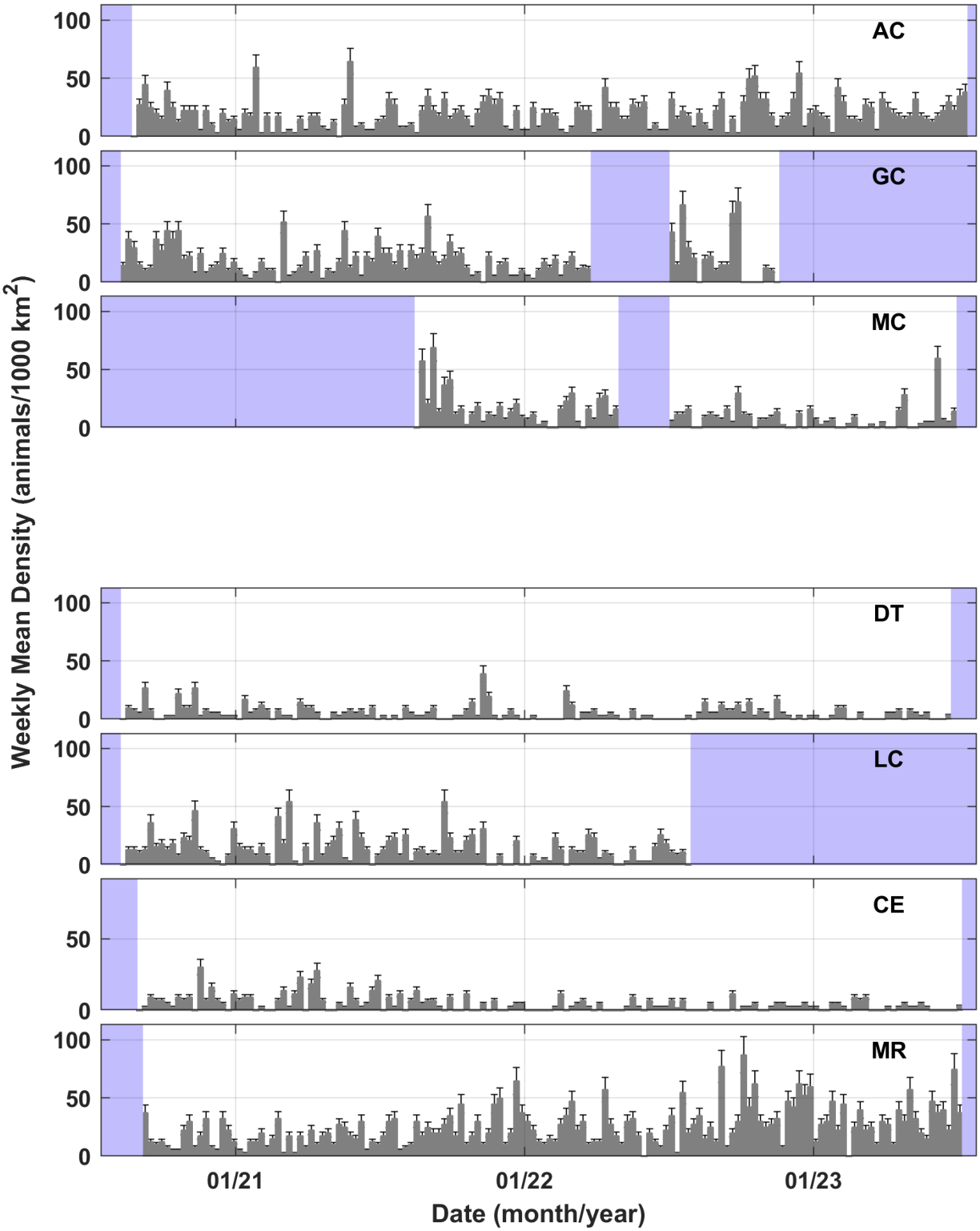


**Figure 57:** Weekly mean daily density (gray bars) of *Kogia* spp. at long-term sites from 2020 to 2023. Error bars represent ± 1 standard deviation. Shaded blue sections represent periods with no recording effort. Note: y-axis values vary for each site based on maximum densities. *Kogia* spp. densities were not estimated for the shallow site DC.

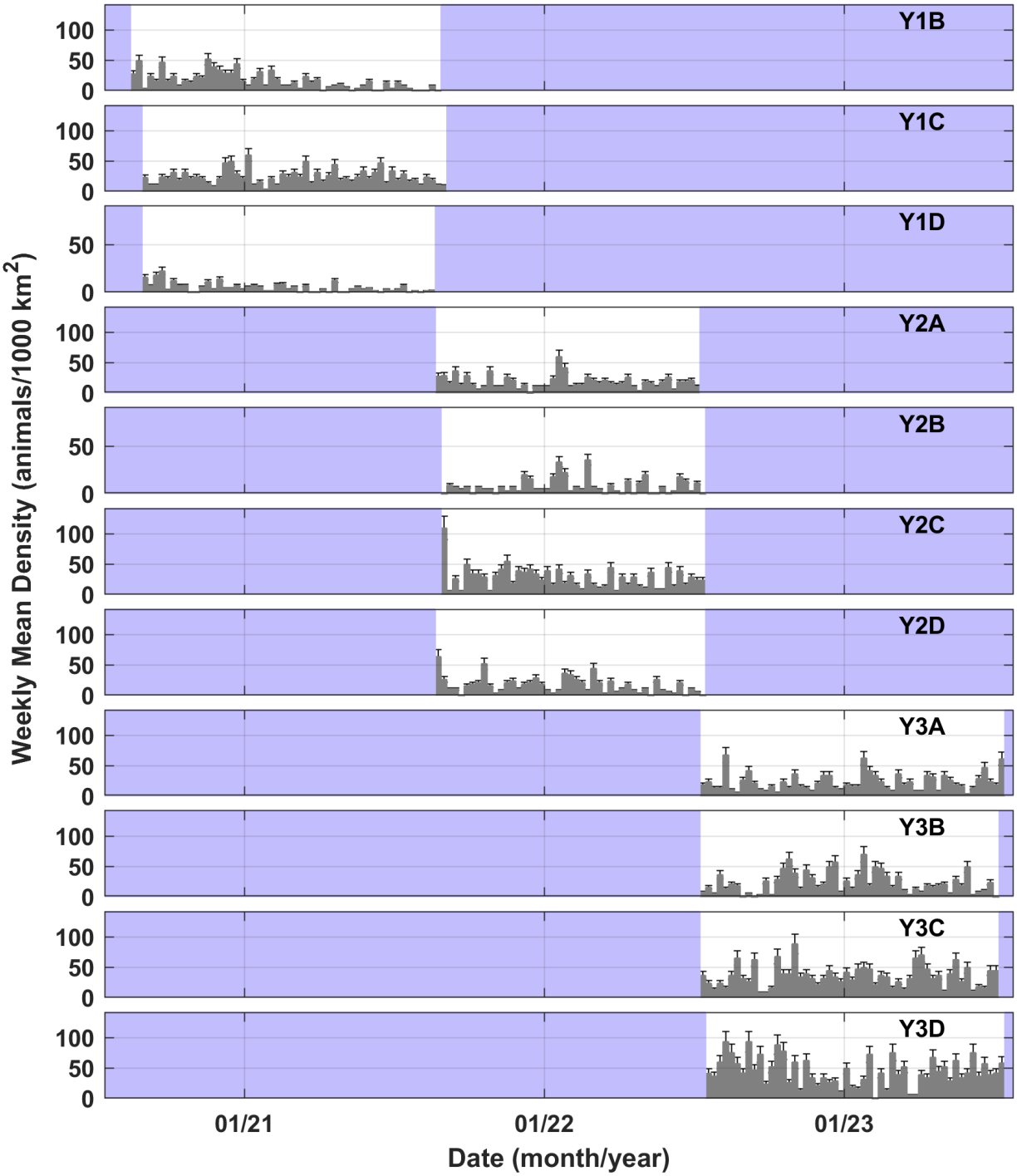


**Figure 58:** Weekly mean daily density (gray bars) of *Kogia* spp. at short-term sites from 2020 to 2023. Error bars represent ± 1 standard deviation. Shaded blue sections represent periods with no recording effort. Note: y-axis values vary for each site based on maximum densities.

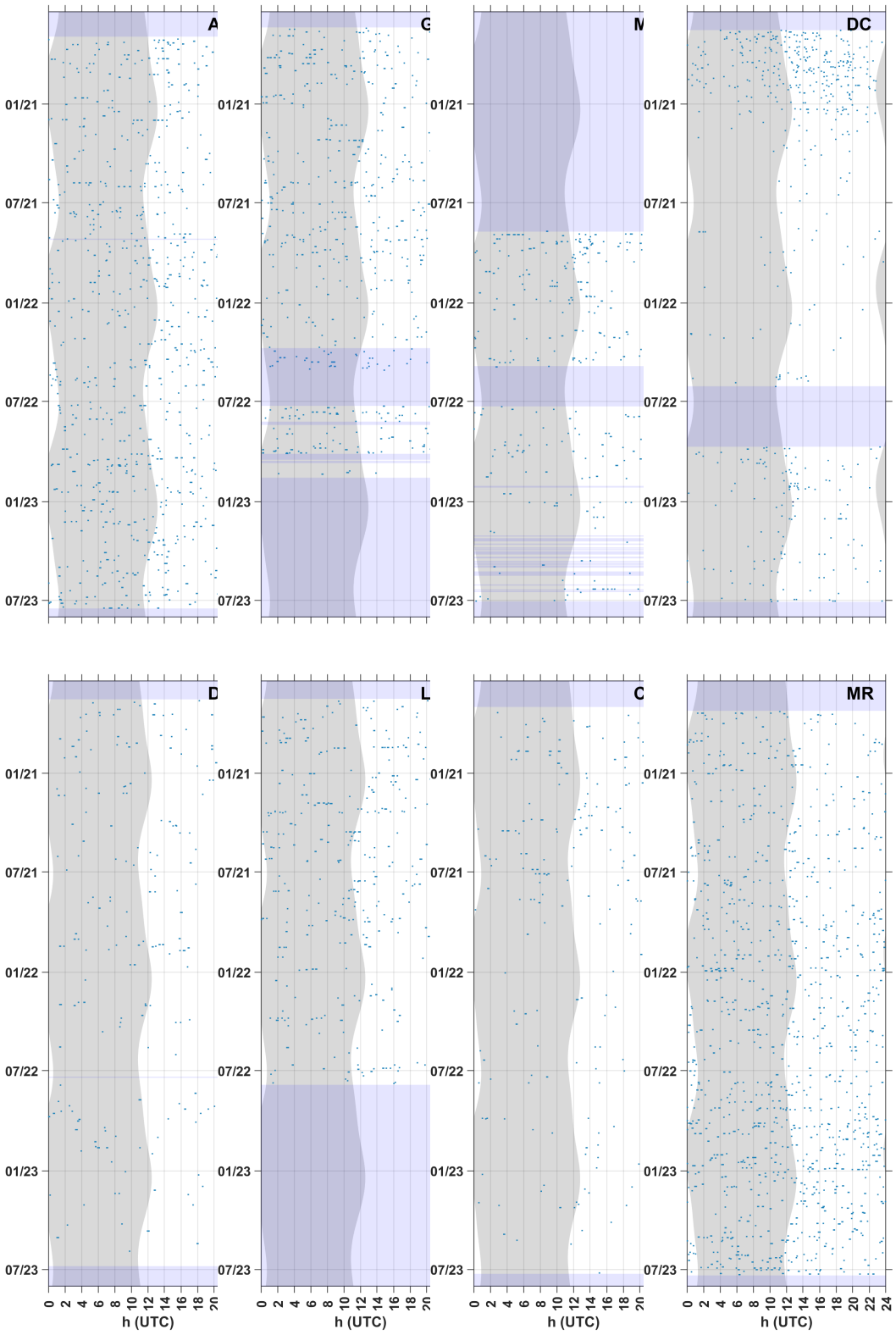


**Figure 59:** *Kogia* spp. echolocation clicks in five-minute bins at long-term sites from 2020-2023. Gray vertical shading denotes nighttime and light blue horizontal shading denotes absence of acoustic data. Color denotes number of detections per 5 minutes (light blue: <100; mid blue: 100-1000; dark blue: >1000).

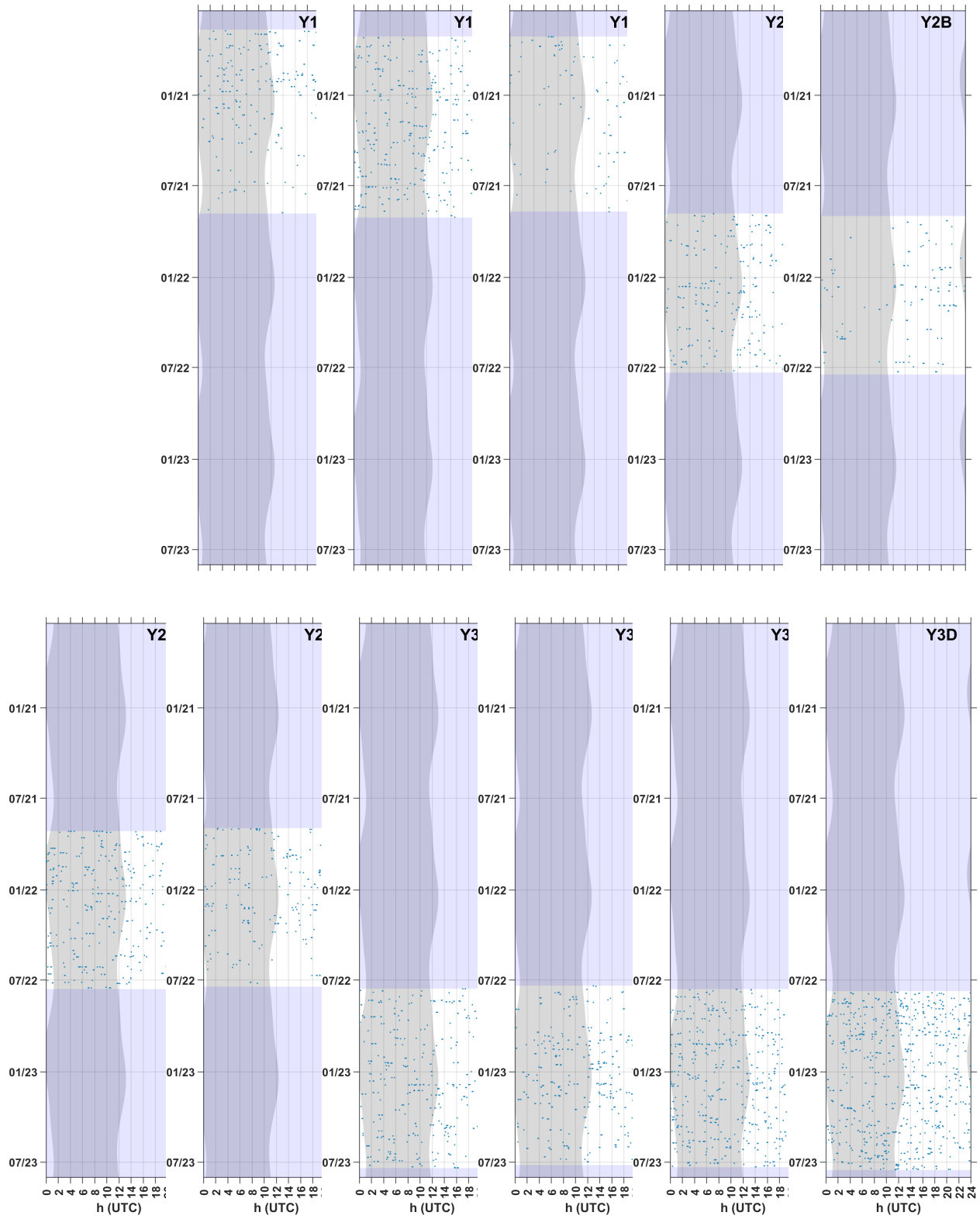


**Figure 60:** *Kogia* spp. echolocation clicks in five-minute bins at short-term sites from 2020-2023. Gray vertical shading denotes nighttime and light blue horizontal shading denotes absence of acoustic data. Color denotes number of detections per 5 minutes (light blue: <100; mid blue: 100-1000; dark blue: >1000).

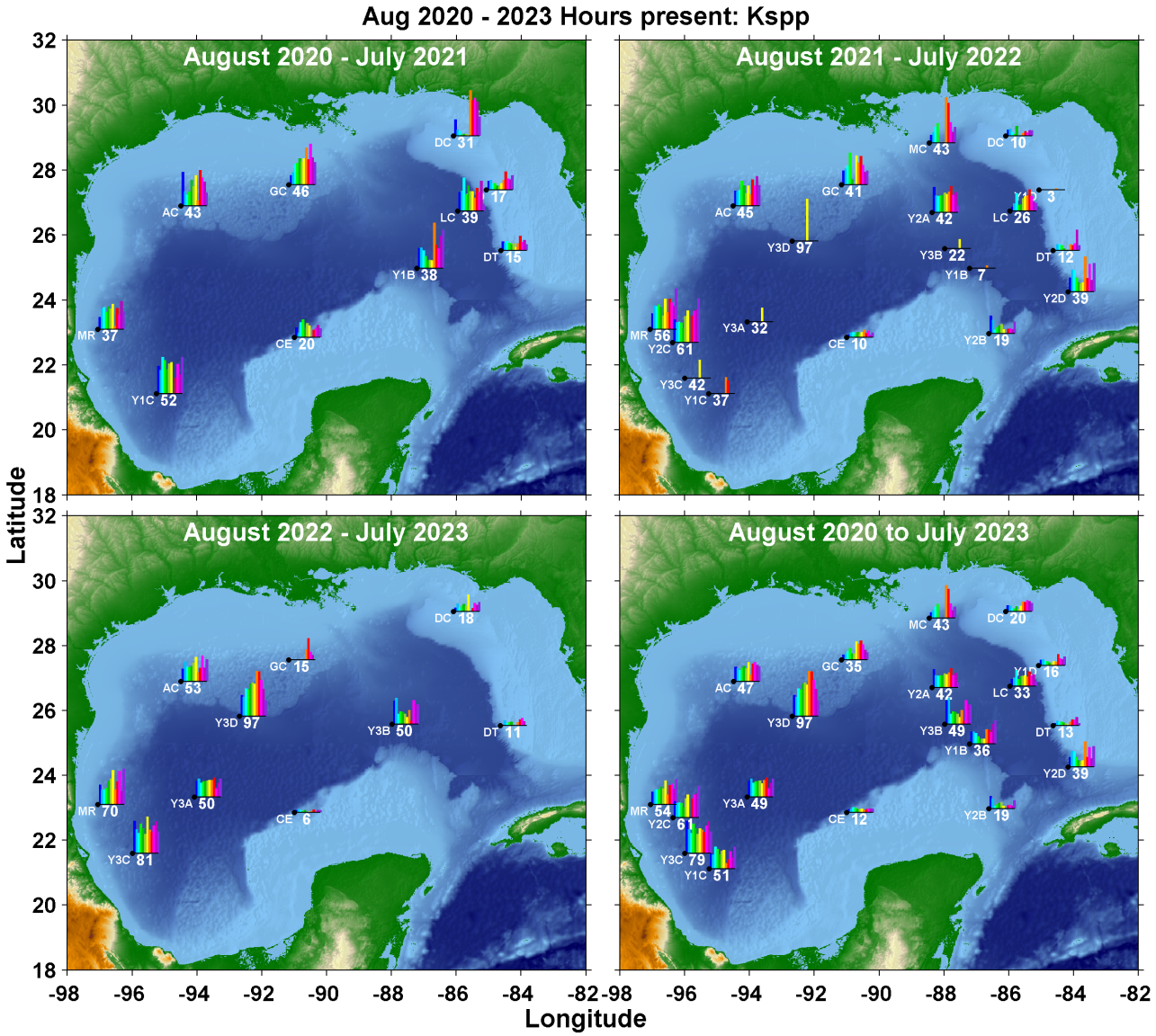


**Figure 61:** Average hourly presence of *Kogia* spp. echolocation clicks per month, represented as bar plots, from 2020-2023. Values below bar plots represent mean hours of presence per year. Panels represent presence in each of the three years of recordings with the bottom right panel representing all years combined.

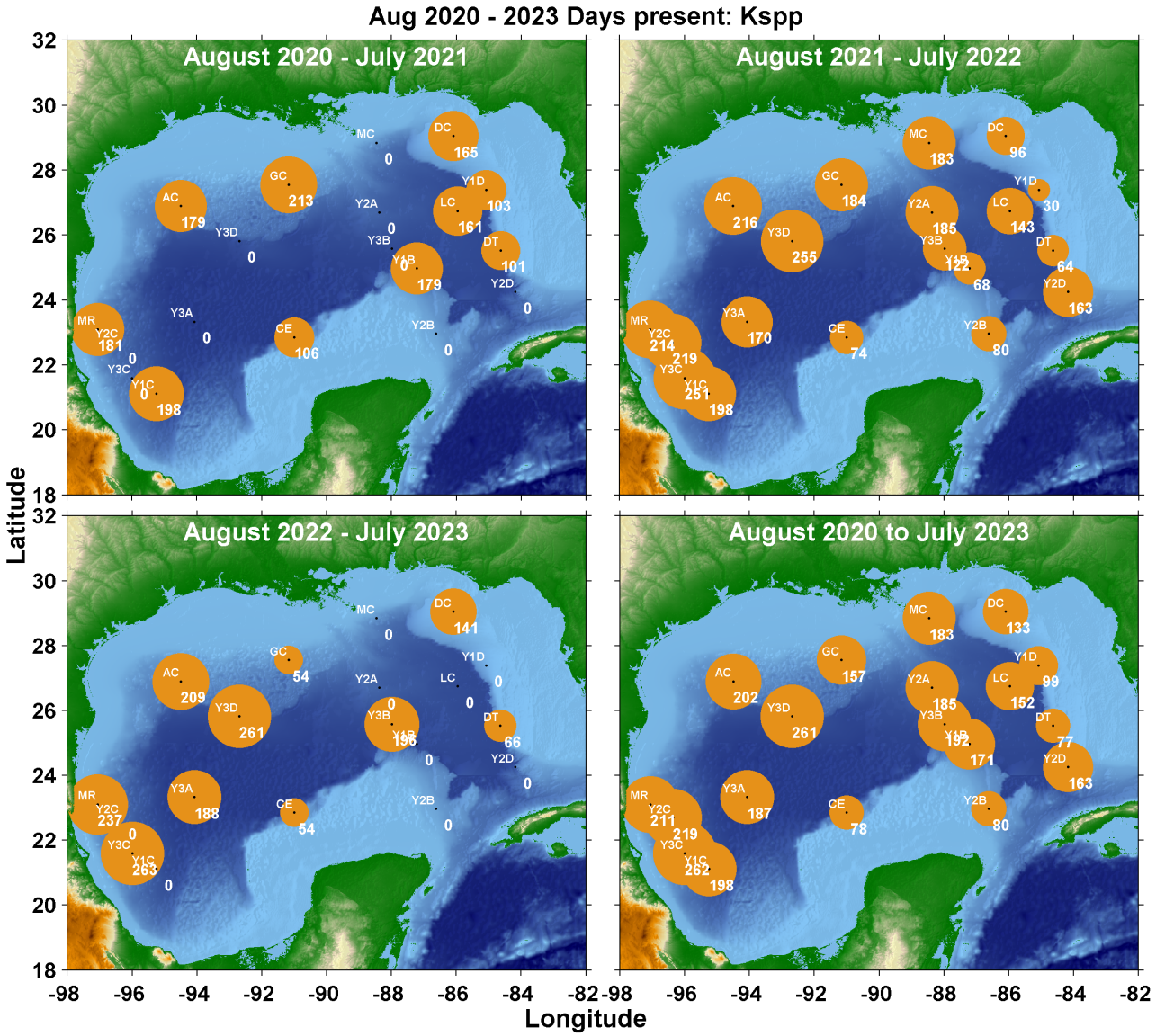


**Figure 62:** Days with presence of *Kogia* spp. echolocation clicks from 2020-2023. Panels represent presence in each of the three monitoring years, with the bottom right panel representing yearly means computed across the three years, adjusted for recording effort.

### 4.1.6 Risso's Dolphin

Risso's dolphin densities were highest at eastern Gulf sites with estimated mean densities of 99.8 animals per 1,000 $km^2$ at site DT and 45.5 animals per 1,000 $km^2$ (5) at site Y1D. Densities were moderately high at sites Y2B and Y2D (22.0 and 19.2 animals per 1,000 $km^2$, respectively), while densities at all other sites were considerably lower, ranging from 0.9 to 9.6 animals per 1,000 $km^2$ (5). Densities at sites MC and GC were lower than historic estimates, with 9.7 and 4.7 animals estimated per 1,000 $km^2$ during 2020-2023 compared with 27.7 and 11.7 animals per 1,000 $km^2$ estimated for 2010, respectively (Frasier et al. In Review). Densities appeared to increase relative to historic estimates at site DT (62.8 animals per 1,000 $km^2$ estimated in 2010). Clear seasonality is observed at most sites for this species, however the timing and strength of seasonal peaks differs among sites. At the highest density site DT, located toward the southern end of the West Florida Shelf, seasonal peaks occur in late fall and winter, while at site MC in the north central Gulf, peaks occur in spring, and at sites AC and CE in the western Gulf, peaks occur in summer (Figures 51 & 52).

A strong tendency toward nocturnal detections is visible at nearly all sites and is most apparent at sites DT and Y1D where Risso's dolphin densities were highest (Figures 65 & 66). Patterns at the shallow site DC are notably different. A possible seasonal pattern with higher numbers of daytime detections in winter, shifting to higher numbers of nighttime encounters in summer is observed. Although they are present at most sites on numerous days each year, Risso's dolphins hourly presence and densities were markedly higher in the southeastern Gulf, at Loop-Current-associated sites (Figure 67). A short-term recording station in the Sigsbee Deep region (Y3A) recorded the fewest number of Risso's dolphin click-positive days (9 days per year), compared with a high of 256 average days of presence per year at site DT (Figure 68).

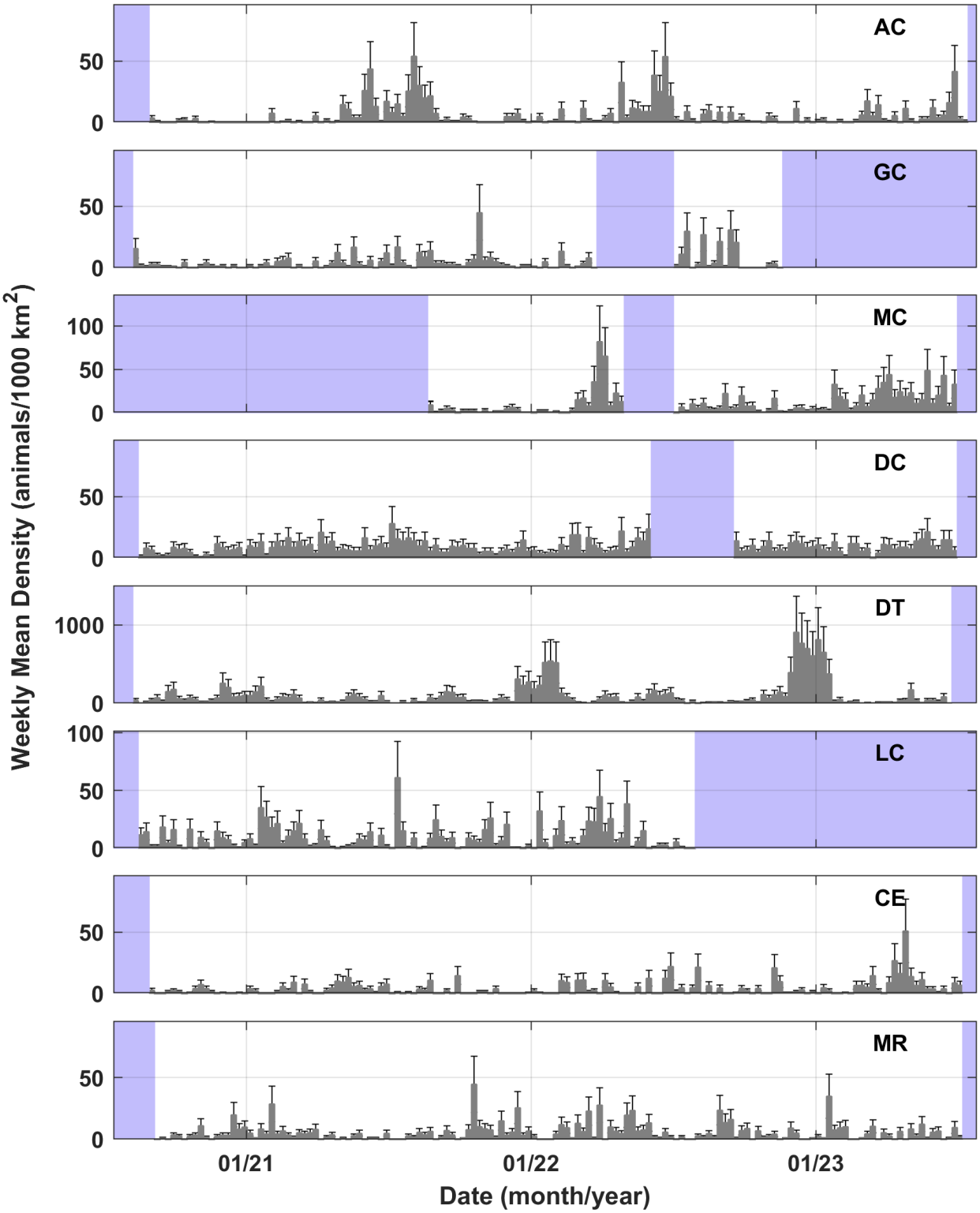


**Figure 63:** Weekly mean density (gray bars) of Risso's dolphins at long-term sites from 2020 to 2023. Error bars represent ± 1 standard deviation. Shaded blue sections represent periods with no recording effort. Note: y-axis values vary in some cases based on maximum densities.

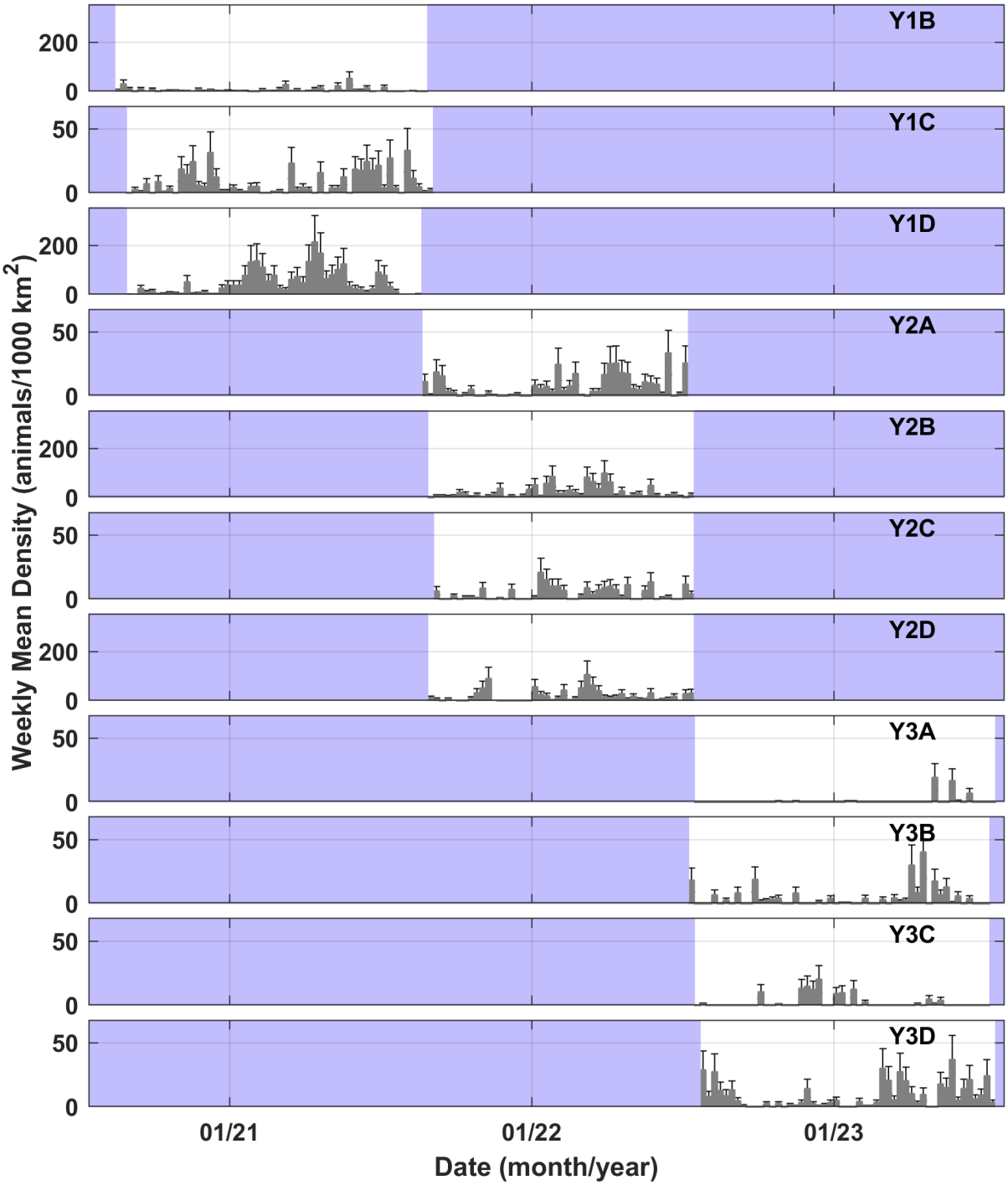


**Figure 64:** Weekly mean density (gray bars) of Risso's dolphins at short-term sites from 2020 to 2023. Error bars represent ± 1 standard deviation. Shaded blue sections represent periods with no recording effort. Note: y-axis values vary in some cases based on maximum densities.

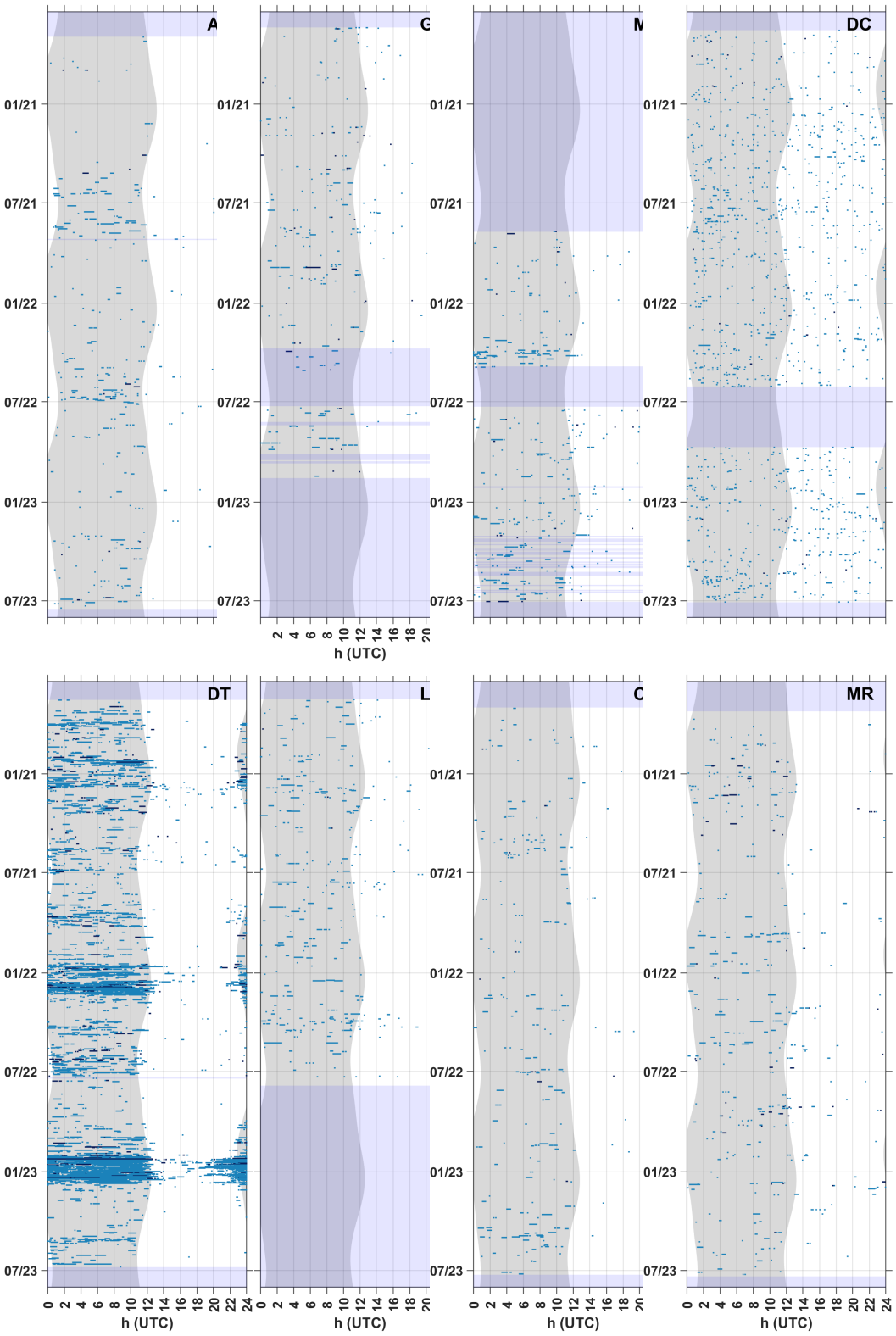


**Figure 65:** Risso's dolphin echolocation clicks in five-minute bins at long-term sites from 2020-2023. Gray vertical shading denotes nighttime and light blue horizontal shading denotes absence of acoustic data. Color denotes number of detections per 5 minutes (light blue: <100; mid blue: 100-1000; dark blue: >1000).

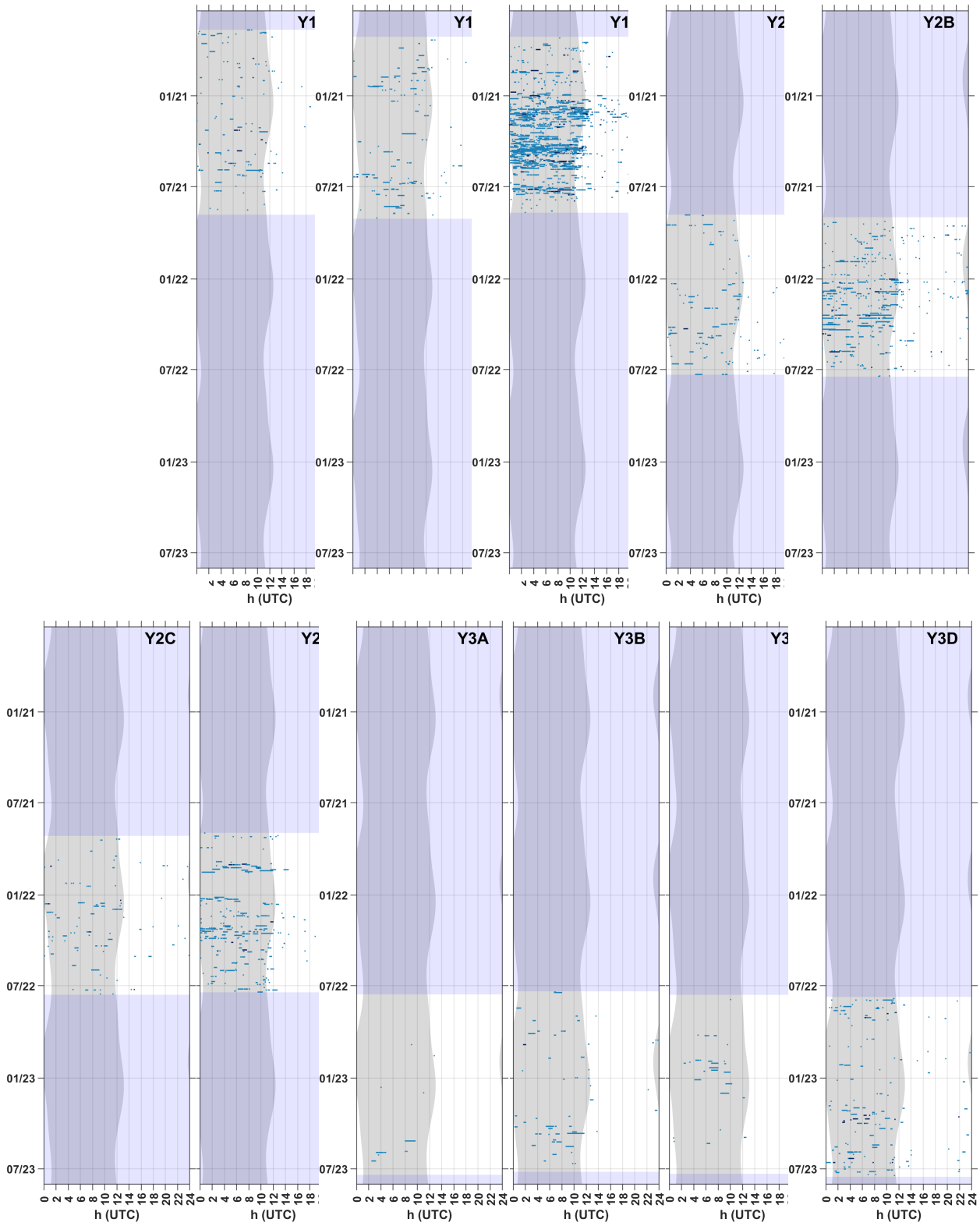


**Figure 66:** Risso's dolphin echolocation clicks in five-minute bins at short-term sites from 2020-2023. Gray vertical shading denotes nighttime and light blue horizontal shading denotes absence of acoustic data. Color denotes number of detections per 5 minutes (light blue: <100; mid blue: 100-1000; dark blue: >1000).

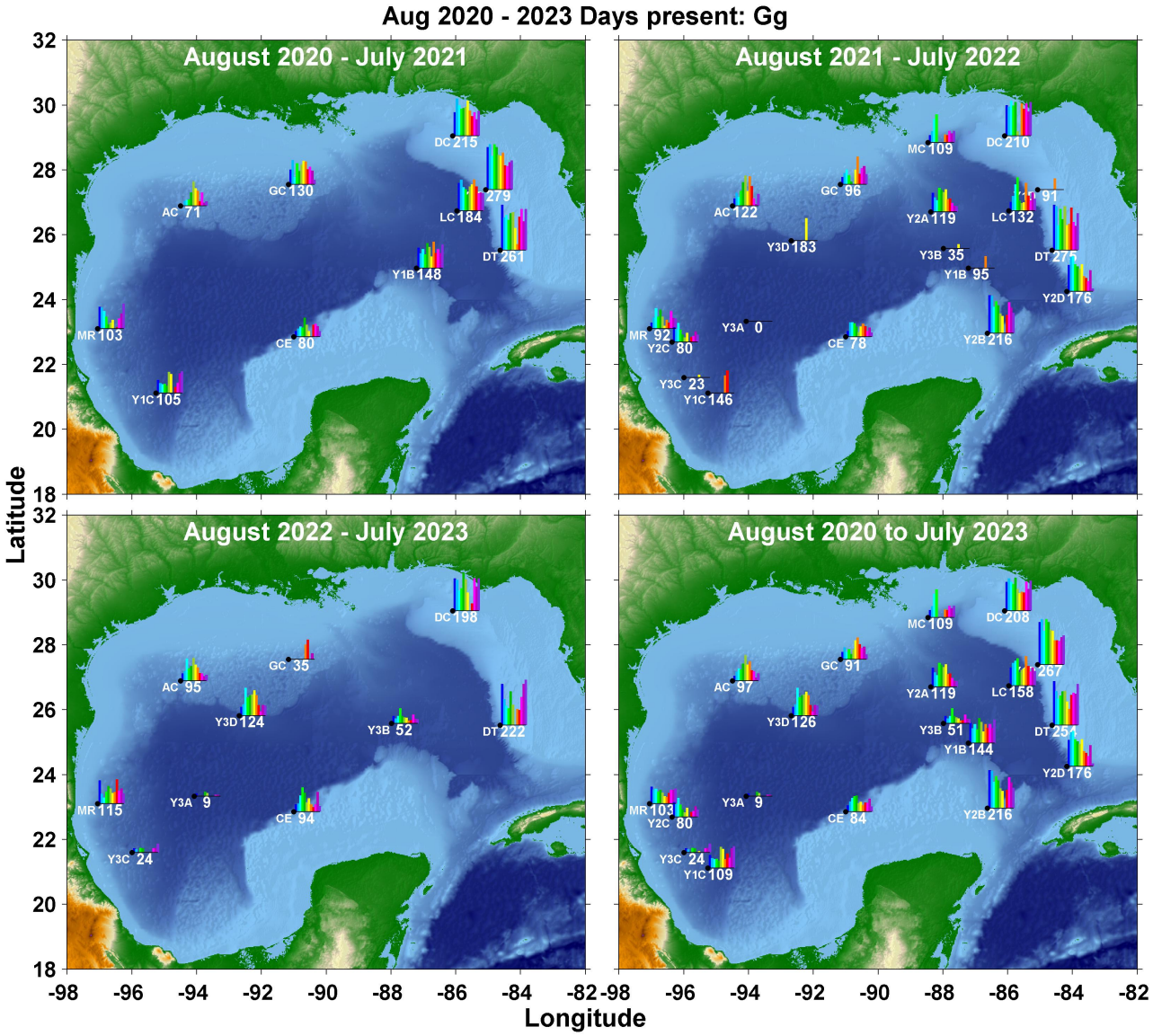


**Figure 67:** Average hourly presence of Risso's dolphin echolocation clicks per month, represented as bar plots, from 2020-2023. Values below bar plots represent mean hours of presence per year. Panels represent presence in each of the three years of recordings with the bottom right panel representing all years combined.

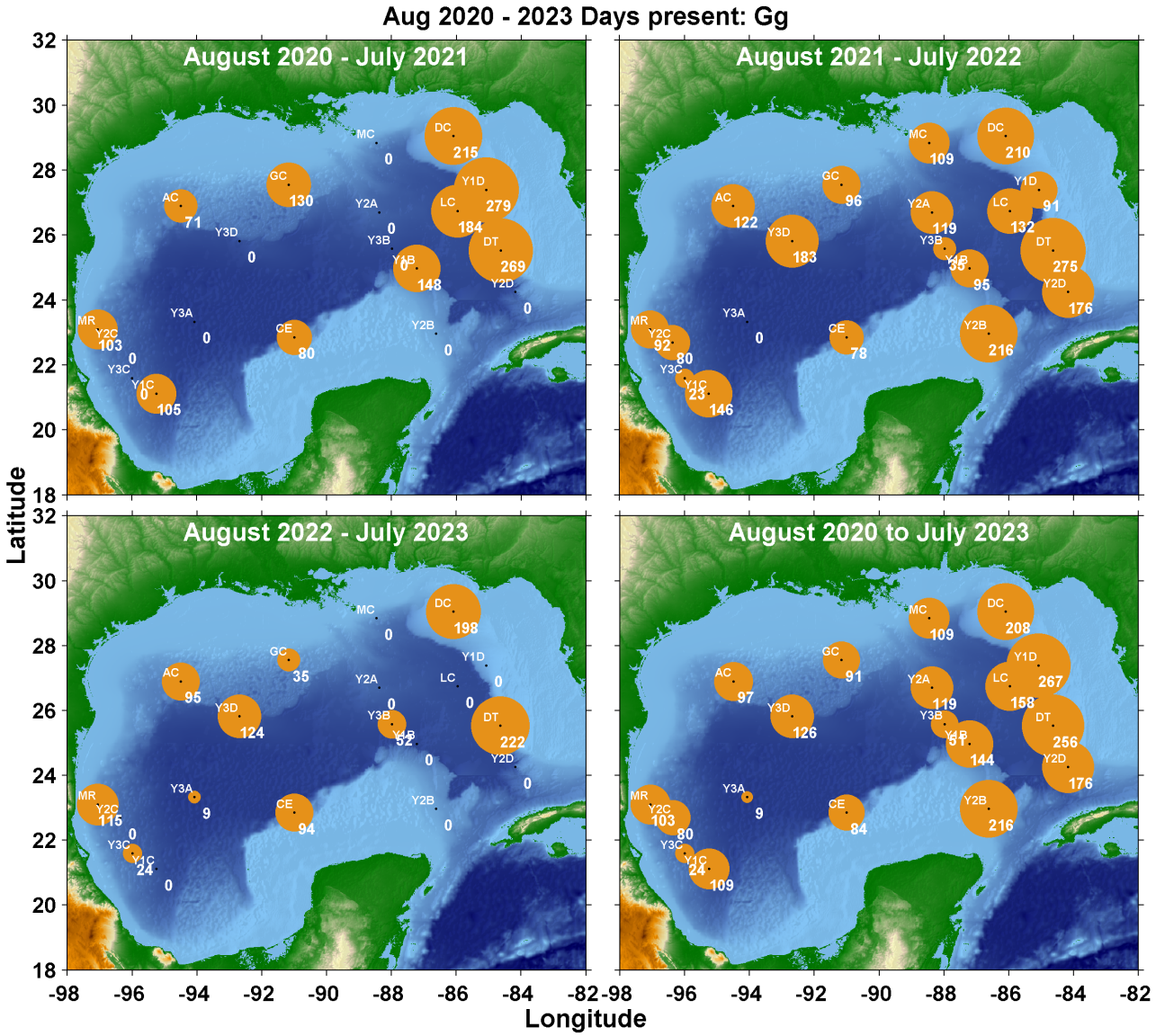


**Figure 68:** Average annual days with Risso's dolphin echolocation click presence from 2020-2023. Panels represent presence in each of the three monitoring years, with the bottom right panel representing yearly means computed across the three years, adjusted for recording effort.

### 4.1.7 Unidentified Dolphins: High-Frequency

Mean densities for unidentified high-frequency dolphins (UD, presumed primarily *Stenella* spp. and offshore *Tursiops truncatus*) were generally high relative to all other marine mammal types (Table 5). Estimated densities at long-term sites were highest at site MC with 703.2 animals per 1,000 $km^2$ , followed by eastern sites DT and LC (622.6 and 508.3 animals per 1,000 $km^2$, respectively), and short-term eastern Gulf sites Y2A, Y2D, and Y3B had high densities between 432.8 and 583.5 animals per 1,000 $km^2$. Long-term sites CE and DC had low densities of high-frequency dolphins (91.5 and 98.8 animals per 1,000 $km^2$ respectively), as did short-term site Y1C in the Bay of Campeche. At site DC, low densities of this high-frequency delphinid class may be related to the dominant presence of a different dolphin class (UD 3P). At site CE, where beaked whale presence was high, dolphin presence was low overall. Preliminary high-frequency dolphin densities during this period were generally lower on than historic estimates of 2010 levels, which ranged from a low of 618.2 to a high of 993.3 animals per 1,000 $km^2$ at sites DC and MC respectively (Frasier et al. In Review).

Densities appear to vary seasonally at many sites, peaking in summer months at sites AC, MC, and DT, as well as site Y2D (Figures 69 & 70). Some single year sites appeared to have winter peaks in density, including Y2B in the southeastern Gulf, and Y3B located in the deep north-central Gulf near site LC. However, one year of data is insufficient to determine whether this is a consistent pattern. Seasonal patterns were less apparent at sites in the southwestern Gulf, including the Bay of Campeche.

A strong tendency toward nocturnal detections is visible at all sites (Figures 71 & 72). However, this pattern is weaker at shallow site DC (Figure 71). This may reflect differences in foraging behavior or foraging preferences related to prey availability, and may also be related to differences in delphinid species composition relative to deeper sites. Unidentified high-frequency dolphin hourly presence was highest at the eastern Gulf sites, including relatively high densities and occurrence at abyssal plain sites with bottom depths greater than 2,500 m (LC, Y2A & Y3A; Figure 73). Species in this unidentified high-frequency dolphin category were detected on an average of 31-35% of days annually at the lowest occupancy sites, and identified on over 70% of days at the highest occupancy sites (Figure 74).

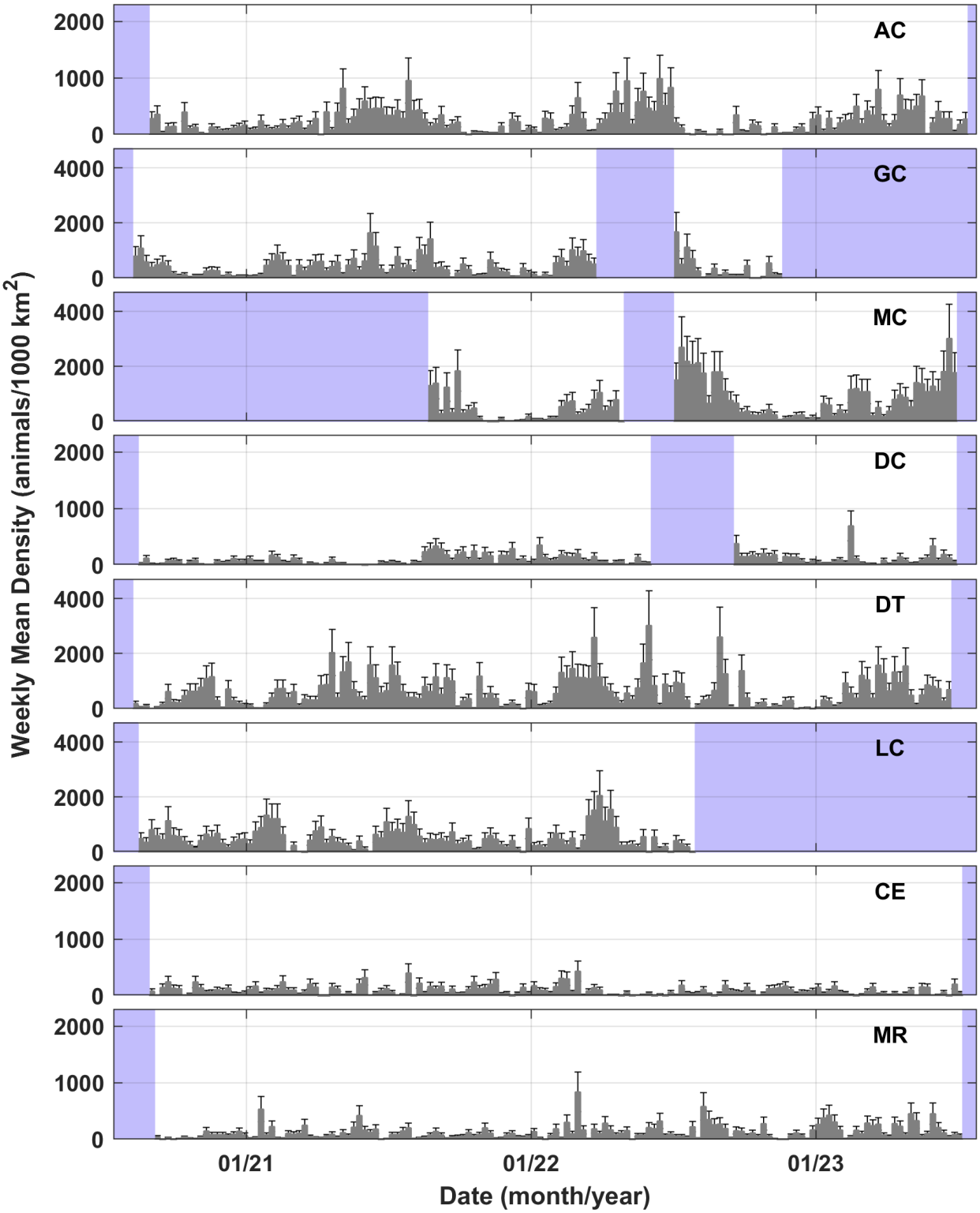


**Figure 69:** Weekly mean density (gray bars) of unidentified high-frequency dolphins at long-term sites from 2020 to 2023. Error bars represent ± 1 standard deviation. Shaded blue sections represent periods with no recording effort. Note: y-axis values vary for each site based on maximum densities.

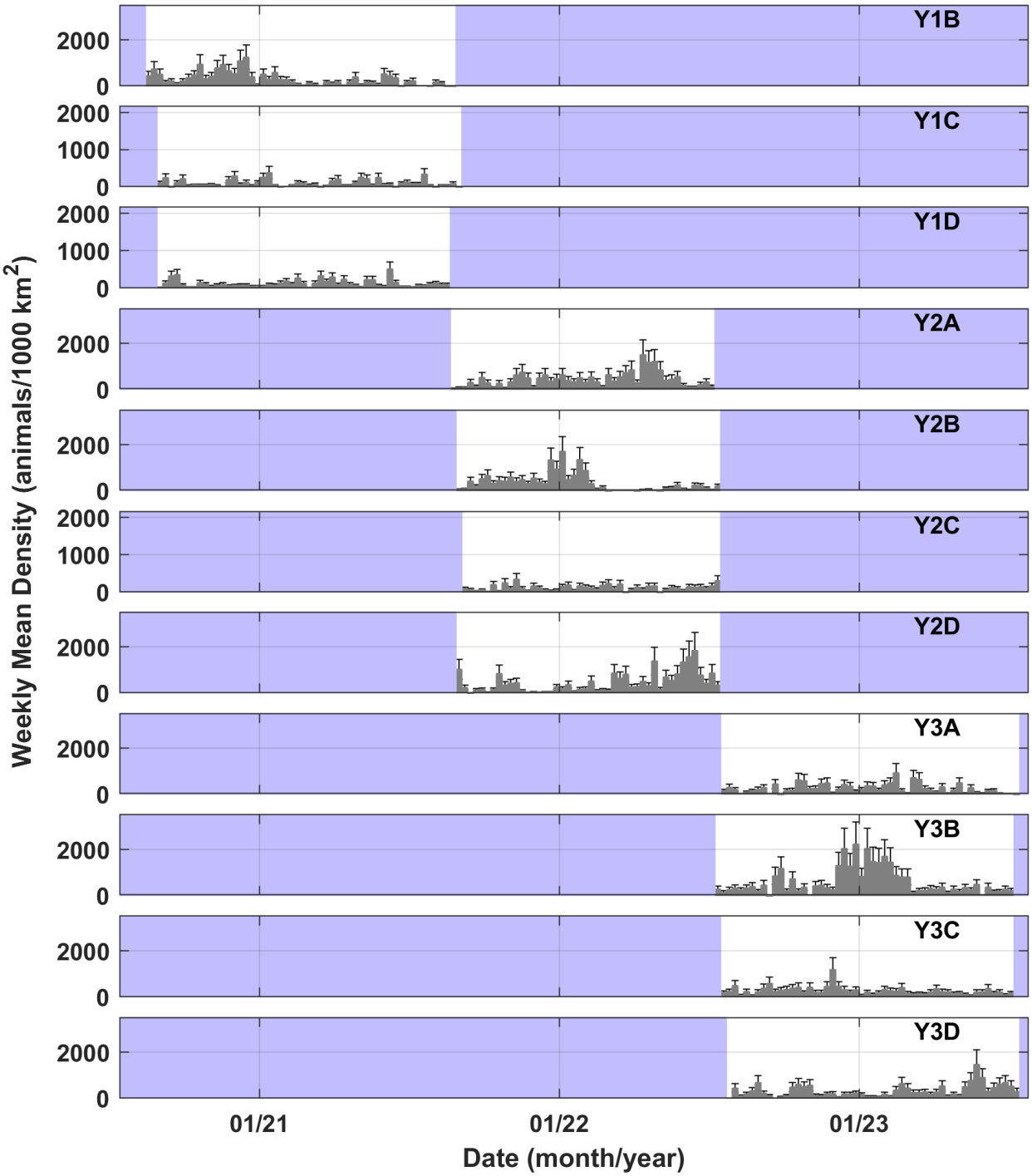


**Figure 70:** Weekly mean density (gray bars) of unidentified high-frequency dolphins at short-term sites from 2020-2023. Error bars represent ± 1 standard deviation. Shaded blue sections represent periods with no recording effort. Note: y-axis values vary for each site based on maximum densities.

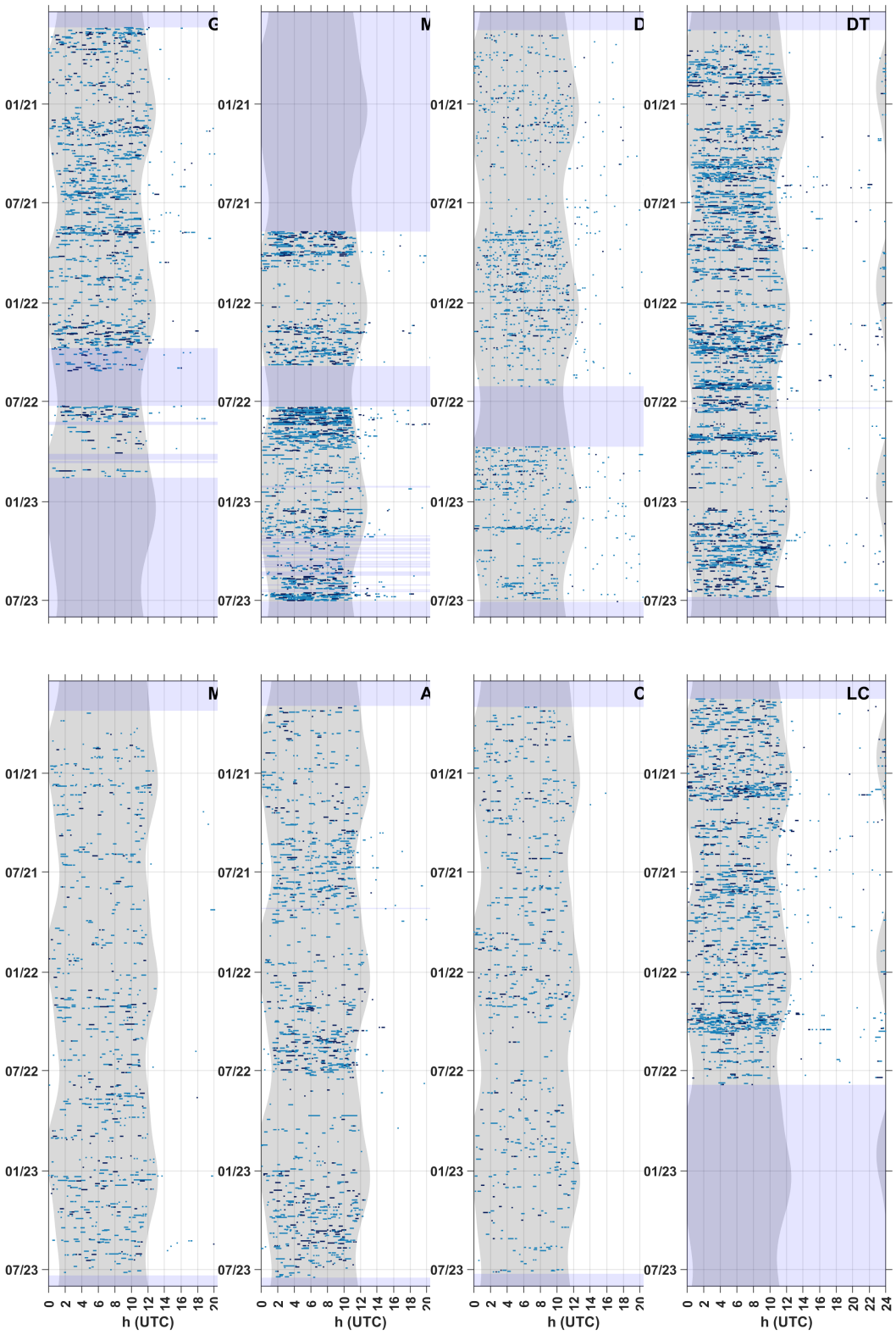


**Figure 71:** Unidentified high-frequency dolphin echolocation clicks in five-minute bins at long-term sites from 2020-2023. Gray vertical shading denotes nighttime and light blue horizontal shading denotes absence of acoustic data. Color denotes number of detections per 5 minutes (light blue: <100; mid blue: 100-1000; dark blue: >1000).

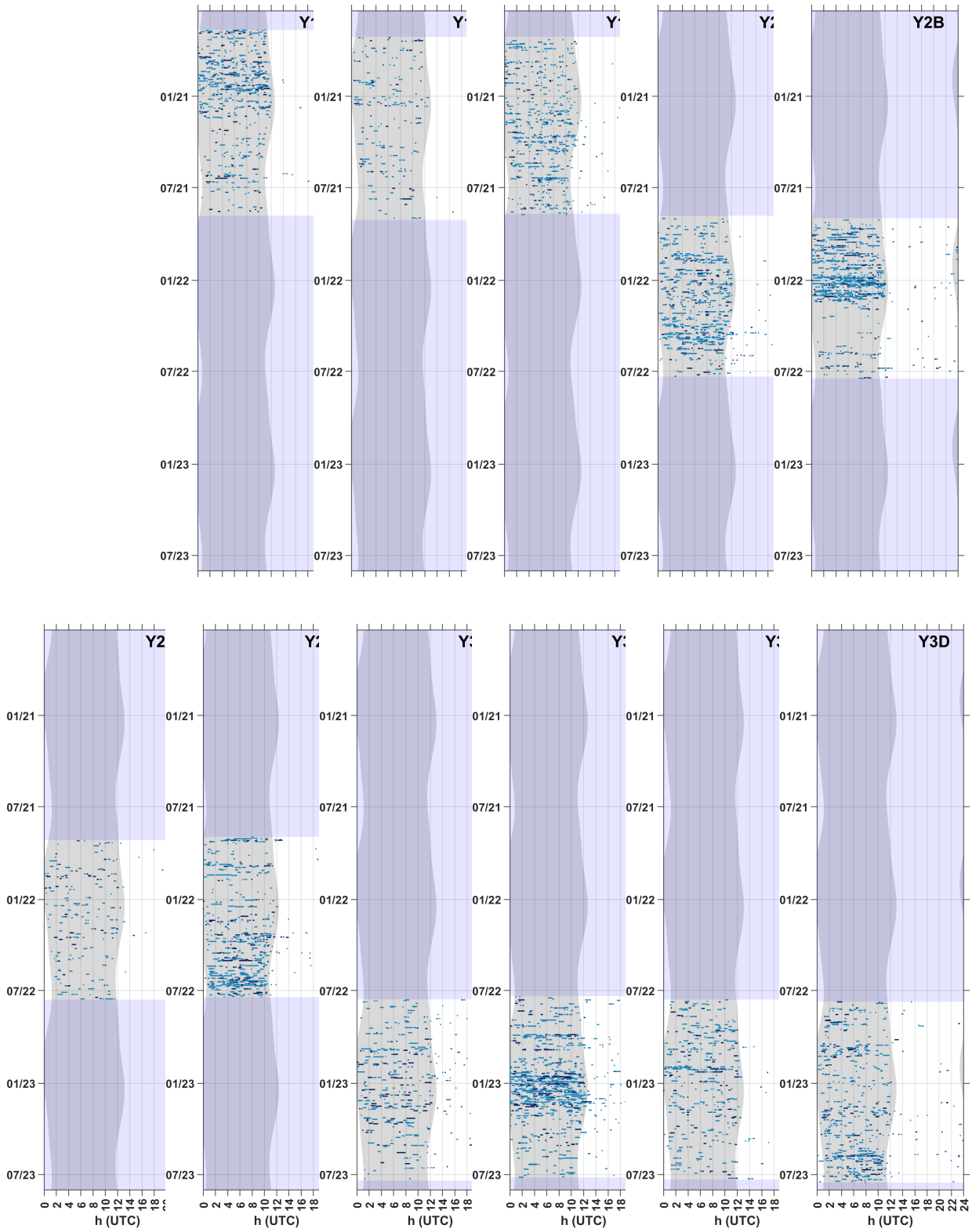


**Figure 72:** Unidentified high-frequency dolphin echolocation clicks in five-minute bins at short-term sites from 2020-2023. Gray vertical shading denotes nighttime and light blue horizontal shading denotes absence of acoustic data. Color denotes number of detections per 5 minutes (light blue: <100; mid blue: 100-1000; dark blue: >1000).

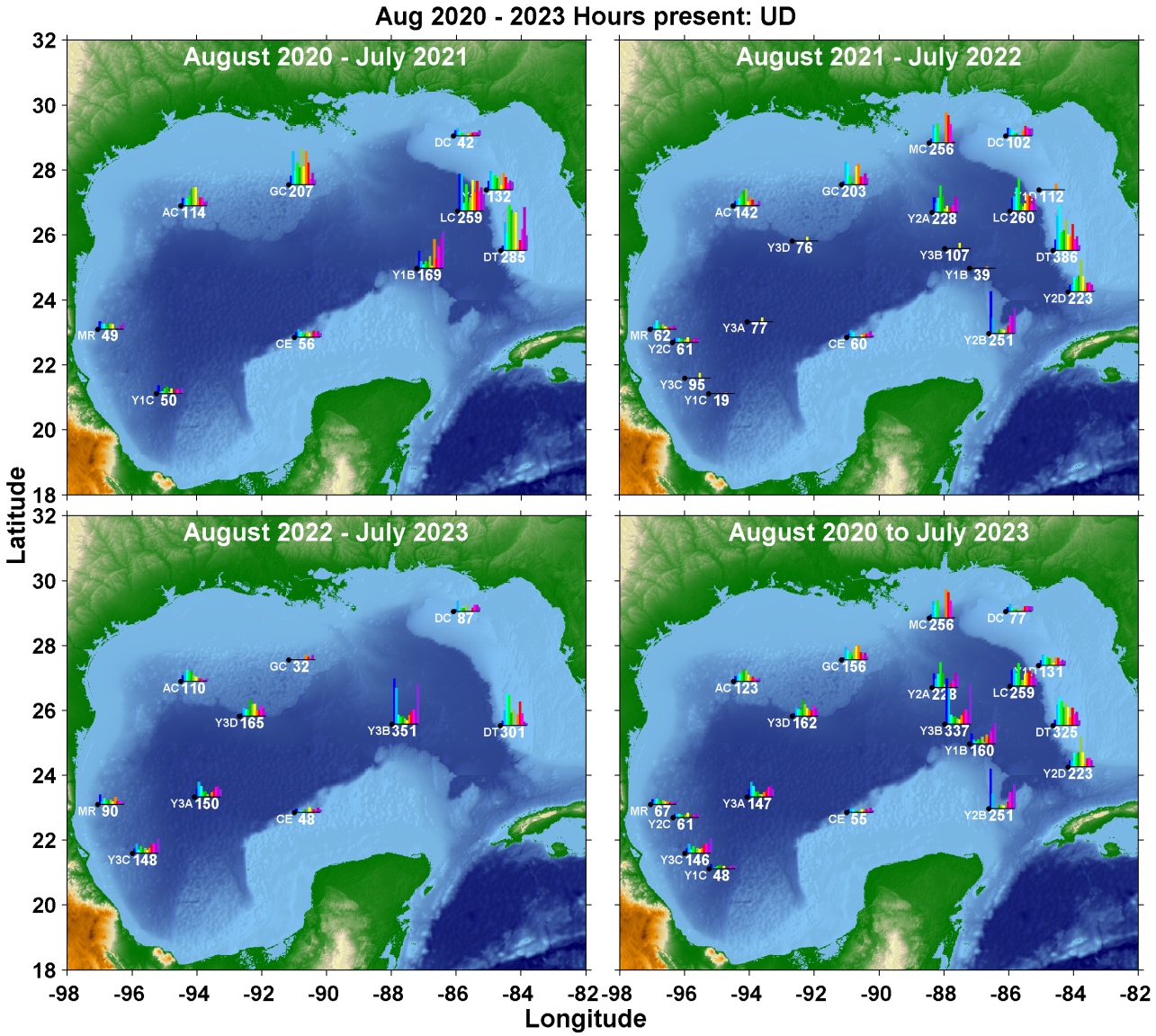


**Figure 73:** Average hourly presence of unidentified high-frequency dolphin echolocation clicks per month, represented as bar plots, from 2020-2023. Values below bar plots represent mean hours of presence per year. Panels represent presence in each of the three years of recordings with the bottom right panel representing all years combined.

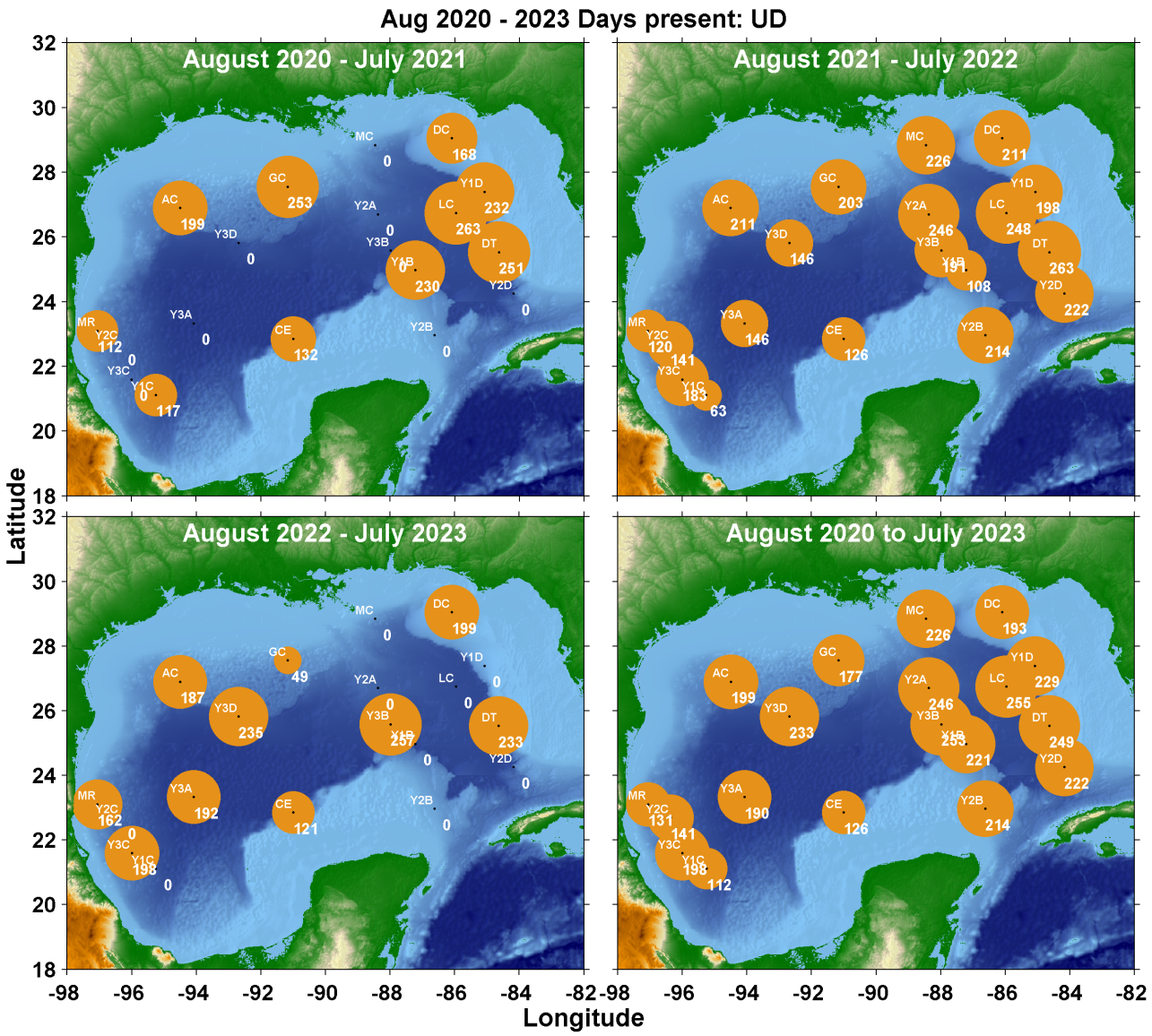


**Figure 74:** Days with presence of unidentified high-frequency dolphin echolocation clicks from 2020-2023. Panels represent presence in each of the three monitoring years, with the bottom right panel representing yearly means computed across the three years, adjusted for recording effort.

### 4.1.8 Unidentified Dolphins: Three-Peak

Mean densities of the unidentified three-peak delphinid type (UD 3P) were high at shallow site DC with 565.6 animals per 1,000 $km^2$ (Table 5). This click type was also identified in relatively high densities at site Y2B, on the eastern side of the Yucatan Peninsula (79.5 animals per 1,000 $km^2$; bottom depth $\sim$700m). Mean estimated densities at all other sites were low, ranging from 3.2 to 29.7 animals per 1,000 $km^2$ (Table 5). At site DC, UD 3P densities remained relatively constant year-round, but were elevated in the spring through late summer of 2021 (Figure 75). A brief period of high density of UD 3P was observed at site DT from December 2022 to January of 2023. Densities were higher in summer, fall and winter than spring at site Y2B (Figure 76).

UD 3P clicks were more commonly-detected during daylight hours during the monitoring period, with some evidence of increased acoustic detections at sunrise. During summer, nocturnal detections seems to increase relative to nocturnal detection levels in winter (Figures 77 & 78). However, at sites Y2B and DT, the acoustic detections were primarily nocturnal. UD 3P hourly presence was highest at site DC, with UD 3P representing over 75% of the species encounters by hour (Figure 31). This class was detected on approximately 311 days per year on average, or over 85% of days (Figures 79 & 80). UD 3P echolocation click days present per year are generally lower across all other sites, ranging from 17 to 168, with detections on more days at sites in the eastern Gulf than the western Gulf (Figure 80).

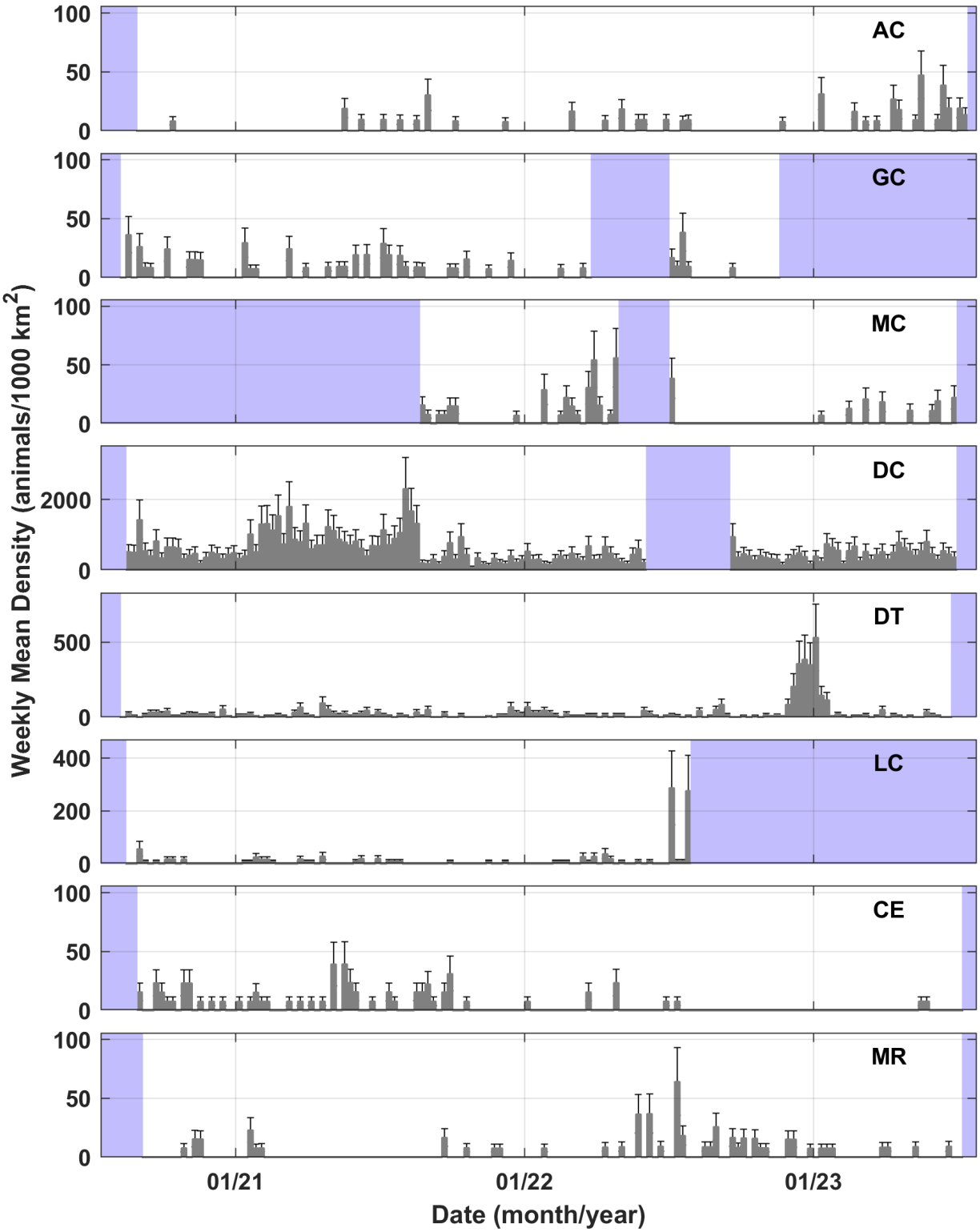


**Figure 75:** Weekly mean daily density (gray bars) of Unidentified three-peak dolphin (UD 3P) echolocation clicks at long-term sites from 2020 to 2023. Error bars represent ± 1 standard deviation. Shaded blue sections represent periods with no recording effort. Note: y-axis values vary for each site based on maximum densities.

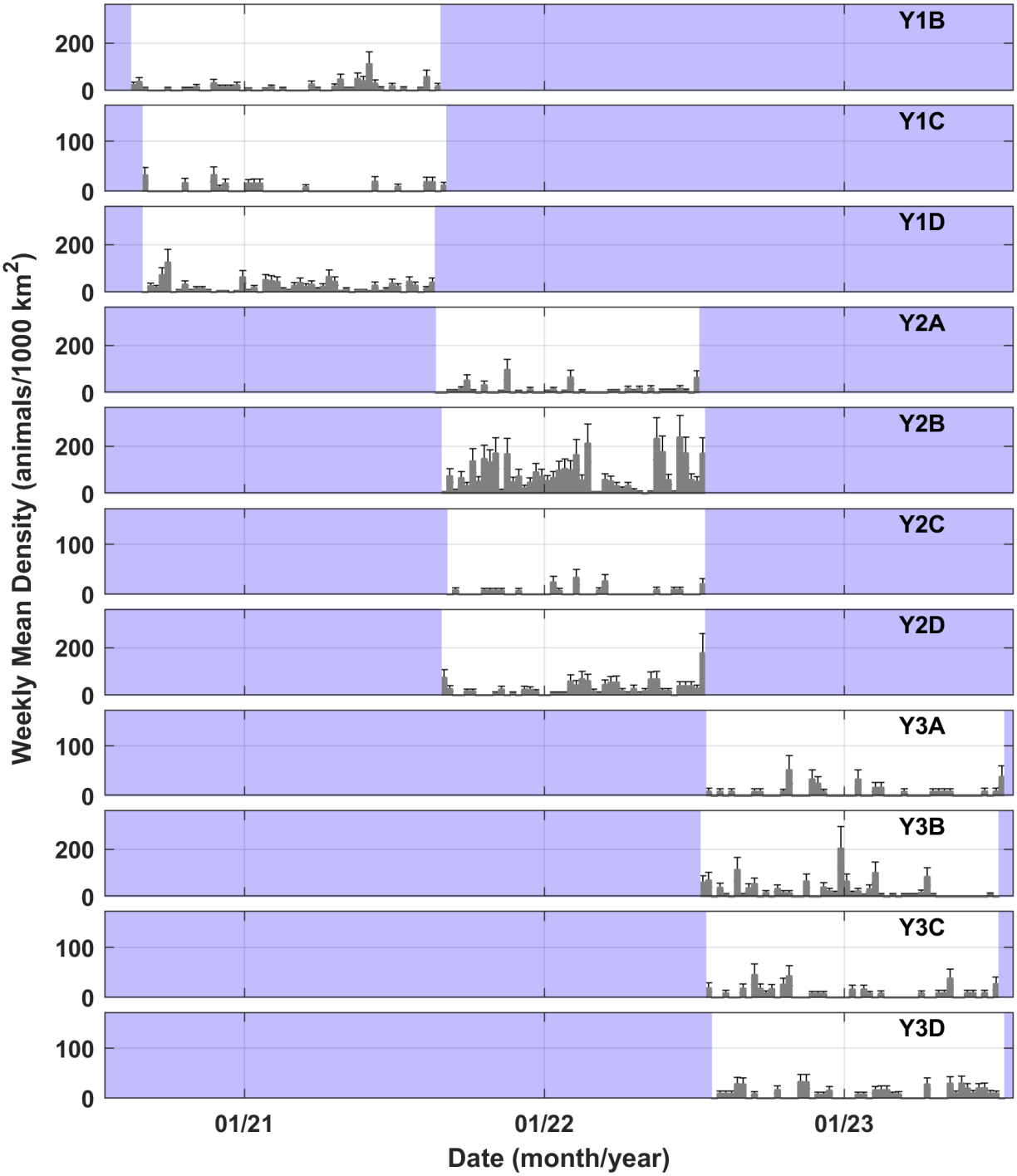


**Figure 76:** Weekly mean daily density (gray bars) of Unidentified three-peak dolphin (UD 3P) echolocation clicks at short-term sites from 2020 to 2023. Error bars represent ± 1 standard deviation. Shaded blue sections represent periods with no recording effort. Note: y-axis values vary for each site based on maximum densities.

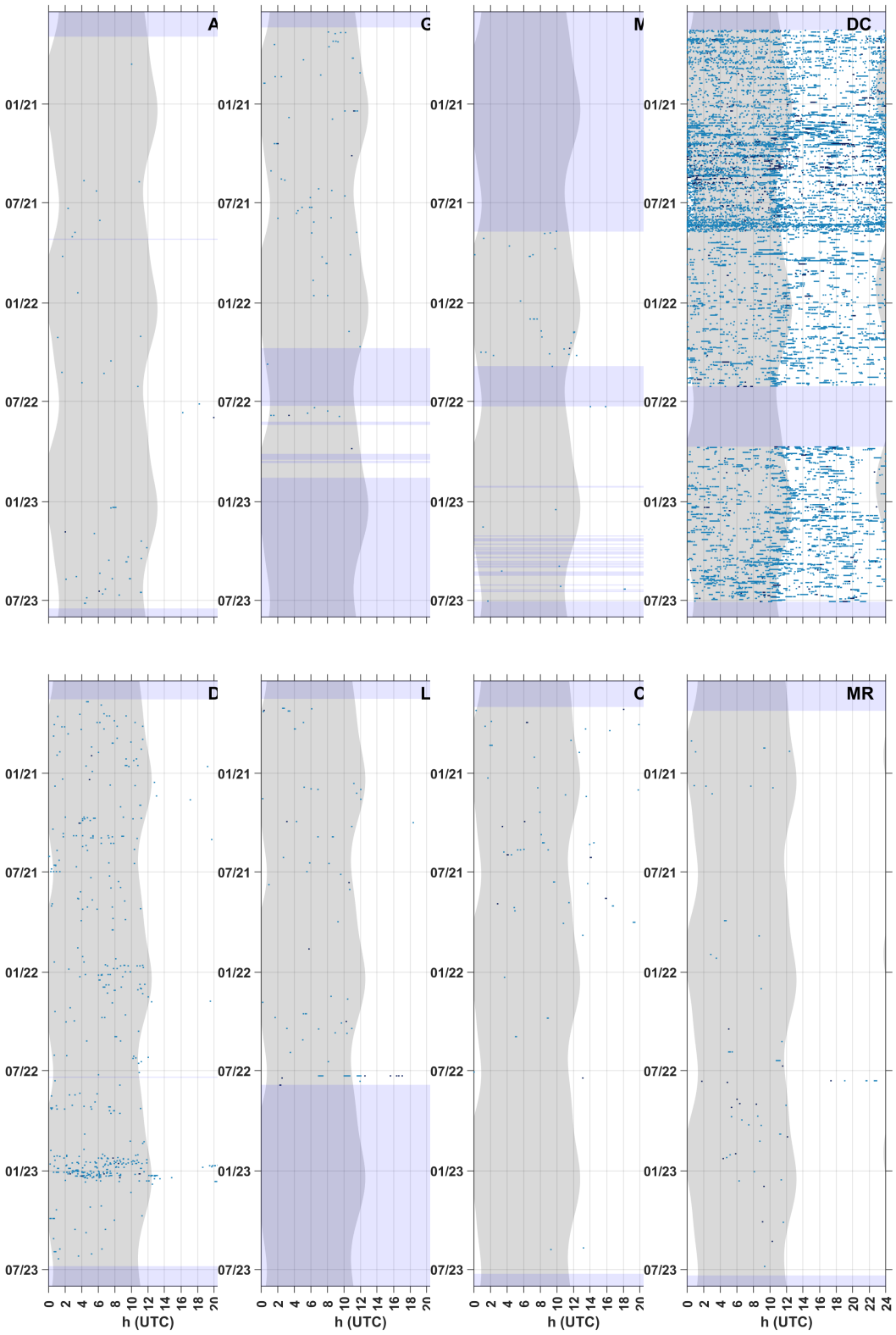


**Figure 77:** Unidentified three-peak dolphin (UD 3P) echolocation clicks in five-minute bins at long-term sites from 2020-2023. Gray vertical shading denotes nighttime and light blue horizontal shading denotes absence of acoustic data. Color denotes number of detections per 5 minutes (light blue: <100; mid blue: 100-1000; dark blue: >1000).

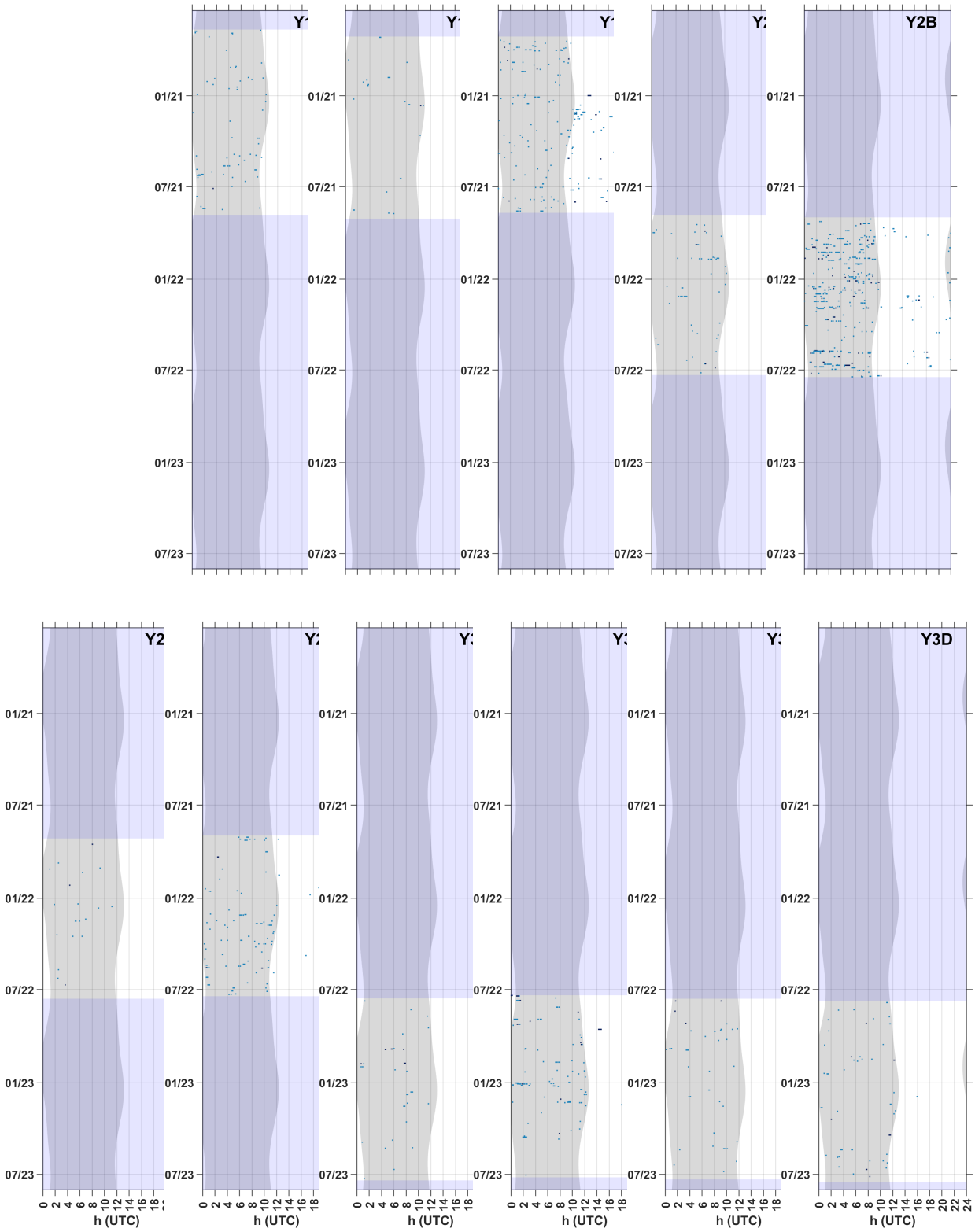


**Figure 78:** Unidentified dolphin three-peak (UD 3P) echolocation clicks in five-minute bins at short-term sites from 2020-2023. Gray vertical shading denotes nighttime and light blue horizontal shading denotes absence of acoustic data. Color denotes number of detections per 5 minutes (light blue: <100; mid blue: 100-1000; dark blue: >1000).

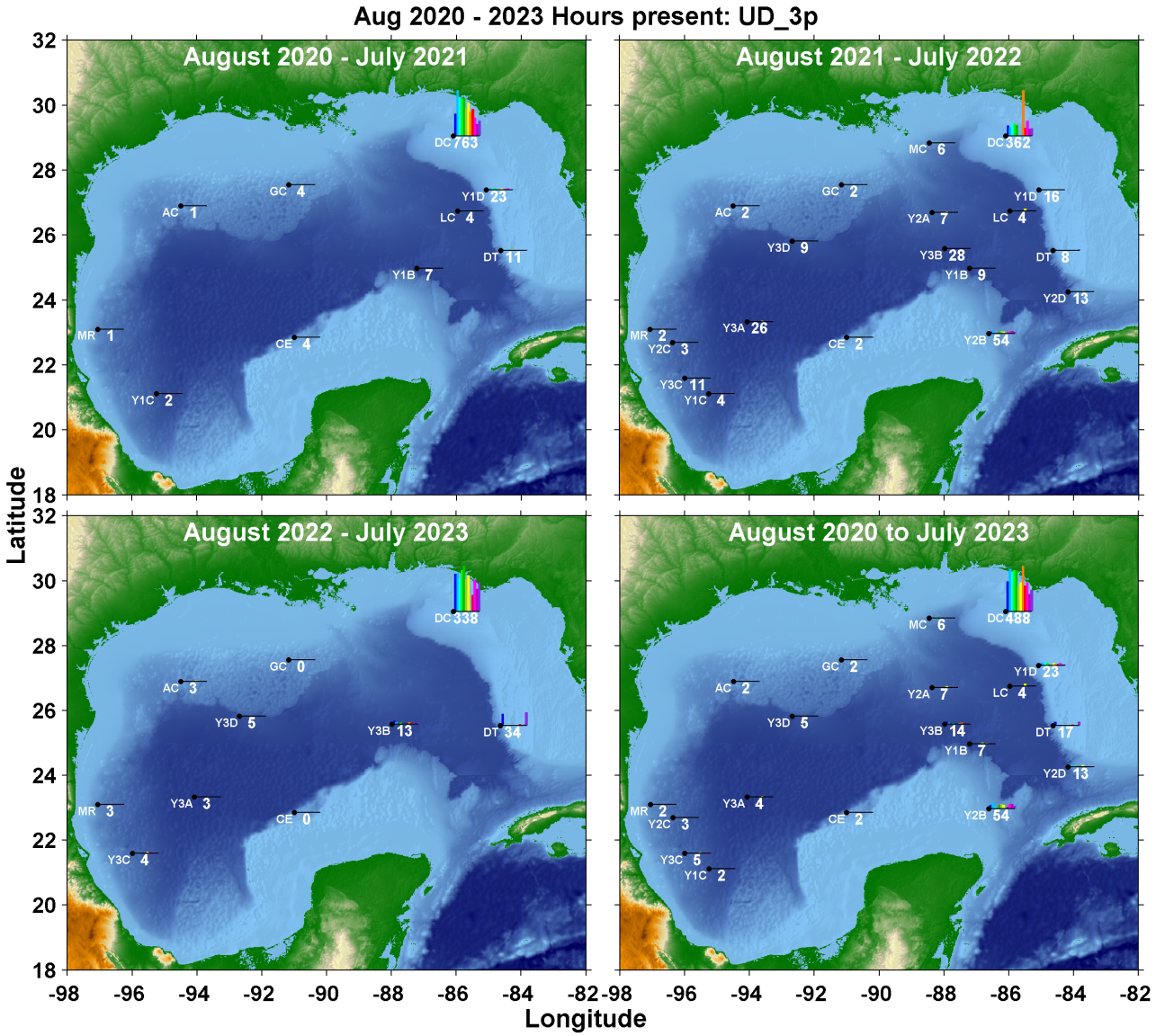


**Figure 79:** Average hourly presence of unidentified three-peak dolphin echolocation clicks (UD 3P) per month, represented as bar plots, from 2020-2023. Values below bar plots represent mean hours of presence per year. Panels represent presence in each of the three years of recordings with the bottom right panel representing all years combined.

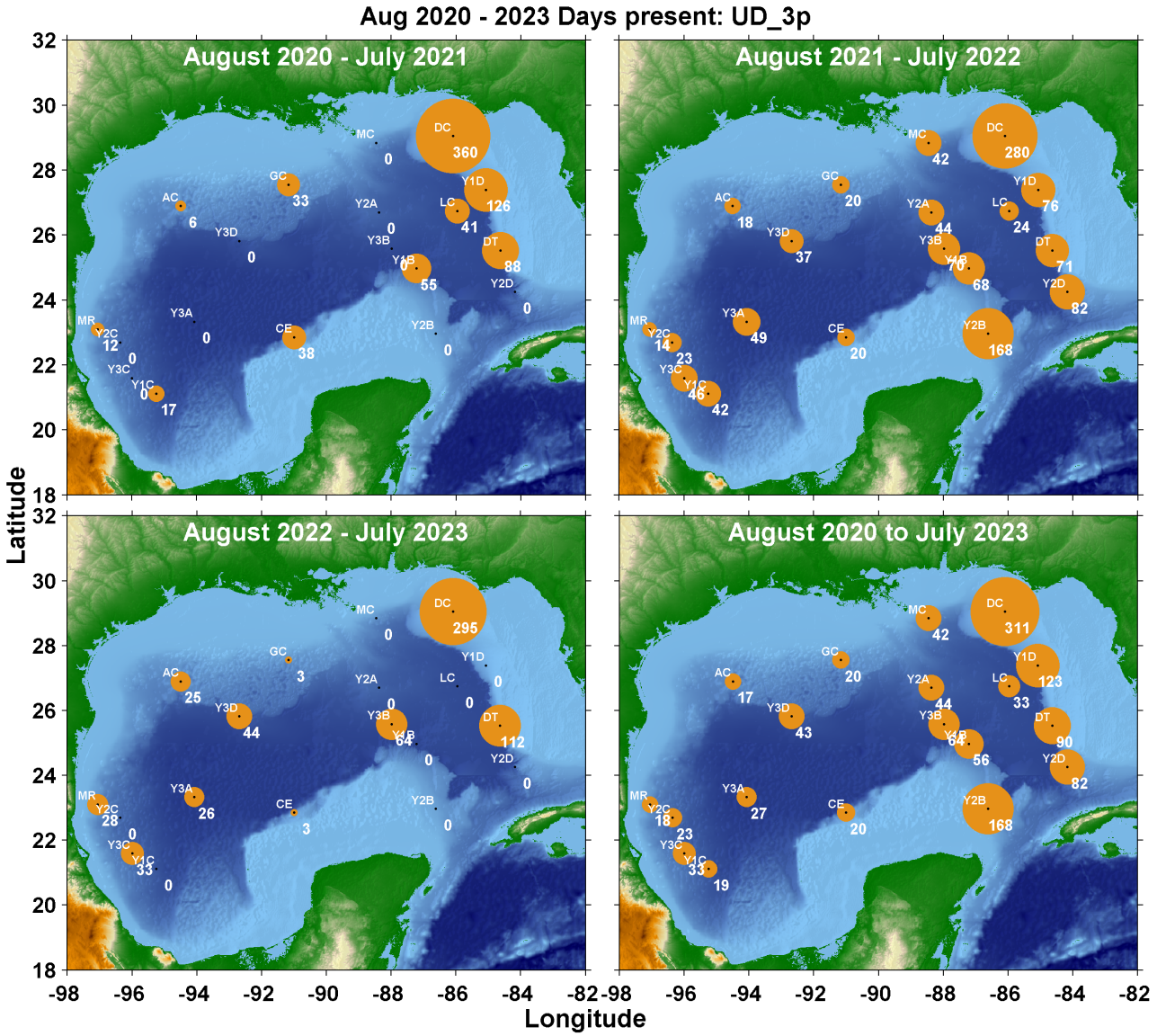


**Figure 80:** Days with presence of unidentified three-peak dolphin echolocation clicks (UD 3P) from 2020-2023. Panels represent presence in each of the three monitoring years, with the bottom left panel representing yearly means computed across the three years, adjusted for recording effort.

### 4.1.9 Unidentified Dolphins: Low-Frequency

Unidentified low-frequency dolphins (UD LF, presumed to include short-finned pilot whale, melon-headed whale, false killer whale, and killer whale) were detected at all sites in relatively low numbers. Occurrence was consistent over time but sparse. Estimated densities were highest at Y3A, a short-term site in the Sigsbee Deep region, with 40.6 animals per 1,000 $km^2$, followed by sites MR and Y1C with 37.1 and 34.1 animals per 1,000 $km^2$, respectively (Table 5). Moderate densities were found at sites Y2C, and Y3C (23.5 and 25.0 animals per 1,000 $km^2$, respectively; Table 5), highlighting the importance of the southwestern Gulf waters for this species group. Site DC had the lowest density of unidentified low-frequency dolphins, at 1.3 animals per 1,000 $km^2$ ; Table 5). Densities for the remaining sites range from 7.2 to 20.4 animals per 1,000 $km^2$ (Table 5). Densities of this species group have been stable or increasing in at the historic sites (2010-2020) and preliminary density estimates at those sites during this monitoring period were similar to 2010 estimates, with the exception of site GC (2010: 19.9 animals per 1,000 $km^2$; 2020-2023: 11.3 animals per 1,000 $km^2$; Frasier et al. In Review).

No clear evidence of seasonality was observed for unidentified low-frequency dolphins (Figures 69 & 70). Diel patterns characterized by increased nocturnal click detections are observed, though detections also occurred during daylight hours (Figures 83 & 84). Similar to patterns for density, unidentified low-frequency dolphin mean hourly presence was highest at sites in the southwestern Gulf, including the Sigsbee Deep, Mexican Ridges and Bay of Campeche, in contrast with the high-frequency delphinid category (Figure 85). Mean daily presence per year was generally lower across sites than for all other species groups except Blainville's beaked whales, ranging from 4% at site DC to 34% at site Y3A (Figure 86).

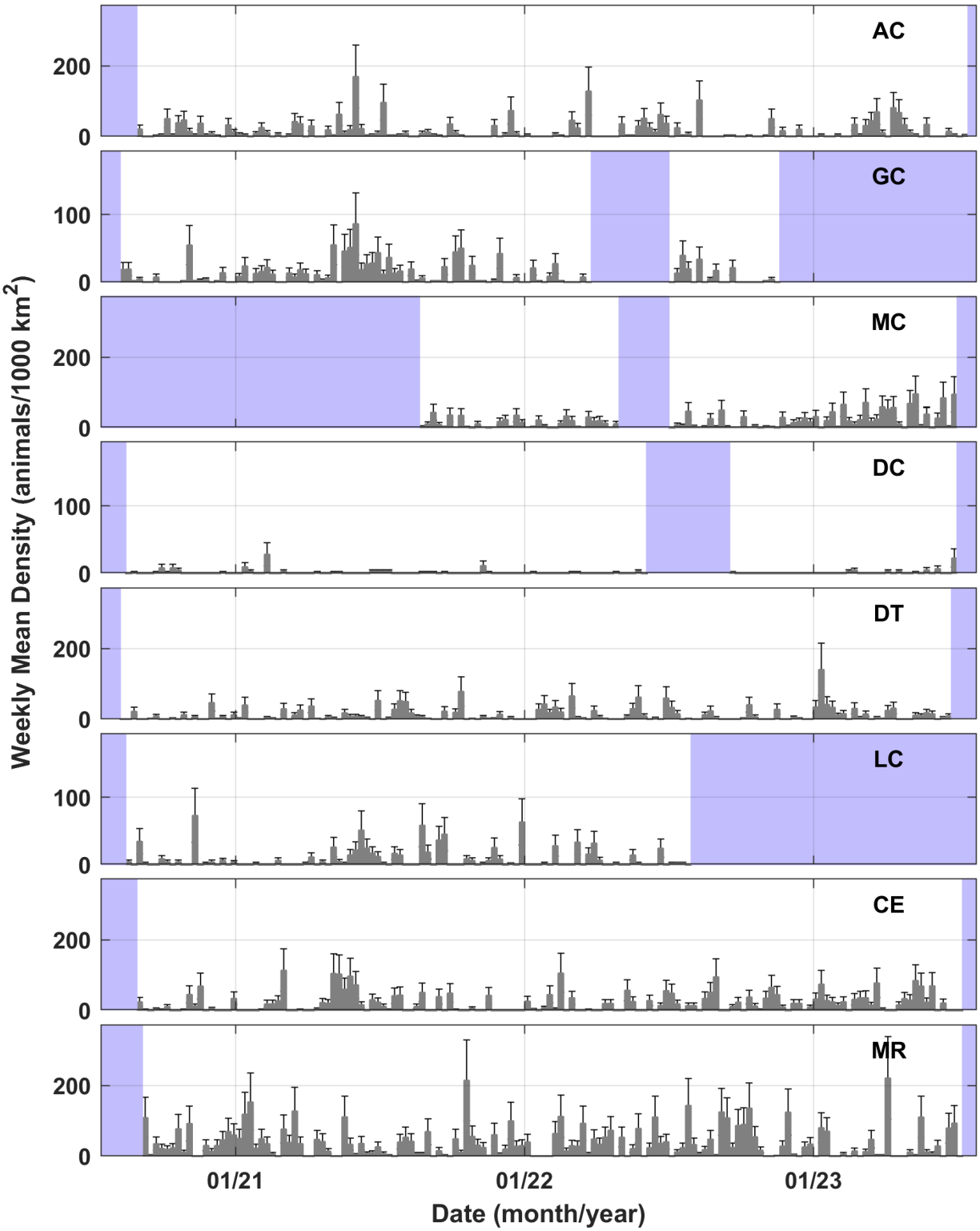


**Figure 81:** Weekly mean density (gray bars) of unidentified low-frequency dolphins (UD LF) at long-term sites from 2020 to 2023. Error bars represent ± 1 standard deviation. Shaded blue sections represent periods with no recording effort. Note: y-axis values vary in some cases based on maximum densities.

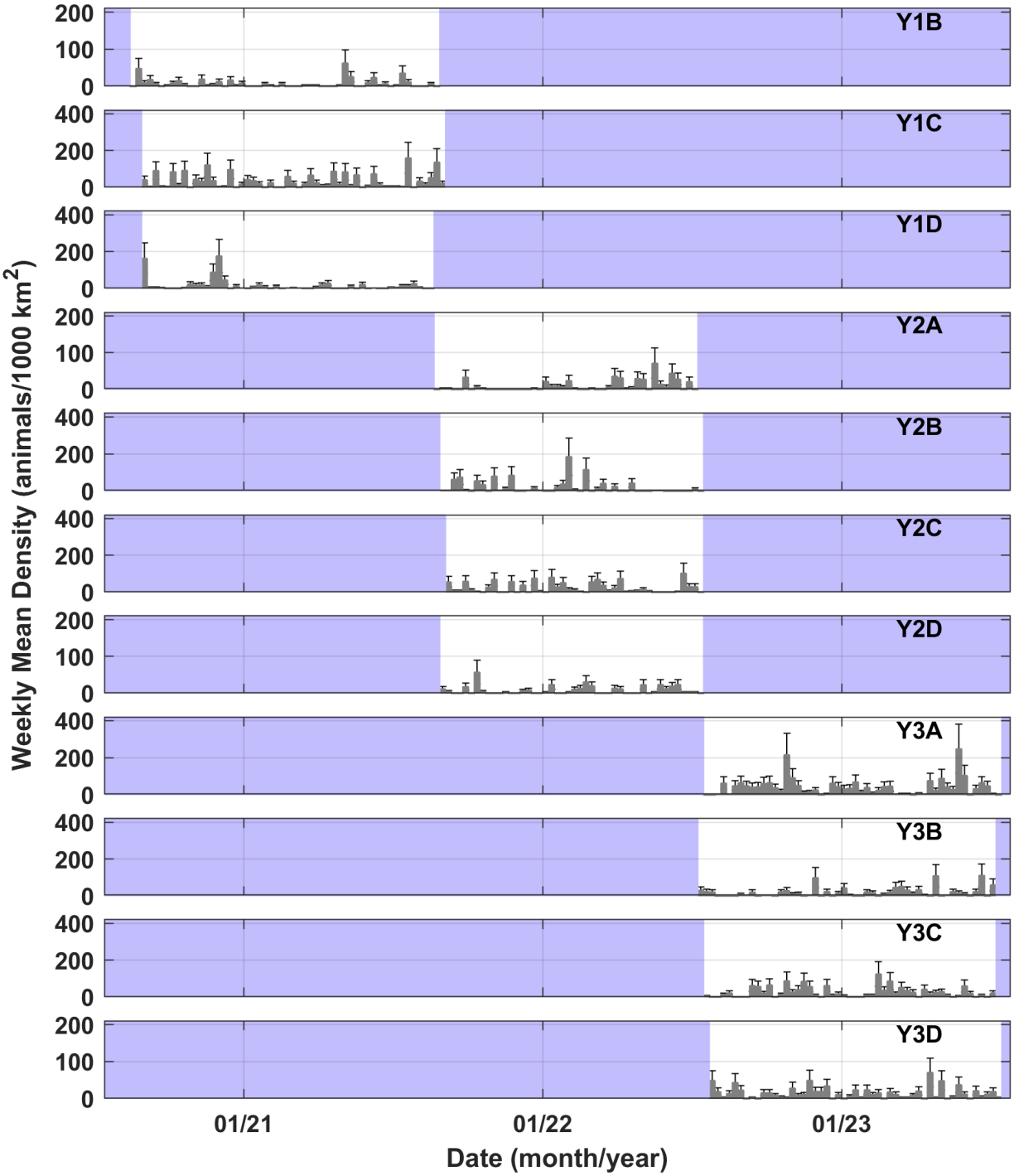


**Figure 82:** Weekly mean density (gray bars) of unidentified low-frequency dolphins (UD LF) at short-term sites from 2020 to 2023. Error bars represent ± 1 standard deviation. Shaded blue sections represent periods with no recording effort. Note: y-axis values vary in some cases based on maximum densities.

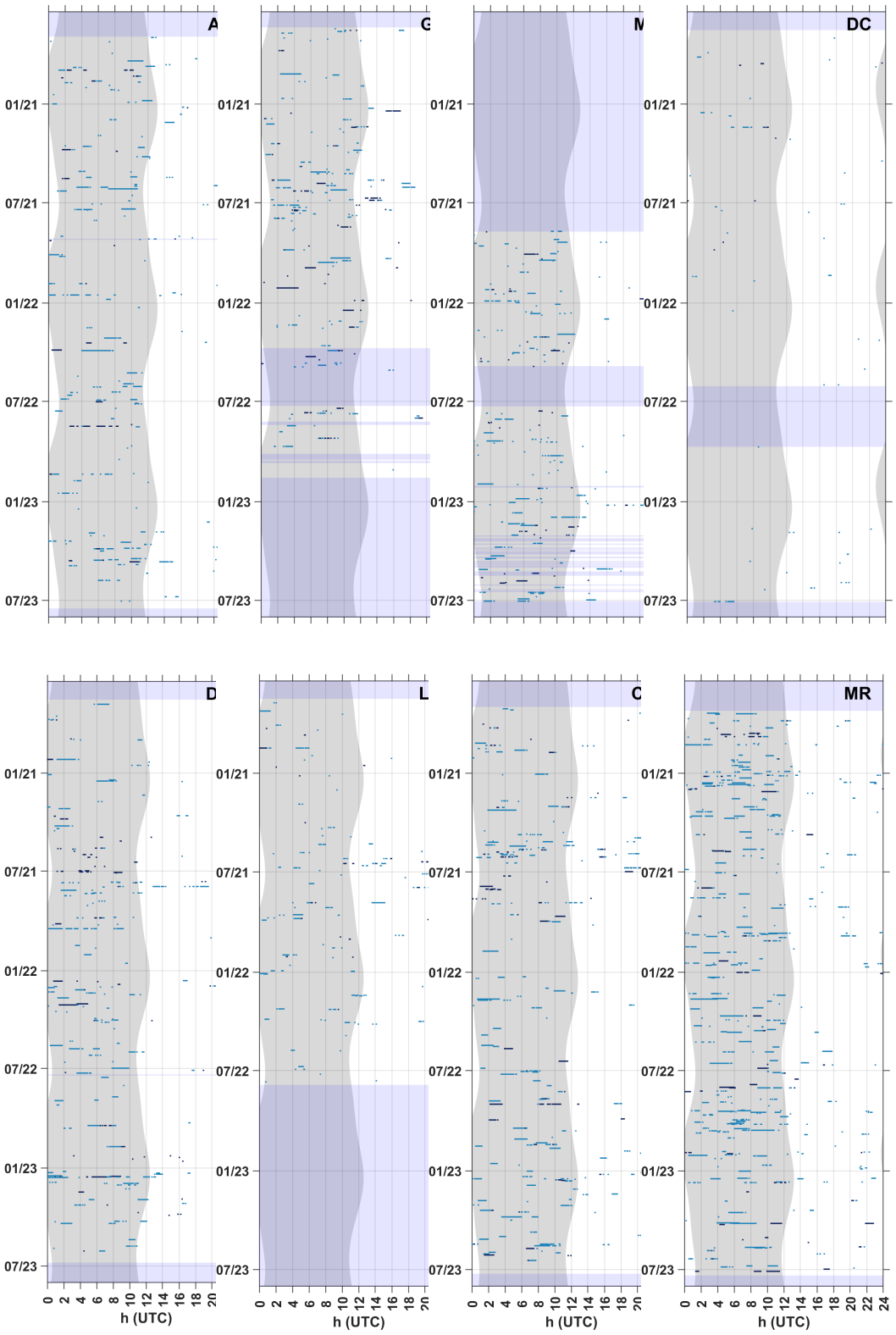


**Figure 83:** Unidentified low-frequency dolphin echolocation clicks in five-minute bins at long-term sites from 2020-2023. Gray vertical shading denotes nighttime and light blue horizontal shading denotes absence of acoustic data. Color denotes number of detections per 5 minutes (light blue: <100; mid blue: 100-1000; dark blue: >1000).

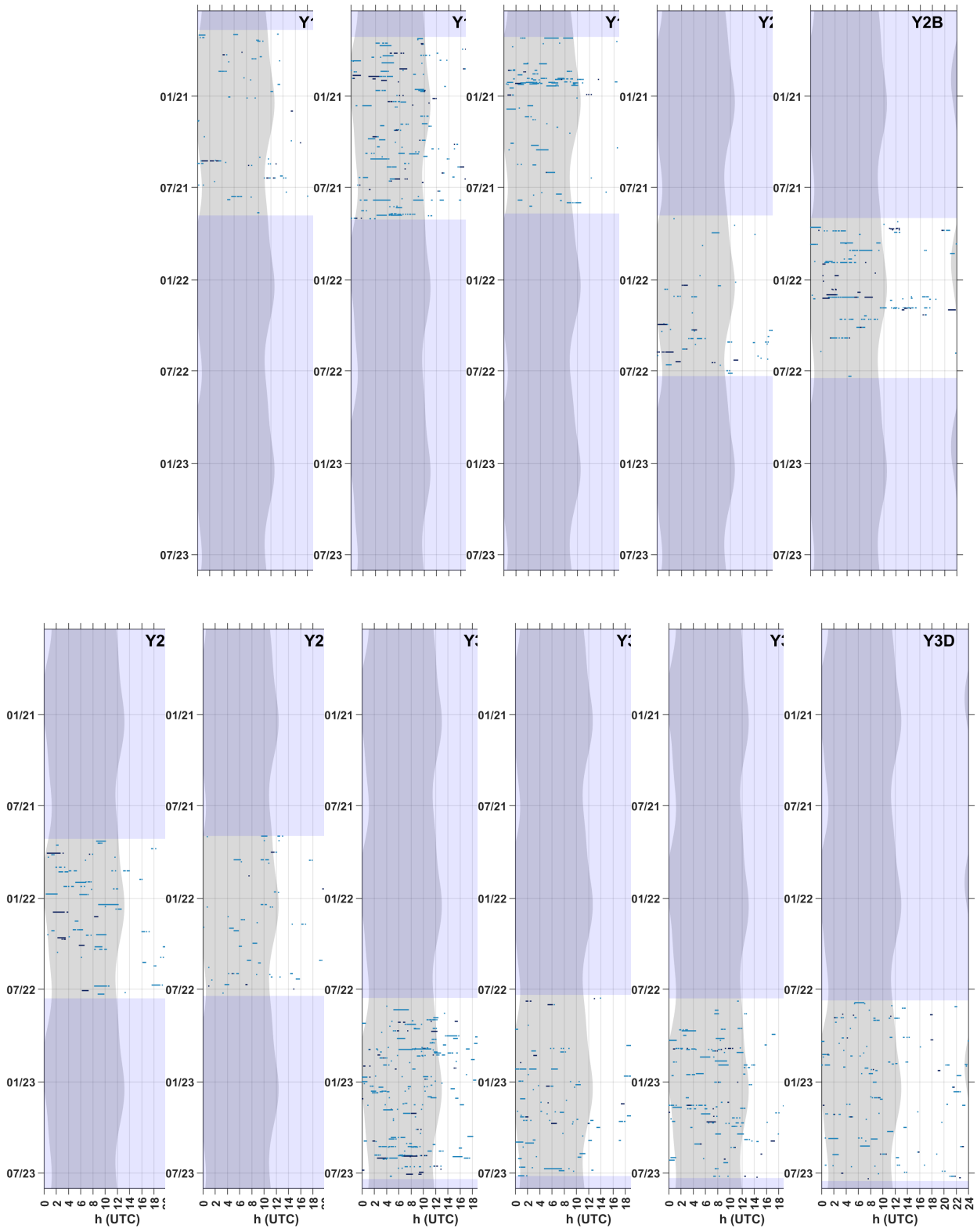


**Figure 84:** Unidentified low-frequency dolphin echolocation clicks in five-minute bins at short-term sites from 2020-2023. Gray vertical shading denotes nighttime and light blue horizontal shading denotes absence of acoustic data. Color denotes number of detections per 5 minutes (light blue: <100; mid blue: 100-1000; dark blue: >1000).

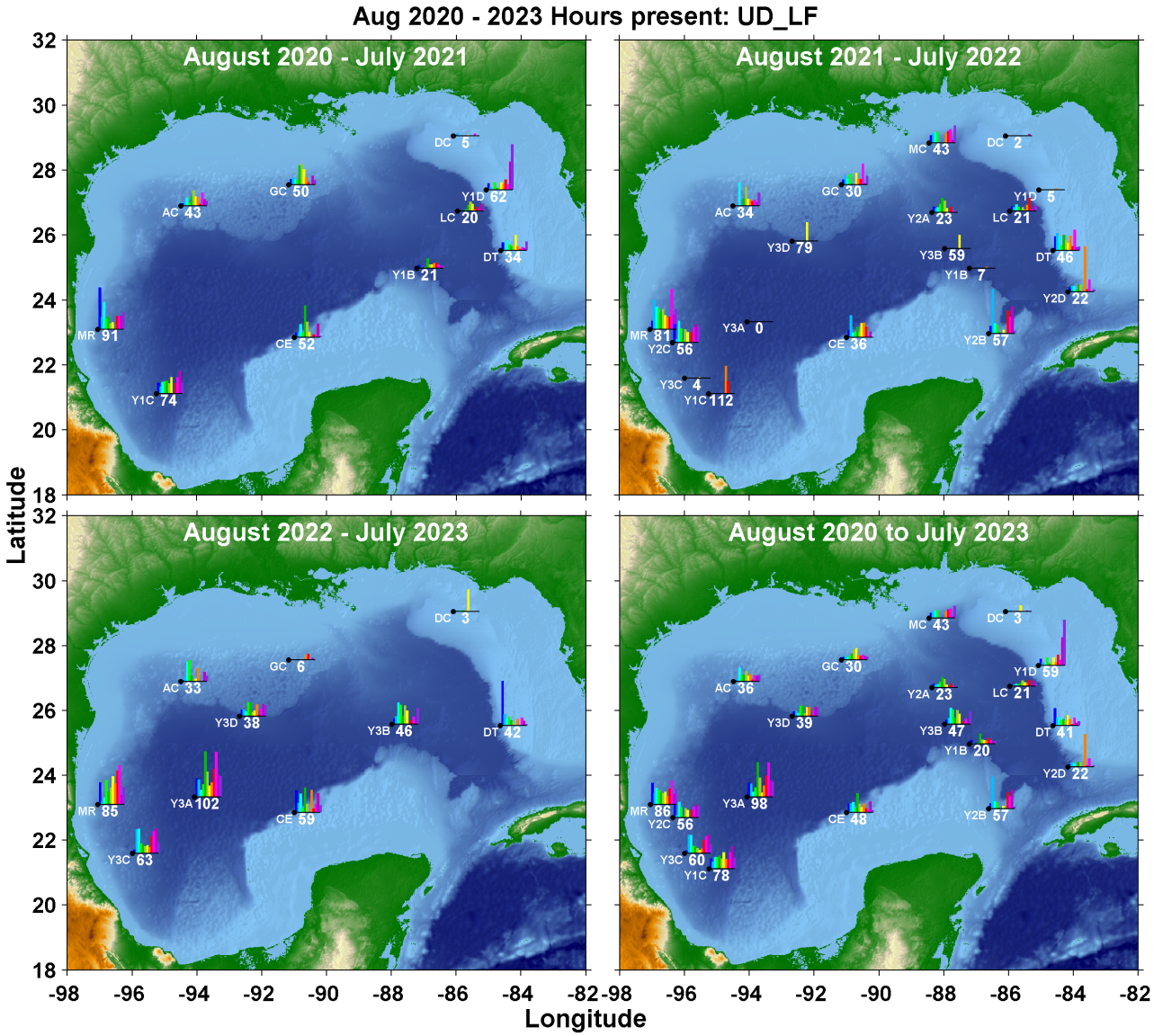


**Figure 85:** Average hourly presence of low-frequency dolphin echolocation clicks per month, represented as bar plots, from 2020-2023. Values below bar plots represent mean hours of presence per year. Panels represent presence in each of the three years of recordings with the bottom right panel representing all years combined.

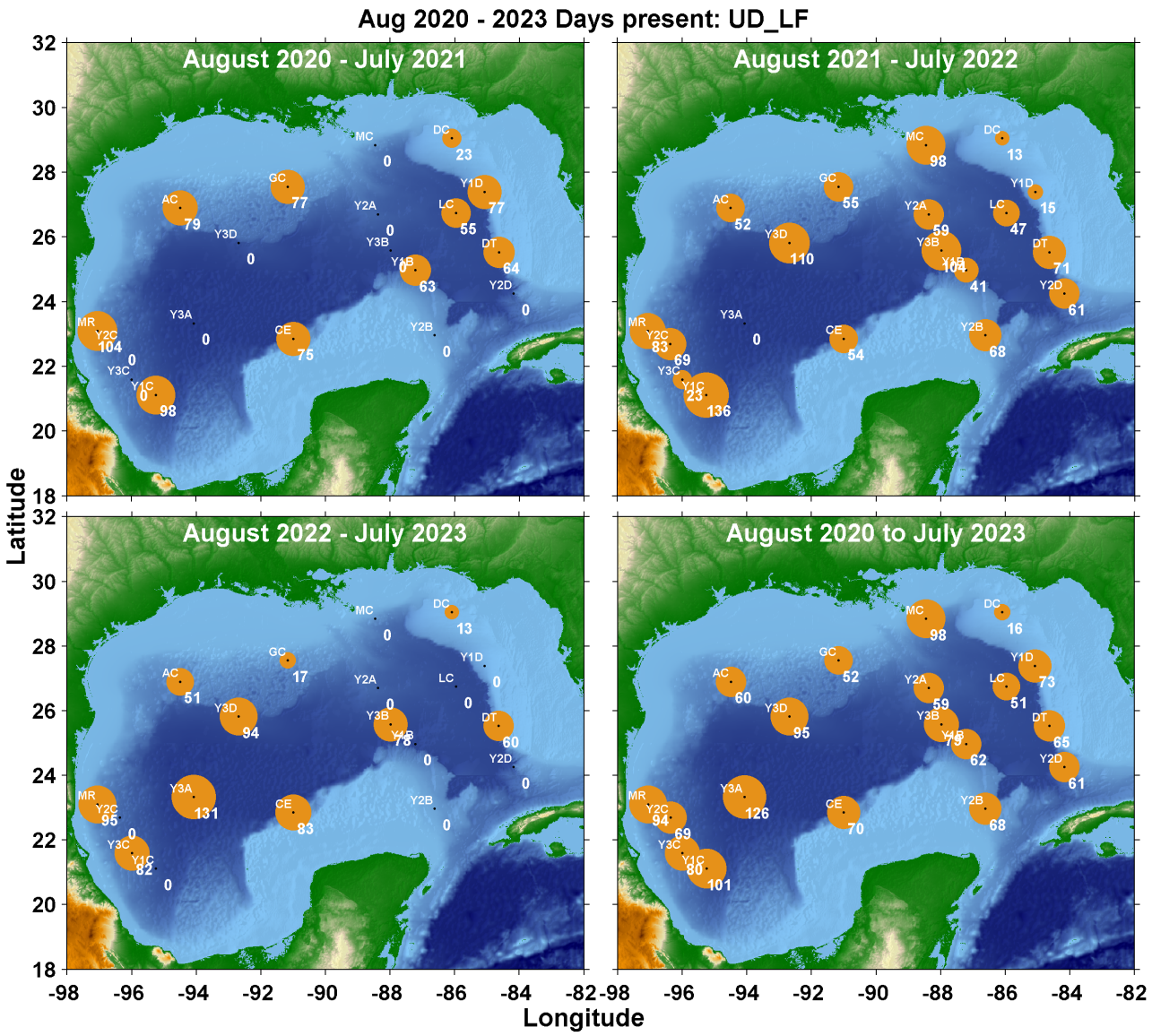


**Figure 86:** Days with presence of unidentified low-frequency dolphin (UD LF) echolocation clicks from 2020-2023. Panels represent presence in each of the three monitoring years, with the bottom right panel representing yearly means computed across the three years, adjusted for recording effort.

### 4.1.10 Beaked Whale Tracking

During the GC tracking array deployment from 9/7/2021 to 3/25/2022, there were 198 days of data available on both tracking HARPs for tracking the three beaked whale species to obtain acoustic and dive behavior parameters for improved density estimation. From these data, twenty-six Cuvier's beaked whale dives, twenty-five Gervais' beaked whale dives, and only two Blainville's beaked whale dives (due to their rare presence at this site) were selected for tracking (Figure 87). Dive segment durations ranged from 7 to 42 min for Cuvier's beaked whales, from 7 to 19 min for Gervais' beaked whales and from 11 to 16 min for Blainville's beaked whales (Figure 87).

Results show that Cuvier's, Gervais' and Blainville's beaked whales were detected at mean depths of 981 m (standard deviation = 97 m), 863 m (sd = 70 m), and 795 m (sd = 36 m), respectively (Figure 87, Table 6). Dives were divided into three phases: descent, bottom, and ascent. For Cuvier's beaked whales, the overall mean swim speed during the bottom phase of dives was 1.15 m/s (sd = 0.64 m/s) with a range from 0.29 to 3.19 m/s (Table 6). For Gervais' beaked whales, the overall mean swim speed during the bottom phase was 1.14 m/s (sd = 0.28 m/s) with a range from 0.56 to 1.83 m/s (Table 6). For Blainville's beaked whales the mean swim speed during the bottom phase was 1.09 m/s (sd = 0.36 m/s). Descent rates for Cuvier's, Gervais' and Blainville's beaked whales were 1.36 m/s (sd = 0.14 m/s, *n* = 8), 1.20 m/s (sd = 0.16 m/s, *n* = 4), and 1.14 m/s, *n* = 1, respectively (Table 6). Ascent rates for Cuvier's and Gervais' were 1.40 m/s (sd = 0.16 m/s, *n* = 3), and 1.19 m/s (sd = 0.06 m/s, *n* = 3), respectively (Table 6). Neither of the Blainville's beaked whale tracks included an ascent; thus, ascent rate was not estimated for this species.

To quantitatively characterize the directionality of the clicks produced by beaked whales, the $SL_{PP}$ estimates from tracking HARP GC 01 were plotted against their off-axis angles (Figure 88). As expected, beaked whales have a narrow transmission beam and at off-axis angles, the observed $SL_{PP}$ distribution decreases dramatically.

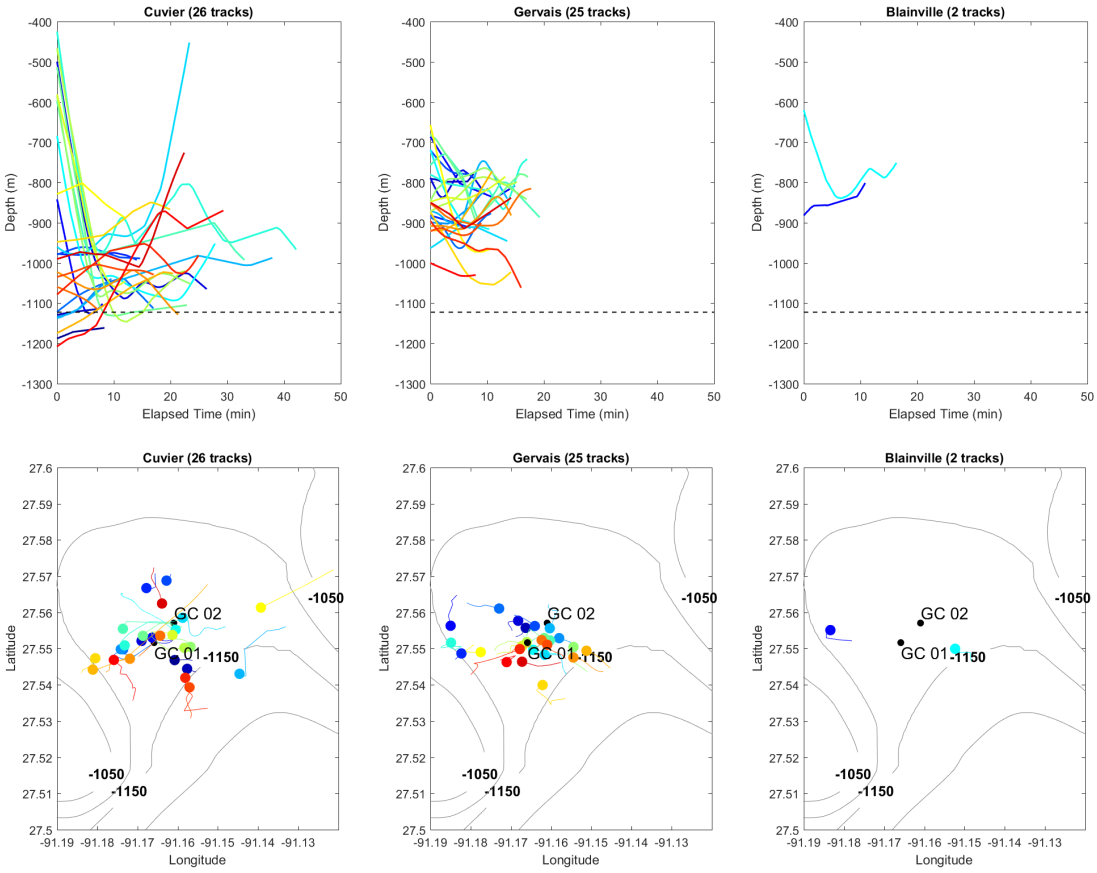


**Figure 87:** Top panels: Estimated depths (in m) as a function of elapsed time (in min) for acoustically-tracked beaked whale dives for three beaked whale species (left: Cuvier's beaked whales, n = 26 tracks; middle: Gervais' beaked whales, n = 25 tracks; right: Blainville's beaked whales, n = 2 tracks). Dashed black line indicates nominal seafloor depth at the two tracking HARPs. Bottom panels: Track locations of tracked beaked whale dives for three beaked whale species (left: Cuvier's beaked whales; middle: Gervais' beaked whales; right: Blainville's beaked whales). Locations where tracks end are indicated with filled circles (colors correspond to the top panels). Tracking HARP positions are indicated by black dots with GC 01 and GC 02 labels. Bathymetry (in m) is indicated in bold.

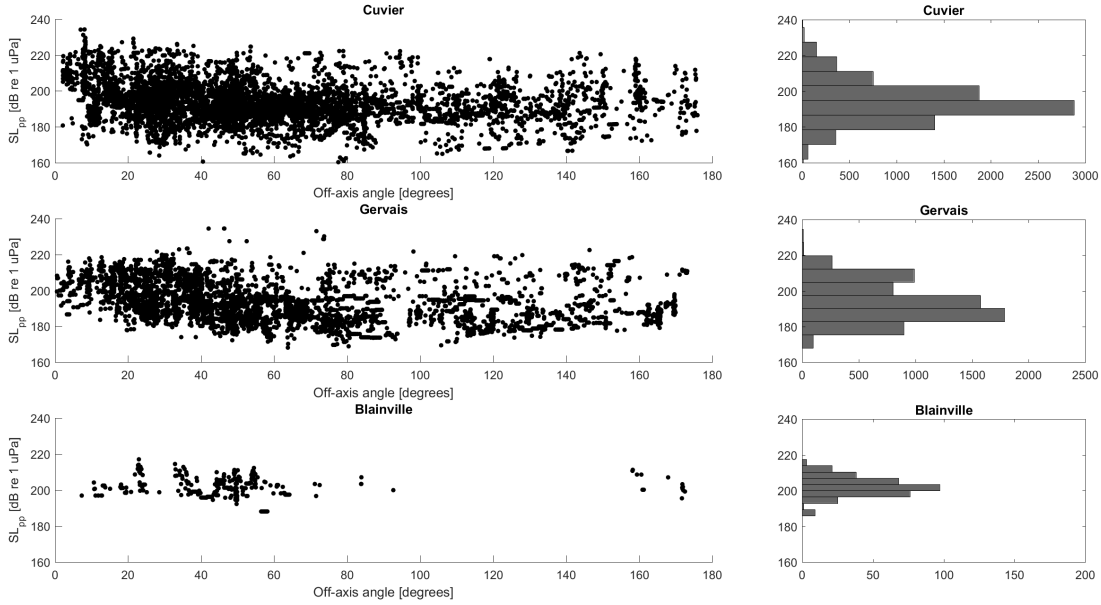


**Figure 88:** Left Panels: Peak-to-peak source level estimates ($SL_{pp}$) of Cuvier's (top, 7,859 clicks), Gervais' (middle, 6,428 clicks), and Blainville's (bottom, 338 clicks) beaked whale clicks as a function of off-axis angle to the GC 01 4-channel HARP for the selected tracks. Right Panels: Source level distribution for each species.

| | Minimum Depth (m) | | | Maximum Depth (m) | | | Mean Depth (m) | | |
|---|---|---|---|---|---|---|---|---|---|
| | **Zc** | **Me** | **Md** | **Zc** | **Me** | **Md** | **Zc** | **Me** | **Md** |
| **n (dives)** | 26 | 25 | 2 | 26 | 25 | 2 | 26 | 25 | 2 |
| **Average** | 816 | 799 | 711 | 1075 | 910 | 861 | 981 | 863 | 795 |
| **SD** | 229 | 82 | 91 | 80 | 69 | 21 | 97 | 70 | 36 |
| **Max** | 1162 | 1000 | 801 | 1208 | 1062 | 882 | 1172 | 1026 | 831 |
| **Min** | 425 | 657 | 620 | 888 | 786 | 839 | 838 | 770 | 759 |

| | Descent Speed (m/s) | | | Ascent Speed (m/s) | | | Bottom Speed (m/s) | | |
|---|---|---|---|---|---|---|---|---|---|
| | **Zc** | **Me** | **Md** | **Zc** | **Me** | **Md** | **Zc** | **Me** | **Md** |
| **n (dives)** | 8 | 4 | 1 | 3 | 3 | 0 | 26 | 25 | 2 |
| **Average** | 1.36 | 1.20 | 1.14 | 1.40 | 1.19 | N/A | 1.15 | 1.14 | 1.09 |
| **SD** | 0.14 | 0.16 | N/A | 0.06 | 0.06 | N/A | 0.64 | 0.28 | 0.36 |
| **Max** | 1.59 | 1.35 | N/A | 1.62 | 1.26 | N/A | 3.19 | 1.83 | 1.44 |
| **Min** | 1.20 | 0.93 | N/A | 1.24 | 1.11 | N/A | 0.29 | 0.56 | 0.73 |

**Table 6:** Summary statistics for the minimum, maximum and mean depth estimated for each beaked whale species (top) and statistics for estimated dive speed (descent, ascent and bottom) for each species (bottom).

## 4.2 Mysticetes

### 4.2.1 Rice's Whales

Analyses of the 2020-2022 deployments found Rice's whale call detections at seven of the 17 sites, including some unexpected sites (Table 7). Eastern call types, including long-moans, downsweep pulse sequences, and tonal sequences were commonly detected at sites DC and Y1D within the Rice's whale core distribution area, with over 200,000 and 10,000 manually validated calls, respectively. Additionally, 10 western long-moan variants were detected at site DC (Table 7, Figures 89 and 90). Rice's whale calls were present at DC and Y1D on 99% and 54% of days, respectively (Table 7, Figure 91). A few rare faint eastern long-moans were also detected at site LC.

Over the 2020-2022 period, nearly 600 Rice's whale western long-moan variant calls, including 150 Hz tones, were detected at sites GA and MR, and 150 Hz tones were detected at sites SL and YC2 on 1 and 162 occasions, respectively (Table 7, Figures 89 & 90). Rice's whale calls were present at sites GA, MR, and Y2C on 11%, 15%, and 19% of days, respectively. Calls at site MR were only detected during the final month of the first year of recordings, while they were more commonly detected throughout the second year (Figures 89 & 90). Calls at Y2C were typically detected on the same days as calls were detected at site MR during the second year (Figures 89 & 90).

Rice's whale calls are not commonly detected at the deeper sites, with no Rice's whale calls detected at sites AC, CE, DT, GC, MC, Y1B, Y1C, Y2A, Y2B, or Y2D (Table 7) over the 2020-2022 period. Call detections at sites DC, Y1D, and GA were expected based on previously identified habitat in the 100 to 400 m water depth range of the northern Gulf of Mexico. Call detections at the deep LC site in the northern Gulf, and the deep MR and Y2C sites in the southern Gulf were unexpected. These results indicate Rice's whales do occur in the southern Gulf (Soldevilla et al. 2024) but it remains undetermined whether they occur in deeper waters. Sites MR, Y2C, and LC are 30, 96, and 112 km away from the 400 m isobath, and Rice's whale calls have been detected at least as far as 75 km away in the northeastern Gulf (Rice et al. 2014). With only a single acoustic sensor on the HARP, it cannot be determined whether the whales occur in deeper waters or if the whales producing the calls detected at sites MR, Y2C, and LC were located in the typical 100 to 400 m water depths. Preliminary estimations of call detection ranges based on hourly-averaged ambient noise conditions at these sites include shelf-break waters (Figures 92 and 93; See Ambient Noise section for additional details). No strong seasonal patterns in call detections or hourly presence are evident at sites during this deployment period (Figures 89 & 90).

| Site | Effort (Days) | Effort (Hours) | Eastern Calls | Western Calls | Presence (% Days) | Presence (% Hours) |
|---|---|---|---|---|---|---|
| **AC** | 690 | 16,576 | - | - | 0.0 | 0.0 |
| **GC** | 632 | 15,019 | - | - | 0.0 | 0.0 |
| **MC** | 450 | 10,757 | - | - | 0.0 | 0.0 |
| **DC** | 656 | 15,722 | 223,988 | 10 | 99.2 | 87.4 |
| **DT** | 695 | 16,660 | - | - | 0.0 | 0.0 |
| **LC** | 689 | 16,452 | 5 | - | 0.6 | 0.0 |
| **CE** | 683 | 16,404 | - | - | 0.0 | 0.0 |
| **MR** | 680 | 16,329 | - | 579 | 14.9 | 1.9 |
| **GA** | 691 | 16,561 | - | 602 | 11.0 | 1.2 |
| **SL** | 632 | 15,096 | - | 1 | 0.2 | 0.0 |
| **Y1B** | 371 | 8,885 | - | - | 0.0 | 0.0 |
| **Y1C** | 364 | 8,725 | - | - | 0.0 | 0.0 |
| **Y1D** | 364 | 8,726 | 10,760 | - | 54.4 | 23.0 |
| **Y2A** | 321 | 7,672 | - | - | 0.0 | 0.0 |
| **Y2B** | 319 | 7,645 | - | - | 0.0 | 0.0 |
| **Y2C** | 319 | 7,638 | - | 162 | 19.4 | 1.7 |
| **Y2D** | 319 | 7,647 | - | - | 0.0 | 0.0 |

**Table 7:** Summary of Rice's whale call detections and recording effort over the 2020 – 2022 period.

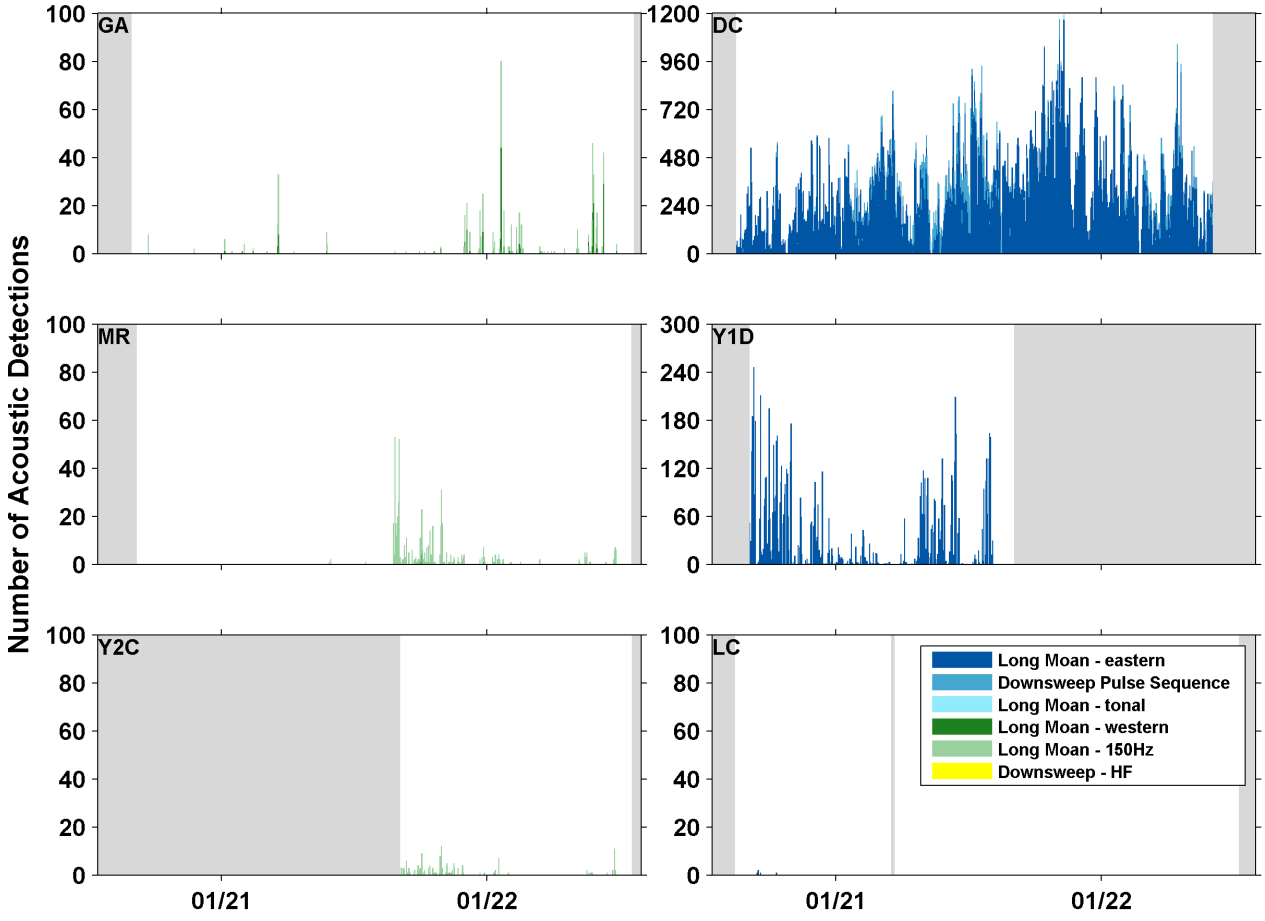


**Figure 89:** Daily Rice's whale call detections by call type (stacked bars) between 2020 to 2022 at sites GA, DC, MR, Y1D, Y2C, and LC. Only one positive call and 3 possible detections occurred at site SL (not shown). No detections were found at the remaining sites during this time period. Shaded gray sections represent periods with no recording effort. Note: y-axis values vary for each site based on detection levels.

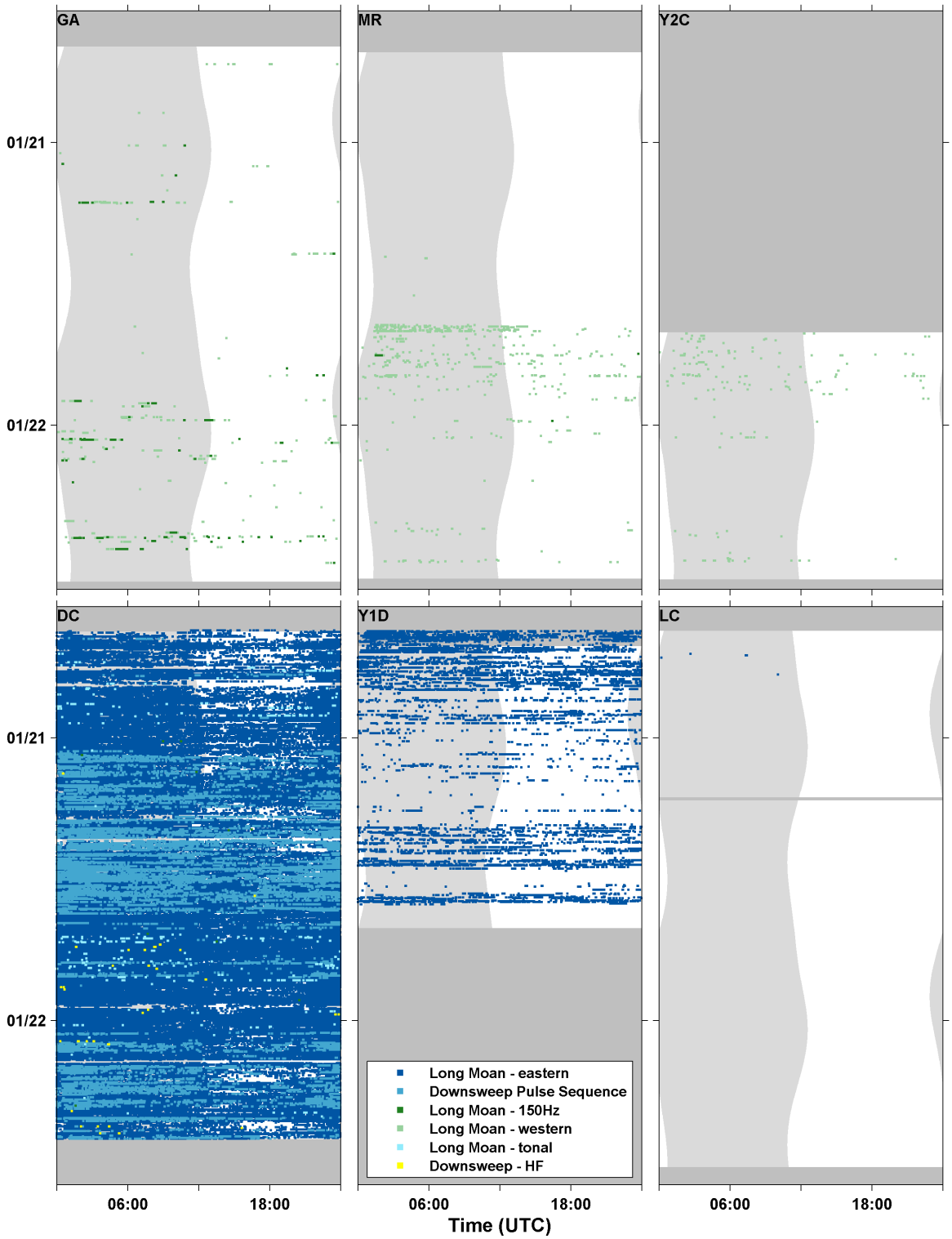


**Figure 90:** Rice's whale calls by call type in one-minute bins over the 2020 to 2022 period at sites GA, MR, Y2C, DC, Y1D, and LC. Light gray vertical hourglass shading denotes nighttime and dark gray horizontal shading denotes absence of acoustic data. Color denotes call type presence.

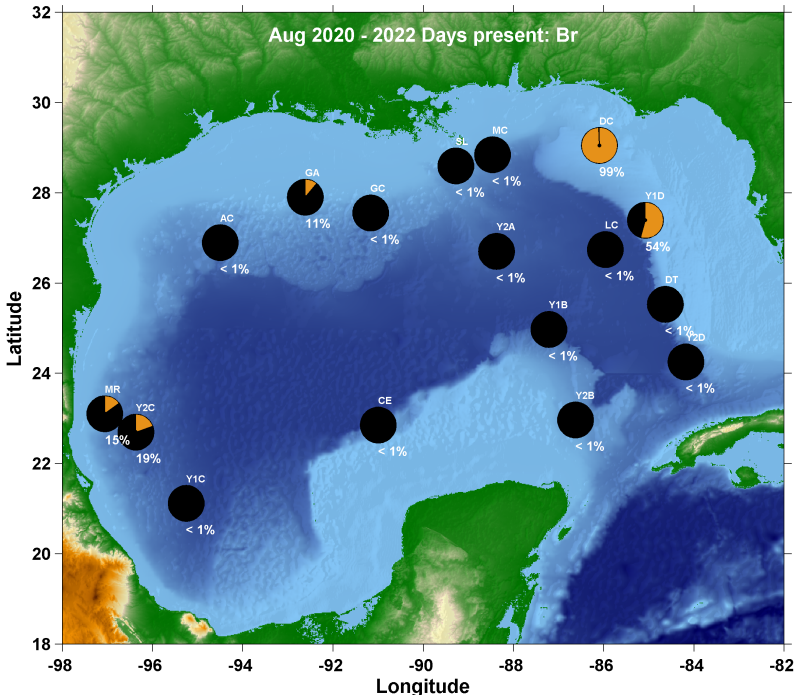


**Figure 91:** Average days present per year for all Rice's whale call types at LISTEN GoMex sites from 2020-2022.

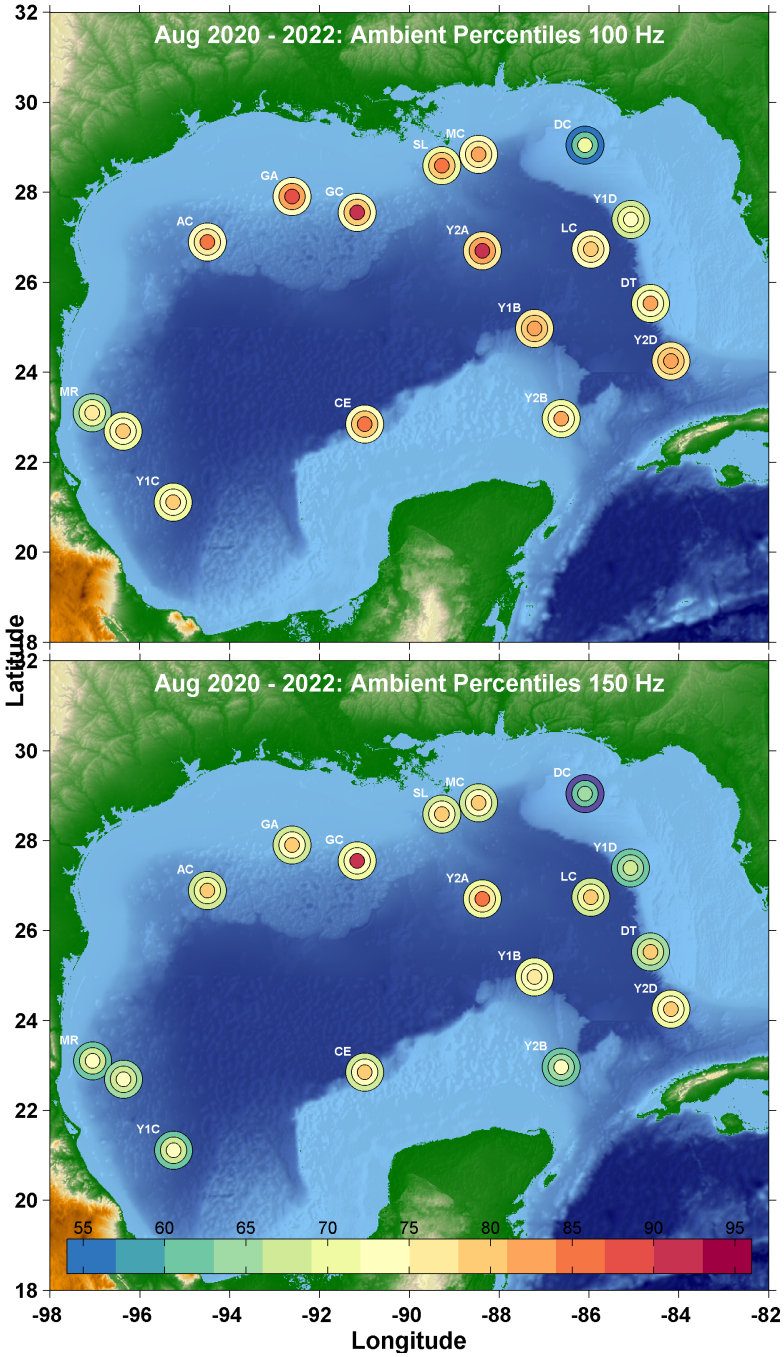


**Figure 92:** Distribution of 100 Hz (top panel) and 150 Hz (bottom panel) ambient sound pressure spectrum levels at LISTEN GoMex sites from 2020-2022. Bullseye circles at each site represent the 5th, 50th, and 95th percentile noise levels as the outer, middle, and inner circles, respectively. Circle fill color represents the sound level, per the color bar.

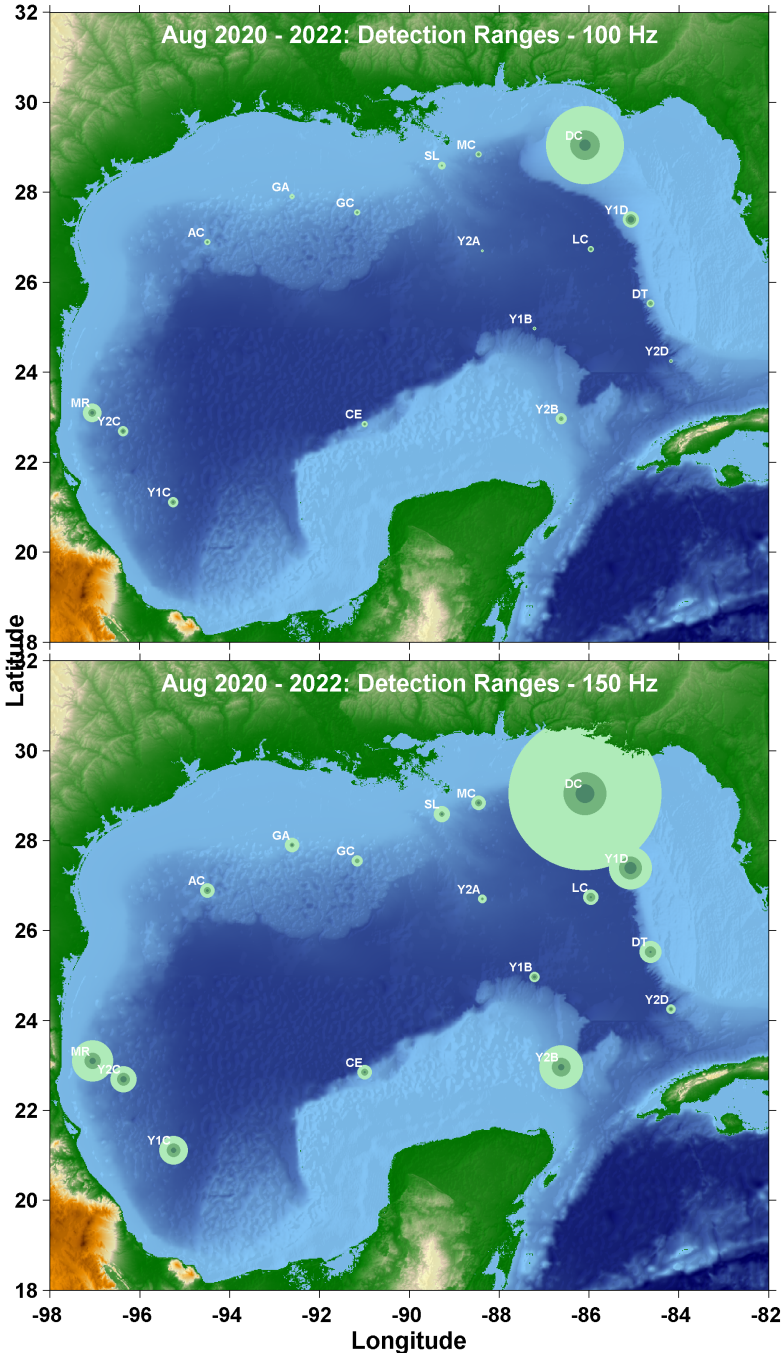


**Figure 93:** Example estimated maximum detection ranges for Rice's whale calls at LISTEN GoMex sites based on measured ambient noise levels at 100 Hz (top panel) and 150 Hz (bottom panel) from 2020-2022. The three concentric circles at each site represent the maximum estimated detection ranges given the 5th, 50th, and 95th percentile noise levels at each 100 or 150 Hz as the outer, middle, and inner circles, respectively. Detection range estimates are based on assumptions of call source levels of 145 dB, 10 dB call detection thresholds, and a geometric spreading loss factor of 15. Detection range estimates are examples only, and require further refinement based on empirically derived source levels, detection thresholds, and spreading loss factors.

## 4.3 Ambient and Anthropogenic Noise

### 4.3.1 Ambient Noise

At most of the 21 locations over the August 2020 to July 2023 recording period, the ambient soundscape below 100 Hz is dominated by seismic survey signals (airguns) nearly year-round (Figures 94 and 95). This is most apparent at site CE (Figure 94), where airgun signals were detected in 2/3 of recording hours over the 3-year period (Section 4.3.4 below). Individual surveys up to months long in duration are visible in the long spectrograms at all of the sites. Further, throughout the three years, the same surveys appear simultaneously across most acoustic recorders (as seen by similar start and end times of airgun noise in the 10 Hz to 100 Hz frequency band across sites), illustrating the long-range propagation of these intense low-frequency signals. Over this period, sound levels are elevated the most in the airgun frequency band at site GC where substantial survey activity was focused on active lease blocks (Section 4.3.4 below). Deep sites tended to have the most consistent occurrence of seismic survey signals due to long-range propagation across the open Gulf. Transmission of airgun signals up slope from deep into shallow water environments is weak; therefore, levels in the seismic band are generally lower at sites DC, GA, SL, and Y1D.

During the 2020 to 2021 deployment, a series of distinct seismic survey events from November to December 2020 and March to May 2021 were strongly visible across all sites, with the exception of the three northeastern sites SL, MC, and DC, which may be due to acoustic shadowing based on the bathymetry between survey locations and those recorders (Figures 94 and 95). Seismic survey signals occurred nearly constantly across all sites over the 2021 to 2022 deployment, though signals quiet down at some sites in March 2022 (e.g. DC, GC, MR, Y2C), while picking up at that time at other sites (e.g. MC; Figures 94 and 95). Over the 2022 to 2023 deployment, three primary seismic survey periods were evident in the long spectrograms across most sites from July to October, December to April, and June to July (Figures 94 and 95).

During quieter periods between seismic surveys, moderately elevated sound levels in the 30 to 90 Hz frequency band are evident at nearly all sites (e.g. at AC during most times from summer 2021 on, and at DT and LC in summer 2021), representing the near constant chronic noise from distant commercial vessel traffic, as well as episodic closer approaches (Figures 94 and 95). This 30 to 90 Hz commercial vessel traffic noise signal is most elevated at site GA (Figure 94), which is directly below the major shipping lane out of Houston, Texas, where thousands of tanker and cargo ship passages per year occur within 2 km of the site (Section 4.3.2 below). The energy peak is present but less evident at the shipping lane site SL (Figure 94), below the major shipping lane out of Southern Louisiana, where approximately half as many passages of cargo, tanker, passenger, and offshore supply vessels occur each year within 2 km of the site (Section 4.3.2 below). Elevated noise levels in the commercial-vessel-traffic frequency range also occurred at sites AC and Y3D (Figures 94 and 95), which are both near shipping lanes with primarily tanker traffic (Section 4.3.2 below) and sites Y1B and Y2B (Figure 95), which are both near shipping lanes with tanker and cargo vessel traffic (Section

4.3.2 below). At the remaining sites, the shipping traffic noise signal was primarily evident during periods in between seismic surveys (Figures 94 and 95).

Across all sites, and particularly evident at the quieter DC site, vertical stripes across the 100-1000 Hz frequency band indicate periods of increased noise levels due to weather events (noise from wind, waves, and precipitation; Figures 94 and 95). These tend to have similar patterns in occurrence across neighboring sites, and generally are increased during the winter period compared to the summer. At sites near the Loop Current (LC, Y1B, Y2A, Y2B) and at site SL, mooring-line strumming noise, primarily below 30 Hz, occurs occasionally (e.g. March 2021 at LC) when the current is strong. Elevated sound levels in the first half of the SL time-series may be partially related to a hydrophone malfunction.

Statistical distributions of the median daily sound pressure levels during the 2020-2023 recording period are presented for each site (Figures 96 and 97). A typical curve is observed across all sites, with sound levels highest at the lower frequencies (<100 Hz), followed by a steep drop off between 100 and 200-300 Hz, and then a continuing drop-off or leveling out between 200 to 1000 Hz. Variance tends to be highest below 100 Hz and above 200 Hz, primarily driven by the presence of airgun noise at low frequencies and weather noise at higher frequencies. At shipping lane sites GA and SL, the shipping noise signal is evident as a hump in sound levels between 30 and 90 Hz, and a similar pattern is seen in the lower end of the noise level distribution across most sites. Sites AC, GC, CE, MR, Y1C, Y2A, Y2C, Y3A, Y3B, and Y3C show a strong airgun noise signal with particularly high sound levels from 10 to 60 Hz, including harmonic peaks evident at 7, 14, and occasionally 21 Hz due to resonance features of airgun pulses. At several sites (e.g. CE, LC, Y1B, Y2A, Y2D, and all Y3 sites), an additional sound level hump is evident between 110 and 210 Hz (Figures 96 and 97) that appears to be associated in time with airgun surveys in the March to May 2021 and May to July 2023 periods (Figures 94 and 95). In some cases, a bi-modal distribution in sound levels is evident (e.g. sites DT, MC, CE, LC, MR) with both the lower amplitude shipping traffic signal and higher amplitude airgun survey signal evident in the statistical distributions below 200 Hz (Figures 96 and 97). Over this three-year period, the overall lowest sound levels occur at site DC, followed by sites MR, Y1D, Y2C, and Y3C. While DC had low noise levels throughout most of the first year from 2020 to 2021, noise from airgun signals were more commonly recorded during the 2021 to 2023 period, leading to increased noise levels below 100 Hz during these times (Figures 94, 95, 96, and 97).

A review of the spatial distribution of yearly medians of hourly-average octave band-levels at each site over the 2020 - 2023 period highlights the spatial distribution of some of the noise sources described above (Table 8). The 31.5 Hz octave-band-level represents sound from airgun surveys well, the 63 and 125 Hz band-level represents noise from shipping traffic (e.g. Marine Strategy Framework Directive, Descriptor 11), and the 500 Hz band-level represents noise from weather. The 31.5 Hz octave band-levels are generally higher in the northwestern, central, and deeper waters of the Gulf compared to the southwestern and the eastern Gulf (Figure 98), which is expected given the typical distribution of airgun survey effort in the northwestern and northcentral Gulf of Mexico, as well as longer-range sound propagation in

Table 8: Minimum and maximum ambient band-levels received over the August 2020-2021 period in the octave bands centered on 31.5 Hz, 63 Hz, 125 Hz, and 500 Hz.

| Octave Band (Hz) | Minimum RL (dB re $\mu$Pa$^2$) | Maximum RL (dB re $\mu$Pa$^2$) |
|---|---|---|
| **16** | 83.0 | 110.2 |
| **31.5** | 84.9 | 114.4 |
| **63** | 82.4 | 115.3 |
| **125** | 77.0 | 105.4 |
| **250** | 74.7 | 99.7 |
| **500** | 77.8 | 93.8 |

deep waters where seafloor absorption is lower. During the 2021-2022 period, 31.5 Hz noise levels were especially high at the central Gulf sites with yearly median noise levels of 112 dB re 1$\mu$Pa$^2$/Hz at site GC (Figure 98). This spatial distribution of noise levels corresponds well with locations of seismic survey activity described below in section 4.3.4.

Received levels in the 31.5 Hz octave band are lowest in the Rice's whale core distribution area (site DC) across all years, though levels were elevated during the 2nd and 3rd years of deployments, when airgun noise was more common, compared to the first year. Sites Y1D and MC also had relatively lower levels in this frequency band during 2020-2021. While the 63 Hz and 125 Hz octave band-levels are typically representative of shipping noise, maps of yearly medians of hourly-average band-levels (Figure 98) follow similar patterns to those for the 31.5 Hz band-levels indicating seismic signals are still dominating these bands most of the time. In the Rice's whale core distribution area, site DC has substantially lower noise levels in the 125 Hz octave band, which encompasses Rice's whale call frequencies, with average levels of 82 dB, compared to the next lowest levels of 89 dB (with 6 dB representing a doubling in noise levels on the log scale) at sites Y1D and MR during 2020-2021. Central sites had median yearly noise levels ranging from 99 to 105 dB in the 125 Hz octave-band (Figure 98). Noise levels in the 500Hz band continue to show similar patterns as those seen at the lower frequencies at the yearly scale, with highest levels in the central and northwestern Gulf, and lower levels at southwestern sites and at DC and Y1D (Figure 98). Interannual differences follow the same patterns as seen at lower frequencies (Figure 98), which may reflect the 200-300 Hz peak in energy that was associated with airgun activity at several sites (Figures 94, 95, 96, and 97).

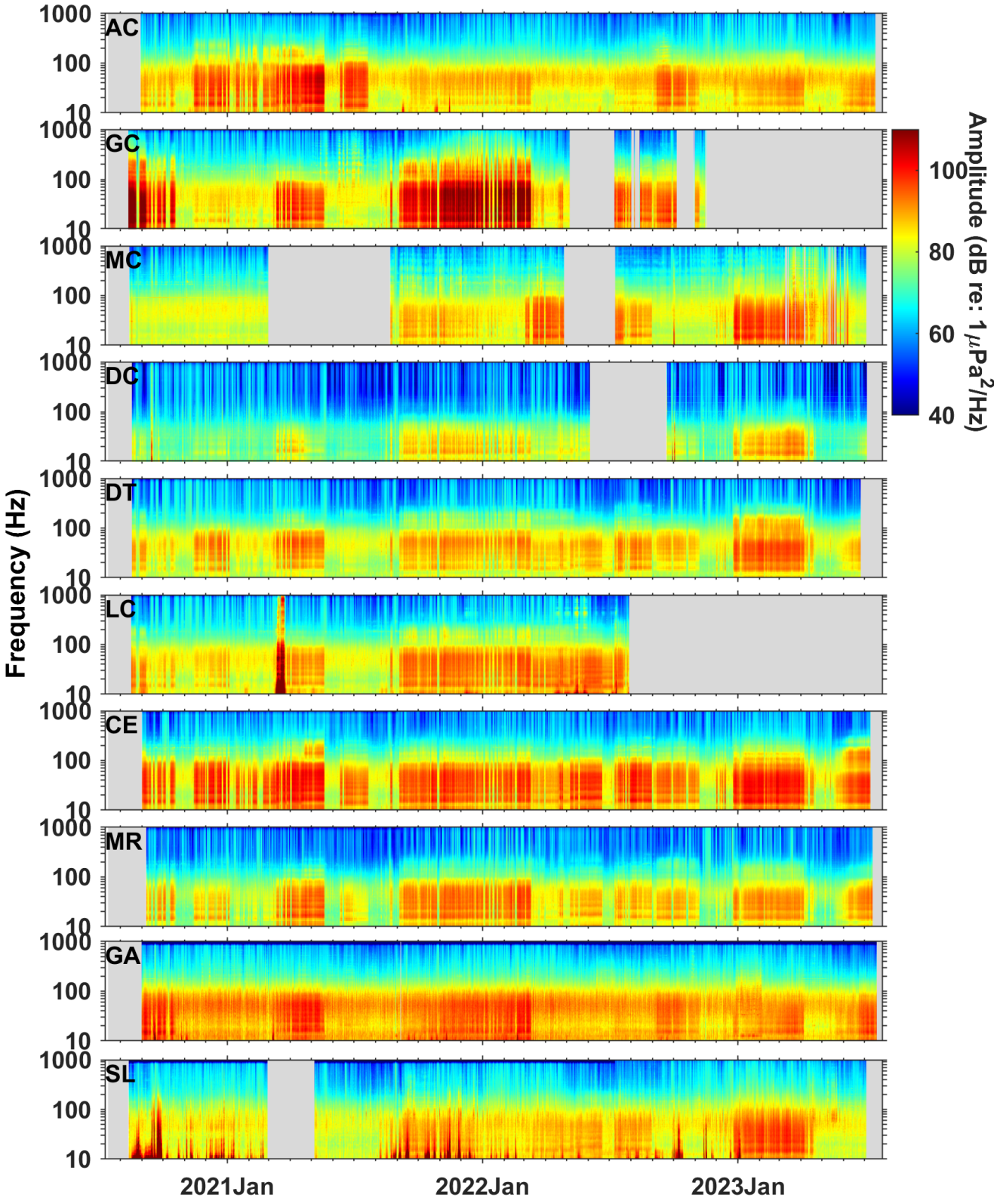


**Figure 94:** Long spectrograms using daily-averaged spectra for 2020-2023 data recordings at long-term sites. Gray blocks represent periods with no data recording.

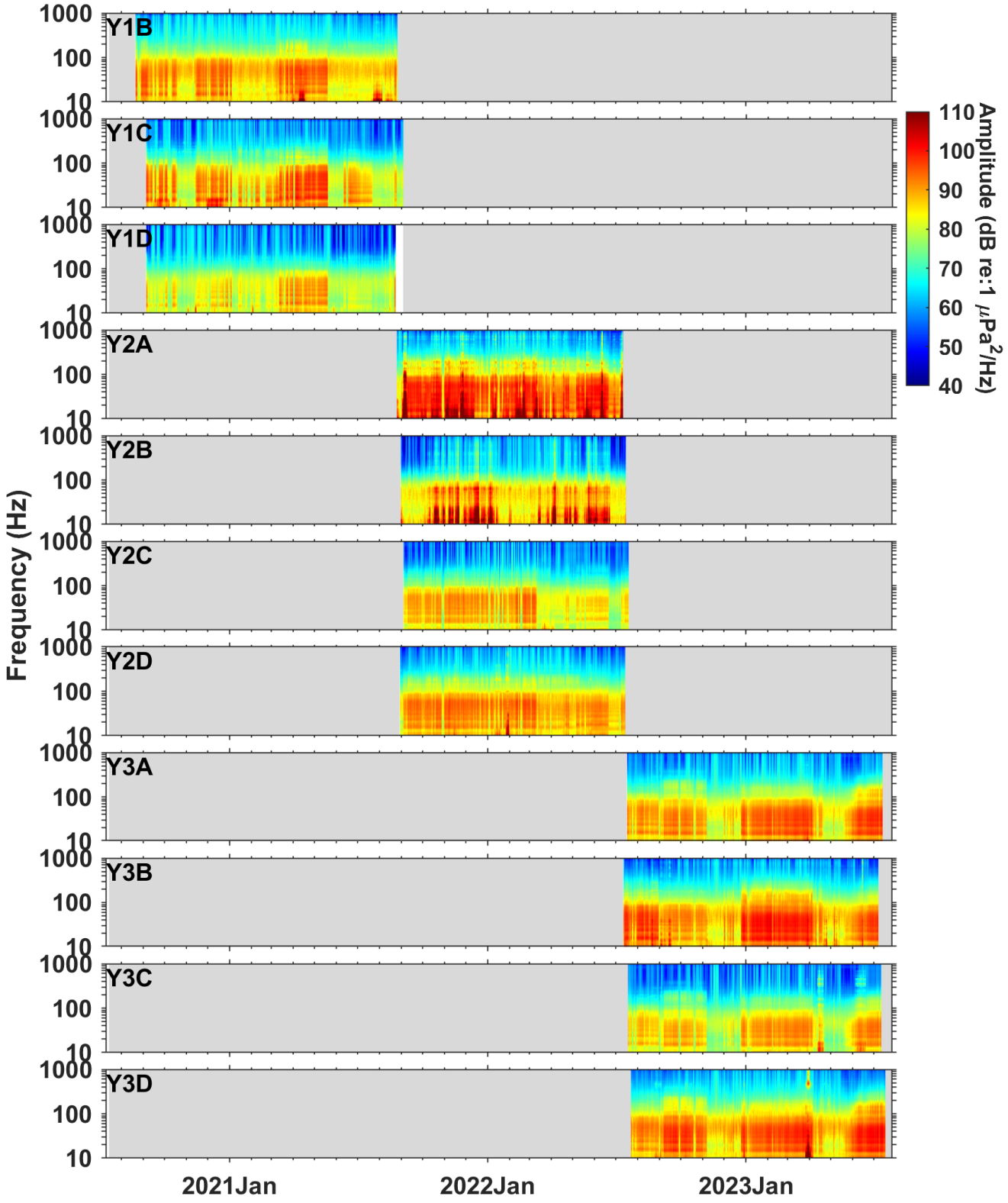


**Figure 95:** Long spectrograms using daily-averaged spectra for 2020-2023 data recordings at short-term sites. Gray blocks represent periods with no data recording.

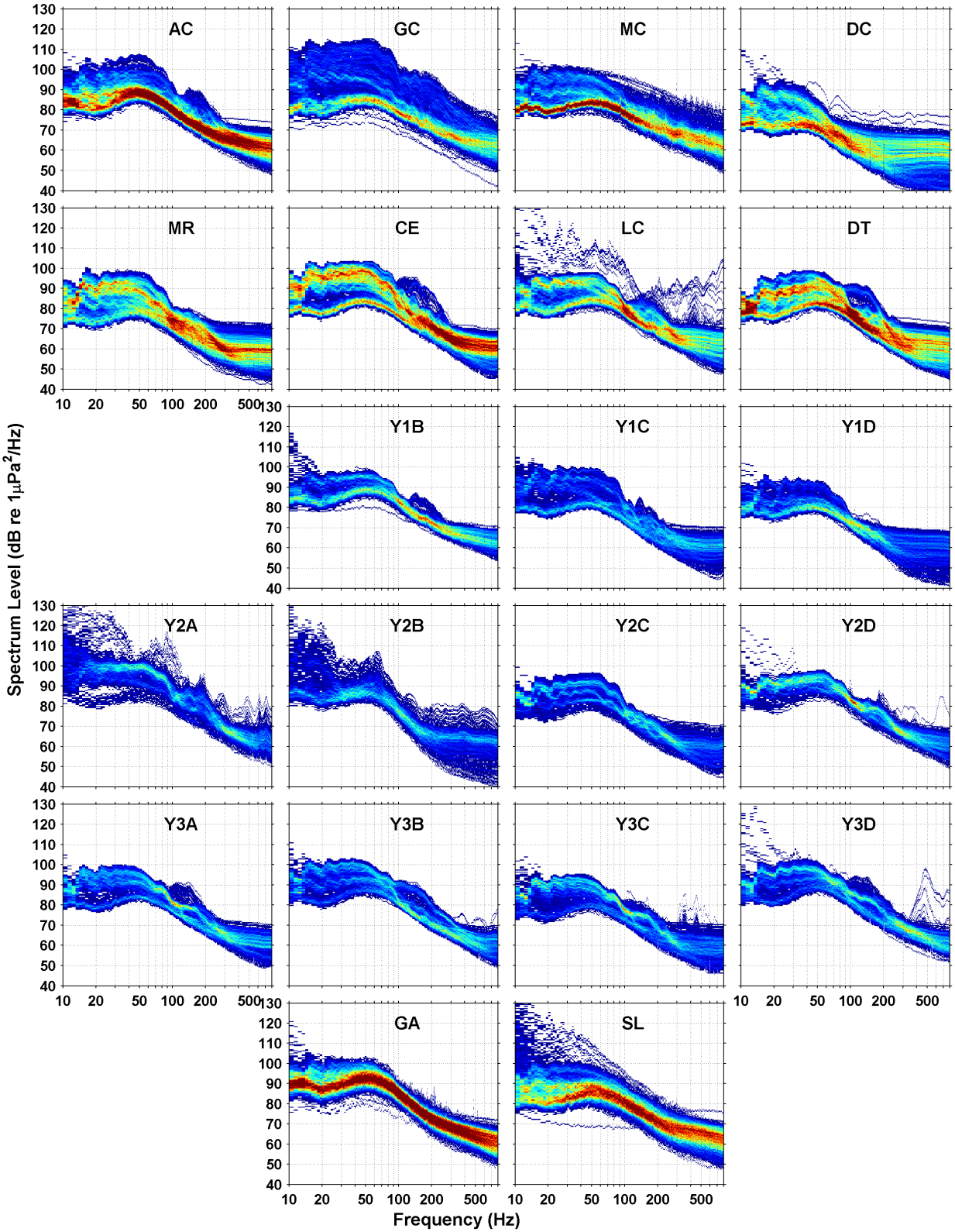


**Figure 96:** Heat map distribution of daily-mean ambient soundscape spectra for HARP and MARP sites from 2020-2023. Cool colors indicate lower frequency of occurrence while warmer colors indicate higher frequency of occurrence.

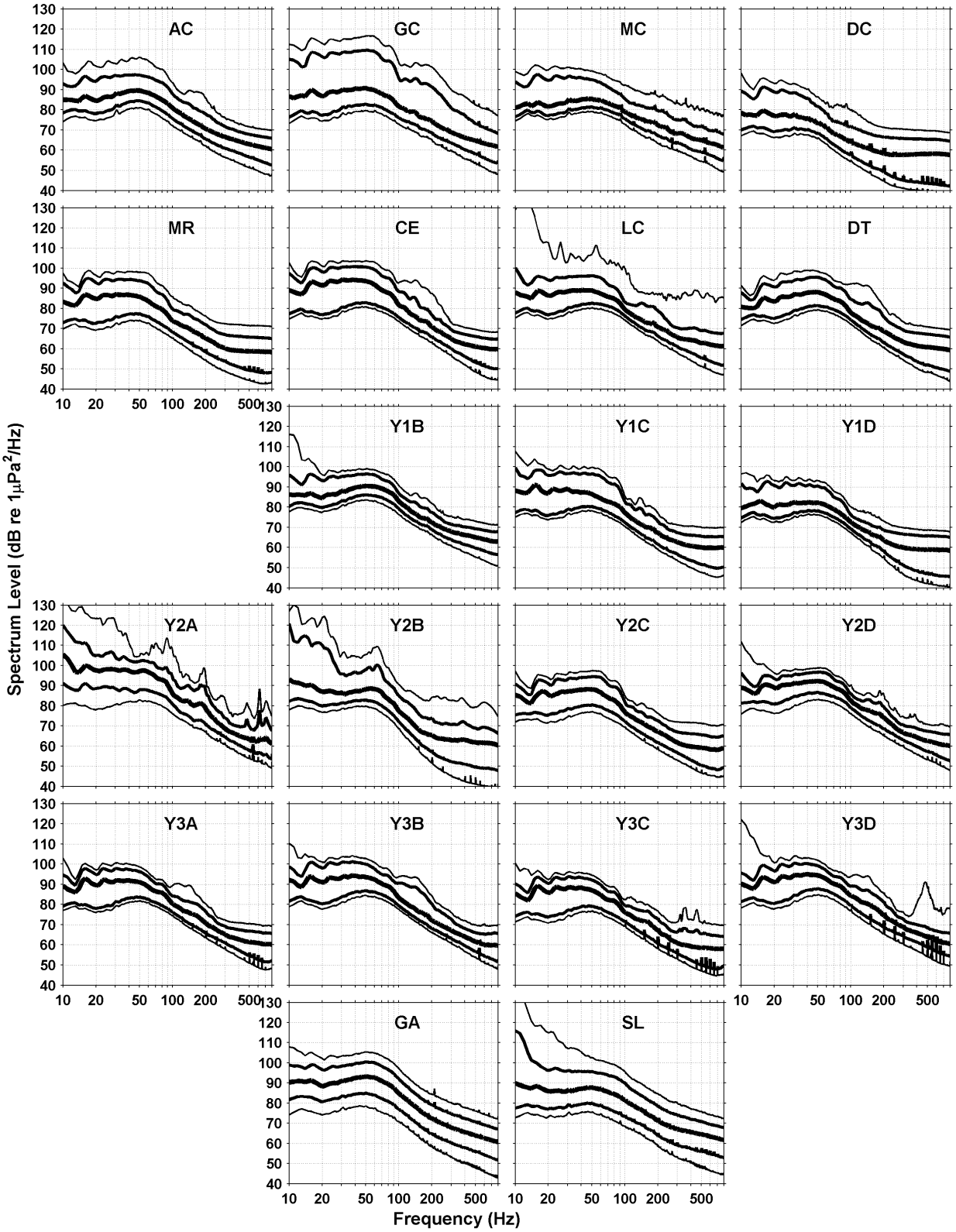


**Figure 97:** Statistical distribution of daily-mean ambient soundscape spectra for HARP and MARP sites from 2020-2023. The 50th (thickest), 10th and 90th (medium thickness), and 1st and 99th (thinnest) percentiles of hourly mean spectra are represented by solid lines.

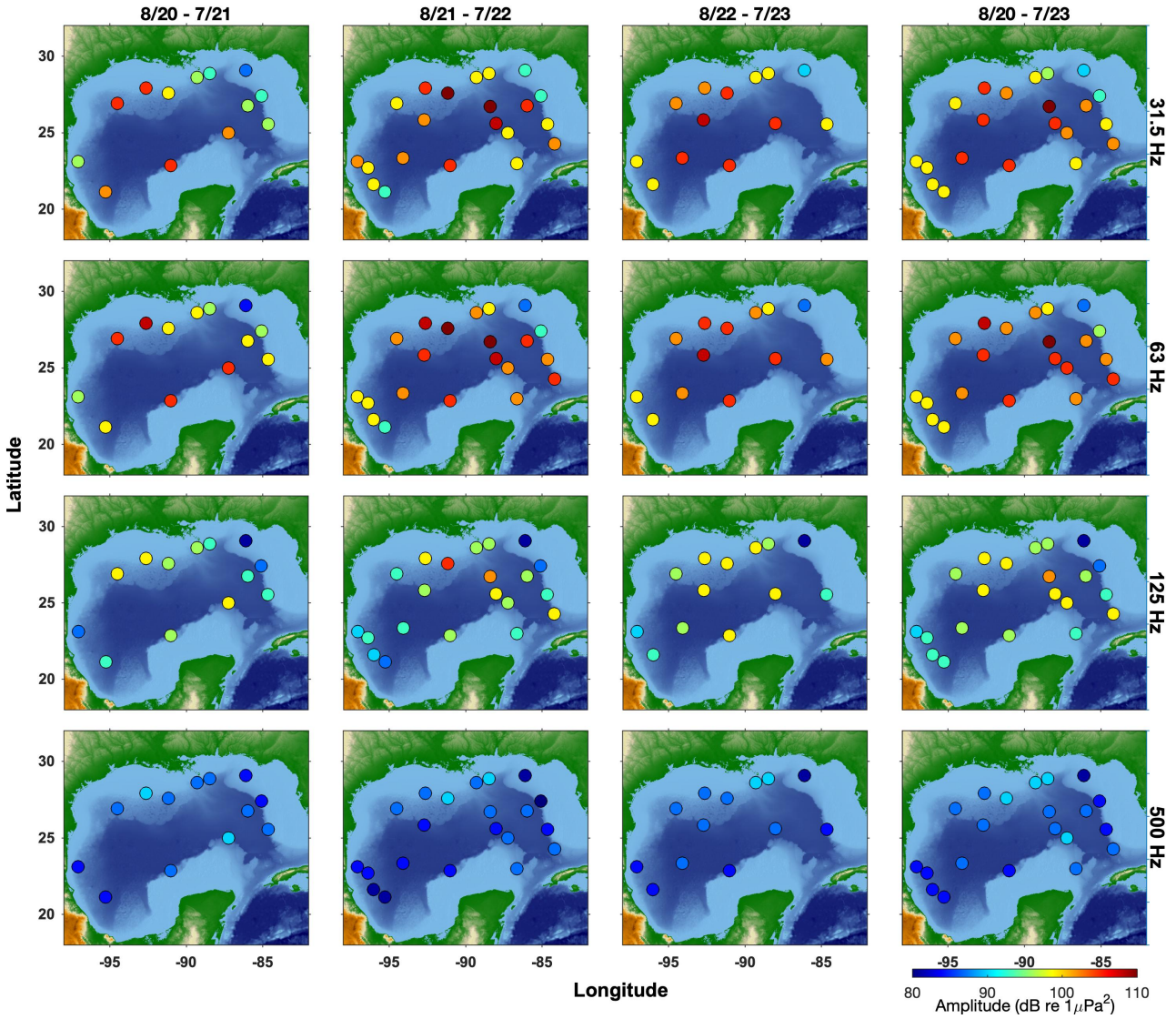


**Figure 98:** Yearly median of hourly-mean ambient octave-band-levels received at each site over the August 2020-2023 period, in the octave bands centered on 31.5 Hz (upper line), 63 Hz (second line), 125 Hz (third line), and 500 Hz (bottom line). Filled circles are colored by octave-band-level measured as the sum over the respective octave bands (rows) according to the color bar (bottom right). Columns represent each of the three monitoring years, with the furthest right column representing medians over the full three year period.

### 4.3.2 Broadband Ships

Analyses of broadband shipping noise detections and AIS ship track data from ships passing close to HARP sites highlight the high levels of shipping activity in the Gulf of Mexico, and the variability in activity, noise levels, and vessel types among sites. Over 63,000 close ship transits were detected across all sites during this three year period. Analyses of data from 2020-2023 indicate the highest number of detections and longest durations of ship noise presence occurred at sites GA (total 20,399 detections, mean 138.6 detections per week; mean 61.2 hours present per week; Figures 99 and 100) and SL (total 13,871 detections, mean 95.2 detections per week; mean 44.7 hours present per week; Figures 99 and 100; Table 9), the two sites located within major shipping lanes. Sites AC, Y1B, Y2B, and Y3D also had elevated numbers of nearby ship transits, likely due to their proximity to heavy shipping traffic (Figures 99, 100 & 101). These four sites, especially site AC, also had long durations of ship noise present, with means of 31.7-42.2 hours per week (Figures 99 & 100; Table 9). Sites GC and MC have moderately elevated numbers of ship transits (Figure 99), likely due to the presence of major shipping lanes and oil rigs nearby (Figure 101). Site DC had low numbers of ship detections but elevated durations of ship noise presence, possibly indicating that ships are passing at slower speeds or that they are detectable for longer periods due to the relatively quiet conditions found at this site. Sites DT, MR, Y2D, and Y3B had relatively low numbers of ship detections and durations compared to the previously mentioned sites, and sites CE, LC, Y1C, Y1D, Y2A, Y2C, Y3A, and Y3C had the fewest ships detected as well as lower durations of ship noise presence. The spatial patterns in durations per year with close-passing vessel noise present (Figure 102) closely follows the spatial density of AIS ship tracks (Figure 101).

The AIS data indicated substantial variability in ship types, number of ships, and closest point of approach of ships at the different sites. The “other” ship type category included industrial ships, mobile offshore drilling units, offshore supply vessels, and research vessels, which were all ship types classified individually prior to 2018, and are more often classified individually after 2021. This category also included additional less common ship types.

Cargo ships and tankers were the most common, passing by most sites (Figures 103 & 104). Cargo ships were the dominant ship type at sites DC (mostly passing at distances >13 km), CE (similar numbers between 0-14 km), MR (with greater numbers >4 km away), Y1B (similar numbers at distances >1 km), Y2A (with greater numbers >5 km away), Y2C (with greater numbers 11-12 km away), Y2D (similar numbers >1km away), Y3B (greater numbers >10 km away), and SL (especially within 2 km) (Figure 103). Sites MR, Y1B, Y2A, Y3B, and SL also had large numbers of tankers, passing at relatively similar distances at sites MR, Y2A, and Y3B, and passing mostly within 2 km at site SL. At site SL, passenger ships and other ship types become more common after 3 km, the distance at which the number of ships passing substantially decreased (Figure 103).

Tankers made up more than 50% of the shipping traffic at sites AC, Y2B, Y3A, and Y3D, and the majority of traffic at sites GA, and GC (Figures 103 & 104). The tankers mainly passed within 8-9 km at sites GC and AC, at similar distances at site Y3A and Y3D, and within 2 km at

site GA. The number of ships passing by site GA significantly dropped after 3 km. Site GC also had elevated numbers of other ship types, which likely included offshore supply vessels due to its proximity to oil rigs.

Site MC had the greatest number of other ship types (Figures 103 & 104), peaking at 4 km and distances >13 km away. Similar to GC, this other category likely included mostly offshore supply vessels due to its proximity to oil rigs. Site MC also saw high numbers of cargo ships, passenger ships, and tug tows. Site DT, which was near a shipping lane, had primarily cargo ships, tankers, and tug tows, with most ships >7 km away. Site Y1D had a variety of ship types – including cargo ships, fishing vessels, pleasure vessels, tankers, and tug tows. Finally, it is important to note the AIS data were especially sparse for sites LC, Y1C, Y2C, Y3A, and Y3C.

Ship broadband RLs for the automated ship detections varied across sites (Figures 105 & 106), with the lowest broadband RLs found at site DC and the highest broadband RLs found at sites GA and SL. Moderately-high received levels were common at long-term sites AC, GC, and MC, and short-term sites Y2A and Y2B. It is not surprising that the two shipping lane sites had the highest broadband RLs, as a majority of ship passings occurred within 3 km of the HARPs, closer than any other site. Likewise, with most ships passing greater than 13 km away, it is not unexpected for site DC to have lower broadband RLs. Within sites, decreasing broadband RLs with greater distances were evident for acoustically detected ships that were equipped with AIS (Figures 107 & 108), as expected given sound propagation losses with distance.

Given the high levels of shipping activity in the Gulf of Mexico, it is unsurprising that some ships were detected multiple times over the current three year study period. Between 2020-2023, tens of thousands of ships passed within 15 km of the Gulf HARPs with thousands passing multiple times, and some making 100 – 1500 different close approaches to the HARPs (Figure 109). Passenger ships, tankers, tug tows, and other ship types (including offshore vessel supply ships) were the most common ship types to be detected repeatedly, while cargo ships and fishing vessels were less likely to be detected more than 1-5 times. Ships with repeated passages through the Gulf contribute to the Gulf soundscape more frequently than those which only pass through occasionally.

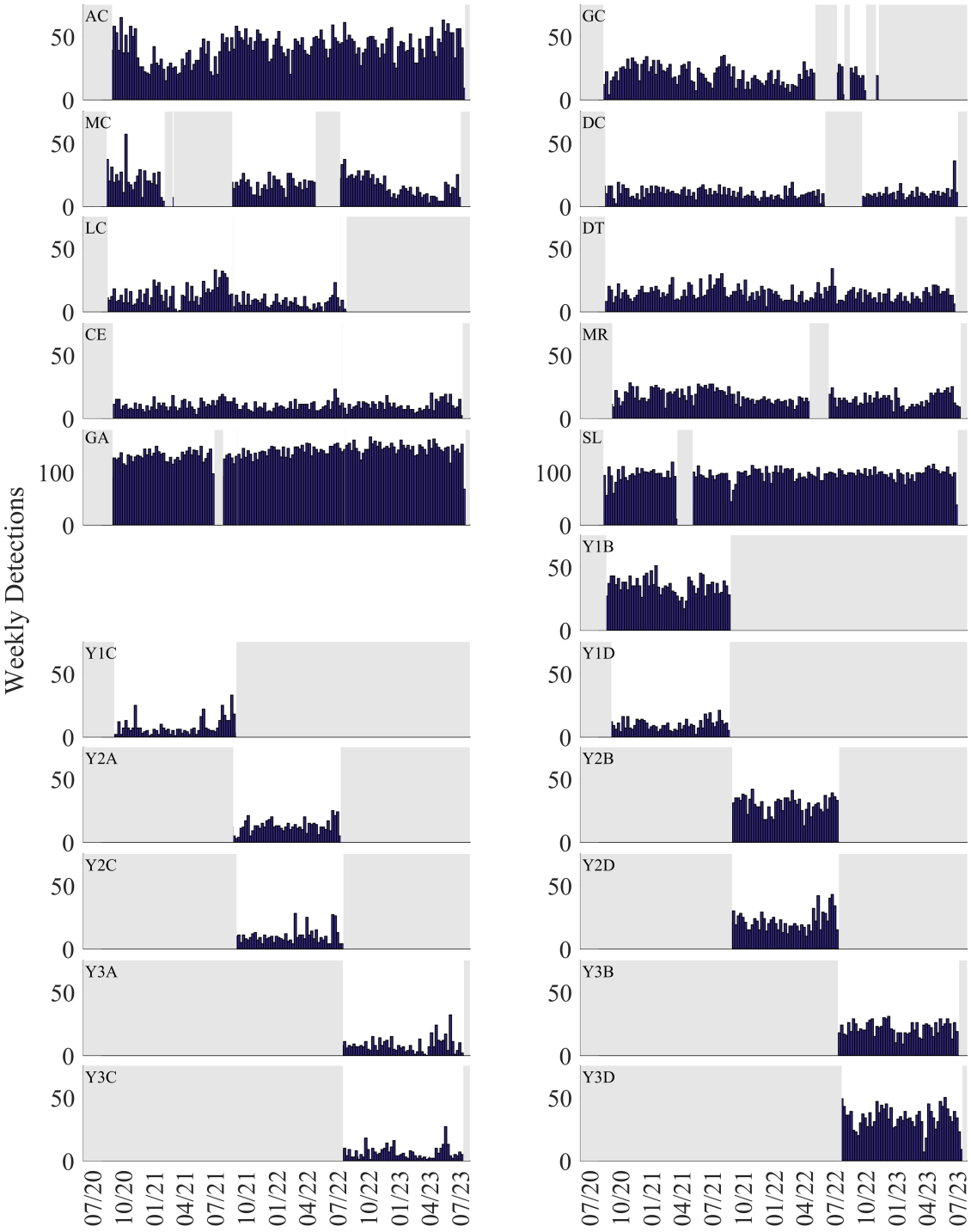


**Figure 99:** Cumulative weekly counts of close-approach ship transits acoustically detected in Gulf of Mexico HARP recordings between 2020-2023. Note: Sites GA and SL have a different scale on the y-axis due to the higher number of ship transits in these shipping lane sites.

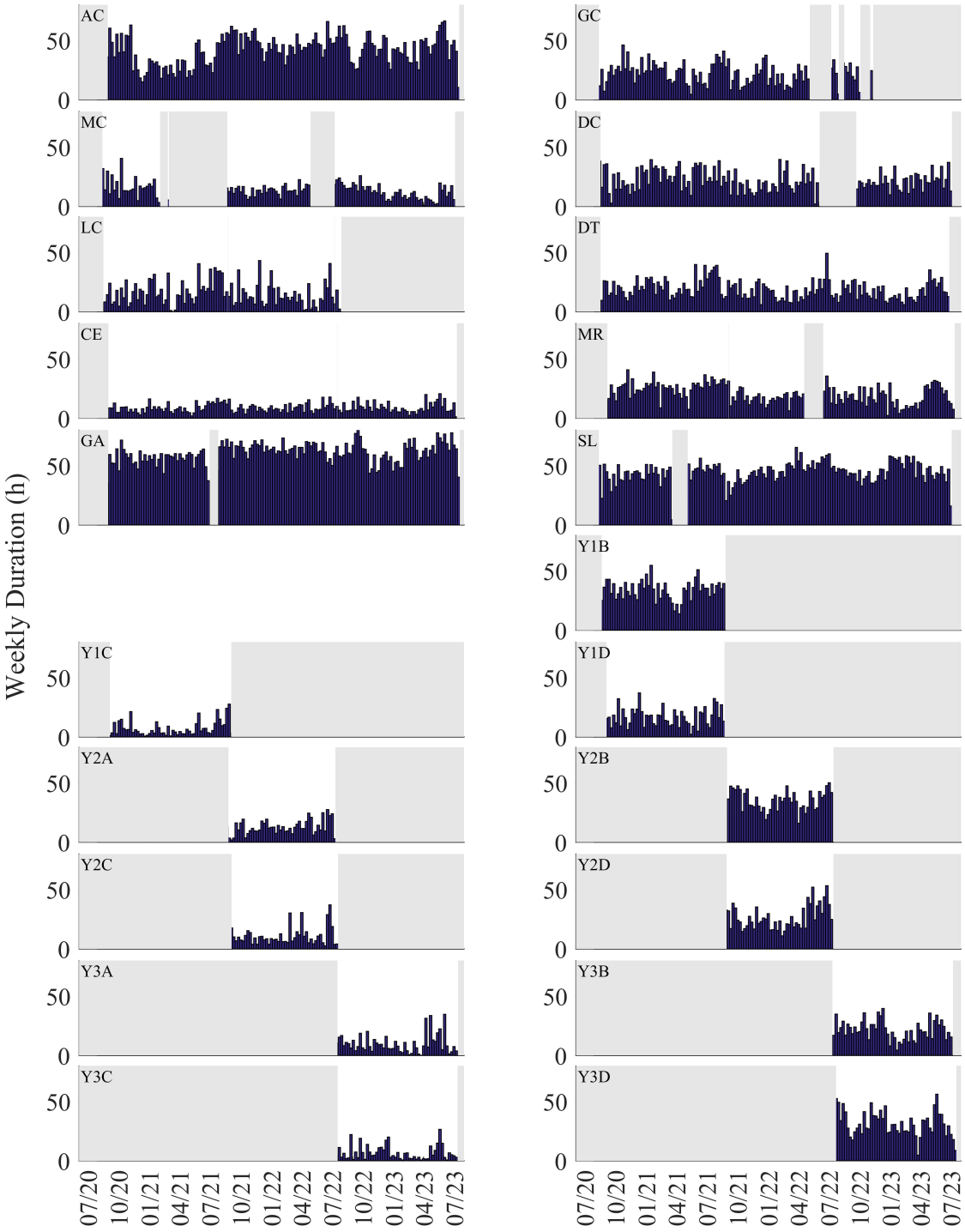


**Figure 100:** Weekly cumulative hours present for close-approach ship transits acoustically detected in Gulf of Mexico HARP recordings between 2020-2023.

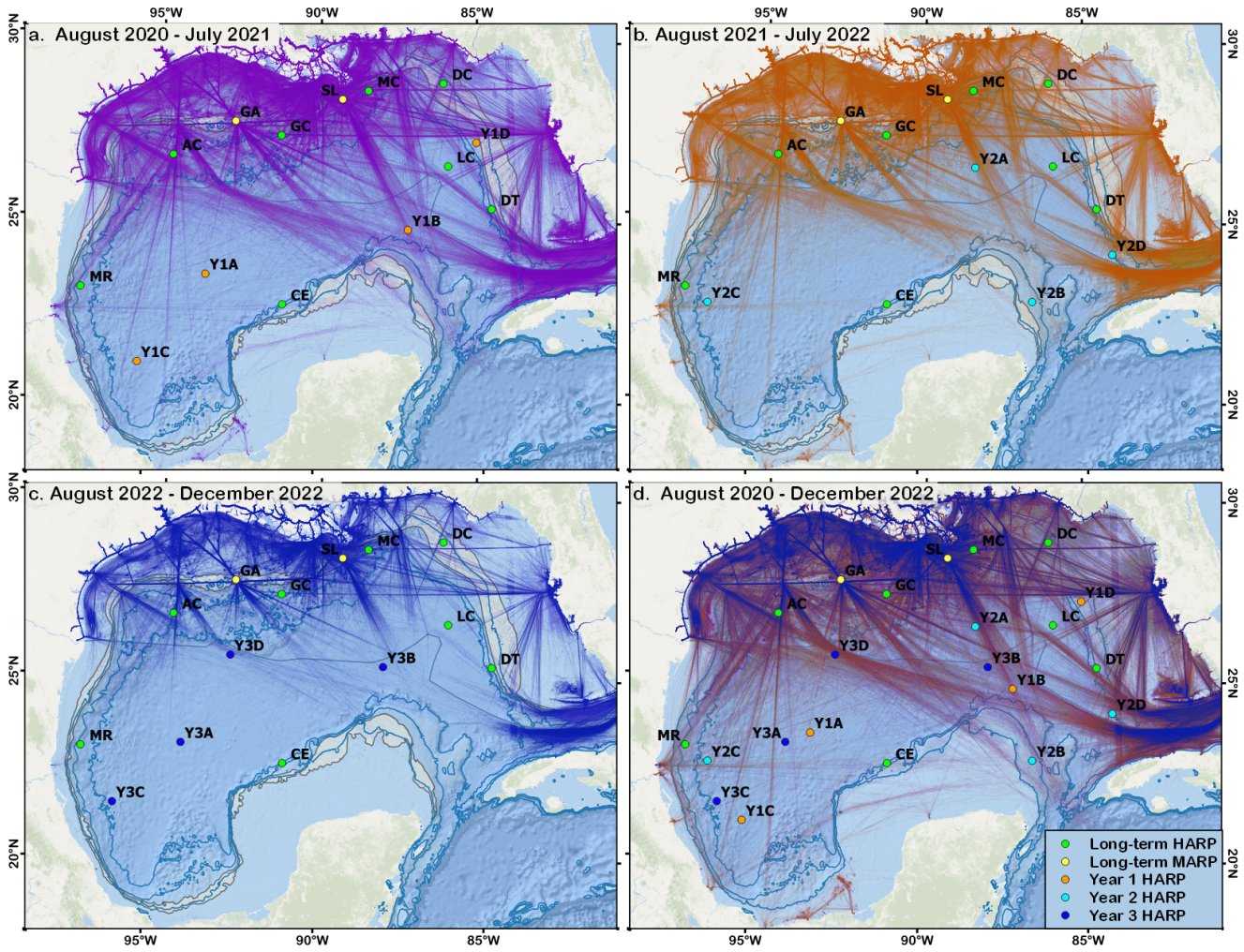


**Figure 101:** AIS-based vessel tracks (from MarineCadastre) in the Gulf of Mexico over the August 2020 to December 2022 period. Panels represent vessel tracks in each of the three years of recordings with the bottom right panel representing all years combined. Vessel track data for January to July 2023 is not included as it is not yet available from MarineCadastre. Lighter levels in the southern Gulf are an artifact of lower AIS-receiver coverage in that region within the Marine Cadastre dataset.

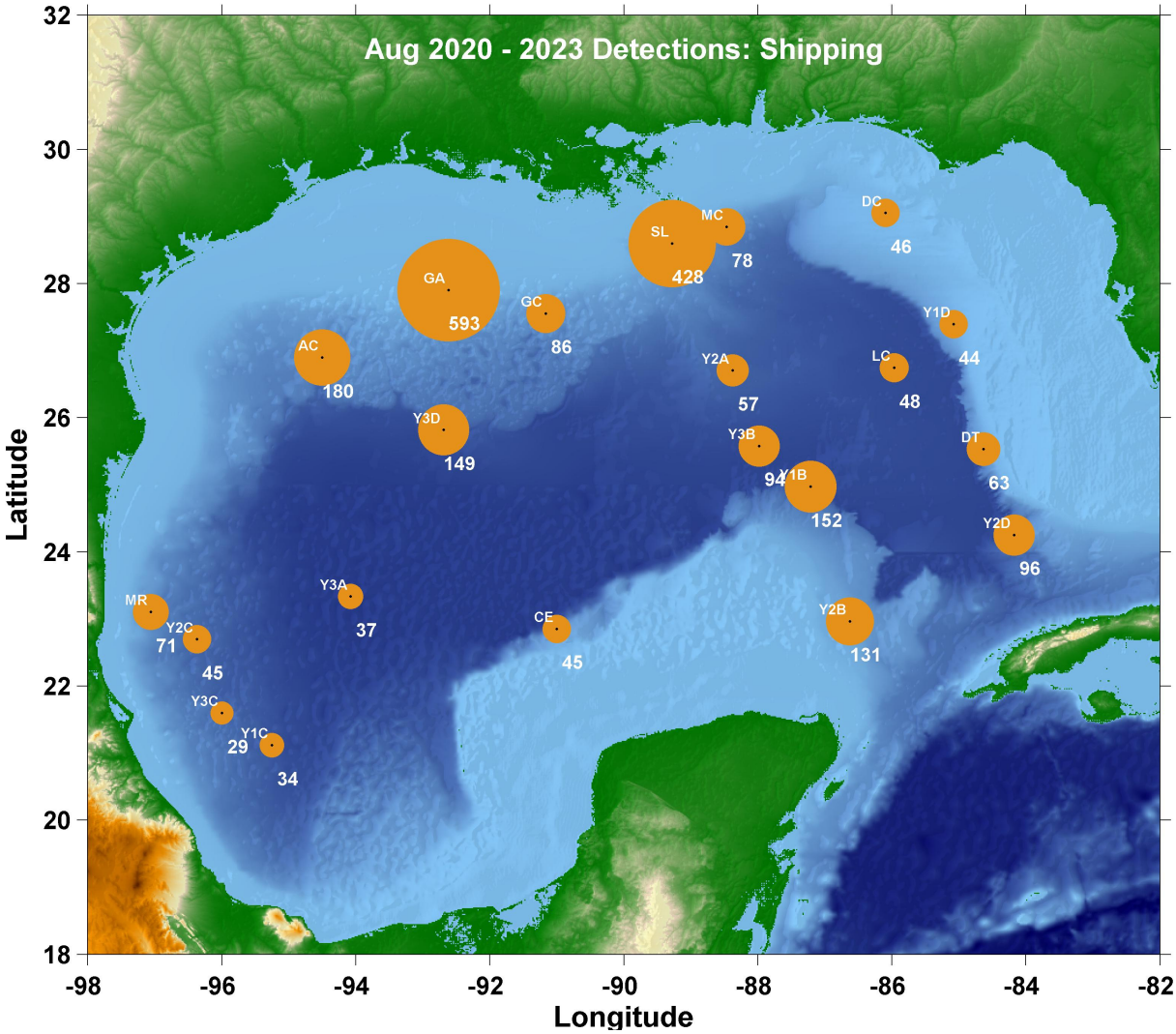


**Figure 102:** Average detections per month per year of broadband shipping noise at each HARP location from 2020-2023.

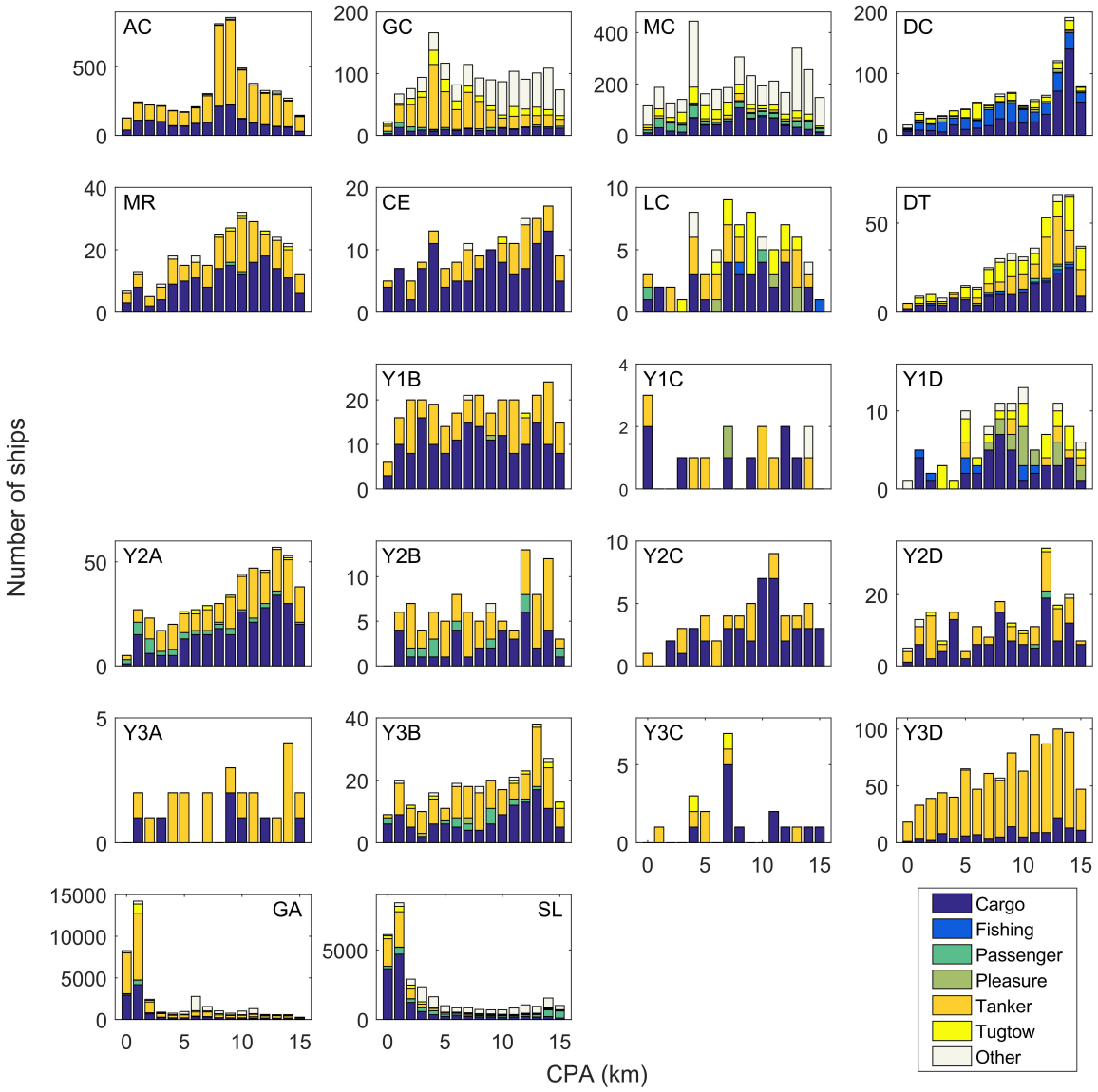


**Figure 103:** Ship closest point of approach (CPA) by vessel category for 2020-2023, based on AIS data (from Marine Cadastre) for ships transiting within 15 km of each HARP site. The number of ships is cumulative over the 2020-2023 period for all sites.

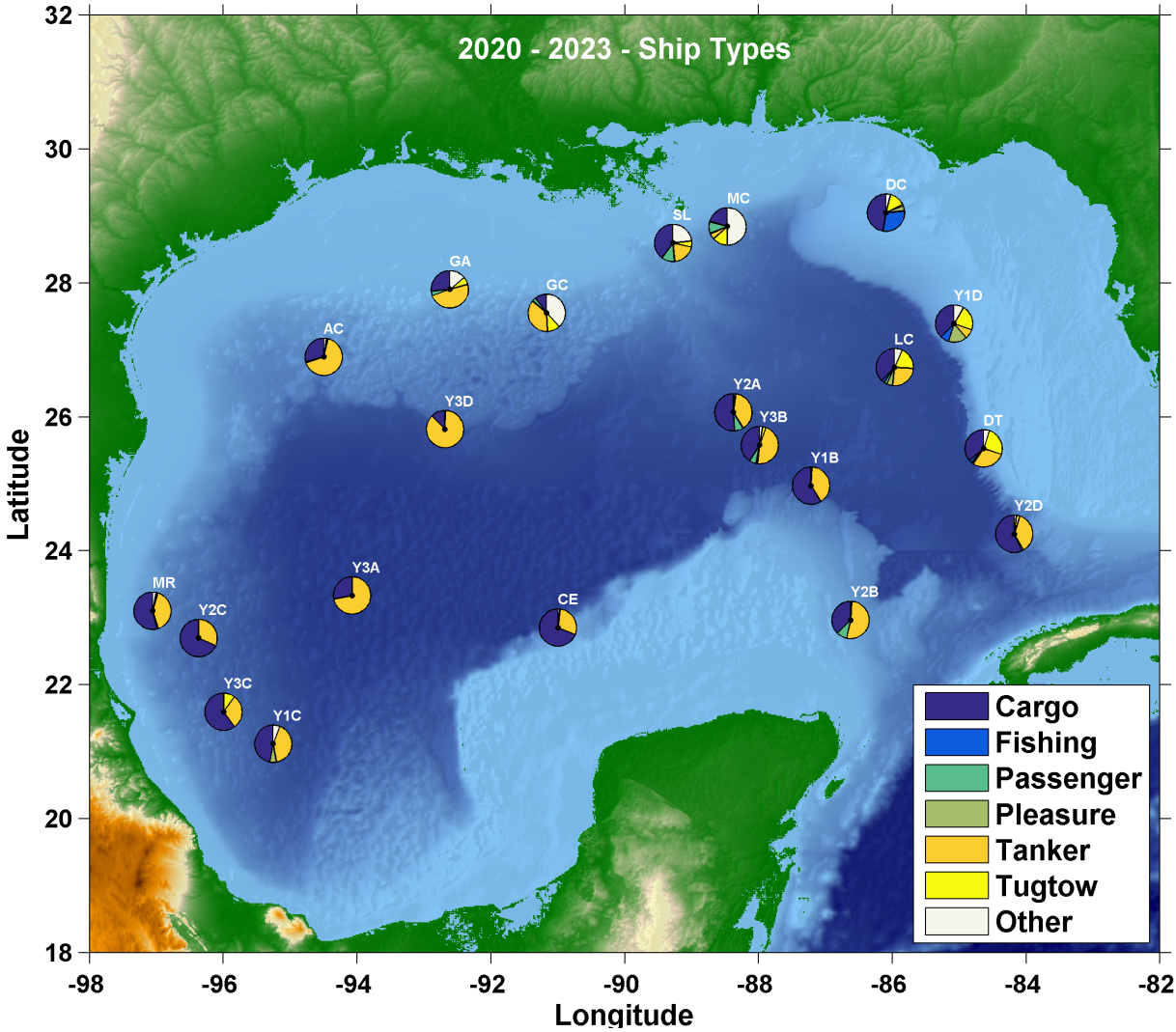


**Figure 104:** Proportion of ship types transiting within 15 km of each HARP location based on AIS data (from MarineCadastre) from 2020-2023, represented as pie charts.

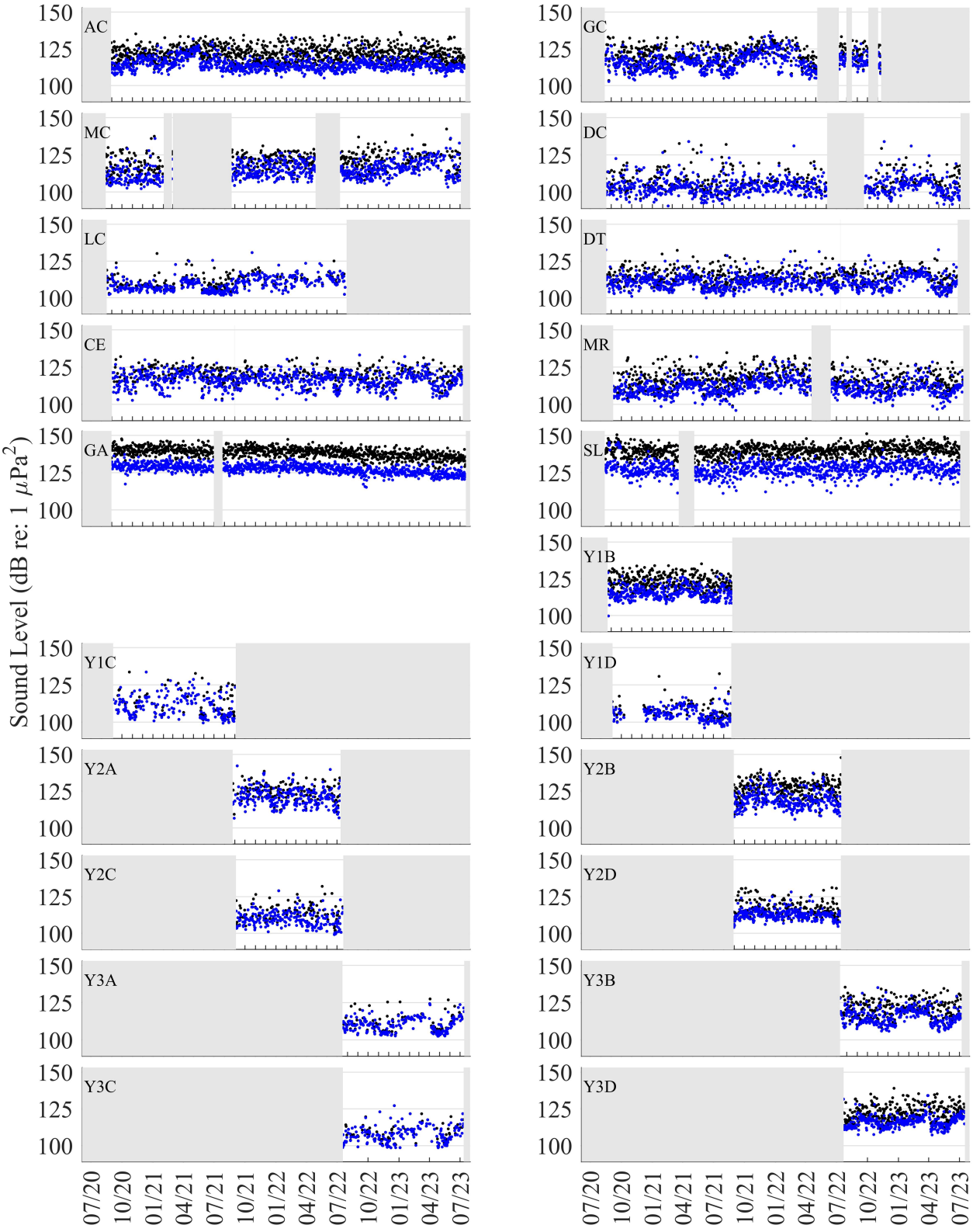


**Figure 105:** Weekly distribution of received sound levels (50th and 95th percentiles) at the acoustically-derived closest point of approach for ship transits acoustically detected in Gulf of Mexico HARP recordings between 2020-2023. Received levels are calculated as a summed band level over the 10-5000 Hz band.


**Figure 106:** Statistical distribution of received sound levels for close-approach ship transits acoustically detected in Gulf of Mexico HARP recordings at 21 sites between 2020-2023 using the automated ship sound detector. Red outlines indicate the distribution of received levels, normalized such that the maximum width is constant across sites. Red boxes within the distribution hourglasses span the 25th to 75th percentiles, with a horizontal line at the median. Red dots indicate outliers. Received levels are calculated as a summed band level over the 10-5000 Hz band.

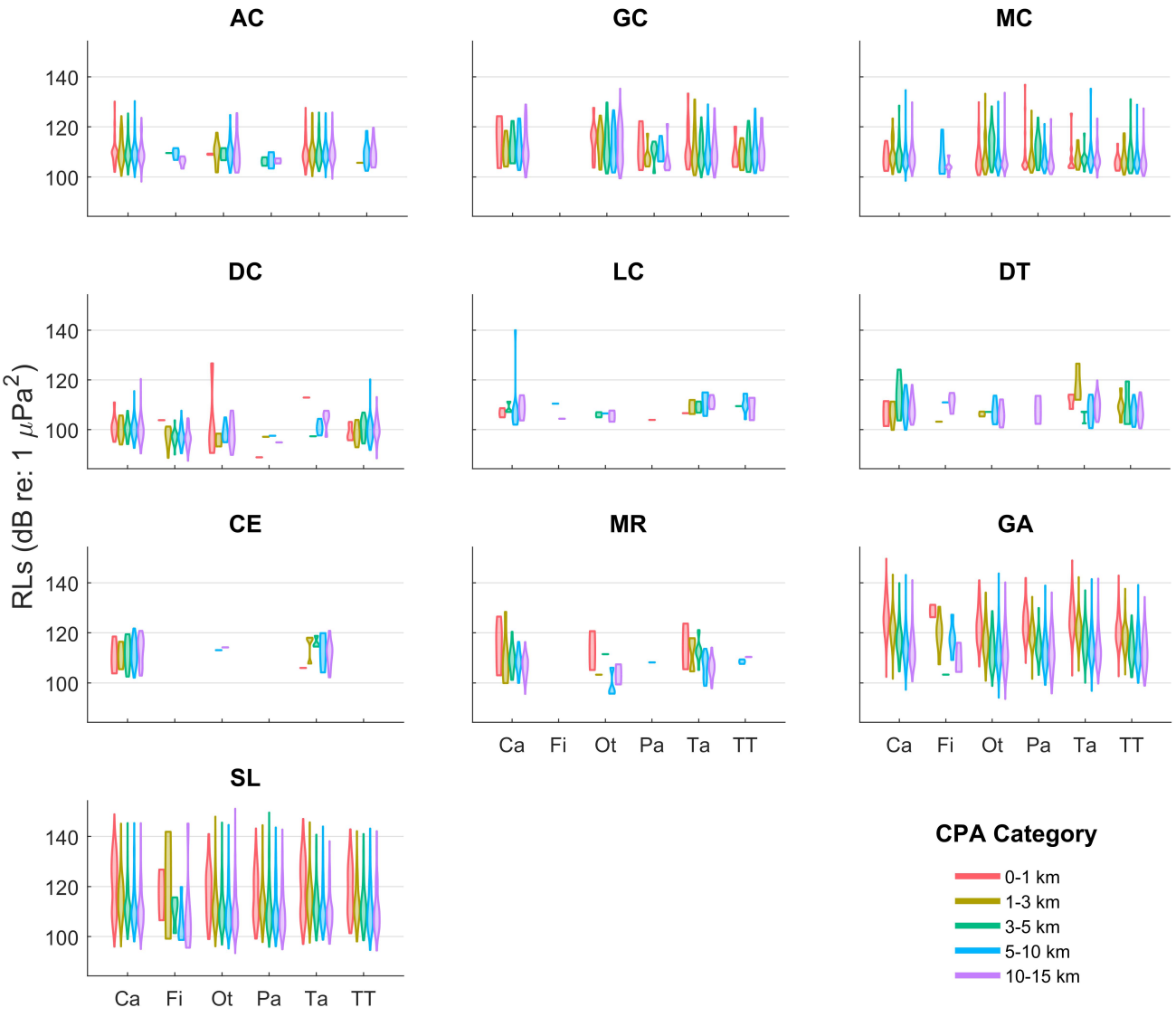


**Figure 107:** Sound levels by vessel category for close-approach AIS-equipped ship transits acoustically detected in Gulf of Mexico HARP recordings between 2020-2023 at long-term sites. Received levels are calculated as a summed band level over the 20-1000 Hz band. Shapes represent the distribution of the measured sound levels at each site, normalized to a constant width across sites. Ca = cargo ships, Fi = fishing vessels, Pa = passenger vessels, Pl = pleasure vessels, Ta = tankers, and TT = tug tows.

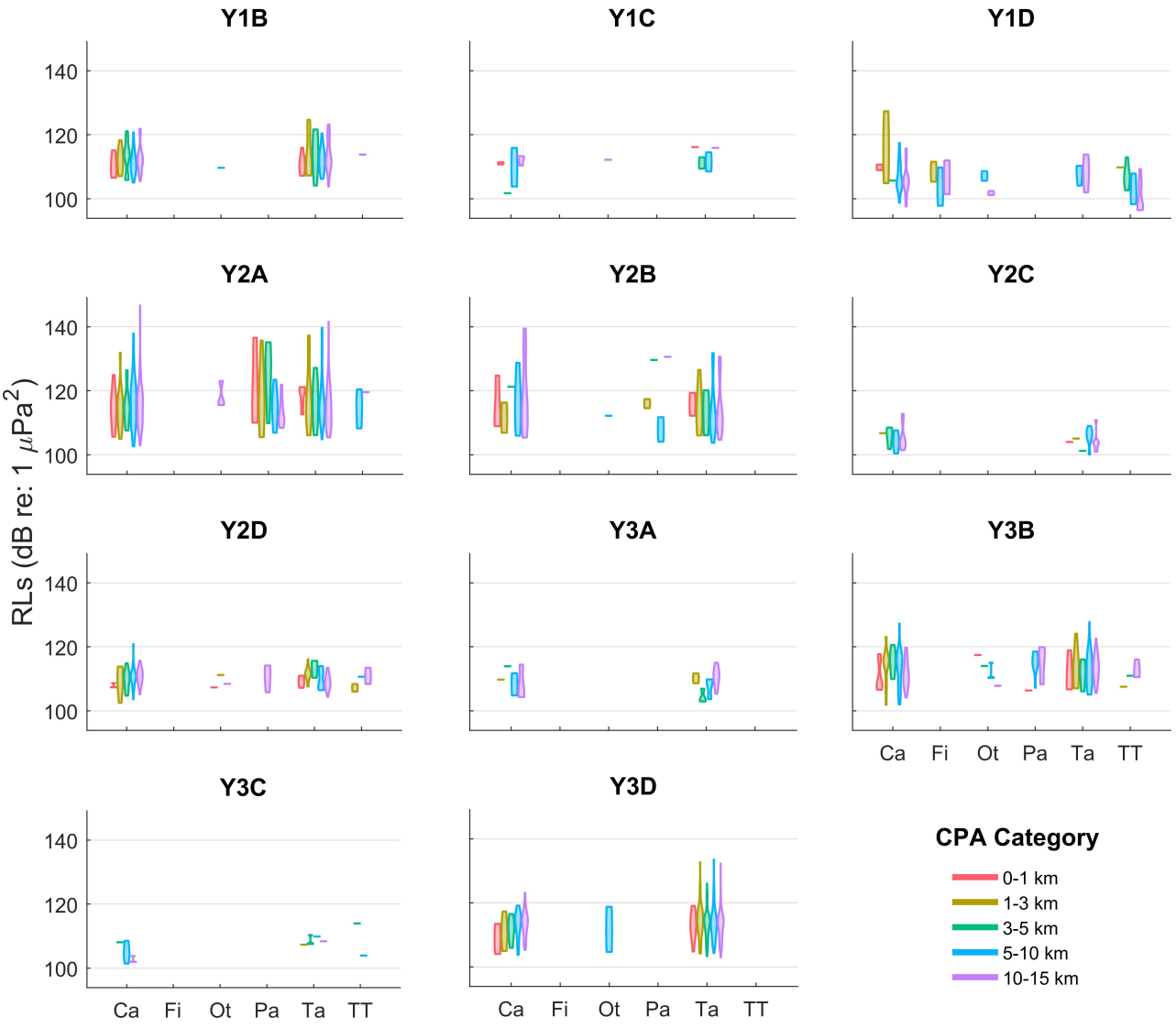


**Figure 108:** Sound levels by vessel category for close-approach AIS-equipped ship transits acoustically detected in Gulf of Mexico HARP recordings between 2020-2023 at short-term sites. Received levels are calculated as a summed band level over the 20-1000 Hz band. Shapes represent the distribution of the measured sound levels at each site, normalized to a constant width across sites. Ca = cargo ships, Fi = fishing vessels, Pa = passenger vessels, Pl = pleasure vessels, Ta = tankers, and TT = tug tows.

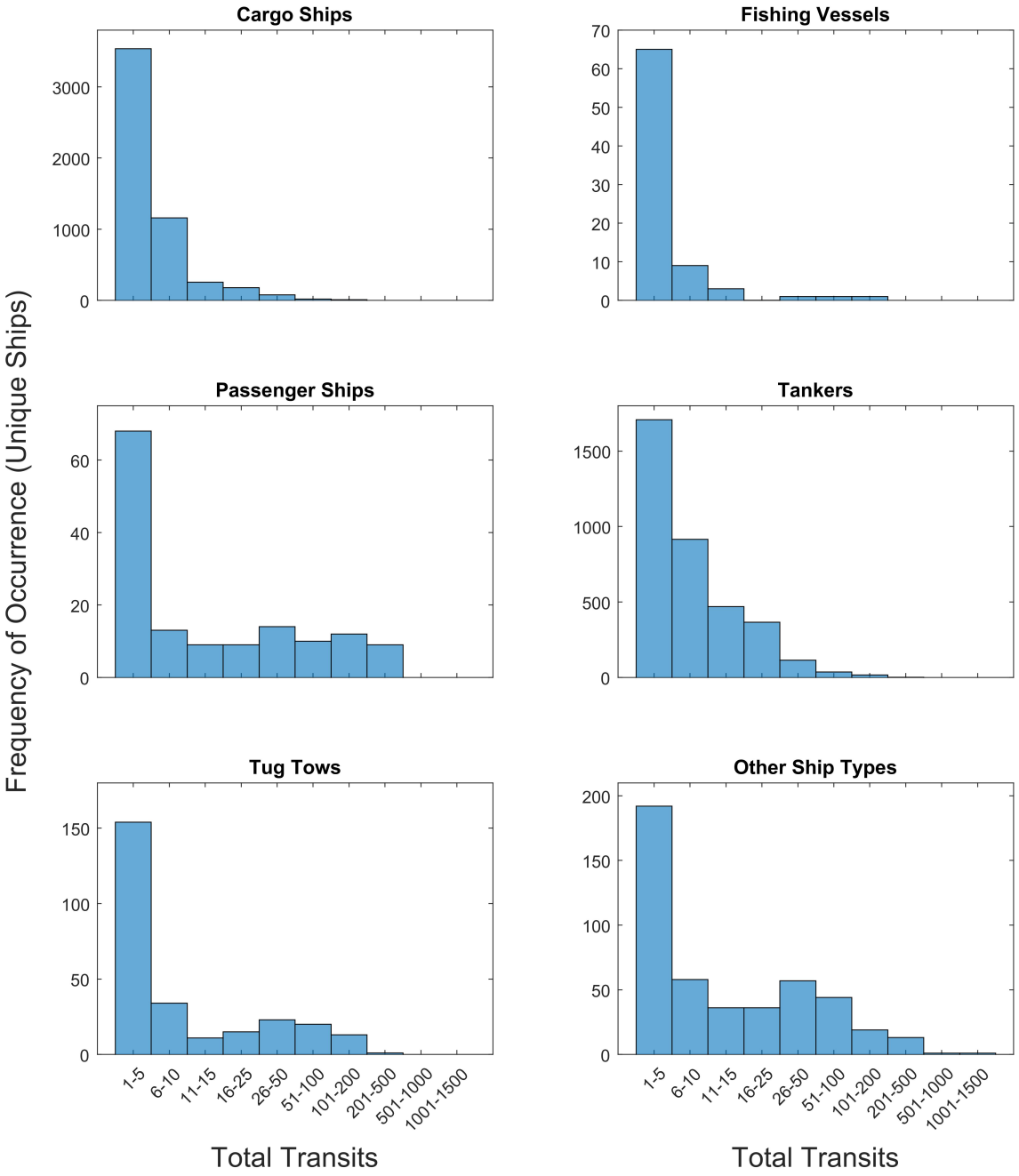


**Figure 109:** Number of transits of individual ships (i.e., repeat transits) passing within 15 km of at least one Gulf of Mexico HARP, identified and classified by AIS (Marine Cadastre) as cargo ships, fishing vessels, passenger ships, tankers, tug tows, and other ship types.

| | Ship Detector | | AIS | | Airguns | |
|---|---|---|---|---|---|---|
| **Site** | **Detections** | **Presence (h)** | **Detections** | **Presence (h)** | **Detections** | **Presence (h)** |
| **AC** | 41.2 | 42.2 | 38.7 | 25.5 | 14,840 | 3,749 |
| **GC** | 19.6 | 22.2 | 15.0 | 11.9 | 20,273 | 3,382 |
| **MC** | 17.6 | 13.5 | 29.4 | 28.1 | 8,114 | 2,036 |
| **DC** | 10.4 | 22.0 | 7.6 | 6.5 | 1,697 | 532 |
| **DT** | 14.4 | 18.7 | 3.3 | 1.8 | 17,556 | 3,651 |
| **LC** | 11.3 | 16.0 | 0.8 | 0.5 | 14,855 | 2,979 |
| **CE** | 10.3 | 9.1 | 1.2 | 0.6 | 33,723 | 6,283 |
| **MR** | 16.4 | 21.1 | 2.1 | 1.3 | 15,354 | 2,938 |
| **GA** | 138.6 | 61.2 | 277.9 | 116.7 | 9,874 | 3,005 |
| **SL** | 95.2 | 44.7 | 228.6 | 130.6 | 9,311 | 3,304 |
| **Y1B** | 34.9 | 34.0 | 7.2 | 3.9 | 7,946 | 1,699 |
| **Y1C** | 7.8 | 7.1 | 0.4 | 0.2 | 8,725 | 1,539 |
| **Y1D** | 9.7 | 16.8 | 2.1 | 1.3 | 1,486 | 626 |
| **Y2A** | 12.9 | 13.1 | 11.6 | 5.7 | 13,198 | 2,698 |
| **Y2B** | 30.0 | 35.3 | 2.3 | 0.9 | 3,720 | 1,559 |
| **Y2C** | 10.3 | 10.8 | 1.3 | 0.8 | 5,957 | 1,088 |
| **Y2D** | 22.1 | 26.5 | 4.6 | 2.7 | 10,308 | 1,872 |
| **Y3A** | 8.6 | 10.3 | 0.5 | 0.5 | 9,536 | 2,056 |
| **Y3B** | 21.6 | 21.8 | 5.9 | 3.3 | 9,904 | 2,428 |
| **Y3C** | 6.6 | 7.0 | 1.7 | 1.7 | 4,318 | 1,149 |
| **Y3D** | 34.3 | 31.7 | 20.1 | 12.1 | 10,580 | 2,536 |

**Table 9:** Columns 1 & 2: Weekly count of broadband ship detections and total detection durations from the automated ship detector. Columns 3 & 4: AIS-based ship transit counts and duration of presence within a 15 km radius of each site. Columns 5 & 6: Airgun pulse detection counts and cumulative hours containing detections. Counts and durations span the 2020-2023 monitoring period.

### 4.3.3 Vessel Source Levels

Vessels transiting over the MARP (within 200m) in the Galveston shipping lane site (GA) were primarily tankers (1,908 transits) and cargo ships (1,198 transits) (Figure 110). In contrast, vessels transiting over the Southern Louisiana shipping lane site (SL) were predominantly cargo ships (1,475 transits) with roughly half as many tanker transits (790) (Figure 111). Tug tows were the third most common vessel category at both sites (63 and 75 transits at GA and SL respectively). Small site position adjustments (within 100 m) in 2021 improved the site alignment within their respective shipping lanes, resulting in more close transits in years 2 and 3 (Figures 115 & 114). Transit speeds were similar at the two sites, with a subset of higher speed transits (>15 knots) recorded at GA. Transit speeds appear to be stable over time. The variability of harmonic mean sound speed estimates derived from HYCOM hindcasts was slightly higher at the SL location (Figure 115), with overall higher values at site GA (Figure 114). Northbound transits were more common at close range than southbound transits at site GA, while southbound transits were slightly more common at Site SL after the site was re-positioned in August 2021.

Monopole source level (MSL) estimates for the major vessel categories were very similar across the two shipping lane sites (Figures 112 & 113), indicating that the modified Lloyd's mirror model largely accounts for site specific differences for these close-approaching transits. A declining trend in received levels at site GA from July 2021 to July 2023 is currently unexplained, and results in a similar trend in MSL estimates. Median MSL was comparable for the two largest categories, cargo ships and tankers, at both sites, with an energy peak around 50 Hz. Tug/Tow vessel source levels were 5-10 dB lower at 50 Hz than the cargo ships and tankers, and passenger vessels were 10-15 dB lower. MSLs of the remaining vessel categories were highly variable, likely due to small sample sizes.

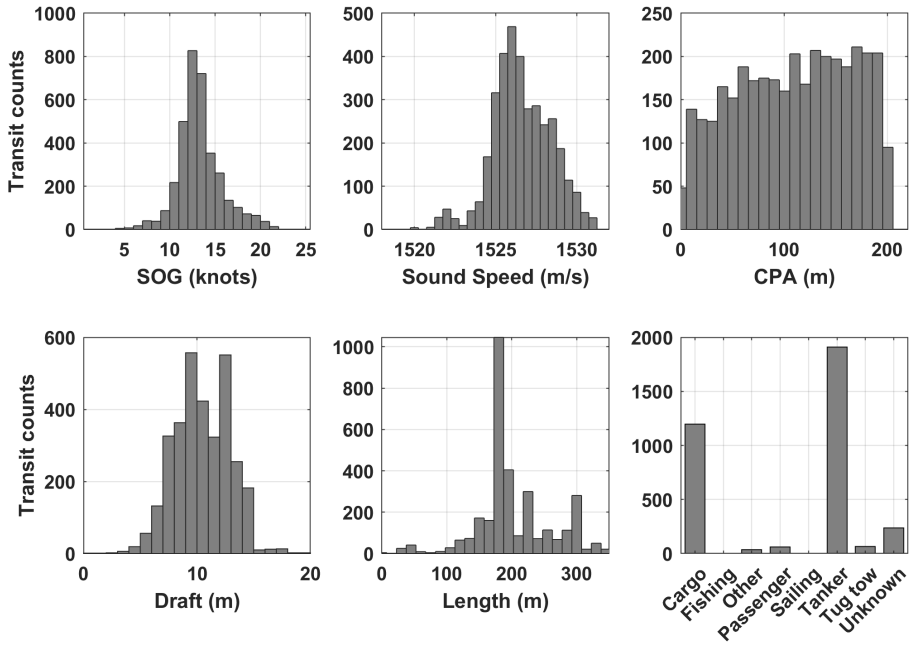


**Figure 110:** Distributions of AIS-derived vessel descriptors for vessel transits passing within 200 m of the GA HARP from mid 2020-2023.

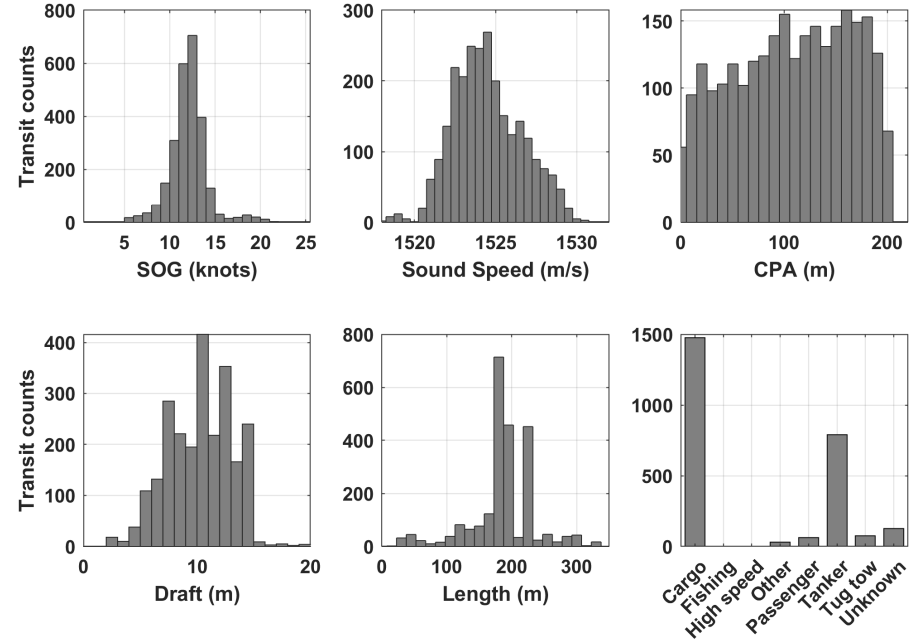


**Figure 111:** Distributions of AIS-derived vessel descriptors for vessel transits passing within 200 m of the SL HARP from mid 2020-2023.

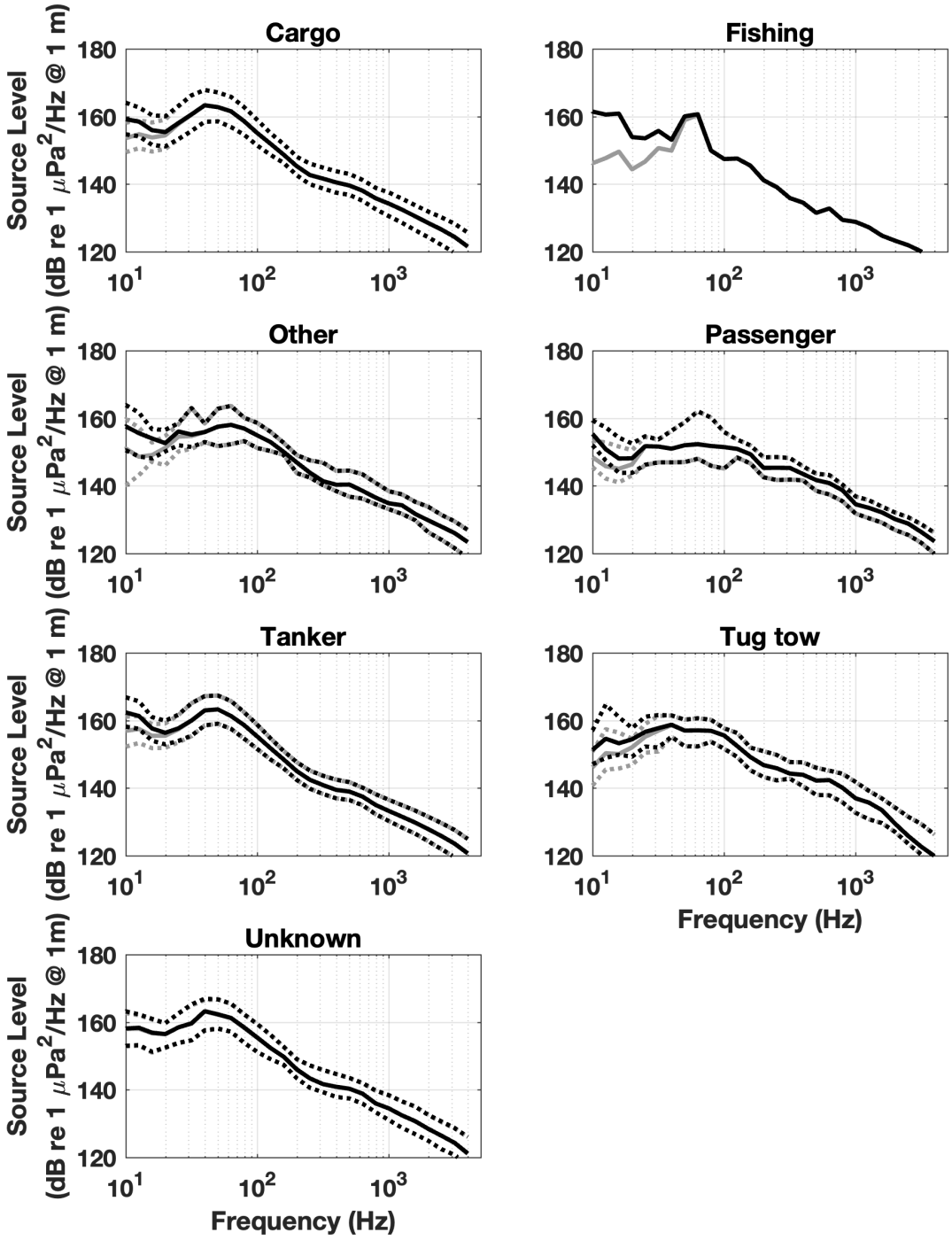


**Figure 112:** Mean (solid line) and 25th and 75th percentiles (dashed lines) of third-octave band MSL (black) and RNL (gray) estimates for different categories of vessels passing within 200 m of the GA HARP from mid 2020-2023.

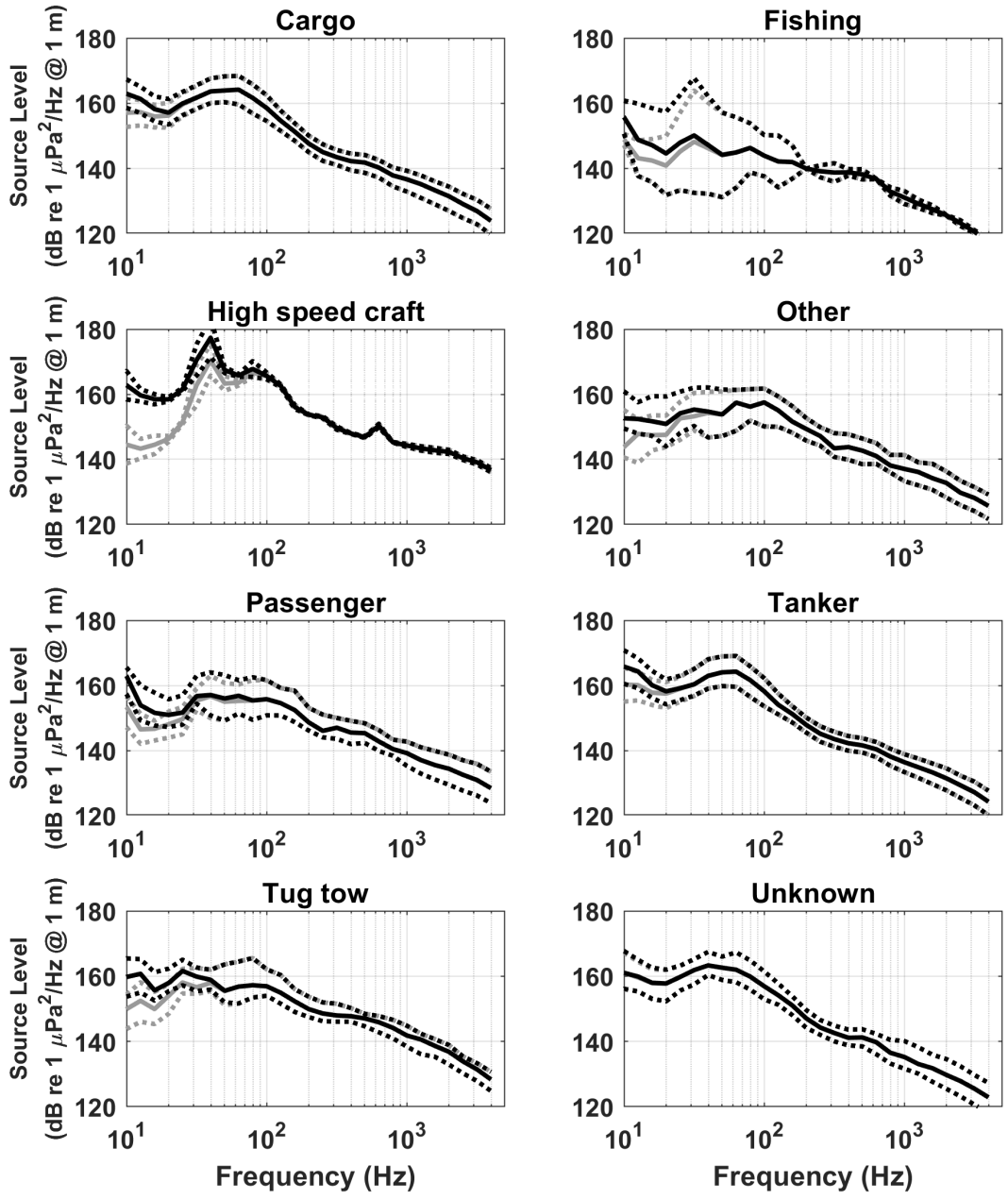


**Figure 113:** Mean (solid line) and 25th and 75th percentiles (dashed lines) of third-octave band MSL (black) and RNL (gray) estimates for different categories of vessels passing within 200 m of the SL HARP from mid 2020-2023.

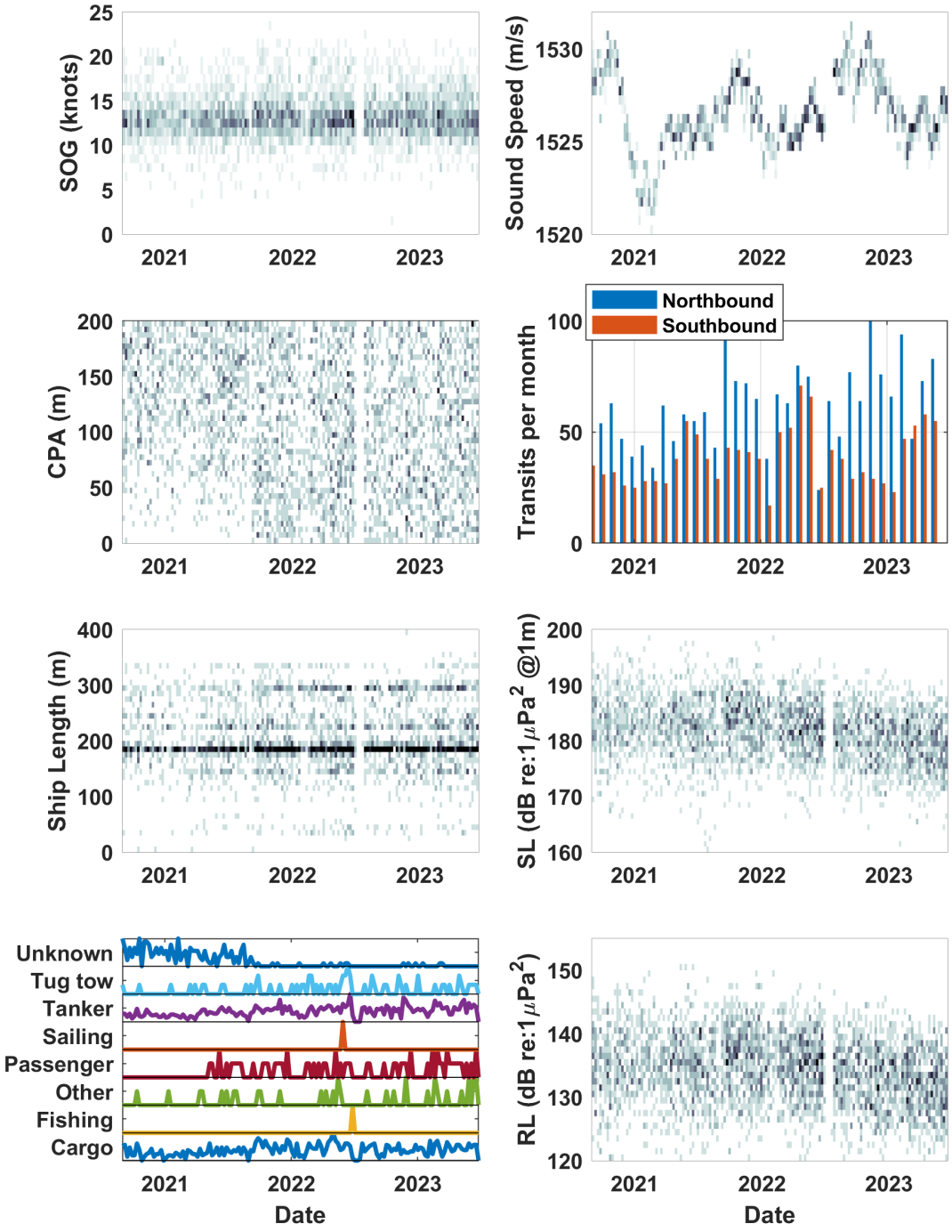


**Figure 114:** Temporal patterns in vessel transit descriptors, broadband received levels and estimated broadband source levels (15 - 1,000 Hz) at site GA over 2020 - 2023. Note that this site's position was adjusted slightly in mid-2021 to increase close transit counts, therefore inter-annual trends in counts may be unreliable.

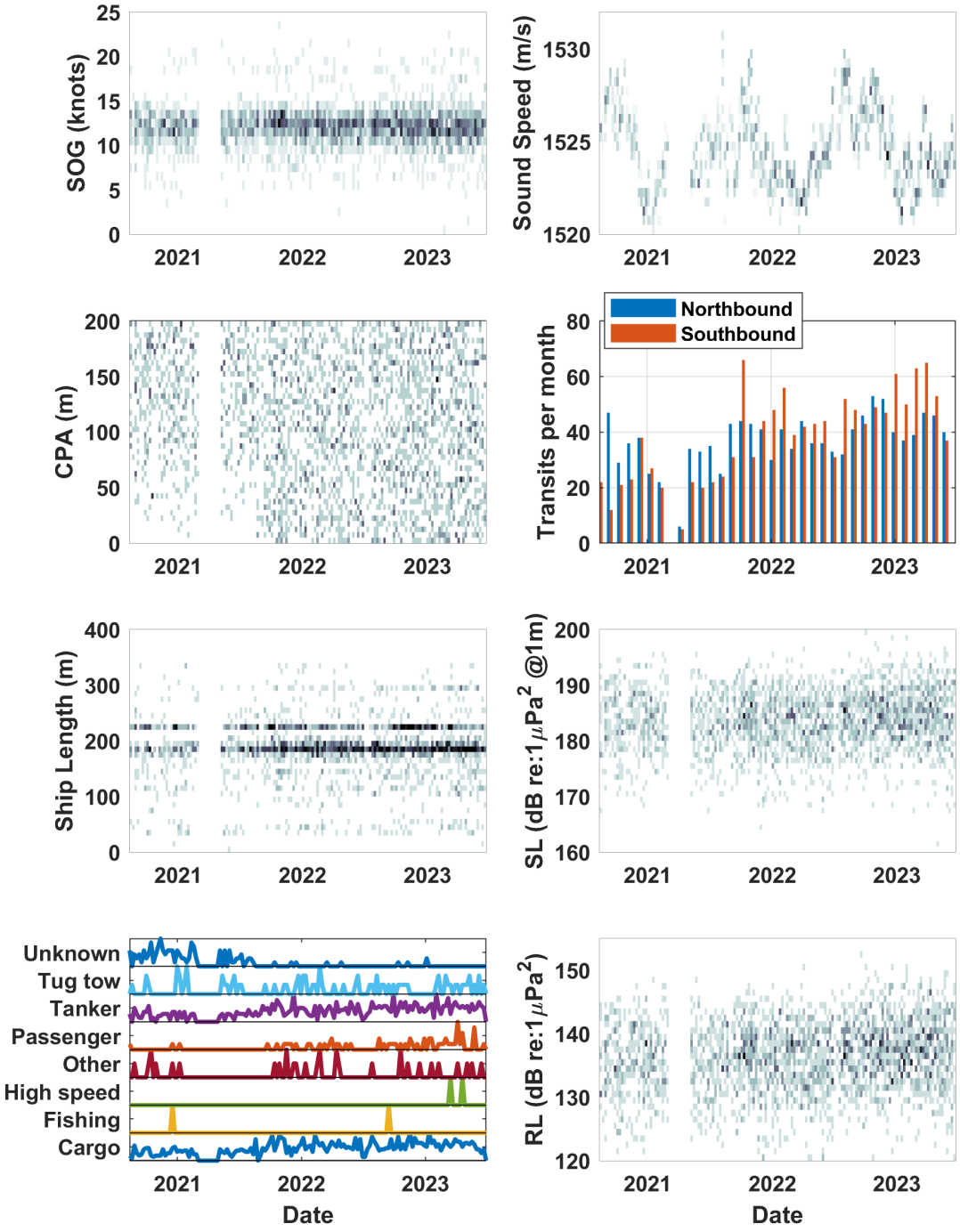


**Figure 115:** Temporal patterns in vessel transit descriptors, broadband received levels and estimated broadband source levels (15 - 1,000 Hz) at site SL over 2020 - 2023. Note that this site's position was adjusted slightly in mid-2021 to increase close transit counts, therefore inter-annual trends in counts may be unreliable.

### 4.3.4 Airguns

Seismic survey airgun pulse signals with energy greater than 120 $dB_{PP}$ re $1\mu Pa^2$ were commonly present, and detected in high numbers, throughout the recordings at all HARP sites over the 2020-2023 period (Table 9). Airgun pulses were detected in highest numbers on average at site CE (over 33,000 detections per week) followed by sites GC, DT, and MR. Lowest numbers of detections were observed at the shallow sites DC and Y1D; however, over one thousand pulses on average per week were still detected at these locations. The consistent detection of airgun signals at the western and deep-water sites, and large number of detections at site DT and Y1D despite these site's locations in the Eastern Planning Area at considerable distances from the majority of presumed survey activity in the Central and Western Planning Areas, is notable.

Within each recording site, detection events are grouped temporally in batches associated with months-long surveys. Additionally, airgun pulse detections had similar patterns of occurrence across sites (Figures 116 &117) indicating the same surveys were detected at multiple sites spread broadly throughout the Gulf. In many instances, surveys were detected on all or nearly all sites Gulf-wide. At the sites with the highest detection rates, minutes per day containing detections are typically present more than 50% of the time, and can approach 100% (Figures 116 &117). There was no clear seasonal pattern in airgun detections, and no apparent diel patterns, as surveys were conducted throughout the day and night (Figures 118 & 119).

Airgun pulse detection received levels were highest at site GC, particularly in the fall of 2020 and winter of 2022, when surveys were conducted for many months at close range. In these cases, nearly all pulses had received levels of 165 $dB_{PP}$ re $1\mu Pa^2$ or higher, as this was the maximum level capable of being recorded by the HARPs. Received levels were also high at site AC throughout the winter and spring of 2021, and at site MC in winter 2022 and spring 2023. At site CE, where the largest number of detections occurred, received levels were moderately high throughout the entire recording period, averaging 140 $dB_{PP}$ re $\mu Pa^2$, but were lower than at sites on the western shelf, and detected surveys appear to include both western and central Gulf surveys. Short-term sites Y2A and Y2B also had moderately high airgun pulse received levels over the durations of their deployments, with levels averaging 140 $dB_{PP}$ re $1\mu Pa^2$, and periodically exceeding 150 $dB_{PP}$ re $1\mu Pa^2$. Received levels were low at sites where detection rates were low, including DC and Y1D, indicative of attenuation of the distant signals over long distances and absorption into the shallower seafloor.

A spatial comparison of monthly occurrence patterns and monthly mean received levels of detected airgun pulses with locations of presumed seismic survey vessels from AIS tracks (from MarineCadastre) each year begins to give insight into the large-scale propagation of seismic survey airgun pulses throughout the Gulf of Mexico (Figures 122, 124, & 125).

- During November 2020 to early January 2021, seismic survey activity was primarily occurring just south of the US/Mexico EEZ in the western Gulf, between sites AC and MR

(Figure 125), and airgun pulse detections and presence with similar patterns occurred at primarily southern sites across the Gulf during this period, with limited detections at sites GA, GC, SL, MC, and DC in the north (Figures 116 and 117). Surprisingly, during this period, the number and occurrence of detections was among the highest at sites DT and Y1B, in the eastern Gulf, with high detections also occurring at sites AC, Y1C, and CE (Figure 122). It is unknown whether an additional survey was occurring in the southeastern Gulf during this time that has not been identified, or whether sound propagation conditions through the deep ocean led to high detectability in these waters compared to waters (e.g., sites MR and GC) closer to the survey.

- During January through April 2021, the primary seismic survey activity was occurring in the western Gulf, just southwest of sites AC and GA (Figure 125). During Jan – Apr, pulse detections following similar patterns occurred at sites AC, Y1C, CE, Y1B, LC, Y1D, and DT, while not being detected at the four northernmost sites or, surprisingly, at nearby MR and GC for January and February survey activity (Figures 116 & 117). Monthly median received levels during these months were highest at sites AC and CE (139-142 $dB_{PP}$ re $1\mu Pa^2$) followed by sites Y1C and Y1B (135-138 $dB_{PP}$ re $1\mu Pa^2$; Figures 120 & 121). Overlapping this period, another seismic survey south of site GA occurred during March to April (Figure 125). This may have primarily been detected at sites GA and GC (Figure 116), where monthly median received levels reached 134-138 $dB_{PP}$ re $1\mu Pa^2$. Further, during April to May there was additional seismic survey activity slightly northwest of the previously described survey, at similar distances from sites AC and GA, and some additional activity may have been occurring around MC during April in multiple small patches. Airgun pulse detections remained high from March through May at sites AC, Y1C, CE, and DT and could have included detections from any of these surveys during that time (Figures 116 & 122). An increase in detections at sites MR and LC during April to May 2021 may correspond to the survey between AC and GA (Figure 116 & 122).
- A smaller survey in July 2021 south of site AC was detected at sites AC (144-145 $dB_{PP}$ re $1\mu Pa^2$), CE, and Y1C. This may have been a lower amplitude survey, with more limited long range propagation.
- Monthly median received levels of airgun pulses reached the highest levels of any site (over 160 $dB_{PP}$ re $1\mu Pa^2$) at GC from September 2021 to January 2022 (Figure 124). Received levels were so elevated at this location that the recordings became clipped, and levels cannot be accurately measured for the closest survey approaches. This 5 month or longer survey (or set of closely positioned surveys), which covered an area over 200 km by 100 km that went directly over site GC during December and January (Figure 125), was widely detected across all recording sites, with the exception of limited detections at sites SL and DC.
- Notable eastern surveys occurred in June and July 2022, with a survey southeast of MC, and another north of Y2A (Figure 125). These appear to have been most strongly detected at sites MC, DT, MR, CE, and SL, and a number of the Y3C sites. A third survey was active southeast of site GC at this time, and is also a source of detected events.

- During the final year of deployments, AIS track data are only currently available from August to December 2022, during which seismic survey activity can be seen occurring in the middle of sites AC, GA, GC, and Y3D during September to November, while numerous smaller surveys were also occurring near sites SL and GC (Figure 125). Airgun detections were commonly detected across all HARP sites during this period.

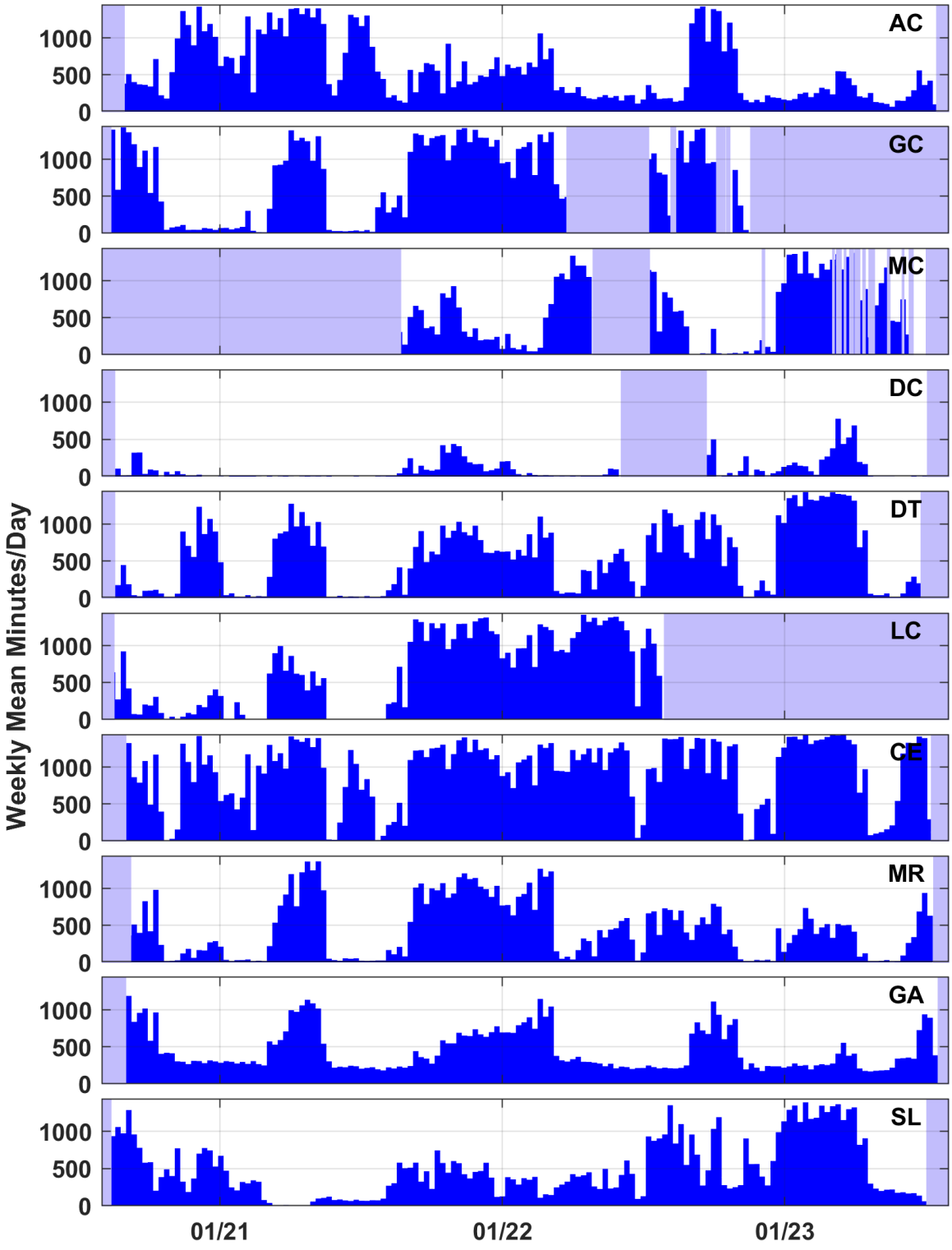


**Figure 116:** Weekly mean minutes-per-day presence (dark blue bars) of airgun pulses between 2020-2023 at long-term Gulf of Mexico HARP sites. Shaded blue sections represent periods with no recording effort.

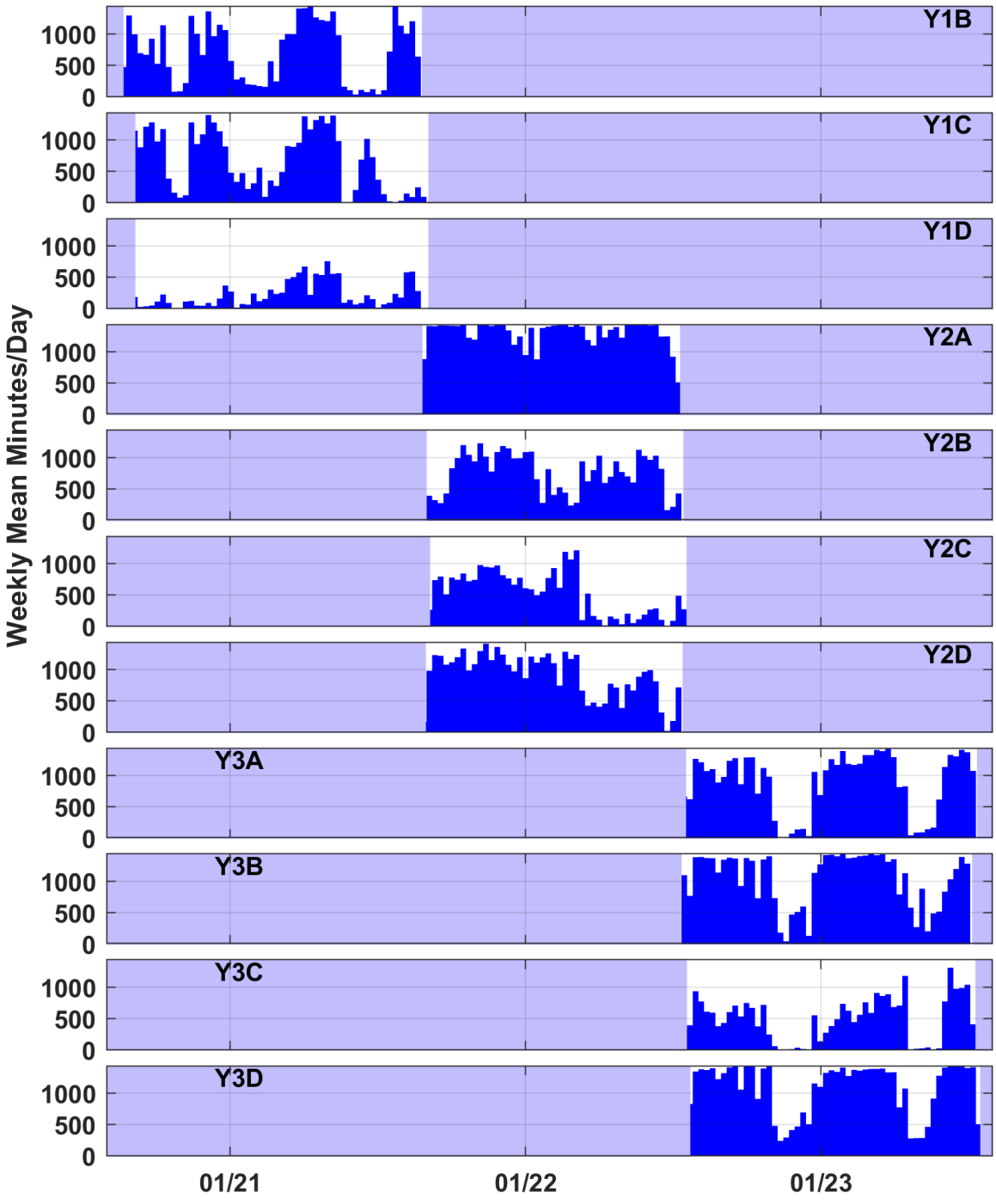


**Figure 117:** Weekly mean minutes-per-day presence (dark blue bars) of airgun pulses between 2020-2023 at short-term Gulf of Mexico sites. Shaded blue sections represent periods with no recording effort.

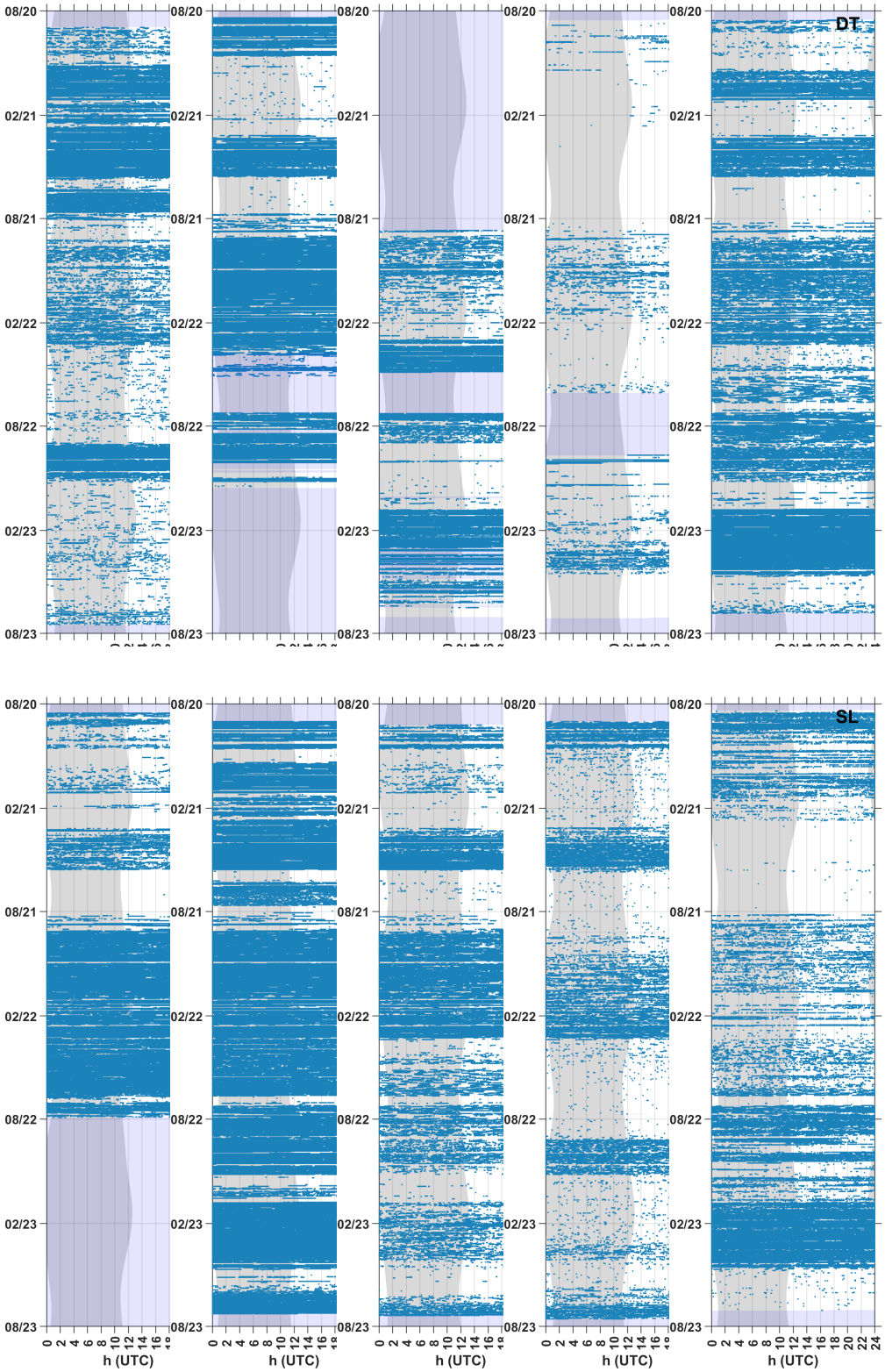


**Figure 118:** Airgun pulse detections in five-minute bins (blue bars) at long-term sites. Shaded blue sections represent periods with no recording effort.

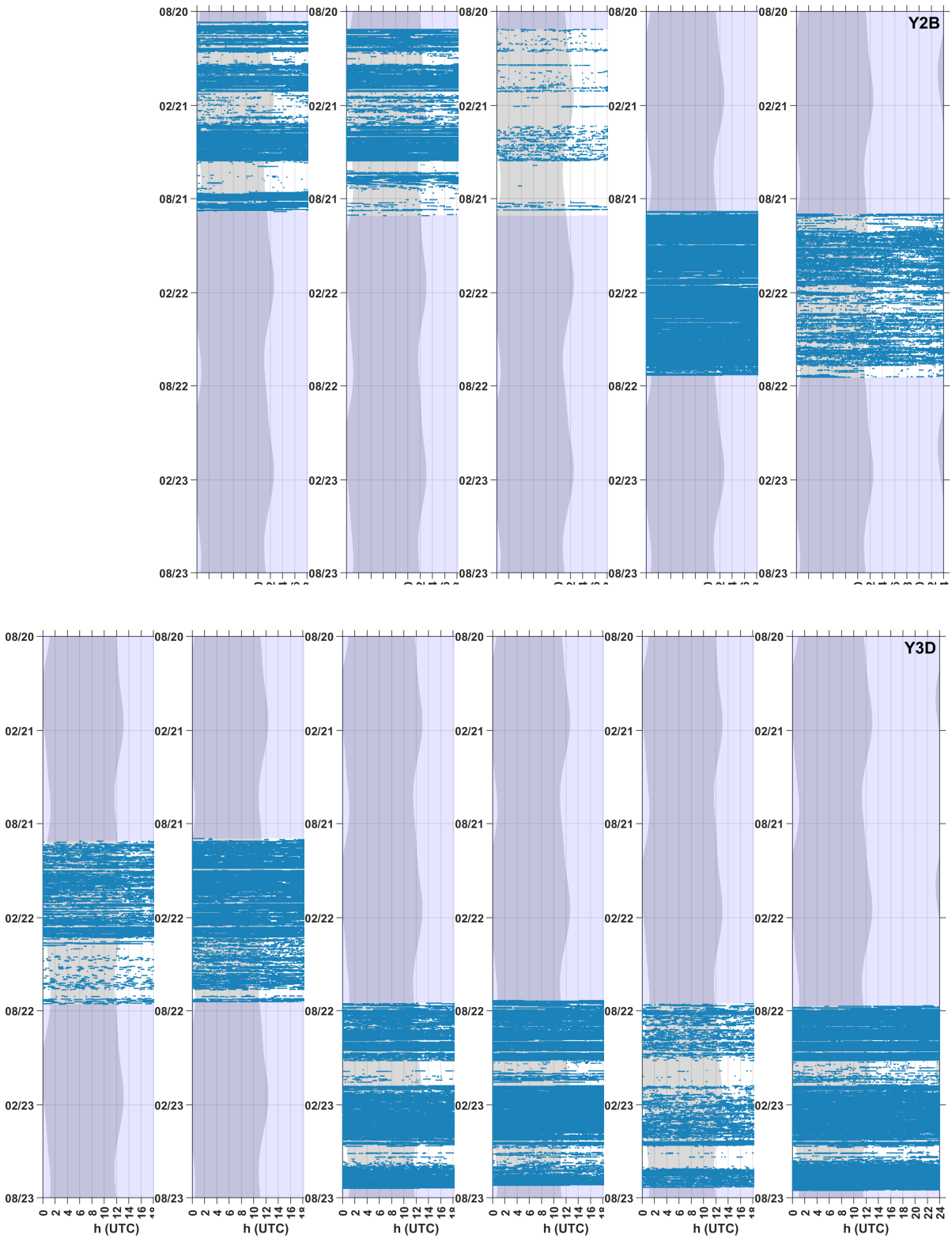


**Figure 119:** Airgun pulse detections in five-minute bins (blue bars) at short-term sites. Shaded blue sections represent periods with no recording effort.

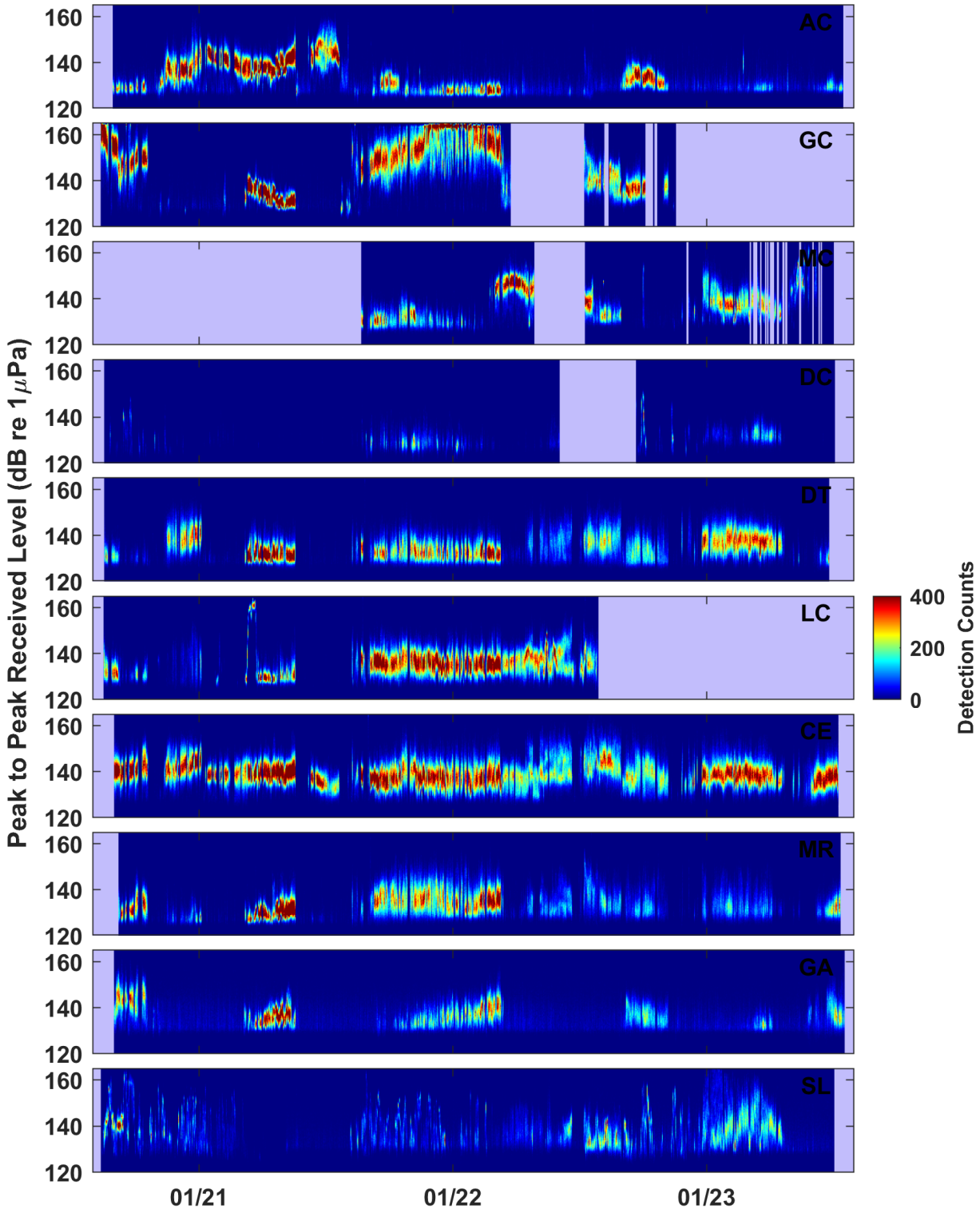


**Figure 120:** Daily peak-to-peak received level distributions of airgun signals detected at long-term sites, represented as heat maps. A minimum received level of 120 dB_pp has been applied. Purple shaded areas indicate periods with no effort.

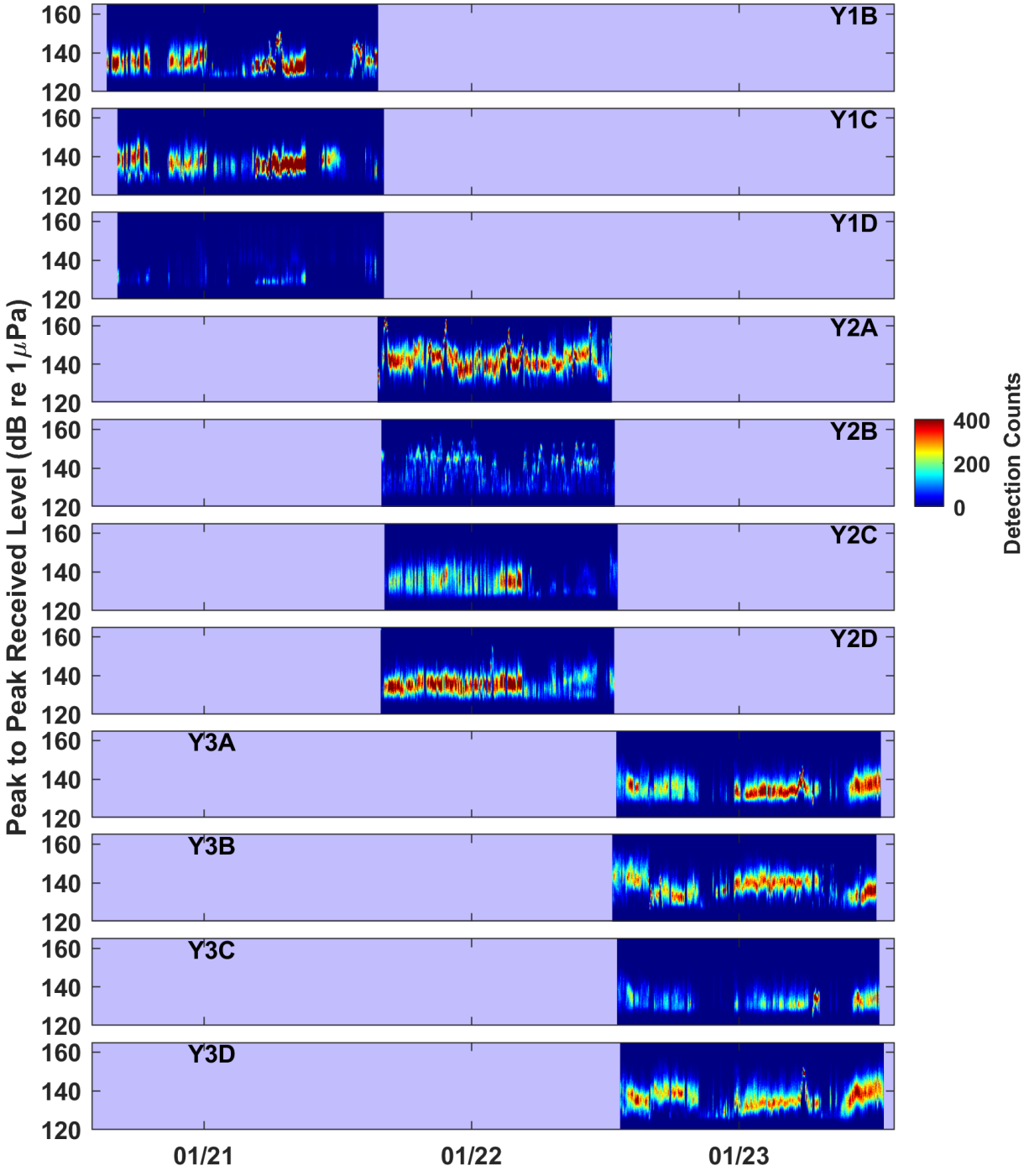


**Figure 121:** Daily peak-to-peak received level distributions of airgun signals detected at short-term sites, represented as heat maps. A minimum received level of 120 dB_pp has been applied. Purple shaded areas indicate periods with no effort.

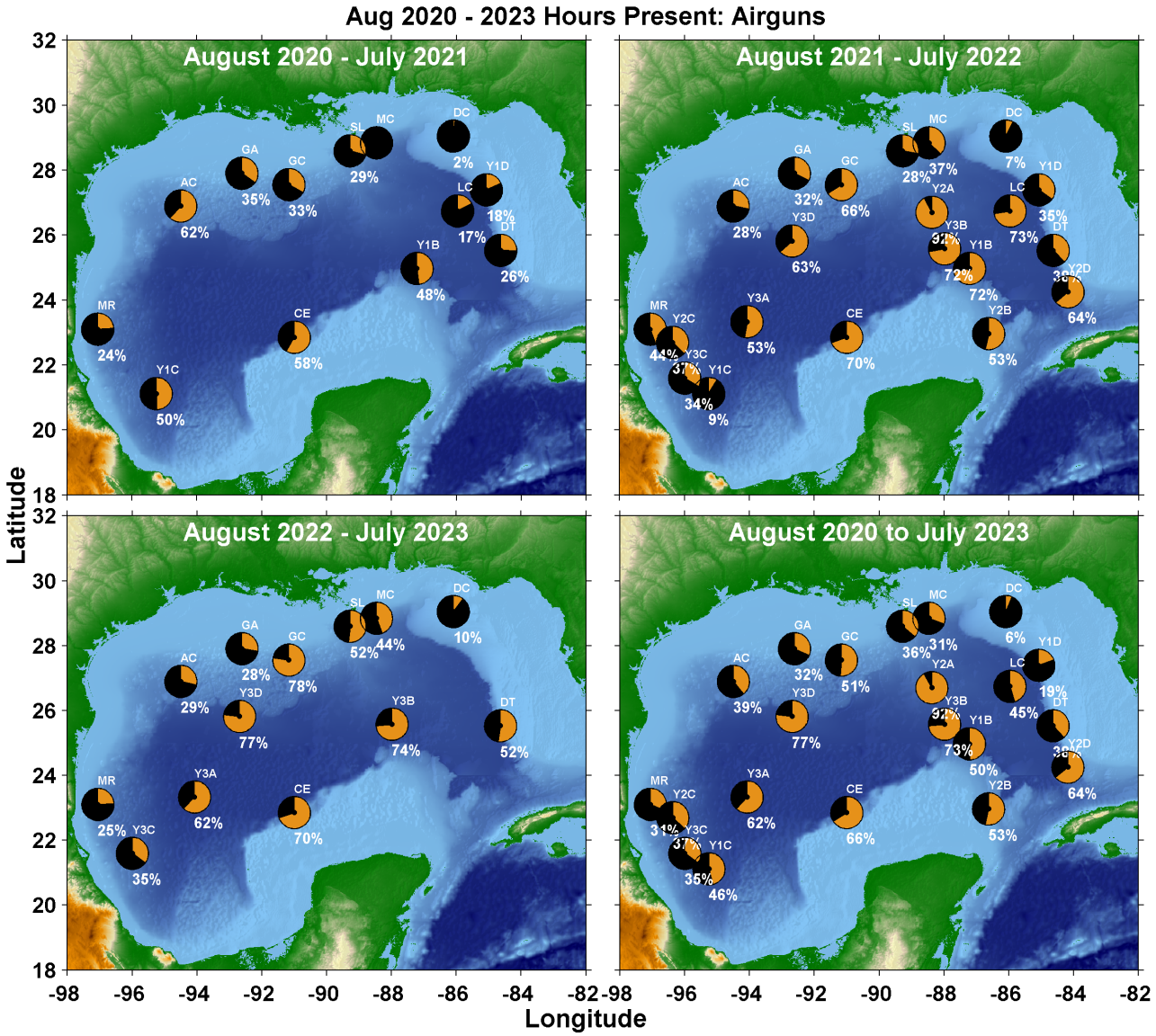


**Figure 123:** Proportion of time airgun pulse detections with ppRLs of at least 120 dB are present in Gulf of Mexico HARP recordings at each HARP site from 2020-2023. Panels represent proportional hourly presence in each of the three years of recordings, with the bottom right panel representing all years combined.

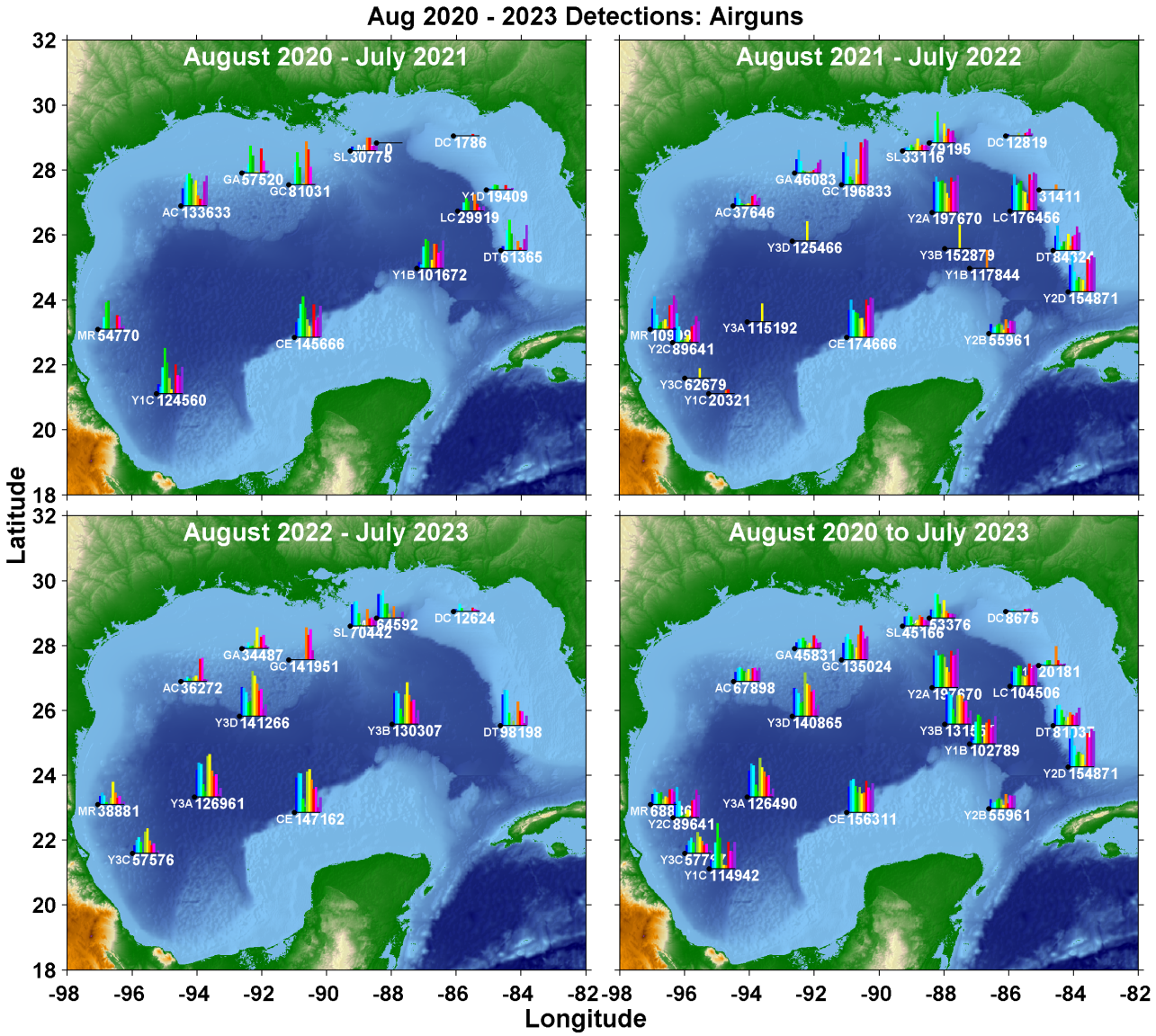


**Figure 122:** Airgun pulse detections per month, represented as bar plots, per HARP site from 2020 to 2023. Values below bars represent average monthly airgun pulse detections over the recording period. Panels represent detections in each of the three years of recordings, with the bottom right panel representing all years combined.

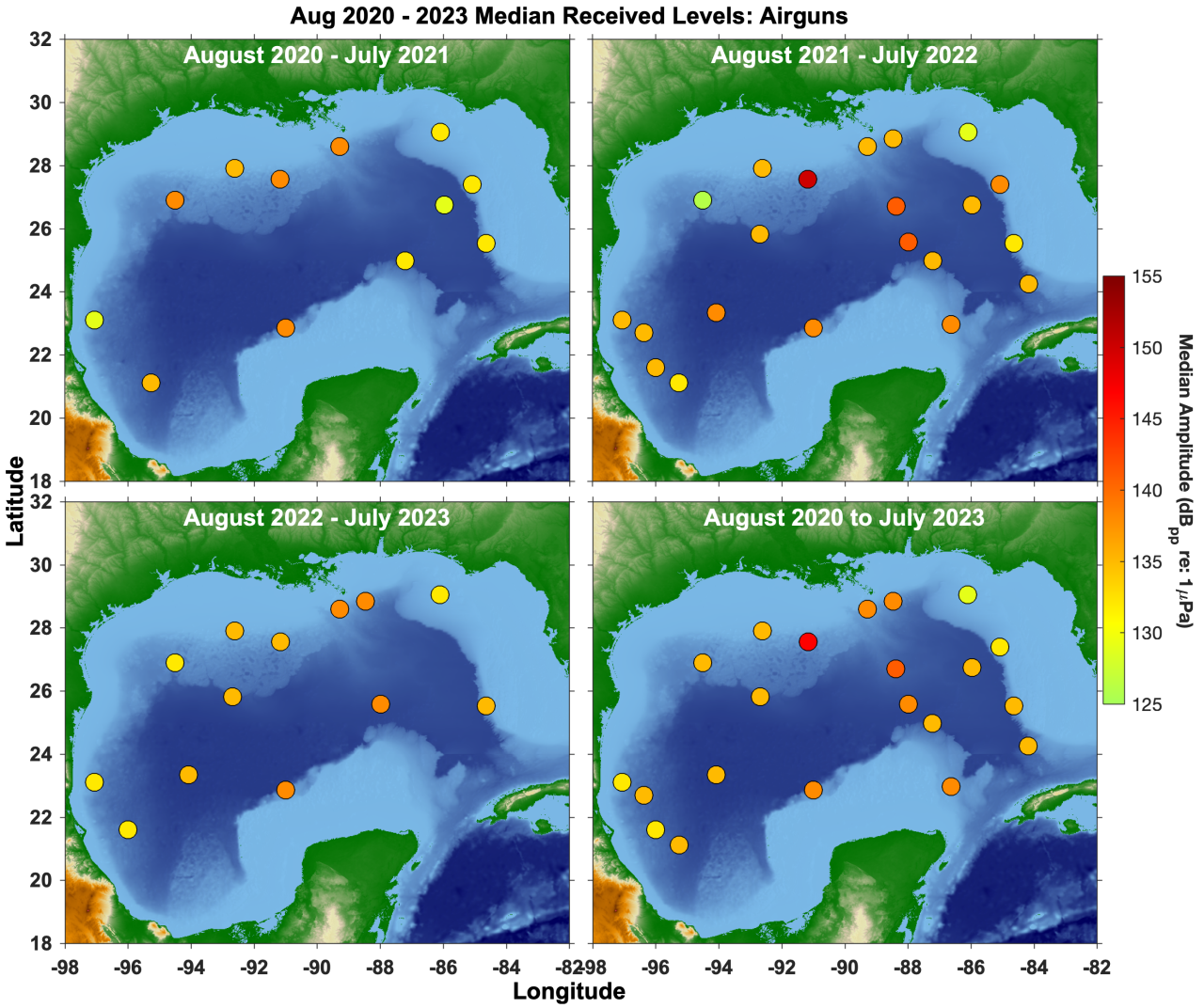


**Figure 124:** Median RLs for all airgun detections with ppRLs of at least 120 dB detected from 2020-2023. Filled circles are colored by peak-to-peak received level according to the color bar (right). Panels represent received levels in each of the three years of recordings, with the bottom right panel representing all years combined.

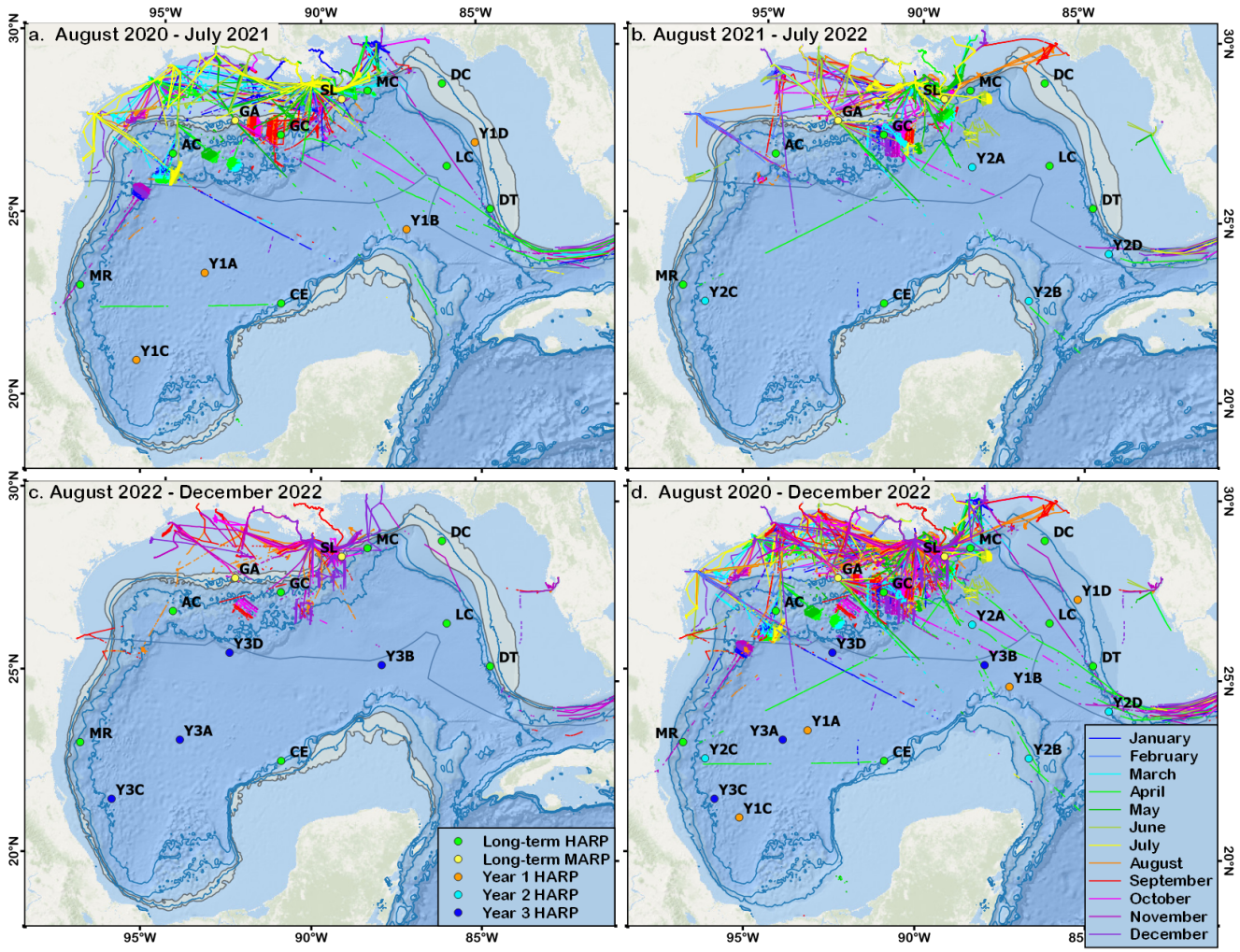


**Figure 125:** Vessel tracks (from MarineCadastre AIS data) for ships that conduct seismic airgun surveys, for the August 2020 to December 2022 period, by deployment year: August 2020 to July 2021 (Top Left), August 2021 to July 2022 (Top Right), August 2022 to December 2022 (remaining data to July 2023 are not yet available; Bottom Left), and all tracks from August 2020 to December 2022 (Bottom Right). Areas with dense track lines are presumed to be indicative of airgun survey activity while single longer lines may represent periods when vessels are just transiting.

### 4.3.5 Seismic Airgun Survey: Detailed Analysis

To further investigate the influence of seismic airgun surveys on the Gulf-wide soundscape, some surveys can be investigated in further detail by linking acoustic recordings across all Gulf sites, AIS vessel tracks, and summary monitoring reports from survey activities (source: www.fisheries.noaa.gov/marine-mammal-protection/issued-letters-authorization-oil-and-gas-industry-geophysical-survey). As an example, a single survey was identified occurring between December 2022 and April 2023 being conducted by two vessels just east of the GC site (Figure 126). During this period, this survey can be detected on acoustic recorder sites across the entire Gulf (Figure 127). The survey start can be identified very clearly at most sites, while the end of the survey is identifiable but slightly less defined, due to the presence of other surveys at that time. This Ocean Bottom Node (OBN) survey used two source vessels each towing two identical arrays with a total of 28 airguns per array; each array was comprised of three sub arrays totaling a nominal source array volume of 5,240 cubic inches with resulting source levels of approximately 262 $dB_{pp}$ re 1$\mu$Pa  1 m (RPS Group 29 June 2023). There appears to be a bathymetric effect on the received levels observed at the various sites, with substantially greater transmission loss along the source-to-receiver path in shallower waters compared to deeper waters. Higher received levels are observed at the distant CE and DT sites where the transmission path occurs downslope and across deep waters compared to the closer GA and AC sites where the transmission path occurs along or upslope. The potential long-range transmission and impact of bathymetry on sound-propagation is important when evaluating the contribution of airguns to the Gulf-wide soundscape.

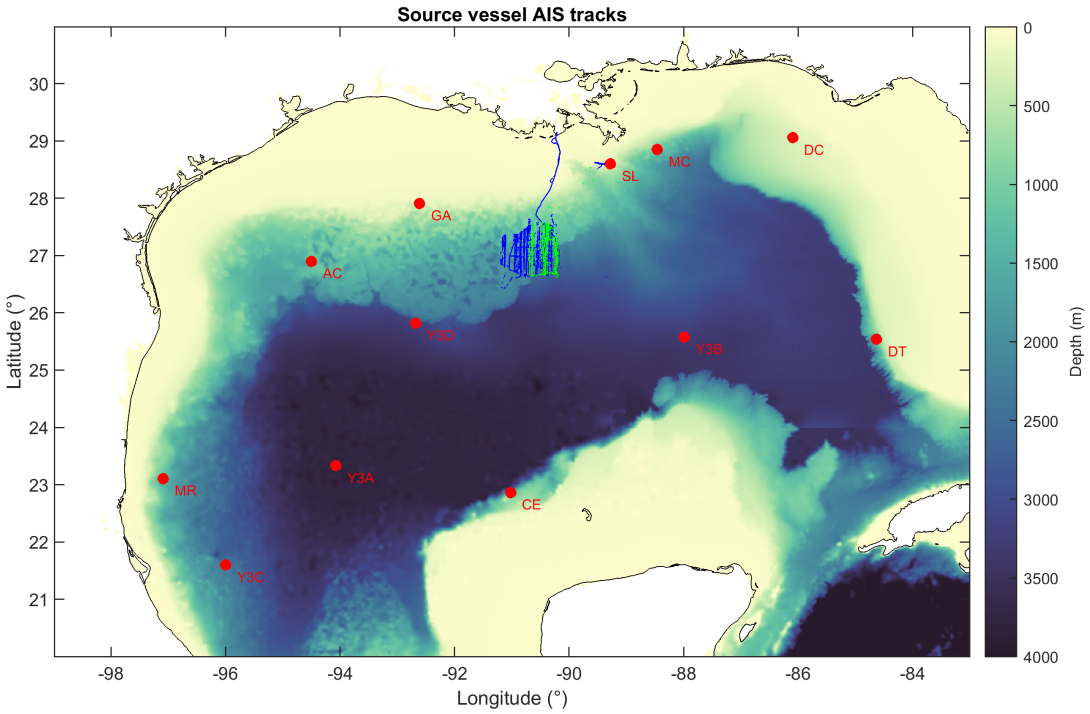


**Figure 126:** AIS tracks of two source vessels (green and blue lines) conducting the December 2022 to April 2023 airgun survey. LISTEN GoMex HARP sites deployed during these airgun operations are shown (red circles).

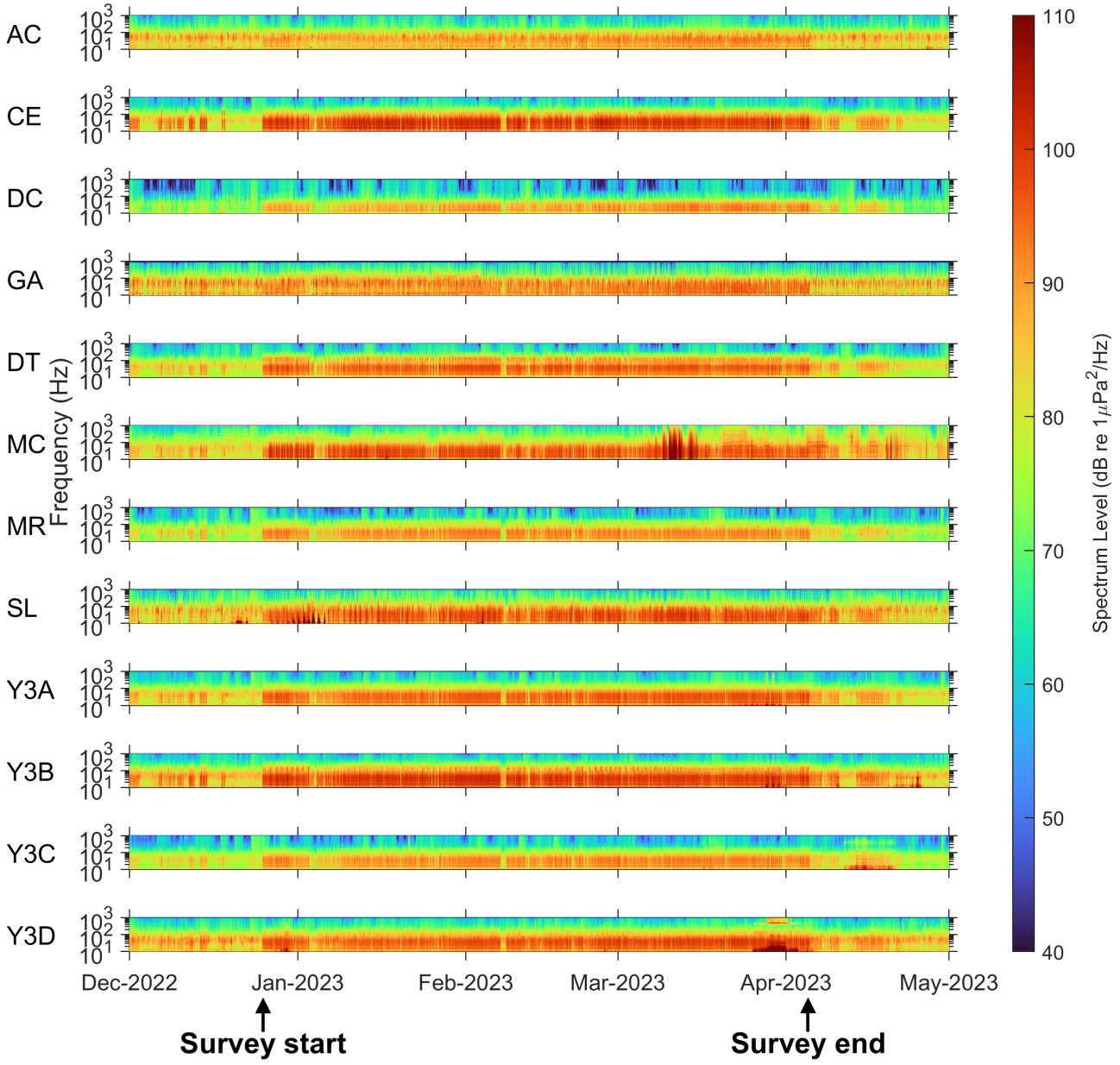


**Figure 127:** Long spectrograms (hourly averaged spectra) illustrating how specific seismic airgun surveys can be detected at sites across the entire Gulf of Mexico. The survey shown here starts at the end of December 2022 and ends in early April 2023.

# 5 Future Steps

Data results included in this report include the preliminary marine mammal occurrence and density estimates, and ambient and anthropogenic noise analyses from the 2020-2023 LISTEN GoMex data. Data collection and analyses for this 2020-2024 passive acoustic monitoring program are ongoing. Future annual reports and manuscripts for peer-review will include preliminary marine mammal occurrence and density estimates for each year of data collected, along with more in-depth analyses of long-term density trends, spatio-temporal occurrence patterns, and predictive spatially-explicit models of marine mammal density related to environmental drivers. Future work will also include analyses of finer taxonomic resolution of odontocete echolocation clicks.

# 6 Acknowledgments

Gabrielle Arrieta, Ashley Cook, Bruce Thayre, Eva Hildalgo Pla, Gania Figueroa, Itzel Carballo, John Hurwitz, Josh Jones, Kieran Lenssen, Kristen Rosier, Natalie Posdaljian, Ryan Pierson, Sam Wagner, Sean Wiggins, and Vanessa ZoBell assisted with building, deploying and recovering of HARPs. Erin O'Neill, Diego Majewski, and Shelby Bloom processed the acoustic data. Vanessa ZoBell, Alba Solsana Berga, Jenny Trickey and Kieran Lenssen assisted with data analysis. Captain Tad Berkey and the crew of the R/V Pelican made the field work possible. Len Thomas assisted with the LISTEN GoMex survey design. Laura Engleby, Jason Gedamke, and Leila Hatch advised on shipping lane locations for the noise-focused HARP sites.

# 7 Funding Sources

Funding for the LISTEN GoMex program is provided by NOAA's RESTORE Science Program, the *Deepwater Horizon* Open Ocean Trustee Implementation Group, and the Office of Naval Research Task Force Ocean. Funding for the 2010-2020 historic HARP data leveraged by the LISTEN GoMex program were provided by the *Deepwater Horizon* Natural Resource Damage Assessment program, the Gulf of Mexico Research Initiative through C-IMAGE at USF (Steve Murawski and Sheryl Gilbert), and NOAA NMFS' Office of Science and Technology (Mridula Srinivasan), NOAA's Southeast Regional Office (Laura Engleby).

Acoustic data collection at three long-term sites (MR, CE, and LC), twelve short-term sites (Y1A, Y1B, Y1C, Y1D, Y2A, Y2B, Y2C, Y3D, Y3A, Y3B, Y3C, Y3D), and six tracking sites (MC-4CH-1, MC-4CH-2, GC-4CH-1, GC-4CH-2, MR-4CH-1, MR-4CH-2) over the 2020-2023 period, marine mammal occurrence analyses in these recordings, and beaked whale tracking analyses from the 2020-2023 recordings were funded as part of the "Assessing long-term trends and processes driving variability in cetacean density throughout the Gulf of Mexico

using passive acoustic monitoring and habitat modeling" project under federal funding opportunity Grant No. NOAA-NOS-NCCOS-2019-2005608 from the National Oceanic and Atmospheric Administration's RESTORE Science Program through the Gulf Coast Restoration Trust Fund to the NOAA Southeast Fisheries Science Center.

Acoustic data collection at five long-term sites (AC, GC, MC, DC, DT) and two noise-focused sites (GA, SL) over the 2020-2023 period, marine mammal occurrence analyses in these recordings, and all ambient and anthropogenic noise analyses from the 2020-2023 recordings were funded by the *Deepwater Horizon* Open Ocean Trustee Implementation Group's "Reduce Impacts of Anthropogenic Noise on Cetaceans" project to restore natural resources injured by the 2010 Deepwater Horizon oil spill in the Gulf of Mexico.

Ship-time aboard the R/V Pelican for HARP deployment and servicing cruises in August 2020, August 2021, and July 2022, HARP equipment upgrades, and airgun detection algorithm development were funded under the Office of Naval Research Task Force Ocean (Robert Headrick).

# References

Au, Whitlow WL (1993). *The sonar of dolphins*. Springer Science & Business Media.

Audoly, Christian and Valentin Meyer (2017). "Measurement of radiated noise from surface ships–Influence of the sea surface reflection coefficient on the Lloyd's mirror effect". In: *Proceedings of Acoustics*. Vol. 19. 22.

Baumann-Pickering, Simone et al. (2013). "Species-specific beaked whale echolocation signals". In: *The Journal of the Acoustical Society of America* 134.3, pp. 2293–2301.

Baumann-Pickering, Simone et al. (2014). "Spatio-temporal patterns of beaked whale echolocation signals in the North Pacific". In: *PloS one* 9.1, e86072.

Blackman, Donna K et al. (2004). "Testing low/very low frequency acoustic sources for basin-wide propagation in the Indian Ocean". In: *The Journal of the Acoustical Society of America* 116.4, pp. 2057–2066.

Cohen, Rebecca E et al. (2022). "Identification of western North Atlantic odontocete echolocation click types using machine learning and spatiotemporal correlates". In: *PloS one* 17.3, e0264988.

Cox, Henry (2004). "Navy Applications of High-Frequency Acoustics". In: *AIP Conference Proceedings*. Vol. 728. 1. American Institute of Physics, pp. 449–455.

Frasier, Kaitlin E et al. (2016). "Delphinid echolocation click detection probability on near-seafloor sensors". In: *The Journal of the Acoustical Society of America* 140.3, pp. 1918–1930.

Frasier, Kaitlin E et al. (2017). "Automated classification of dolphin echolocation click types from the Gulf of Mexico". In: *PLoS computational biology* 13.12, e1005823.

Frasier, Kaitlin E et al. (In Review). "A decade of declines in toothed whale densities following the Deepwater Horizon oil spill". In: *TBD*.

Frasier, Kaitlin Emily (2015). *Density estimation of delphinids using passive acoustics: A case study in the Gulf of Mexico*. University of California, San Diego.
Gassmann, Martin, Sean M Wiggins, and John A Hildebrand (2015). "Three-dimensional tracking of Cuvier's beaked whales' echolocation sounds using nested hydrophone arrays". In: *The Journal of the Acoustical Society of America* 138.4, pp. 2483–2494.
– (2017). "Deep-water measurements of container ship radiated noise signatures and directionality". In: *The Journal of the Acoustical Society of America* 142.3, pp. 1563–1574.
Gillespie, Douglas et al. (2009). "Field recordings of Gervais' beaked whales Mesoplodon europaeus from the Bahamas". In: *The Journal of the Acoustical Society of America* 125.5, pp. 3428–3433.
Goold, John C and Sarah E Jones (1995). "Time and frequency domain characteristics of sperm whale clicks". In: *The Journal of the Acoustical Society of America* 98.3, pp. 1279–1291.
Henderson, EE et al. (2022). *Standardized Unclassified Nomenclature to Describe Navy Sonar Signals*. Naval Information Warfare Center Pacific (NIWC Pacific) TECHNICAL REPORT 3273.
Hildebrand, John A (2009). "Anthropogenic and natural sources of ambient noise in the ocean". In: *Marine Ecology Progress Series* 395, pp. 5–20.
Hildebrand, John A et al. (2015). "Passive acoustic monitoring of beaked whale densities in the Gulf of Mexico". In: *Scientific reports* 5.1, pp. 1–15.
Hildebrand, John A et al. (2019). "Assessing seasonality and density from passive acoustic monitoring of signals presumed to be from pygmy and dwarf sperm whales in the Gulf of Mexico". In: *Frontiers in Marine Science* 6, p. 66.
Johnson, Mark et al. (2004). "Beaked whales echolocate on prey". In: *Proceedings of the Royal Society of London. Series B: Biological Sciences* 271.suppl_6, S383–S386.
Leu, Amanda A et al. (2022). "Echolocation click discrimination for three killer whale ecotypes in the Northeastern Pacific". In: *The Journal of the Acoustical Society of America* 151.5, pp. 3197–3206.
Madsen, PT et al. (2002). "Sperm whale sound production studied with ultrasound time/depth-recording tags". In: *Journal of Experimental Biology* 205.13, pp. 1899–1906.
Marques, Tiago A et al. (2009). "Estimating cetacean population density using fixed passive acoustic sensors: An example with Blainville's beaked whales". In: *The Journal of the Acoustical Society of America* 125.4, pp. 1982–1994.
McKenna, Megan F et al. (2012). "Underwater radiated noise from modern commercial ships". In: *The Journal of the Acoustical Society of America* 131.1, pp. 92–103.
Mellinger, David K and Christopher W Clark (2000). "Recognizing transient low-frequency whale sounds by spectrogram correlation". In: *The Journal of the Acoustical Society of America* 107.6, pp. 3518–3529.
Møhl, Bertel et al. (2003). "The monopulsed nature of sperm whale clicks". In: *The Journal of the Acoustical Society of America* 114.2, pp. 1143–1154.
Rafter, MR et al. (2022). *LISTEN GoMex: 2010-2021-Long-term Investigations into Soundscapes, Trends, Ecosystems, and Noise in the Gulf of Mexico*. Marine Physical Laboratory,

Scripps Institution of Oceanography, University of California San Diego, La Jolla, CA. MPL Technical Memorandum #662.
Rice, Aaron N et al. (2014). "Potential Bryde's whale (*Balaenoptera edeni*) calls recorded in the northern Gulf of Mexico". In: *The Journal of the Acoustical Society of America* 135.5, pp. 3066–3076.
Roch, Marie A et al. (2011). "Classification of echolocation clicks from odontocetes in the Southern California Bight". In: *The Journal of the Acoustical Society of America* 129.1, pp. 467–475.
RPS Group (29 June 2023). *OCS Permit L22-004 WesternGeco Engagement III 3D OBN Survey Protected Species Observer Final Report*.
Širović, Ana et al. (2014). "Bryde's whale calls recorded in the Gulf of Mexico". In: *Marine Mammal Science* 30.1, pp. 399–409.
Soldevilla, Melissa S et al. (2017). "Geographic variation in Risso's dolphin echolocation click spectra". In: *The Journal of the Acoustical Society of America* 142.2, pp. 599–617.
Soldevilla, Melissa S et al. (2022a). "Acoustic localization, validation, and characterization of Rice's whale calls". In: *The Journal of the Acoustical Society of America* 151.6, pp. 4264–4278.
Soldevilla, Melissa S et al. (2022b). "Rice's whales in the northwestern Gulf of Mexico: Call variation and occurrence beyond the known core habitat". In: *Endangered Species Research* 48, pp. 155–174.
Soldevilla, Melissa S et al. (2024). "Rice's Whale Occurrence in the Western Gulf of Mexico from Passive Acoustic Recordings". In: *Marine Mammal Science.*
Solsona Berga, Alba (2019). "Advancement of methods for passive acoustic monitoring: a framework for the study of deep-diving cetacean". In: *Universitat Politècnica de Catalunya*.
Solsona-Berga, Alba et al. (2020). "DetEdit: A graphical user interface for annotating and editing events detected in long-term acoustic monitoring data". In: *PLoS computational biology* 16.1, e1007598.
Solsona-Berga, Alba et al. (2022). "Echolocation repetition rate as a proxy to monitor population structure and dynamics of sperm whales". In: *Remote Sensing in Ecology and Conservation*.
Solsona-Berga, Alba et al. (Submitted). "Accounting for sperm whale population demographics in density estimation using passive acoustic monitoring". In: *TBD*.
Watwood, Stephanie L et al. (2006). "Deep-diving foraging behaviour of sperm whales (*Physeter macrocephalus*)". In: *Journal of Animal Ecology* 75.3, pp. 814–825.
Welch, Peter (1967). "The use of fast Fourier transform for the estimation of power spectra: a method based on time averaging over short, modified periodograms". In: *IEEE Transactions on audio and electroacoustics* 15.2, pp. 70–73.
Wiggins, Sean M and John A Hildebrand (2007). "High-frequency Acoustic Recording Package (HARP) for broad-band, long-term marine mammal monitoring". In: *2007 Symposium on Underwater Technology and Workshop on Scientific Use of Submarine Cables and Related Technologies*. IEEE, pp. 551–557.

Wiggins, Sean M, Mark A McDonald, and John A Hildebrand (2012). “Beaked whale and dolphin tracking using a multichannel autonomous acoustic recorder”. In: *The Journal of the Acoustical Society of America* 131.1, pp. 156–163.

Wiggins, Sean M et al. (2016). “Gulf of Mexico low-frequency ocean soundscape impacted by airguns”. In: *The Journal of the Acoustical Society of America* 140.1, pp. 176–183.

Zimmer, Walter MX et al. (2005). “Echolocation clicks of free-ranging Cuvier’s beaked whales (*Ziphius cavirostris*)”. In: *The Journal of the Acoustical Society of America* 117.6, pp. 3919–3927.

DOI: // 10.25923/3ma1-b145